INVESTIGATION OF MOLECULAR PARAMETERS ON CARTILAGE REGENERATION IN EXPERIMENTAL MODELS OF CARTILAGE DEFECTS AND OSTEOARTHRITIS

By

ELEFTHERIOS A. MAKRIS
M.D. (Aristotle University, Thessaloniki, Greece) 2009

DISSERTATION

Submitted in partial satisfaction of the requirements for the degree of

DOCTOR OF PHILOSOPHY

in

Biomedical Engineering Research

in the

OFFICES OF GRADUATE STUDIES

of the

UNIVERSITY OF THESSALY, GREECE
UNIVERSITY OF CALIFORNIA DAVIS, USA

Eleftherios Makris
March 2014
Biomedical Engineering

INVESTIGATION OF MOLECULAR PARAMETERS ON CARTILAGE REGENERATION IN EXPERIMENTAL MODELS OF CARTILAGE DEFECTS AND OSTEOARTHRITIS

ABSTRACT

Articular cartilage and fibrocartilage have limited abilities to self-repair following disease- or injury-induced degradation. With such cartilages providing the critical roles of protecting the osseous features of the knee joint and ensuring smooth, stable joint articulation, it is therefore critical that treatment modalities are created to promote the repair and/or regeneration of these tissues. A promising novel treatment modality comes from the potential of tissue engineered cartilage. While much progress has been recently made toward achieving engineered articular cartilage and fibrocartilage with compressive properties on par with native tissue values, their tensile properties still remain far behind. It is, therefore, critical that novel treatments be established to generate robust neotissue to address the approximately 46.4 million individuals affected by arthritis in the United States alone.

Motivated by the potential of tissue engineering, this thesis had three global objectives: 1) to investigate novel molecular pathways toward regenerating articular cartilage in *in vitro* and *in vivo* experimental models of cartilage defects and osteoarthritis, 2) to develop and optimize treatment modalities toward engineering neocartilage of clinical applicability, and 3) to promote neotissue maturation and foster integration between self-assembled neocartilage and native tissue. Toward achieving these goals, this thesis sought to tailor the use of exogenous agents to

promote native articular cartilage and fibrocartilage organization in engineered tissues. To begin, a treatment regimen consisting of copper and hydroxylysine was utilized to enhance the collagen crosslink content of self-assembled neocartilage constructs. A hypoxia treatment regimen was also investigated with the similar goal of enhancing the crosslink content and, therefore, the functional properties of engineered cartilage. Given the promising correlation between increased collagen crosslink content and neotissue tensile properties, a more direct approach to increase these crosslinks was established via application of the exogenous agent lysyl oxidase (LOX) to further enhance neotissue functional properties.

Other studies in this thesis focused on developing approaches for enhancing the collagen content and organization of the engineered tissues that, when combined with the novel collagen crosslinking approaches, would potentially result in mature engineered tissues capable of repairing cartilage defects in experimental (animal) models. Specifically, two agents known to modulate intracellular Ca^{2+} signaling (digoxin and adenosine triphosphate) were investigated as an alternative means to improve matrix content and biomechanical properties of neocartilage through promoting both collagen enhancement and collagen crosslinking. In addition, similar studies were focused on optimizing a treatment regimen consisting of the biophysical agent chondroitinase-ABC (C-ABC) and the biochemical agent transforming growth factor-β1 (TGF-β1) to enhance the functional properties of self-assembled neofibrocartilage constructs. Biomechanical stimulation in the form of passive axial compressive loading was also examined to aid in further driving *in vitro* development of self-assembled neofibrocartilage in an organized, shape-specific manner. An additional study investigated the possibility of alternative primary cell sources from the ankle joint as a superior cell source for generating tissue-specific self-assembled neocartilage for ankle joint cartilage defects.

Finally, this thesis investigated the potential of the exogenously applied LOX molecular mechanism to promote integration between neocartilage and native tissue. An initial study investigated the ability of LOX to promote integration between neocartilage and native articular cartilage. Promising results lead to combining LOX with C-ABC and TGF-β1 with the goal of inducing simultaneous neofibrocartilage maturation and integration. Specifically, this novel combination of stimuli was first applied to an *in vitro* model of integration, and then on an experimental animal model of integration to investigate the ability of the *in vivo* environment to further promote such integration.

Overall, the series of studies presented in this thesis represent various novel and potentially clinically significant molecular strategies to enhance the functional properties of a spectrum of collagen-rich tissues. Specifically, copper, endogenous LOX enhancement though hypoxia, and exogenous LOX application were all found to improve the mechanical properties of engineered cartilage, demonstrating the ability of enhancing collagen crosslinks to promote the development of mechanically robust, biomimetic neotissues. Further, agents such as digoxin, adenosine triphosphate, C-ABC, TGF-β1, and static weight application were all found to exhibit significant abilities toward promoting collagen enhancement and collagen crosslinking in neotissues. Finally, exogenous LOX applied alone and in combination with C-ABC and TGF-β1 was found to foster *in vitro* and *in vivo* tissue maturation and integration, illustrating the promise of this novel combination of agents to promote *in vivo* tissue regeneration. Taken together, these studies provide an overview of several exciting and promising technologies to 1) increase the functional properties of both native and engineered tissues, and 2) to enhance their *in vivo* integration potential, highlighting the tremendous potential of such agents toward developing clinically robust neotissues to repair and/or replace those damaged by injury or disease.

ACKNOWLEDGEMENTS

I would first like to thank my dissertation committee members, including Prof. Konstantinos Malizos, Prof. Kyriacos A. Athanasiou, Prof. Aspasia Tsezou, and Prof. Grigoris Haidemenopoulos, for their collective mentoring and great support. I would also like to thank my fellow Athanasiou lab members; my work would not have been possible with out the tremendous foundation and contributions of my predecessors, or the advice and support of those presently in the lab. I would especially like to thank Dr. Regina F. MacBarb, whose continued collaboration has been instrumental to my graduate work and has resulted in numerous high impact publications. In addition, I would also like to thank Dr. Donald Responte and Dr. Nikolaos Paschos for their collaboration, time, and advice.

Beyond the Athanasiou lab, I am very grateful to Dr. Jerry Hu, whose enthusiasm and mentoring has been a tremendous help to me. I would also like to extend remarkable thanks to the entire Orthopedic Department of University Hospital of Larisa and UC Davis Biomedical Engineering Department staff for all of their guidance and support. I am also very grateful for the financial support of NIH grants supported me all these years.

Last but not least, I would like to thank my family and friends, who have provided me with immeasurable encouragement and support. To my dad (Athanasios Makris) mom (Archontia Makri), and my brother (Stergios Makris), who have always believed in me and continually provide me with the love, strength, and courage necessary to always push forward toward achieving my goals. I would not have done any big step without them and I am blessed to have such a wonderful family. I am also grateful for all my friends, but I would like to specially thank my dear friend Tasos (Anastasios Mantikas).

Finally and most importantly, I would like to sincerely thank my PhD advisors Professors Kyriacos A. Athanasiou and Konstantinos N. Malizos, both leaders in their fields, whose excellence in research and science was always for me a great example to mimic and a continues challenge to reach. Their guidance, mentorship, and unswerving belief and support to me over the past four years are unparalleled.

TABLE OF CONTENTS

TABLE OF FIGURES

TABLE OF TABLES

INTRODUCTION – CONCEPTS IN ARTICULAR CARTILAGE REGENERATION: FROM CURRENT REPAIR TECHNIQUES TO FUTURE TISSUE-ENGINEERING APPROACHES

ABSTRACT

Chondral and osteochondral lesions due to injury or other pathologic conditions often result in the development of osteoarthritis, eventually leading to progressive joint destruction. While current progress suggests that biologic agents can delay the advancement of such deterioration, they are incapable of promoting tissue restoration. The limited ability of articular cartilage to self-repair and regenerate renders joint arthroplasty unavoidable, creating the need for alternative means to treat pathologic joints. This review describes current, widely used clinical repair techniques for resurfacing articular cartilage defects; short- and long-term outcomes of these techniques are also discussed. Further, the potential of developing a biologic pipeline of regenerative products to achieve functional articular cartilage healing, including cell-based and cell-free materials, autologous and allogeneic cell-based approaches, and multipotent and pluripotent stem cell-based techniques, and how such techniques will undoubtedly revolutionize joint care over the next decade, is examined. Finally, the prominent role of tissue engineering in the translation of biologic technologies into clinical products with the concomitant regulatory processes will be explored.

Chapter submitted as: Makris, E.A., Gomoll, A.H., Malizos, K.N., Hu, J.C., & Athanasiou, K.A. Concepts in Articular Cartilage Regeneration: From Current Repair Techniques to Future Tissue-engineering Approaches. In *AJSM.* 2014.

INTRODUCTION

The management of articular cartilage defects continues to be one of the most challenging clinical problems for orthopedic surgeons. Articular cartilage is a highly organized tissue exhibiting substantial durability, yet a poor intrinsic capacity for healing; damage from trauma or degeneration inevitably results in morbidity and functional impairment. Given time, both treated and untreated lesions often lead to debilitating joint pain, dysfunction, and degenerative arthritis. The individual and societal burden of joint diseases such as osteoarthritis has prompted the development of regenerative medicine and tissue engineering solutions aimed toward restoring cartilage and bone. Current cartilage repair strategies include bone marrow stimulation techniques, as well as cell-based, cell-plus-scaffold-based, or whole-tissue transplantation techniques. In this review, we discuss the basic science, indications, advantages, shortcomings, and outcomes of cartilage regenerative interventions with the goal of providing an evidence-based assessment for the treatment of articular cartilage pathologic conditions. Moreover, we discuss current and prospective tissue engineering approaches for joint repair, with an emphasis on the different cell types that could be used, the clinical aspects of cell administration, *in vitro* and *in situ* recruitment of mesenchymal stem cells (MSCs), and cell-free or factor-based therapies. Finally, the scientific and regulatory challenges in translating these approaches to the clinic are discussed.

PRESENT REPAIR TECHNIQUES

A. Microfracture

Over the past few decades, the field of orthopedics has seen the development of many surgical approaches for treating chondral and osteochondral lesions. Leading this effort was the microfracture technique, developed in the late 1980s and early 1990s to treat knee cartilage

defects. Microfracture was further adapted for use in the ankle, shoulder, elbow, and hip. The premise of this procedure is to surgically induce lesions that penetrate the subchondral bone, allowing mesenchymal stem cells (MSCs) to migrate from the marrow to the defect site (Fig. 1). The environment of the cartilage defect, however, places the MSCs under numerous biochemical and biomechanical stimuli, causing the cells to dedifferentiate and form a mechanically inferior fibrocartilage-like repair tissue (1). Without the mechanical robustness of a hyaline tissue, the repair tissue is vulnerable to the high mechanical demands of the joint environment, leaving the joint susceptible to bone edema, pain, and progressive degeneration. Failure of this procedure is therefore eminent, with deterioration occurring approximately 23 months post-surgery (1). As a result, microfracture is no longer considered a cartilage regenerative procedure and is now only used as a means to delay cartilage degeneration.

Specific indications have been proposed for performing this technique in cartilage lesions (Fig. 2). When used only for treating full thickness femoral condylar defects 2 – 3 cm^2 in diameter in patients under 40 years old and with a normal body mass index, microfracture has been shown to effectively delay cartilage deterioration (2). However, when used to treat femoral condylar defects of larger sizes, patellofemoral defects of any size, patients of advanced age, or those presenting with abnormally high body mass indices, microfracture has proven ineffective. A detailed description of microfracture and its clinical outcomes are considered outside the scope of this regenerative-strategy focused review. A brief understanding of this technique is important to consider, however, as the shortcomings of microfracture ultimately spurred the development of procedures that aim to fully regenerate cartilage defects with hyaline-like repair tissue.

B. Autologous Chondrocyte Implantation

The impetus to generate techniques that promote hyaline-like repair tissue in cartilage defects lead to the development of autologous chondrocyte implantation (ACI). This procedure, which is conducted via two surgeries, has become one of the most widely used techniques for articular cartilage regeneration. To conduct ACI, a 200-300 mg full-thickness cartilage biopsy from a non-weight-bearing region of the knee joint is first performed. The chondrocytes are then extracted from the biopsy, purified, and expanded for approximately 4 weeks to achieve between 15-20 million cells. Once this critical number is achieved, they are implanted directly into the defect site. This procedure is traditionally finalized by securing the cells under a periosteal flap (Fig. 3A-D). There are two major benefits of ACI: 1) Use of the patients' own cells avoids the potential immune complications that might arise from implanting allogeneic cells or foreign materials. 2) ACI has been found to promote better clinical outcomes and efficacy compared to microfracture (3). Together, these benefits result in a longer lasting repair tissue and, thus, improved outcomes.

Controlled prospective clinical trials have confirmed the improved clinical outcomes of ACI. One of the earliest reports on ACI followed 23 patients, ages 14 – 48, an average of 48 months post-surgery. For osteochondral defects ranging from 1.6 to 6.5 cm^2, biopsy results revealed approximately half the patients to have hyaline-like cartilage filling the defect (4). In a more recent prospective study in young patients (mean age 38.3 years) having a mean defect size of 4.9 cm^2, a 5-year follow up evaluation revealed 50 – 75% improvement in WOMAC subscales; 92% of patients were found to function well and were therefore able to delay the need for joint replacement (5). Similarly, a prospective study was carried out in 126 patients who received ACI after a previously failed cartilage repair procedure (6). When patients were

assessed an average of 4 years post-ACI-surgery based on knee pain, quality of life, and overall health, approximately 76% were found to have overall positive clinical results. The study did not find any differences in outcomes when a patient had previously undergone a different method of articular cartilage repair treatment. This study, therefore, concluded that ACI was an effective means to repair cartilage defects and to improve the quality of life of patients whose first procedure had failed. Finally, long-term evaluation of patients treated with ACI (up to 20 years follow-up) have demonstrated that the technique is an effective and durable solution for the treatment of large surface lesions of the knee joint (7).

Whether ACI is superior to other standard treatments in prospective controlled clinical trials, however, still remains controversial. Superiority in terms of structural outcome was shown with ACI over autologous osteochondral transplantation (mosaicplasty) in a study of 100 patients averaging 31 years in age and having defects of approximately 4.7 cm^2 (8). Good-to-excellent clinical results were found in 88% of ACI patients and 69% of mosaicplasty patients approximately 19 months following the respective procedure. One year later, arthroscopic evaluation revealed good-to-excellent repair to remain in 82% of ACI patients, while only 34% of those receiving mosaicplasty maintained this status. This suggests that ACI provides a better long-term clinical solution for treating articular cartilage defects in comparison to mosaicplasty. In a separate study, 46 patients having lesions greater than 2 cm^2 received either ACI or microfracture surgery. While patients receiving microfracture had a mean Cincinnati score of 1.3 follow surgery, patients receiving ACI had a significantly greater score of 3.1 (9). It should be noted, though, that the microfracture outcomes reported in this study were considerably inferior to those described in other reports (10). In a more recent study, 118 patients were assessed at 12 and 18 months following either ACI or microfracture (11). Clinical outcomes

were similar in both groups, although ACI was associated with increased structural repair. At 5 years, clinical outcomes were again comparable. However, at this time point, ACI was found to be statistically more effective in a subgroup of patients who had undergone the procedures close to presentation of symptoms (12). Finally, a systematic review of the literature found cartilage repair in the knee with microfracture, ACI, or osteochondral autograft to provide only short-term success (13).

In spite of the clinical efficacy and benefits achieved with ACI, there are two major drawbacks to this procedure: 1) the necessity to undergo two operations, and 2) the long recovery time required to ensure proper maturation of the repair tissue. An additional disadvantage of ACI is the tediousness of this procedure. The surgery itself is highly invasive, requiring an open procedure to access the joint space, which leaves the patient susceptible to potential arthrofibrosis and joint stiffness. Further, harvesting of the periosteal patch necessitates an additional incision, leading to the possibility of donor site morbidity, infections and additional post-operative pain. In terms of the implantation itself, the most frequently reported adverse effect is hypertrophy of the periosteal flap. In a report of 52 adverse events following ACI in 101 patients, 26 were found to have hypertrophy of the periosteum, while 7 had complete graft failure (14). To bypass the potential for hypertrophy, the use of porcine collagen I/III matrix as a substitute for periosteal grafts has been presented as an alternative. Finally, in terms of articular cartilage phenotype during expansion, a few reports have described dedifferentiation of the primary cells into fibrochondrocytes (15). Overall, these inherent drawbacks are likely responsible for the inconsistent and irreproducible outcomes of ACI seen in the literature (16).

To standardize clinical outcomes of ACI, patient-specific and defect-specific factors

have been established to generate a treatment algorithm that limits the likelihood of adverse effects from this procedure (Fig. 2). For instance, ACI should only be considered in patients presenting with either trochlear or patellar lesions and only once rehabilitation has failed. Further, in determining the likelihood of success using ACI, surgeons must consider defect size and location, patient body mass index, expectations, and whether the patient has had any previous treatments for this particular defect. ACI has been found to work best for treating medium to large, full-thickness, focal, single or multiple articular cartilage defects. It is also important that the rim of the lesion is intact to best support the sutures used to secure the periosteal or scaffold flap. Furthermore, patients selected for ACI must be capable of following time consuming, tedious rehabilitation regimens and be free of a recent history of inflammatory arthritis or infection. Overall, while adverse events associated with ACI can be unfavorable and require the patient to undergo additional repair surgery, the frequency of such outcomes is quite low compared to other cartilage repair techniques. Therefore, when used within the appropriate indications, ACI remains as one of the most promising repair strategies for patients suffering from cartilage defects.

C. Scaffold-based approaches in clinical practice

In addition to the challenges examined above, the lack of a supportive scaffolding material to guide matrix synthesis and organization may, in part, account for the observed outcome variability across patient populations, as seen in the literature. Successful cartilage regeneration is dependent upon both autologous chondrocyte proliferation rate and differentiation capacity; use of a tissue-engineered, three-dimensional (3D) matrix as a cell carrier has been shown to maintain and support these crucial cellular characteristics (17).

Efforts, therefore, have focused on development of scaffold-based mechanisms for delivering autologous chondrocytes to the defect site, introducing the second generation of ACI. The major advantages of scaffold-based approaches include: 1) increased control over filling the defect site, 2) decreased donor site morbidity 3) a less technical surgical procedure, and 4) decreased recovery time post-surgery due to increased graft stability. Additionally, because the chondrocytes are cultured in a 3D environment, they are less prone to dedifferentiation and therefore better retain the ability to produce a more hyaline-like repair cartilage (18). Further, *in vitro* culture prior to implantation may help to maintain quality control of scaffold-based repair strategies.

There are several important aspects to be considered when designing a suitable scaffold for repairing cartilage defects. The ideal articular cartilage scaffold will excel in three criteria: bioactivity, mechanics, and logistics. First, the scaffolding or matrix material must be both biocompatible and biodegradable so that it degrades safely in accordance with healing time. It is also important that the material promotes even distribution of the cells to encourage uniform deposition of neomatrix fill. Important bioactive aspects include that the scaffold maintains cell phenotype, induces ECM synthesis, lacks immunogenicity, and promotes tissue integration. Since heterogeneous loading of articular cartilage occurs *in vivo* on a daily basis, the implanted material must impart the appropriate mechanical properties, tissue anisotropy, geometry, and lubrication characteristics to function properly immediately upon implantation (19). Finally, the logistics of a successful scaffolding or supportive matrix material must not be unwieldy: supply, processability, and surgical implantation practicality must all be considered.

C.1. Matrix-assisted Chondrocyte Implantation

The most common technique currently in clinical practice for scaffold-plus-cell based therapy is known as matrix-associated chondrocyte implantation (MACI). Similar to ACI, MACI comprises two surgical procedures: The first surgery is conducted to retrieve the autologous tissue from which the patient's chondrocytes are isolated. Once isolated, the cells are expanded in vitro to achieve the desired number and then seeded on an absorbable porcine-derived collagen type I/II 3D matrix for 3 days prior to implantation. These matrices are specifically engineered to have a looser fiber arrangement on one side to promote chondrocyte infiltration and attachment, and a denser, smoother side to facilitate low-friction lubrication. Upon receiving the cell-seeded scaffold, a mini-arthrotomy is performed to expose and debride the lesion, after which the matrix is implanted and secured using fibrin glue such that the cell-laden side faces the subchondral bone and the low-friction surface faces into the joint cavity (Fig. 3A-B,E-F).

The benefits of MACI are best represented through clinical findings. In a prospective study, 21 patients having symptomatic, traumatic articular cartilage defects of the knee (>2cm^2) and presented without knee instability or malalignment, were treated with MACI implants fixed in place with fibrin glue (20). Five years post-surgery, most patients treated with the implants demonstrated significant clinical and radiological outcomes and good quality of repair tissue. Thus, the study concluded MACI to be a safe and effective treatment for symptomatic, traumatic chondral knee defects. In a separate preliminary clinical report, 35 patients presenting with defects averaging 4 cm^2 and treated with MACI were followed for at least 6 months post-surgery (21). Using both subjective parameters and objective outcomes, MACI was concluded to produce a hyaline-like repair cartilage that relieved pain and restored knee function. To assess chondrocyte phenotype after being implanted on collagen type I/III scaffolds, histological

analysis was performed over the course of 6 months in 56 patients receiving MACI (22). Results found chondrocytes to maintain a spherical-like morphology, reminiscent of native tissue cell morphology. Further, the cells were found to express several chondrogenic markers, including aggrecan and collagen type II. Overall, following 6 months of implantation, 75% of the implants resulted in the development of a hyaline-like cartilage within the defect site.

While clinical results of MACI are extremely promising, it is important to note that the majority of the reports are on case studies. One of the few prospective randomized clinical trials conducted thus far to assess MACI evaluated 91 patients presenting with symptomatic chondral defects (23). Patients were treated with either ACI or MACI and evaluated 1-year post-surgery. No significant differences were found between the main clinical scores in MACI-treated patients and ACI-treated patients at the 1-year time point. Further, arthroscopic evaluation at 1 year found hyaline-like repair cartilage to be equally prevalent in approximately 40% of patients following either surgery. In a separate randomized controlled trial 21 patients presenting with full thickness cartilage defects averaging 4.1 cm^2 received either ACI or MACI. Although both Lysholm and Gillquist scores and MRI results initially favored ACI, no differences in any of the outcomes between the two techniques were observed by the 12- and 24-month time points. Further, while a few patients from each procedural group suffered from adverse effects, including transplant delamination, osteochondral dissection, and transplant hypertrophy, the majority of patients remained adverse-free (24). Overall, both studies found MACI and ACI to have similar, mainly positive outcomes.

Recently, a method used to fill deep cartilage defects, called the “sandwich” MACI technique, has been developed. This technique is performed by first securing one cell-seeded membrane into the base of the defect with fibrin glue such that the side seeded with cells faces

up. A second cell-seeded membrane is then secured into place via fibrin glue to the surrounding articular cartilage, this time with the cell-seeded side facing down into the defect. This method was used in 5 patients having defects greater than 8 mm in depth, with improvements in both the Cincinnati knee and Stanmore functional rating 6 months following surgery (25). One year post-surgery, 4 of the patients received arthroscopy, showing a well-formed repair tissue. The ability of the "sandwich" technique to fill deep cartilage defects further encourages future studies to investigate the true potential of MACI.

C.2. Hyaluronan-Based Scaffolds

Another means recently being explored to introduce chondrocytes within 3D, biodegradable environments is via hyaluronan-based scaffolds. These scaffolds contain fibers 20 mm thick in diameter, having interstices of varying sizes. Similar to porcine collagen derived matrices, hyaluronan-based scaffolds provide an environment intended to maintain the chondrocytic phenotype and genotype during in vitro culture, as well as to provide structural support for the cells following implantation. An added advantage of this material is that its degradation rate can be precisely tailored to match the rate of the cell-induced matrix to aid in integration with the defect site (26).

Delivering autologous chondrocytes on hyaluronan-based scaffolds has displayed much promise as a method for treating cartilage defects, with accounts of a hyaline-like cartilage developing approximately 1 year post-implantation. For instance, in a case series, hyaluronan-based MACI was used to treat 32 patellofemoral chondral lesions averaging 4.7 cm^2 in size (27). Cell-seeded scaffolds were implanted either arthroscopically or via mini-arthrotomy following debridement of the defect site. ICRS-IKDC scoring was found to improve

dramatically in all patients at both a 1- and 2-year time point, while MRI at the later time point showed complete filling of the defects with signals very similar to that of native articular cartilage in 71% of patients. Patients were also reported to have positive clinical outcomes at the 2-year assessment, with arthroscopy revealing a hyaline-like histology in 6 of the patients. In a cohort study, 41 professional or semi-professional male soccer players were treated surgically and evaluated prospectively at 2 years and again at a minimum of 4 years post-surgery (28). Of these patients, 21 were treated arthroscopically using a hyaluronan-based MACI technique, while the remaining 20 received microfracture surgery. In both groups, patients were found to have significantly improved clinical scores by the final follow-up time point, with nearly 80% of patients receiving microfracture and 86% receiving hyaluronan-based MACI to return to competition. Players who had microfracture required at least 8 months of recover prior to returning to the field, while those receiving MACI required 12.5 months.

Recently, a multicenter study evaluated patients receiving autologous chondrocyte seeded hyaluronan-based scaffolds an average of 38 months following implantation (29). Of the 141 patients, results found 96% to have normal or near-normal physician evaluations, while 92% had enhanced IKDC scores. In a separate study, patients receiving either hyaluronan-based MACI or microfracture repair techniques were compared 5 years post-respective surgery. Results found those having the hyaluronan-based scaffold implantations to have overall higher IKDC objective and subjective scores than those undergoing microfracture, although both groups did have significantly higher IKDC scores compared to their pre-surgical conditions. Such promising results likewise merits future research on the potential of hyaluronan-based MACI techniques. Overall, in spite of the demonstrated potential of MACI, such techniques are only thus far approved in Europe; FDA approval is currently pending in the USA.

While the clinical outcomes of MACI have been shown to be similar to ACI, there are several important technical considerations that use of a matrix helps to solve. For instance, due to the ease of implantation when using a scaffold cell carrier as opposed to that of traditional ACI, MACI has been found to be less technically demanding and to reduce surgery time by approximately 19.2 minutes (30). Further, MACI, which can be performed using minimally invasive procedures, avoids the need for a periosteal harvest, thus avoiding the possibility of donor site morbidity and graft hypertrophy. While use of a 3D scaffold does suggest a more supportive environment that promotes cellular adhesion, proliferation, and development of a more hyaline-like cartilage, quantitative assessments have yet to prove such assumptions. Likewise, whether MACI decreases the likelihood of graft delamination or dislocation has yet to be fully explored.

FUTURE REGENERATIVE APPROACHES

A. Ex Vivo Engineered Tissue Using Autologous Chondrocytes

Aside from the technical advantages of MACI, studies thus far have revealed clinical outcomes of this method to be very similar to those of ACI. A plausible explanation is that following chondrocyte expansion, the collagen matrices are implanted into the patient within 3 days of cell seeding, leaving the neotissue implant in an immature, and therefore, vulnerable form. To improve the efficacy of such tissue engineered procedures, novel approaches are under development in which autologous chondrocytes are introduced to a 3D matrix and cultured *in vitro* for longer periods, typically around 4 – 6 weeks. During this time, chondrocytes induced by external stimuli produce their own ECM components within the 3D environment, resulting in an implant with biochemical and, subsequently, functional integrity closer to that of native

articular cartilage prior to implantation. Surgical techniques similar to those established for MACI are used to both obtain the autologous tissue and perform the implantation. Overall, the enhanced mechanical robustness following *ex vivo* 3D culture renders implants better suited to the joint environment, and may improve overall patient outcomes.

While *in vitro* culture of 3D matrices seeded with autologous chondrocytes may result in more robust chondral implants, time alone is not enough to promote sufficient maturation of the implants. Thus, researchers have sought out exogenous stimuli representing those chondrocytes typically face *in vivo* to promote mechanically robust implants. Coming from a complex, highly loaded environment, chondrocytes are extremely responsive to mechanical stimulation; in the body, these cells can experience loads approximately six times body weight (31). Exogenous mechanical stimulation has been introduced to cell-laden matrices in the form of either hydrostatic pressure (32) or dynamic compression supplemented with the growth-factors, such as TGF–β3 (33, 34). Such stimulation aids in maintaining the native chondrocyte phenotype and, thus, promotes the development of implants donning structure-function relationships closer to those of native articular cartilage. Overall, implants formed using such stimulation have been shown to develop more hyaline-like properties compared to those formed in the absence of such stimulation (32-34).

There are only a few clinical reports currently available on the outcomes of using autologous chondrocyte-laden, tissue engineered scaffolds subjected to *in vitro* culture. One such study reports the results of an FDA phase I clinical trial on 8 patients receiving tissue-engineered collagen type I scaffolds seeded with autologous chondrocytes (35). These cell-seeded scaffolds were subjected to hydrostatic pressure for several weeks via a bioreactor prior to implantation. Results found patients to have decreased pain scores in as little as 12 months

post-surgery. At the 1-year time point, 7 of 8 patients were found to have almost fully or completely filled defects, and remained as such in 6 patients 2 years following surgery. Further, this study found no adverse responses to the treatment, and that the defects filled with a mature and organized repair tissue. Based on these promising results, a phase II clinical trial was conducted comparing the use of autologous chondrocyte-seeded tissue-engineered collagen type I scaffolds to microfracture (36). Overall, this phase II trial found the cell-seeded scaffold to have similar outcomes to microfracture, with greater clinical efficacy 2 years post-implantation.

B. Alternative cell sources

Thus far, current cell-based clinical practices for treating articular cartilage defects and degeneration only utilize autologous chondrocytes. In spite of efforts to try and more closely recapitulate the *in vivo* environment through 3D culture systems, bioreactors, and exogenous mechanical and biochemical stimulation, a repair tissue achieving native hyaline cartilage properties prior to implantation remains elusive. Thus, in an effort to avoid the many drawbacks associated with autologous chondrocytes, methods are currently being developed around the use of stem cells, many of which are currently in queue for FDA approval to proceed with clinical studies.

B.1. Bone marrow MSCs

Of the various types of stem cells found in the body, bone marrow-derived mesenchymal stem cells (bMSCs) offer many advantages. First, they are comparatively easy to both isolate and expand, allowing the potential to obtain bMSCs from allogeneic donors and store them in readily available cell banks. Further, extensive work has found bMSCs capable of

differentiating into both cartilage and bone, meriting their use for regeneration of both osteochondral and chondral defects (37, 38). Another beneficial trait of bMSCs is their ability to selectively migrate toward diseased tissues and organs, where they have been found to secrete immunosuppressive mediators for T cells (39). Thus, in the case of articular cartilage repair, use of bMSCs may provide a more targeted repair system that releases factors of interest directly into chondral lesions (40). Through promoting a more regenerative environment, bMSCs may also encourage the patient's own stem cells to enter the defect and aid in the regeneration of the damaged tissue.

Preliminary studies utilizing bMSCs have been conducted in humans. In one such study, the knee joints of 4 osteoarthritis-afflicted patients were injected with bMSCs; 1 year after injection, the patients were found to have decreased pain and improved joint mobility without any noticeable side effects (41). In a larger scale study, 72 patients presenting with cartilaginous lesions were treated with either ACI or injected with bMSCs. The stem cells, which were found to treat the chondral defects as effectively as ACI, were associated with comparatively lower costs while avoiding the risk of donor site morbidity (42). The reported favorable outcomes of cartilage healing and regeneration with direct injection of bMSCs into affected knee joints, however, lacks the benefit of tissue engineering-based approaches. Thus, MACI-based strategies have been developed to employ stem cells. Thus far, three case studies have been conducted using bMSC-seeded collagen scaffolds (43-45). A separate study found bMSCs derived from patients with advanced osteoarthritis to respond well to *ex vivo* culture, and in the presence of transforming growth factor-β1, to maintain a chondrocytic phenotype. Further, re-implantation of these cells using MACI techniques resulted in the regeneration of a hyaline-like cartilage (46, 47). The positive outcomes of these studies have shed light onto the tremendous

potential of bMSCs for cartilage repair. While it remains to be seen how bMSC-based techniques compare to more established procedures via controlled studies, further investigation of the use of bMSCs isolated from healthy allogeneic donors is necessary to enhance the cartilage forming potential of these cells, as well as to better understand the clinical feasibility of this cell source.

B.2. Other MSC sources

Thus far, most work concerning the use of MSCs has been carried out on those of the bone marrow lineage, as the characteristics of these cells are best known among MSCs. Furthermore, aspiration methods for obtaining bMSCs, although painful, are well known, making it easy to retrieve these cells from either allogeneic or autologous sources. However, there are several other sources from which stem cells can be derived, including adipose tissue, muscle, synovium, periosteum, and umbilical cord (48). Of these other sources, stem cells derived from adipose tissue are readily accessible and have been shown to have similar proliferative profiles and differentiation capacities to those of bMSCs (49, 50). An advantage of adipose derived stem cells over bMSCs is their ability to be isolated in comparatively large quantities (51). Both *in vitro* and *in vivo* work has shown stem cells derived from synovial tissue, on the other hand, to have a marked chondrogenic potential over other sources (52, 53). Further work with MSCs derived from sources other than bone marrow will answer the many questions concerning the clinical applicability of these cells.

B.3. Pluripotent stem cells

An additional means for obtaining clinically relevant cells comes from the promise of induced

pluripotent stem cells (iPSCs). These recently discovered cells have been shown to be capable of differentiating into both cartilage and bone, and have been speculated to be the precursor cells to those comprising adult joint tissues (54). Chondrogenically differentiated iPSCs derived from adult mouse fibroblasts were used in an *in vitro* cartilage defect model with promising results, indicating the potential of iPSC-derived cells to contribute to cartilage regeneration (55). In a separate study, iPSCs derived from synovial fibroblasts of patients presenting with advanced osteoarthritis have been used to generate MSCs, chondrocytes, and osteoblasts (56). In spite of the promising results observed thus far with this autologous cell source, several questions remain to be answered, including: 1) the use of viral vectors in forming iPSCs, 2) the best practices to differentiate these cells ex vivo, 3) the potential of teratoma formation *in vivo*, and 4) the status of iPSCs with regulatory agencies. Although much remains to be understood, the enormous potential of iPSCs for treating cartilage degeneration merits future studies to find answers to these underlying uncertainties.

C. Novel cell-free biomaterials

While autologous chondrocytes and MSC-based cell techniques offer much promise for articular cartilage repair, methods for extracting, expanding, and differentiating cells are both timely and costly. Further, because MACI- and hyaluronan scaffold-based techniques contain cells, they may be considered both a medical device and biologic from the FDA's perspective, resulting in long and costly regulatory approval processes. Products that do not contain cells, therefore, intend to offer advantages to those that contain cells. Recent research has thus begun to consider cell-free material-based products for cartilage regeneration and repair.

One example of a cell-free method is autologous matrix-induced chondrogenesis

(AMIC), a technique that can be performed in a single surgery. To perform AMIC, a mini-arthrotomy is first used to expose and clean the defect site. Next, microfracture is employed to release both blood and bone marrow containing MSCs, followed by suturing or gluing of a collagen I/III matrix into the defect site (57). The implanted collagen matrix may stabilize the resulting blood clot, helping to promote early mechanical stability and aid in cartilage regeneration. Studies have found AMIC to be both safe and effective in treating full-thickness cartilage defects (58), with comparable outcomes to ACI, MACI, and microfracture in terms of pain relief, restoration of joint functionality, and cartilage regeneration (59). For instance, one study used AMIC to treat localized full-thickness cartilage defects averaging 4.2 cm^2 in diameter in 27 patients. Patients were followed for up to 5 years post-surgery, with significant improvements in Tegner, Lysholm, ICRS, and Cincinnati scores as early as 12 months post-surgery. Further, MRI results revealed moderate to complete filling of all chondral defects (60). Interestingly, unlike microfracture, ACI, or MACI, results with AMIC did not find a correlation between clinical outcomes and a patient's age, body mass index, or number of previous operations. The simplicity and cost-effectiveness of this procedure, therefore, merits more work in terms of identifying the quality of neocartilage formation, the repeatability of the technique, and potential pitfalls, in order to fully understand its potential impact.

C.1. Active in situ approaches

A novel approach to enhance AMIC is to deliver factors known to selectively recruit and stimulate MSCs from the subchondral bone marrow within cell-free materials. The goal of this technique is to further enhance cartilage formation in the defect site. Such factors can be tailored to also activate chondrocytes in the surrounding, healthy tissue to aid in the remodeling

of the repair tissue filling the defect site. Through such a combination, these materials specifically target the area most in need of cartilage repair and regeneration.

As a strategy for active *in situ* AMIC, one study investigated the effects of implanting polyglycolic acid polymer-based materials combined with autologous serum or platelet-rich plasma (PRP) and hyaluronic acid following initial microfracture of the defect (61). This particular approach is novel in its use of autologous serum or PRP, as these agents have been found to recruit bMSCs from the underlying subchondral bone, while hyaluronic acid may help the bMSCs differentiate toward a chondrogenic phenotype. A prospective study using this approach found 52 patients receiving the treatment to have improved KOOS scores 1 year following surgery. Histological evaluation of the repair cartilage from the same patient population identified the defects to fill with a hyaline-like repair tissue (62).

While active *in situ* regeneration in combination with AMIC offers much promise as a clinical treatment for cartilage degeneration, knowledge of factors that both recruit and stimulate MSCs must be enhanced before such methods will be clinically applicable. For example, factors known to effect MSC recruitment, which include bone morphogenetic proteins, whole blood serum, chemokines, and PRP, do so in dose-dependent and tissue-specific manners (63). Thus, different active agents may need to be used depending on a patient's condition as well as the location of the defect. Growth factors, such as those belonging to the TGF-β and fibroblast growth factor families, have also been shown to aid in the development of robust cartilage repair tissue (64). Methods are therefore being developed that combine both growth factors and active agents to further enhance cartilage regeneration. To do so effectively, such systems are being tailored to release the agents, which are typically secured to the surface of matrices or included within nanoparticles, in a controlled manner.

D. Scaffoldless Approaches

While several tissue-engineering approaches for cartilage repair forgo the use of either cells or exogenous stimulation, another option more recently being explored is to omit the use of scaffolds. Without a scaffold to interrupt cell-cell signaling and stress shielding, the resulting neotissue may have a more bioactive microenvironment, which may enhance its ability to both respond to stimuli and integrate with surrounding tissue upon implantation. Studies have found subjecting scaffold-free articular cartilage to various exogenous stimuli, including biochemical, biophysical, and biomechanical stimulation, to promote the development of robust neotissue with functional properties approaching those of native cartilage (65, 66). Such work has also found the scaffold-free neotissue capable of both integration and *in vivo* maturation (67-71). Studies comparing scaffold-free to scaffold-based techniques have found scaffoldless neotissue to have greater mechanical properties and higher ECM content (72, 73). Thus, scaffold-free neotissue presents as a promising new avenue for generating highly bioactive implants to enhance cartilage repair.

There are currently two scaffold-free technologies for articular cartilage regeneration undergoing clinical trials. The first technology is based on generating spheroids of autologous chondrocytes for implantation. In an animal study, the chondrospheres were able to adhere and integrate with full-thickness cartilage defects and produce a cartilaginous ECM (74). This process is currently in a phase I clinical trial. The second scaffold-free technology utilizes juvenile allogeneic chondrocytes; pre-clinical studies found the cells to have a significantly stronger and more stable chondrogenic activity *in vitro*, and to avoid any immunologic responses *in vivo* (75). The resulting graft, which is implanted in a single step procedure, has

been found to form hyaline-like tissue upon implantation (76). This technology is currently in phase III clinical trials.

CONCLUSIONS

This review focused on the basic science, indications, advantages, disadvantages, and outcomes of current and future cartilage regenerative strategies. An emphasis was placed on tissue engineering approaches as such techniques are forming the basis for the next generation of novel cartilage regeneration technologies. Specifically, tissue-engineering aims to develop biomimetic tissues that recapitulate the biological, structural, and functional features of native tissue, increasing the ability of implants to withstand and adapt to the highly loaded environment of the knee. Such strategies are targeted to not only stop the progression of cartilage degeneration, but to restore a patient's joint back to its original state. These novel biomimetic solutions will help to diminish the currently overwhelming proportion of individuals facing cartilage pathologies, and equally importantly, the tremendous healthcare costs.

In spite of the many efforts outlined above, the generation of truly biomimetic chondral and osteochondral replacements still remains elusive; however, technology development is occurring rapidly from many different directions (Fig. 4). For instance, tissue engineering approaches using a variety of cell sources, including autologous, allogeneic, xenogeneic, and stem cell approaches, have yielded repair tissues having hyaline-like characteristics, annulling patient pain, and delaying the process of degenerative pathologies such as osteoarthritis. While a gold standard cell source has yet to be identified, stem cells do stand out among the rest in terms of their availability and minimization or complete lack of donor site morbidity. Further, the combination of tissue engineering technologies with both biochemical and biomechanical

exogenous stimulation has resulted in repair tissues displaying even greater hyaline-like properties. Other promise has been seen in the absence of cells all together, via tissue engineered, cell-free scaffolds, as well as via cell-based, scaffold-free approaches.

Overall, a technology has yet to be developed that satisfies all of the fundamental requirements of a successful chondral defect; namely, one which embodies the appropriate structure-function relationships, ECM organization, bioactivity, and surgical logistics. To address these success criteria, work must be conducted to improve not only the mechanical properties of the tissue, but to shape and organize their development in a way that better mimics native morphogenesis. Further, an emphasis must be placed on the degradation characteristics of scaffold-based approaches to ensure degradation rates match tissue regeneration. In cell-based applications, a thorough understanding of how to maintain the chondrocytic phenotypic of autologous and allogeneic chondrocytes, and how to foster complete chondrogenic differentiation of stem cells, must be established. Once technologies are able to capture all of the necessary success criteria, stringent manufacturing methods that ensure reproducibility of the resulting implants and functional clinical outcomes in humans will need to be developed. Further, standardization of the approval process should be attempted and streamlined across countries, as current practices in Europe allow faster translation of promising technologies than does the FDA, hindering progress in the US.

Crucial to all of these endeavors is to develop better chondral defect animal models for *in vivo* testing prior to implanting technologies into patients in well-designed prospective, randomized, and controlled clinical trials. Further, it is important that such clinical studies compare novel technologies to current “gold standard” clinical approaches. The resulting repair tissue must also be subjected to rigorous biochemical and biomechanical evaluation to

specifically determine how close the regenerative tissue is to native tissue. Further, what quantifies a robust, hyaline-like repair tissue, and what threshold of such quantifiable characteristics is necessary for successful clinical outcomes, must be clearly determined. Use of non-invasive, quantitative measures both pre- and post-surgery is also important for determining long-term clinical outcomes of such trials. Such information will be especially critical to determining which technologies result in the best outcomes: those that result in repair tissue that truly captures the structure-function relationships of native, healthy cartilage. Equally important, measures should be taken to determine the appropriate indications, contradictions, patient selection criteria, and surgical practices for each technology developed. The idea of minimizing health care costs must be also importantly considered. All in all, the idea of biomimetic cartilage regenerative therapies are the focus of novel techniques, and while much work remains, we are closer than ever to making such a concept a clinical reality.

FIGURES

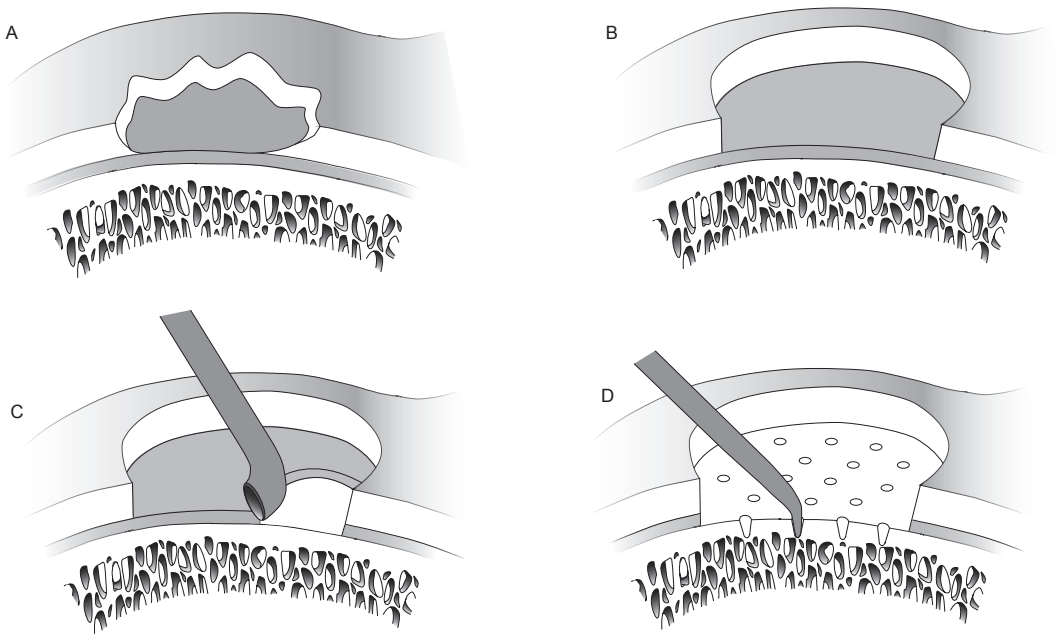

FIGURE 1.1 – OVERVIEW OF THE MICROFRACTURE TECHNIQUE. A) Full-thickness focal chondral lesion. B) Debridment of the lesion to ensure healthy, stable margins for integration of the fill tissue. C) Removal of the calcified zone of articular cartilage to promote clot adhesion. D) Channels created using a 45° awl, spaced 3-4 mm apart, and made deep enough to penetrate the subchondral marrow.

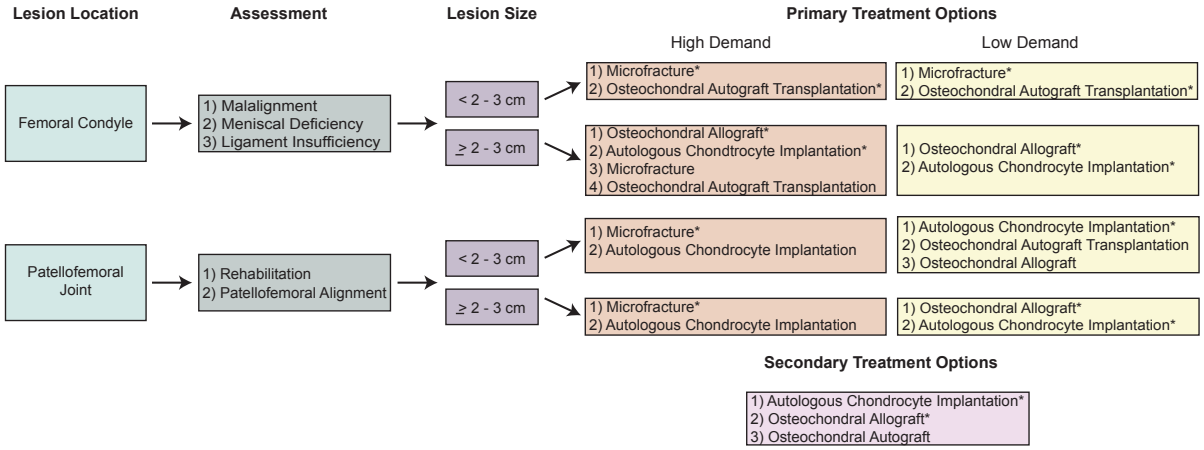

FIGURE 1.2 – ALGORITHM FOR TREATING FOCAL CHONDRAL LESIONS. Once it has been established that rehabilitation is not a viable option for a patient, the surgeon should assess both the size and location of the defect, determine whether the patient desires a more active (high demand) or sedintary (low demand) lifestyle, and find out if the patient has sought previous treatment. Answers to such questions will aid as a guide toward performing the appropriate surgical procedure for a given patient. The asterix indicates the best treatment option for a given situation.

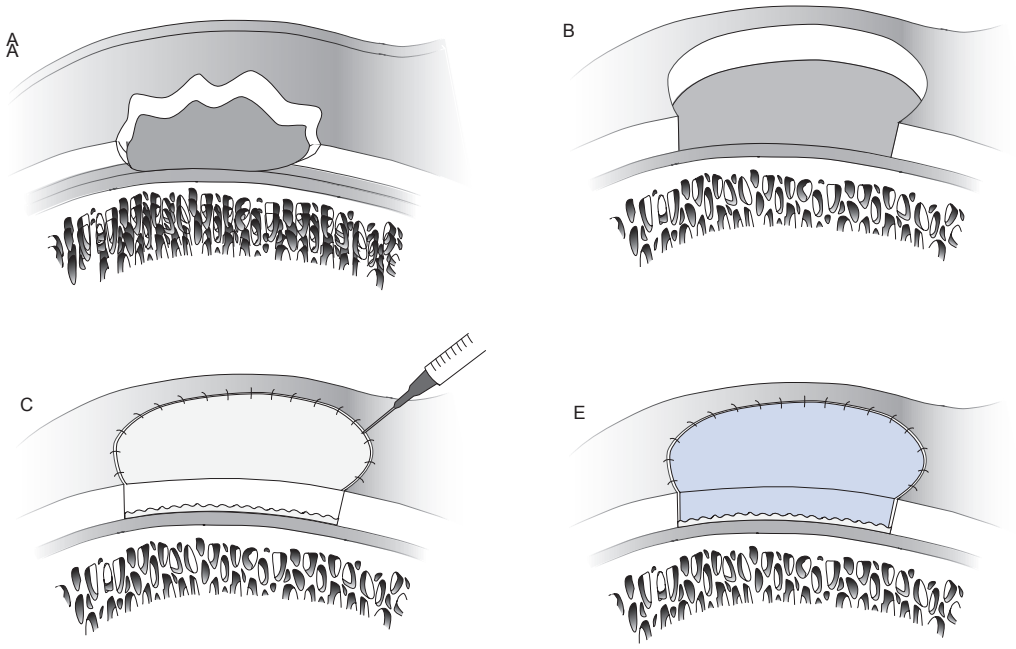

FIGURE 1.3 – OVERVIEW OF ACI AND MACI TECHNIQUES. A) Full-thickness focal chondral lesion. B) Debridment of the lesion to ensure healthy, stable margins for integration of the fill tissue. C) Drided lesion is covered with a periostal flap or collagen type I/III membrane, and filled with expanded autologous chondrocytes for ACI. D) Arthroscopic photograph of ACI-induced neocartilage.

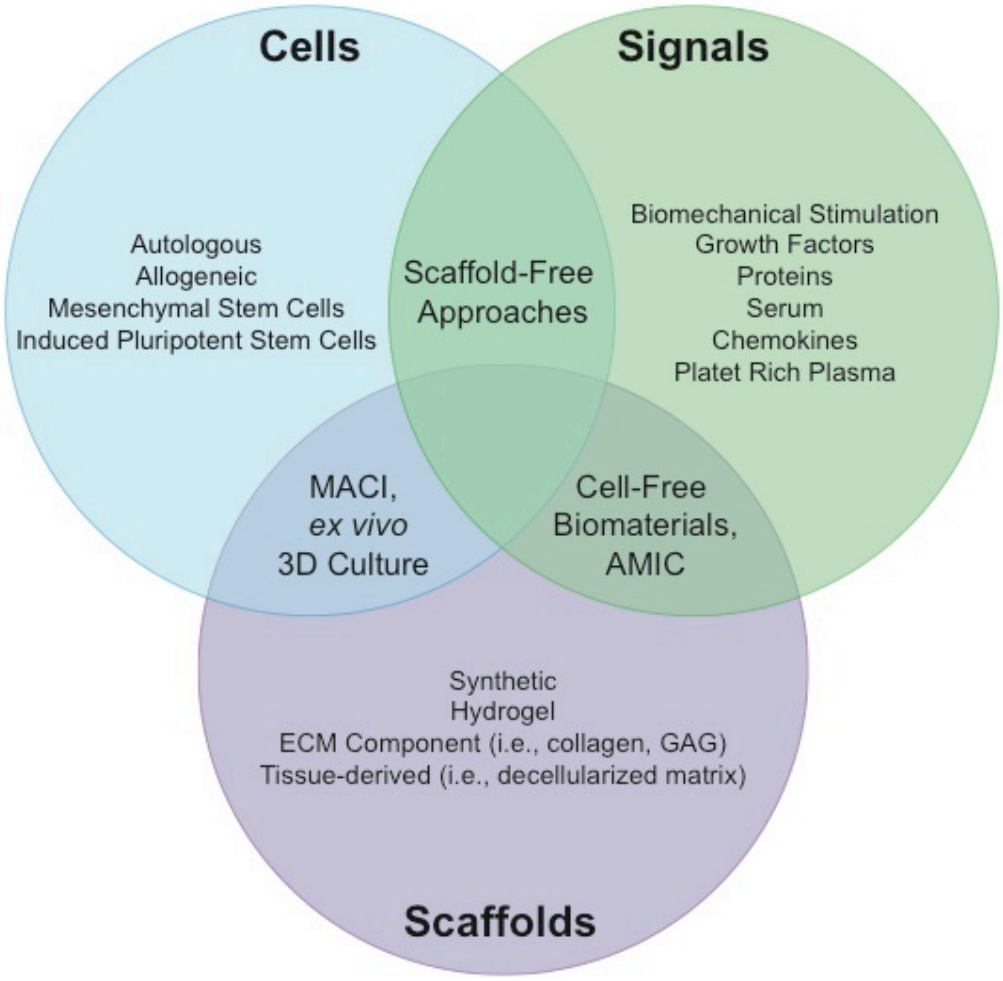

FIGURE 1.4 – SCHEMATIC REPRESENTATION OF THE TISSUE ENGINEERING PARADIGM. Figure is tailored to the specific tissue engineering approaches discussed in this review. The paradigm shows that cells, signals, and scaffolds are the major elements of tissue engineering approaches, which may be used either alone or in combination.

CHAPTER 1 – THE KNEE MENISCUS: STRUCTURE-FUNCTION, PATHOPHYSIOLOGY, CURRENT REPAIR TECHNIQUES, AND PROSPECTS FOR REGENERATION

ABSTRACT

Extensive scientific investigations in recent decades have established the anatomical, biomechanical, and functional importance that the meniscus holds within the knee joint. As a vital part of the joint, it acts to prevent the deterioration and degeneration of articular cartilage, and the onset and development of osteoarthritis. For this reason, research into meniscus repair has been the recipient of particular interest from the orthopedic and bioengineering communities. Current repair techniques are only effective in treating lesions located in the peripheral vascularized region of the meniscus. Healing lesions found in the inner avascular region, which functions under a highly demanding mechanical environment, is considered to be a significant challenge. An adequate treatment approach has yet to be established, though many attempts have been undertaken. The current primary method for treatment is partial meniscectomy, which commonly results in the progressive development of osteoarthritis. This drawback has shifted research interest towards the fields of biomaterials and bioengineering, where it is hoped that meniscal deterioration can be tackled with the help of tissue engineering. So far, different approaches and strategies have contributed to the *in vitro* generation of meniscus constructs, which are capable of restoring meniscal lesions to some extent, both functionally as well as anatomically. The selection of the appropriate cell source (autologous, allogeneic, or xenogeneic

Chapter submitted as: Makris, E.A., Hadidi, H., & Athanasiou, K.A. The knee meniscus: Structure–function, pathophysiology, current repair techniques, and prospects for regeneration. In *Biomaterials.* 32(30): 7411-7431, 2011

cells, or stem cells) is undoubtedly regarded as key to successful meniscal tissue engineering. Furthermore, a large variation of scaffolds for tissue engineering have been proposed and produced in experimental and clinical studies, although a few problems with these (e.g., byproducts of degradation, stress shielding) have shifted research interest towards new strategies (e.g., scaffoldless approaches, self-assembly). A large number of different chemical (e.g., TGF-β1, C-ABC) and mechanical stimuli (e.g., direct compression, hydrostatic pressure) have also been investigated, both in terms of encouraging functional tissue formation, as well as in differentiating stem cells. Even though the problems accompanying meniscus tissue engineering research are considerable, we are undoubtedly in the dawn of a new era, whereby recent advances in biology, engineering, and medicine are leading to the successful treatment of meniscal lesions.

INTRODUCTION

Six decades ago, the discovery that removing the meniscus from the knee joint—then commonly seen as the sole technique for treating sports-related injuries—resulted in the deterioration of articular cartilage and the gradual development of arthritis, radically changed the approach for treating meniscus-related problems [1]. In 1982, partial meniscectomy was suggested as an alternative to complete meniscectomy [2], while the first published account of a meniscus transplant dates back to 1989 [3]. These studies are landmarks in understanding the anatomical and functional utility of the knee meniscus, and have since resulted in numerous investigations into different treatment approaches.

The current prevailing trend in repairing meniscus-related lesions is to maintain the tissue intact whenever possible [4-6]. However, the inability of surgeons to restore the tissue—both anatomically and functionally—in cases of complex or total traumatic lesions continues to

present challenges. The simultaneous inability to delay the progressive development of osteoarthritis presents a similar motivation to search for new therapeutic avenues.

This review will cover current knowledge regarding anatomical and biochemical characteristics of the knee meniscus, and discuss the tissue's biomechanical and functional properties. The review will also address the causal pathologies precipitating the need for meniscus treatment, and the effectiveness of current tissue repair methods, among different age groups. Finally, current therapeutic developments in repairing the meniscus will be discussed, focusing especially on the field of tissue engineering. Within this topic, special emphasis will be placed on advances in scaffolds and scaffold-free approaches to regenerate meniscal tissue. Finally, perspectives for the future of meniscus repair will be given.

STRUCTURE AND FUNCTION OF THE KNEE MENISCUS

2.1 Meniscus Anatomy

The knee joint contains the meniscus structure, comprised of both a medial and a lateral component situated between the corresponding femoral condyle and tibial plateau (Figure 1) [7]. Each is a glossy-white, complex tissue comprised of cells, specialized extracellular matrix (ECM) molecules, and region-specific innervation and vascularization. Both menisci are critical components of a healthy knee joint [7-12]. The main stabilizing ligaments are the medial collateral ligament, the transverse ligament, the meniscofemoral ligaments, and attachments at the anterior and posterior horns (Figure 2) [8]. The meniscofemoral ligaments, also known as the Humphrey and Wrisberg ligaments, connect the posterior horn of the lateral meniscus to a location near the insertion site of the posterior cruciate ligament on the medial femoral condyle. Though only 46% of people have both of these ligaments, 100% of people have at least one of

them [8]. The meniscus surface appears smooth upon both gross inspection and microscopically [9]. Human medial and lateral menisci have distinctly different dimensions: lateral menisci are approximately 32.4-35.7 mm in length and 26.6-29.3 mm wide, while medial menisci are 40.5-45.5 mm long and 27 mm wide [10, 11]. Though both menisci are roughly wedge-shaped and semi-lunar, lateral menisci display greater variety in size, shape, thickness, and mobility than medial menisci [12, 13]. Lateral menisci also cover a larger portion of the tibial plateau (75-93% laterally) in comparison to medial menisci (51-74% medially) [13].

Vascularization in this tissue is of high relevance. From prenatal development until shortly after birth, the meniscus is fully vascularized. Afterwards, however, vascularization appears to subside. At 10 years of age, vascularization is present in around 10-30% of the meniscus, and at maturity the meniscus contains blood vessels and nerves only in the peripheral 10-25% of the tissue [13]. Subsequently, two distinct regions of the meniscus can be distinguished: the outer, vascular/neural region (red-red zone), and the inner, completely avascular/aneural region (white-white zone). These two areas are separated by the red-white region, which presents attributes from both the red-red and white-white regions (Figure 3). Critically, the healing capacity of each area is directly related to blood circulation, leaving the white region susceptible to permanent post-traumatic and degenerative lesions [14].

2.2 Biochemical Content

Regarding composition by wet weight, the meniscus is highly hydrated (72% water), with the remaining 28% comprised of organic matter, mostly ECM and cells [15]. In general, collagens make up the majority (75%) of this organic matter, followed by GAGs (17%), DNA (2%),

adhesion glycoproteins (<1%), and elastin (<1%) [15, 16]. The above proportions might vary depending on age, injuries, and other pathological conditions [17, 18].

Although collagen is the main fibrillar component of the meniscus, different collagen types exist in varying quantities in each region of the tissue. In the red-red zone, collagen type I is predominant, at approximately 80% composition by dry weight, with other collagen variants (type II, III, IV, VI, and XVIII) present at less than 1%. In the white-white zone, collagen makes up 70% of the tissue by dry weight, of which 60% is collagen type II and 40% is collagen type I [19]. Aside from collagen, another fibrillar component is elastin: a combination of mature and immature elastin fibers has been found in very low concentrations (<0.6%) in the adult meniscus. Elastin's exact biochemical and functional importance in the meniscus has yet to be determined [9, 18, 20].

Proteoglycans are heavily glycosylated molecules that constitute a major component of the meniscus ECM [21]. These molecules are comprised of a core protein which is decorated with glycosaminoglycans (GAGs). The main types of GAGs found in normal human meniscal tissue are chondoitin-6-sulfate (60%), dermatan sulfate (20-30%), chondroitin-4-sulfate (10-20%), and keratin sulfate (15%) [15]. Aggrecan is the major large proteoglycan of the meniscus while biglycan and decorin are the main small proteoglycans [22]. Regional variation of these molecules has also been observed, with the inner two-thirds containing a relatively higher proportion of proteoglycans than the outer one-third [22]. Their main function is to enable the meniscus to absorb water, whose confinement supports the tissue under compression [22, 23]. Adhesion glycoproteins are also indispensible components of the meniscus matrix, as they serve as a link between ECM components and cells. The main adhesion glycoproteins present in the human meniscus are fibronectin, thrombospondin, and collagen VI [18, 24].

2.3 Meniscus Cells

During early development, all meniscus cells present the same cellular morphology—in terms of both size and shape—with no regional variations. However, later in development, morphologically and phenotypically-distinct cells appear, which also vary in terms of number and topographic localization (Figure 3) [25]. Ghadially et al. [9] suggested categorization of meniscus cells according to their shape and the presence or absence of territorial matrix. Under this classification method, chondrocytes, fibroblasts, or intermediate cells exhibiting characteristics of both were identified. Today, the characterization of meniscus cells appears somewhat controversial in the literature, with a number of different terms being used (i.e., fibrocytes, fibroblasts, meniscus cells, fibrochondrocytes, and chondrocytes) [25]. Regardless of the varying terminology used, it is apparent that outer zone cells have an oval, fusiform shape and are similar in appearance and behavior to fibroblasts. Thus, they may be described as fibroblast-like cells. These cells also display long cell extensions, which facilitate communication with other cells and the extracellular matrix. The matrix surrounding these cells is mainly comprised of type I collagen, with small percentages of glycoproteins and collagen types III and V present [26, 27]. In contrast, cells in the inner portion of the tissue appear more round and are embedded in an ECM comprised largely of type II collagen intermingled with a smaller but significant amount of type I collagen and a higher concentration of GAGs than in the outer region. This relative abundance of collagen type II and aggrecan in the inner region is more reminiscent of hyaline articular cartilage. Therefore, cells in this region are classified as fibrochondrocytes or chondrocyte-like cells [27, 28]. A third cell population has also been recognized in the superficial zone of the meniscus. These cells possess a flattened, fusiform morphology and are absent of cell extensions. It has been suggested that these cells are possibly

specific progenitor cells with therapeutic and regenerative capabilities [29]. In summary, cell phenotype and ECM composition render the outer portion of the meniscus akin to fibrocartilage, while the inner portion possesses similar, but not identical, traits to articular cartilage.

2.4 Biomechanical and Functional Properties

The meniscus withstands many different forces such as shear, tension, and compression. It also plays a crucial role in load-bearing, load transmission, shock absorption, as well as lubrication and nutrition of articular cartilage [16, 30-33]. These multiple and complex functions require a specialized form. Since the tissue is wedge-shaped, it proves highly adept at stabilizing the curved femoral condyle during articulation with the flat tibial plateau [17, 34, 35]. During everyday activity, axial tibiofemoral forces compress the menisci. The wedge shape of the meniscus and its horn attachments serve to convert the vertical compressive forces to horizontal hoop stresses (Figure 4). At the same time, shear forces are developed between the collagen fibers within the meniscus while the meniscus is deformed radially [17, 32, 36].

The biomechanical properties of the knee meniscus are appropriately tuned to withstand the forces exerted on the tissue. Many studies have helped to quantify the properties of the tissue both in humans and in animal models (Tables 1 and 2). According to these studies, the meniscus resists axial compression with an aggregate modulus of 100-150 kPa [37]. The tensile modulus of the tissue varies between the circumferential and radial directions; it is approximately 100-300 MPa circumferentially and 10-fold lower than this radially [38]. Finally, the shear modulus of the meniscus is approximately 120 kPa [38].

The contact forces on the meniscus within the human knee joint have been mapped. It has been calculated that the intact menisci occupy approximately 60% of the contact area

between the articular cartilage of the femoral condyles and the tibial plateau, while they transmit >50% of the total axial load applied in the joint [6, 39, 40]. However, these percentages are highly dependent on degree of knee flexion and tissue health. For every 30° of knee flexion, the contact surface between the two knee bones decreases by 4% [41]. When the knee is in 90° of flexion the applied axial load in the joint is 85% greater than when it is in 0° of flexion [40]. In full knee flexion, the lateral meniscus transmits 100% of the load in the lateral knee compartment, whereas the medial meniscus takes on approximately 50% of the medial load [36].

Conversely, of notable interest are the changes in contact area and contact force following partial or total meniscectomy. Paletta et al. [42] investigated the biomechanical effects of total removal of the lateral meniscus in 10 cadaveric knees and reported a 50% decrease in total contact area, resulting in a 235-335% increase in peak local contact load. In a similar study, Kurosawa et al. [43] noted that following total meniscectomy the tibiofemoral contact area decreased by approximately 50%, therefore leading to an overall increase in contact forces by 2-3 times. Correspondingly, partial (16-34%) meniscectomy has been shown to lead to a >350% increase in contact forces on the articular cartilage [44].

MENISCUS PATHOPHYSIOLOGY

In the United States, meniscal lesions represent the most common intra-articular knee injury, and are the most frequent cause of surgical procedures performed by orthopedic surgeons [45, 46]. The mean annual incidence of meniscal lesions has been reported to be 66 per 100,000 inhabitants, 61 of which result in meniscectomy [47, 48]. Men are more prone to such injuries than women, with a male to female incidence ratio between 2.5:1 and 4:1, and overall incidence peaking at 20-29 years of age for both sexes [47, 49, 50]. Meniscal lesions are most commonly

found in the right knee [47] and occur in all age groups, with the main etiological and pathophysiological factors varying and being highly dependent upon the patient's age [46, 51].

3.1 Meniscus Tears in Young People

In young patients, sports-related (football, basketball, soccer, baseball, and skiing in particular) injuries are the most common cause of meniscal lesions, accounting for more than 1/3 of all cases [47, 49]. The underlying mechanism of these injuries usually involves cutting or twisting movements, hyperextension, or actions of great force [12]. Meniscal tearing during these sports is accompanied by anterior cruciate ligament (ACL) tearing in >80% of cases [52-58]. Most patients report an acute onset of sharp pain following a twisting injury with the knee flexed and the foot planted on the ground [59, 60]. Meniscal tears resulting from vehicle accidents are also associated with increased incidences of meniscus lesions in this particular age group [47].

Classification of meniscal injuries occurs depending on location, thickness, and resulting stability [6, 12, 61]. Thus, tears in the peripheral vascularized portion are denoted as red-red tears, in the middle third portion as red-white or white-white tears, and in the inner avascular portion as white-white tears. According to the depth of the tear, injuries are observed as partial or full thickness, of which full thickness injuries can be further categorized as stable or unstable. Another means of classifying meniscal injuries is based on tear pattern [6, 62]. This way, one can distinguish between different types of meniscal tears—the most important being vertical/longitudinal (including bucket handle), flat/oblique, radial/transverse, and horizontal/complex (including degenerative) [63]. The above categorization is highly relevant when deciding upon the most appropriate and effective therapy. Studies have shown that there

is also a significant difference in tear pattern between stable knees and those with concurrent ACL lesions [64-66].

Diagnosing meniscal malfunction is greatly dependent upon both the experience and insight of a physician. A detailed patient history, a thorough physical exam, and modern imaging techniques can help guide the process towards reaching diagnostic consensus. Starting from the patient's history, an accurate description of the injury's acquisition can set the ground for suspected meniscal tearing. Patient complaints concerning pain, swelling, or 'locking', and diagnostic characteristics during physical examination (joint effusion, joint line tenderness), should be taken under serious consideration [12, 67]. The main tests, which will need to be conducted each time a patient's knee presents with any of the above findings, are joint line palpation, the flexion McMurray test, the Apley's grind test, and the Thessaly test [68-70]. Imaging modalities that need to be applied when diagnosing such injuries are X-ray and MRI [12].

3.1.1 Peripheral Meniscal Tears

Numerous techniques have been described and applied regarding surgical meniscus repair in the peripheral (vascular) zone. Though such techniques undergo continuous development, surgical treatment approaches can be classified under four main categories: inside-out, outside-in, and all-inside arthroscopic techniques; and open repair [5, 6, 71]. These techniques have been extensively described in the literature, along with their accompanying complications and appropriate rehabilitation programs, and will therefore not be largely discussed in the present review.

A substantial amount of research has focused on the efficacy and reliability of these repair techniques for achieving anatomical and functional restoration of the meniscus. In general, there is an ever-increasing amount of literature supporting current meniscus repair techniques for treating tears in the vascular zone. Functionally successful outcomes in young individuals with stable knees are fairly frequent, with success rates varying from 63% to 91% [45, 57, 72-76]. However, more long-term follow-up studies need to be conducted so as to robustly confirm such evidence, and exclude the possibility of long-term degenerative deteriorations of the articular cartilage and meniscus.

3.1.2 Avascular Zone Meniscal Tears

Tears in the avascular zone of the meniscus are generally more complex and broad, and are often associated with a poor prognosis following repair. Improving the healing process in this type of injury is an ongoing challenge for clinicians and researchers. Several different therapeutic approaches have been brought forward, with a variety of reported results (Table 3). The most notable of these new approaches are: the use of parameniscal synovial tissue, trephination of the peripheral meniscus rim with suture of the meniscus tear, creation of vascular access channels, and use of mesenchymal stem cells or growth factors [77, 78].

Despite these results, none of the above techniques has been a recipient of general acceptance and application. Therefore, the main strategy for treating such tears is partial meniscectomy, with its related long-term degenerative implications for articular cartilage [79, 80]. The lack of acceptance and clinical application of the above methods is mainly due to a deficiency in long-term follow-up studies and replication of results, which could confirm these findings in a greater number of clinical cases. In future studies, evaluation of articular cartilage

in a long-term follow-up is of special importance. In addition to this, investigation of the biomechanical properties of healed meniscus in experimental and clinical studies is essential.

3.2 Meniscal Tears in Older People and Children

In general, meniscal lesions occur frequently in middle-aged and elderly patients. Tears encountered in patients belonging to this age group usually result from long-term degeneration. Such meniscal lesions lead to joint swelling, joint line pain, and mechanical blocking [81, 82]. The reported prevalence of meniscal lesions in patients with clinical and radiographic findings of osteoarthritis is 68-90% [83-85]. This high correlation creates a series of diagnostic problems, mainly concerning the identification of the main pathology in a symptomatic knee. Therefore, on some occasions, symptoms that may be due to a pathological cause (such as osteoarthritis) may be attributed by the physician to the presence of a meniscal tear in MRI, while on other occasions, symptoms which may result from trauma (such as a meniscal tear) may be attributed to osteoarthritis. This has obvious repercussions on the choice of proper therapy. For example, treatment of meniscal tears with partial meniscectomy is rather unlikely to reduce symptoms caused by osteoarthritis.

Regarding the successful application of meniscus repairs in older people, less promising findings have been reported as compared to patients in younger age groups [72, 81]. The main reason behind such unfavorable results is the degenerative etiology surrounding meniscal tears in such patient groups, as well as the declining vascularization of the aging meniscus. Barrett et al. [81] reported only a small percentage (6%) of repairable meniscal tears in this special aged patient group. In general, the current preferred intervention for the majority

of surgeons is meniscectomy, either partial or total, depending on the degree of meniscal damage.

An increased incidence in meniscal tearing has recently been observed in skeletally-immature children [86, 87]. The main causative factor behind this increased incidence is the growing participation of children in highly-demanding athletic activities. Simultaneously, the expansion in health services focused on child pathology, and the extensive use of highly specialized imaging techniques such as MRI, have aided in contributing to these diagnoses.

Meniscal lesions in children are different than those in adult patients. In children, the vast majority of cases (>71%) are isolated meniscal lesions [88-90]. The main mechanism of meniscal tearing in children is sports-related twisting of the knee. In a small percentage of these cases, a common predisposing factor is a discoid meniscus [91]. Diagnosis is dependent upon the presence of a complete medical history for the patient and a clinical examination. If a meniscal tear is suspected following clinical examination, the application of an imaging technique should be pursued. Nonetheless, the sensitivity and specificity of MRI for diagnosing meniscal lesions in children is considerably less than that for adults [92, 93].

Meniscus pathology in children has received fairly limited attention in the literature with regards to repair techniques. Most of the studies in this field deal with patient groups comprised mostly of adults, with children representing a small portion of cases and with fairly short follow-ups [94-98]. In general, most of these studies report that the overall success rate for meniscal repair in children appears analogous to that observed in adults, especially for cases of isolated tears [96-98].

CELL SOURCES FOR TISSUE ENGINEERING THE KNEE MENISCUS

4.1 Autologous Cells

One of the leading questions in tissue engineering is whether the engineered tissue should be an exact replica of the native tissue, or whether it should merely carry out its main functions. Several researchers argue that the development of a biomimetic replica of the native meniscus necessitates the use of a biodegradable scaffold seeded with native cells that will produce the same fibrocartilaginous ECM [99-101]. However, this approach exhibits several limitations. Two surgical interventions would be required of a patient: a biopsy to obtain autologous meniscal cells, and a second procedure to implant the tissue-engineered meniscus. Moreover, tissue scarcity and current techniques yield only a limited number of isolated cells, of which only cells from the inner part of the meniscus produce sufficient matrix GAGs [102, 103]. To tackle these issues, research has moved to the fairly simple expansion of autologous meniscal cells in monolayer culture. However, monolayer expansion of meniscus cells leads to significant downregulation of ECM gene expression [104]. Similarly, some approaches have included the use of autologous chondrocytes for meniscal tissue engineering, as they have proven to produce more GAGs and collagen II compared to meniscal cells after expansion, although they too undergo differentiation [99, 105, 106].

Though the development of functional tissue-engineered meniscus constructs has advanced, important problems still persist. The limited ability of cell isolation for large-scale constructs is a notable example. Furthermore, the dedifferentiation of cells after expansion, as well as the possibility of autologous cells already being in either a degenerated state, or in an age-related disease state, deem their utility in tissue engineering questionable [107]. For these reasons, a wide variety of cell sources may be considered for meniscus tissue engineering.

4.2 Allogeneic and Xenogeneic Cell Sources

The realization of the fact that the isolation of a sufficient number of healthy, undifferentiated meniscal cells extracted from an injured meniscus ranges from difficult to impossible, and the need for alternative cell sources, has led many researchers to use allogeneic cells for meniscus tissue engineering [25]. The first trials in this direction have been largely based on the positive healing outcomes of allogeneic articular, auricular, and costal chondrocytes in lesions in the avascular zone of the meniscus, in a large animal model study [108]. In another study, both autologous and allogeneic chondrocytes were seeded in a degradable scaffold and implanted in 17 pigs to repair previously inflicted bucket-handle meniscal tears [109]. After 12 wks, the authors found that both allogeneic and autologous-based scaffolds were capable of promoting healing when compared to the control group. The fact that no statistically significant therapeutic outcome was found between the two cell-based implants is of importance, as it suggests that the use of allogeneic cells is feasible [109].

In terms of the use of xenogeneic cells in tissue engineering, increasing amounts of research seem to strongly encourage their use [110-112]. In a study by Ramallal et al. [110], the investigators created cartilage defects in the femoral condyle of 30 rabbits and subsequently tried to repair the injury by suturing a periosteal flap to the articular cartilage, while also infusing cultured pig chondrocytes into the defect void. After 24 wks, the authors reported the appearance of articular cartilage neotissue, which integrated with the native tissue, and an overall lack of measurable immune response. In another study, researchers used four different types of cells: allogeneic chondrocytes, MSCs, fibroblasts, and human umbilical cord blood (hUCB) stem cells, and embedded them in PLA scaffolds to repair cartilage defects in a rabbit model [111]. Although they found better results when using allogeneic MSCs, they reported no immune response when using xenogeneic hUCB stem cells, motivating further investigations in

this area. The results from these studies point towards the possibility of using xenogeneic cell sources in meniscus tissue engineering, which is further supported by unpublished data from our lab based on both *in vitro* and *in vivo* studies.

4.3 Human Embryonic Stem Cells

Lately, an increasing interest in the use of stem cells for regenerating destroyed or degenerative tissue (such as articular cartilage, meniscus, intervertebral disc, TMJ disc, and heart muscle) has been shown [113-117]. Stem cells can play an important role in rectifying meniscal damage through their ability to differentiate and regenerate tissue, and through their ability to produce cytokines and growth factors [118]. Human embryonic stem cells (hESCs) have proven to be an emerging cell source for fibrocartilage tissue engineering [117]. Some of the main characteristics which make this cell source ideal for tissue engineering are pluripotency and unlimited proliferative capacity [119, 120]. Attempts towards tissue-engineering the meniscus using this cell source are still in early phases. A main step in this direction was made by Hoben et al. [121], who investigated hESCs' differentiation potential into fibrochondrocyte-like cells, and characterized the resulting differentiated cells. In this study, hESCs were cultured with growth factors (TGF-β3, BMP-2, BMP-4, BMP-6, PDGF-BB, sonic hedgehog protein), and/or primary cells (chondrocyte or fibrochondrocytes) for 3 wks. Following this time, their ability to produce GAGs and collagen types I, III, and VI was assayed, along with the presence of certain surface markers (CD105, CD44, SSEA, PDGFRa). Following comparison of these treatments, results showed that the combination of TGF-β3 with BMP-4 yielded embryoid bodies positive for collagen type I, II, and VI with 6.7 and 4.8-fold increases in GAG and collagen, respectively. Also, co-culture with fibrochondrocytes led to 9.8-fold increases in collagen II

production. Results from this study point to the suitability of hESCs for meniscal tissue engineering and highlight at least 3 effective strategies to create hESC-derived fibrocartilage [121].

4.4 Adult Stem Cells

While the usage of hESCs in meniscal tissue engineering remains at a preliminary stage, many studies have focused on using mesenchymal stem cells (MSCs) as a potential cell source. MSCs are multipotent progenitor cells of stromal origin whose main source is adult bone marrow, although they may be isolated from other tissues in both adults and fetuses [122-125]. The large scientific interest surrounding these cells is due to two main abilities. First, MSCs have been observed to differentiate into many terminally-differentiated cells which synthesize mesenchymal tissue (i.e., cartilage, bone, ligaments, muscle, fat, dermal, and other connective tissue), and can therefore be used to engineer mesenchymal-derived tissue [126]. Second, MSCs secrete a large variety of immunoregulatory molecules, and contribute to the healing process of injured tissue by providing paracrine trophic mediators [118].

Different strategies for using autologous connective tissue progenitors in MSC-based tissue engineering have been described in the literature. An approach that has been investigated by many researchers is *in situ* activation of the migration, proliferation, and differentiation of local MSCs. This can be achieved by the transplantation of an acellular scaffold [127] or by the local administration of growth factors such as VEGF, which activates these MSC functions [128, 129].

Another strategy is the local administration of autologous MSCs to replenish the population of local cells which has been diminished due to trauma, degeneration, tissue defects,

or compromised vascularity. Currently, many surgeons use this method to transplant bone marrow-derived stem cells (BMSCs) for bone healing applications due to its high value and low risk and cost [130]. This strategy has been the center of much interest as a therapeutic approach for rehabilitating meniscal lesions. Some of the main techniques utilized with this approach include the creation of vascular access channels and vascular tunnels by trephination or rasping in the vascular region of the meniscus. This allows the influx of blood—and subsequently MSCs—into the damaged avascular area [77, 78, 131, 132]. Other techniques use vascularized synovial flaps or fibrin clots, based on the same rationale [133-138]. Results of these techniques appear to conflict in the existing literature.

The transplantation of expanded or modified autologous MSCs is another approach in MSC-based tissue engineering. The first attempt of this took place in 2005, when Izuta et al. [139] used autologous BMSCs from green fluorescent protein transgenic rats; these were isolated, expanded in monolayer culture, and then transplanted into meniscal defects inflicted in the avascular zone. After 8 wks follow-up, the investigators found that MSCs could survive and proliferate in the meniscal tears while also developing an extensive extracellular matrix, aiding the healing process in the avascular meniscus [139]. Similarly, investigators in another study reported that autologous BMSCs injected into meniscal wounds of eight canines improved healing [140]. In the same light, studies have proven the use of MSCs seeded onto scaffolds for meniscus tissue engineering as a rather effective one [141, 142]. Another study showed that undifferentiated MSCs, as opposed to precultured cells, display a more potent healing response [143]. Here, the investigators studied the therapeutic value of autologous MSCs in meniscal tissue lesions in a rabbit model by comparing their action to that of platelet-rich plasma and autologous BMSCs. More specifically, they created circular meniscal punch defects (2mm), and

either left the resulting gap intact, or covered it with hyaluronan-collagen composite matrices using one or none of the above cell categories. Of notable importance is that some of the stem cell matrices were precultured in chondrogenic medium for 14 days prior to transplantation. Twelve wks after transplant the researchers concluded that the non-precultured autologous MSCs led to integrated meniscus-like repair tissue, while the precultured MSCs led only to partial integration [143].

Undoubtedly, the expansion of MSCs *in vitro* has significant advantages and disadvantages. The primary advantage of expansion is an increase in cell number. Disadvantages include possible cell infection during culture, as well as decreased capacity for proliferation prior to implantation [144-146]. Finally, another danger not extensively reported on in the literature is the development of tumor-like abnormalities following implantation of precultured autologous MSCs with mutations or epigenetic changes [130]. This appears to be a relatively unexplored topic, showing the need for more studies.

Finally, another strategy utilizing MSCs is *ex vivo* tissue differentiation/generation, with subsequent transplantation of this tissue. Research using this approach is currently being conducted in the authors' lab to generate fibrocartilaginous tissues, including meniscus tissue. The main challenges in this field coincide with the main challenges of tissue engineering in general: development of functional tissue mirroring the composition of native tissue, which will satisfactorily integrate with the host, and which will allow long-term preservation of cell viability and meniscus function.

SCAFFOLDS FOR TISSUE ENGINEERING THE KNEE MENISCUS

Scaffolds for tissue engineering the meniscus may be categorized into four broad classes: synthetic polymers, hydrogels, ECM components, or tissue-derived materials. Synthetic

polymers are materials that do not exist in the body, at least not in polymer form. Hydrogels are hydrophilic colloids capable of holding large amounts of water, and may be derived from natural or synthetic sources. ECM component scaffolds are comprised of whole materials formed primarily from a component macromolecule of natural matrix, such as collagen or hyaluronan. Finally, tissue-derived materials include decellularized ECM and other significant components or byproducts of living tissue such as small intestinal submucosa. Importantly however, these four categorizations are not mutually exclusive, and rather serve as a broad guide to appreciate significant differences in properties among scaffolds. Hybrids and composites between these materials also exist. Since cell-seeded polymers consistently outperform acellular scaffolds in terms of regenerative capacity [101, 147, 148], this section will primarily focus on studies examining the capabilities of scaffolds incorporating cells.

The ideal meniscus construct will excel in three criteria: mechanics, bioactivity, and logistics (Table 4). Since heterogeneous loading of the meniscus occurs every day *in vivo*, appropriate mechanical properties, tissue anisotropy, geometry [149], and lubrication are requirements of the mechanics criterion. Any implanted meniscus construct will also need to display sufficient bioactivity. This means maintenance of cell phenotype, induction of ECM synthesis, lack of immunogenicity, and capacity for host-tissue integration. Finally, the logistics of a successful construct must not be unwieldy: supply, processability, sterilization, and eventual surgical implantation must all be practical.

5.1 Synthetic Polymer Scaffolds

Synthetic polymers, such as polyurethane (PU), polycaprolactone (PCL), polylactic acid (PLA), polyglycolic acid (PGA), and polylactic co-glycolic acid (PLGA), hold several advantages,

including fabrication under a variety of methods, near-limitless supply, and the potential to achieve appropriate pore size, fiber size, mechanical properties, and scaffold geometry. These advantages are countered by a central weakness—minimal intrinsic biomimetic and bioactive properties. By contrast, the mechanical properties of some more highly bioactive scaffolds, such as small intestinal submucosa, are considerably less than that of some synthetic polymers [158-160]. The lack of inherent biological support among synthetic scaffolds has motivated the exploration and use of many synthetic scaffolds as acellular meniscus prostheses, which provide some biomechanical functionality, as well as modest tissue regeneration, when implanted [150-157].

Tissue engineering has spurred recent advances in synthetic polymer scaffolds that emphasize and build upon the advantages stated above. Methods for generating mechanical anisotropy within synthetic cartilage scaffolds are one example. This characteristic is essential, since loading of the meniscus *in vivo* is highly non-uniform [38, 39]. It has been demonstrated that fibers in PCL scaffolds may be preferentially aligned by the use of a rotating collection platform during electrospinning [161]. When evaluated mechanically, these scaffolds exhibited a 33-fold change in tensile moduli if tested in the direction parallel versus perpendicular to fiber alignment [161]. Aligned scaffolds can also subsequently promote cell and ECM orientation [162-165]. It has been found that aligned PCL scaffolds seeded with meniscus cells and cultured over 10 wks display a 7-fold greater increase in tensile modulus in the direction of alignment than corresponding non-aligned scaffolds [162]. Importantly, collagen per DNA was not statistically different between aligned and non-aligned scaffolds, suggesting differential organization of the existing ECM [162], although some studies have also reported that scaffold

alignment serves to increase matrix deposition [166, 167]. Regardless of the underlying mechanism, scaffold orientation appears to have a beneficial effect.

Recent work has also demonstrated that scaffolds may be physically woven to further increase their compressive, tensile, and shear properties and to introduce scaffold anisotropy [168, 169]. In this strategy, a custom-built weaving loom was used to produce anisotropic PGA or PCL scaffolds with mechanical characteristics generally on the same order of magnitude as native articular cartilage [168, 169]. These woven scaffolds may be combined with hydrogels to make composites capable of supporting seeded articular chondrocytes or adipose-derived stem cells [168, 169]. Although these studies focused on engineering articular cartilage, they would also be highly relevant for recapitulating the mechanical properties and anisotropy of the knee meniscus.

Other recent advances focus on making synthetic polymers more biomimetic and bioactive. One group of investigators recently reported the fabrication of a peptide scaffold sensitive to matrix metalloproteinase-2 (MMP-2) degradation [170]. Although this scaffold has not yet been applied to meniscus tissue engineering, it may greatly aid in coupling cell-mediated matrix remodeling to scaffold degradation. Since native components of the ECM are nanoscale molecules, nanofibrous scaffolds may also help to coax cells to behave as they do in native matrix. One study comparing PLLA nanofiber and microfiber scaffolds reported increased production of sulfated GAGs, cartilage link protein, collagen II, and aggrecan by bovine chondrocytes seeded in the nanofiber scaffolds [171]. Some synthetic polymers may also inherently provide a more biomimetic environment than hydrogels for meniscus cells. A comparison of meniscus cells cultured in PGA or agarose scaffolds over 7 wks reported 2 to 6-fold higher cell numbers, 2 to 4-fold higher GAG production, and 3-fold greater collagen

production in the PGA scaffolds [172]. The authors concluded that cell proliferation and ECM synthesis may be reduced when meniscus cells are forced to assume a round morphology in highly hydrophobic agarose, since meniscus cells display a morphology and phenotype that is representative of elongated fibroblasts as well as chondrocytes [173, 174]. This conclusion is corroborated by other studies of fibroblast functionality in gels, where proliferation diminished as cell spreading was restrained [175, 176].

Despite the recent advances described above, the main disadvantage of synthetic polymer scaffolds still lies in facilitation of the development of a functionally-robust matrix prior to scaffold degradation *in vivo*. Future research in this direction is needed. Integration of synthetic polymer tissue constructs with neighboring host tissue also remains an issue to tackle. Finally, fine-tuning of synthetic polymers, so as to promote joint lubrication and to prevent tissue wear and tear at bone-cartilage interfaces, also represent avenues for further research.

5.2 Hydrogel Scaffolds

Hydrogels have also been investigated for use as meniscus scaffolds. Hydrogels can be synthetic materials such as poly N-isopropyl acrylamide (PNIPAAm), or natural materials such as alginate. The physical properties of hydrogels are largely influenced by their water content, which is often >90%. Hydrogels are also versatile—they may be crosslinked through various methods [177-179], reversibly gelled [180], and patterned with cells [181-184] and growth factors [185, 186]. Many hydrogels can also be synthesized from readily available reagents. However, hydrogels may hamper meniscus cell phenotype by preventing encapsulated cells from assuming their characteristic spread fibroblastic morphology [172, 173, 175]. Additionally, the mechanical properties of hydrogel scaffolds are not as easily manipulated as in

synthetic polymers. Finally, hydrogels such as polyvinyl alcohol (PVA) [187, 188] and fibrin [189, 190] have been investigated as acellular meniscus materials, but these will not be focused on in this review.

Much research has focused on utilizing the versatile chemistry of hydrogels to create more biomimetic structures. The chemical functionalization of hydrogels is one strategy that has been pursued to create a more native microenvironment for cells. Hybrid hydrogels (chitosan-alginate-hyaluronan) have been conjugated with the adhesive arginine-glycine-aspartic acid (RGD) polypeptide and cultured with articular chondrocytes over 1 to 2 wks to show higher collagen and GAG content over unconjugated controls [191]. Hydrogels have also been functionalized to undergo proteolytic degradation by MMPs [192-194]. Both of these approaches are highly relevant to meniscus tissue engineering, but further work is needed to explore these scaffolds in conjunction with meniscus cells. Hydrogel co-cultures may also be created by spatial patterning of different cell types [182-184], using insoluble adhesion molecules or sequential photopolymerization. Fibroblasts have been co-cultured with BMSCs in this manner [183], although the diverse meniscus cell subpopulations have not. This method is one way in which the regional cellular variation of the meniscus may be replicated.

Another principal advantage of hydrogels is their ability to reversibly gel in response to environmental factors such as temperature, pH, electric field, ultrasound, or salt concentration [180]. This has allowed for the development of “smart” biomaterials whose design allows for responses according to the environment, which is favorable for tissue engineering because injectable scaffolds that solidify in the body can be produced. Building on this concept, Chen et al. [195] have produced temperature-sensitive chitosan-hyaluronan-PNIPAAm hybrid gels which maintain meniscus cell viability, encourage native matrix synthesis, and reversibly

solidify in response to temperature. Though an injectable knee meniscus hydrogel is minimally invasive and enticing, a major limiting factor lies in the scaffold's insufficient mechanical properties after solidification. This deficiency may potentially be modulated through increased hydrogel crosslinking, but some crosslinking methods have been shown to affect cytotoxicity and cellular metabolism [196, 197].

Other tissue engineers have taken advantage of various methods to create cell-seeded hydrogel scaffolds that accurately represent the complex geometry of the meniscus. One method combines the imaging capabilities of computed tomography or MRI with robotic printing to automate creation of a geometrically-accurate model of the meniscus [177, 198]. Alginate scaffolds seeded with bovine meniscus cells in high density (50 million/mL) in this manner displayed a high geometrical fidelity to the target shape, high cell viability, and some properties similar to native tissue (50% of aggregate modulus, 33% of GAG content, but 2% of hydroxyproline content), though tensile properties were not examined [198]. However, tissue grown in this manner was highly heterogeneous, possibly due to limited transport in the fairly large construct. Subsequent work demonstrated the use of a magnetic stir bar "mixing bioreactor" to produce constructs with a larger degree of homogeneity, higher equilibrium and tensile moduli, and greater ECM deposition, although detrimental effects were observed at higher stirring intensities [199]. This work underscores the necessity of, and opportunities and challenges associated with, bringing together diverse tools (imaging modalities, processing methods, bioreactors) to successfully tissue engineer the knee meniscus.

Hydrogels represent a versatile class of tissue engineering scaffolds, but their mechanical properties (especially in tension) and bioactivity (especially in promoting meniscus cell phenotype and ECM synthesis) need to be improved. Cell-adhesive hydrogels have been

created, and these may help with cell spreading and phenotype issues [176]. Other research has been directed towards ECM molecule hydrogels, yielding studies on elastin-like polypeptide [200, 201] and collagen-mimetic peptide [202, 203] hydrogels. Further research into these approaches may combine the bioactivity of ECM molecules with the versatility of hydrogel scaffolds.

5.3 ECM Component Scaffolds

ECM component scaffolds are materials formed primarily from a macromolecule abundant in native matrix. Examples include collagen meniscus implants or hyaluronan scaffolds. Combinations of these molecules may also be used (i.e., collagen-GAG scaffolds or scaffolds containing multiple types of collagen). Collagen scaffolds in particular are amenable to several fabrication and processing methods, including nanofiber electrospinning, anisotropic deposition, and crosslinking. Because of these methods, ECM scaffolds may possess strength comparable to synthetic scaffolds. As far as bioactivity, ECM scaffolds would logically constitute a natural environment for seeded cells. Yet, although these scaffolds are made of natural matrix, they may not completely recapitulate the cell microenvironment (i.e., the collagen VI pericellular matrix, collagen IX crosslinks, etc.). In addition, some other scaffold materials such as silk have also been shown to more robustly promote matrix deposition compared to collagen scaffolds [204, 205]. Yet, in general, ECM component scaffolds are more intrinsically biomimetic than synthetic and hydrogel materials.

Since meniscus cells normally rest in a dense network of collagen and GAG molecules, scaffolds made from these components would logically provide a natural environment for the regeneration of meniscus tissue. Interestingly, not all ECM molecules are

equally effective. An early study showed that GAG-collagen II matrices promoted more meniscus cell proliferation, more GAG deposition, and less contraction versus GAG-collagen I matrices [206]. Other researchers have shown that aggrecan surfaces are more effective in encouraging meniscus cell ECM deposition than collagen I surfaces [104]. HYAFF-11 is another ECM component scaffold, made by modifying the glucoronic acid groups in hyaluronan. A study comparing meniscus cells seeded in HYAFF-11 and collagen scaffolds (types I, II, and III) found no differences in GAG and collagen I synthesis [207]. Thus, a variety of results have been observed when comparing the efficacy of different ECM component scaffolds. More research into these ECM component scaffolds and combinations of these scaffolds is needed.

Scaffolds, and especially ECM component scaffolds, can exert a strong effect on seeded cells through the microenvironment they provide. A recent investigation developed a hybrid scaffold consisting of chitosan, hyaluronan, chondroitin-6-sulfate, collagen I, and collagen II molecules [208]. Rat meniscus cells passaged in monolayer underwent conventional dedifferentiation, but those subsequently cultured in these hybrid scaffolds underwent partial redifferentiation over 1 wk. Results from RT-PCR demonstrated the upregulation of collagen I, collagen II, and aggrecan, although not to the levels seen prior to passage [208]. Although these results are exciting in that they show scaffolds may induce redifferentiation of previously dedifferentiated meniscus cells, further studies are needed to characterize the matrix deposited in these systems, especially over longer culture periods.

From a clinical perspective, ECM scaffolds have received perhaps the most attention of all scaffold categories, due to the use of collagen meniscus implants. The collagen meniscus implant is a surgical mesh composed of bovine collagen type I, crosslinked with aldehydes, and

molded in the shape of the lateral or medial menisci [209]. A multi-center clinical trial of collagen meniscus implants showed greater tissue restoration 1 year after operation compared to partial meniscectomy; and activity levels also rose in chronic sufferers of meniscal problems 7 years after implantation [210]. Smaller non-randomized trials report positive patient outcomes over longer periods, with losses in pain and higher activity levels documented [211, 212]. Despite these results, significant scientific and clinical drawbacks associated with the collagen meniscus implant exist. The implant is not an option for patients who have undergone total meniscectomy. In addition, once implanted, scaffold degradation and shrinkage as well as shape incongruency remain significant issues [213, 214]. The technical difficulty of suturing the implant also limits its use [213, 214]. Finally, this acellular scaffold's primary mode of healing is thought to be through host cell migration and subsequent synthesis of meniscus matrix, yet results in sheep have indicated more developed healing if collagen meniscus implants are seeded with autologous fibrochondrocytes [101]. In this work, seeded constructs were significantly larger than unseeded constructs or resection controls after 3 wks of implantation. In addition, histology showed greater ECM deposition and lower cellularity in seeded constructs, suggesting accelerated matrix remodeling [101]. This lends credit to cell-based tissue engineering. Lastly, as of this writing, the FDA approval granted to the collagen meniscus implant in 2008 has been rescinded, and the device has been removed from clinical use.

In general, ECM component scaffolds display a mix of desirable traits between mechanics, bioactivity, and logistics. This category may hold the most promise amongst scaffold-based approaches for meniscus tissue engineering. However, the technology and use of these materials is still relatively new, and the efficient incorporation and development of suitable replacement tissue within ECM scaffolds *in vivo* and *in vitro* remains a topic for more

investigation. The introduction of appropriate lubrication, and the modulation of ECM component scaffold degradation kinetics, also present opportunities for further research in functional tissue engineering.

5.4 Tissue-Derived Scaffolds

Tissue-derived materials comprise the final category of scaffolding currently being investigated for engineering the knee meniscus. Tissue-derived materials include processed whole tissue such as small intestinal submucosa (SIS), decellularized tissue or ECM (dECM), and silk. The hypothesis of using such materials is similar to that of using ECM components: they constitute a natural environment for cell seeding, migration, and ECM deposition. Though geometric fidelity and bioactivity of these scaffolds can be high, they must be procured from natural tissue, and thus supply is problematic. In addition, some decellularization and processing protocols compromise the mechanical integrity of these tissues.

Several investigations have demonstrated the comparatively high bioactivity of processed whole tissue scaffolds. A study of passaged and seeded canine chondrocytes in SIS and PLGA scaffolds, implanted in athymic mice, reported that sulfated GAG and hydroxyproline content was higher in the SIS scaffolds, although collagen II was present only in PLGA scaffolds [158]. SIS has also demonstrated superiority to other tissue-derived meniscus scaffolds. In a fairly recent study, three dermis isolates (human, fetal bovine, and crosslinked porcine) were compared against two small intestine isolates (porcine and crosslinked porcine) in a rat model [215]. Canine meniscal cells, synoviocytes, tendon fibroblasts, and bone marrow progenitor cells were seeded in co-culture in all five scaffolds, and porcine small intestine

(principally the non-crosslinked scaffolds) displayed the greatest capacity for encouraging retention, infiltration, and viability of these cells [215].

Though processed whole tissues such as SIS display significant bioactivity and have been seen to induce some tissue regeneration, the resulting tissue mechanics may be insufficient, which subsequently compromises knee function. An early work studied unseeded porcine SIS implanted in surgically-created canine medial meniscus defects [216]. After 12 wks, improved lameness scores, less articular cartilage erosion, and some tissue growth and retention were observed over controls [216]. Similar results have also been reported in a longer-term study with SIS specimens assessed after up to 12 months of implantation, although the study also reported samples with biomechanics inferior to contralateral meniscectomy [217]. A contrasting study reported meniscal regeneration but increased articular cartilage degeneration (compared to contralateral controls) in the knee joints of goats implanted with unseeded porcine SIS [218]. The fact that tissue growth seems apparent in these studies, but inferior biomechanics and/or cartilage degeneration are observed simultaneously, highlights the possibility that this regenerated tissue is mechanically insufficient.

Other research centers on the considerable difficulty of creating tissue-derived scaffolds with appropriate pore sizes. Studies of native menisci have deemed pore sizes of 100-150 microns as appropriate for meniscus cells [219], yet cell infiltration can be highly variant through the depths of both whole processed tissue (SIS, dermis, etc.) [215] and decellularized meniscus [220], likely due to the dense matrix present even after processing. However, other recent work has achieved progress by increasing decellularized ovine menisci porosity (to a value of 80% in the outer meniscus) as well as connected pore volume, although residual DNA content was still significant and compressive properties trended lower [221].

Though decellularized tissue scaffolds are promising, several studies have reported decreased mechanical properties (especially compressive properties) due to the treatment protocols used for decellularizing tissue. Losses in GAG content are similarly reported. A variety of alternate treatment methods have been investigated. One recent study demonstrated no reaction to MHC1 and MHC2, and preservation of, or even increases in, compressive stiffness after ovine menisci were treated with a self-developed enzymatic solution [222]. Further, ovine meniscus cells were successfully cultured within these scaffolds over 4 wks. Despite these positive findings, a 3-fold GAG loss and non-uniform cell distributions were observed within the re-seeded scaffolds [222]. Decellularization of human meniscus has also been performed [223]. This investigation revealed that collagen structure within the meniscus was intact, and mechanical properties were comparable to native tissue, after a 2 wk treatment with 2% sodium dodecyl sulfate (SDS) [223]. However, the use of SDS is associated with many detrimental side effects. Other work has shown that it is possible to remove the vast majority of cellular DNA as well as the primary xenogeneic epitope galactose-α-1,3-galactose, though significant GAG loss is also observed with this procedure [224].

Despite their advantages, tissue-derived meniscus scaffolds suffer from several drawbacks. Uniform cell infiltration and preservation of mechanics and chief ECM components such as GAGs are two areas for future research. Additionally, biological and mechanical performance after recellularization and *in vivo* implantation represent areas for further exploration. Some work has been done in this regard with devitalized rat menisci re-seeded with BMSCs [220, 225]. Constructs displayed cell migration and increases in compressive stiffness over 4 wks, but collagen and GAG content was not assayed [220]. More work in this area needs to be pursued. By bringing together some of the approaches reviewed above, it may be possible

to resolve these problems. However, the bottlenecks of supply, sterilization, and standardization of tissue-derived scaffolds still need to be addressed for a large-scale tissue engineering solution to be obtained.

SCAFFOLDLESS SELF-ASSEMBLY OF TISSUE

The paradigm of tissue engineering has traditionally been defined as the combination of replacement cells, cell-signaling stimuli (mechanical or chemical/biochemical), and supporting scaffolds (Figure 5). Although the use of these three elements in combination comprises the classical approach to engineering replacement tissue, in recent years cell self-assembly has begun to gain recognition and support in generation of functional cartilage, fibrocartilage, vasculature, and retina [226-231]. In cartilage and fibrocartilage, the self-assembly approach supersedes the need for scaffolds by seeding cells in very high density, possibly promoting cell-cell adhesion, cell-matrix adhesion, and cell-cell signaling; and encouraging cells to rapidly develop and integrate into a matrix with quantifiable mechanical properties [226, 232, 233]. Characterization of this process in articular chondrocytes shows high expression of N-cadherin during cell coalescence, followed by collagen VI pericellular matrix synthesis, and finally collagen II and GAG ECM synthesis [233].

Obviating the need for a support scaffold conveys key tissue engineering advantages. First, the natural synthesis of and adherence to cartilage ECM as it develops bestows the most bioactive microenvironment of any approach. Second, the all-biologic construct greatly increases likelihood of integration with host tissue. Third, since no material is completely biocompatible in every use, the lack of a scaffold diminishes further contributions to an immune response. Fourth, removal of any degradation products minimizes potential toxicity and allows for greater cell viability. Fifth, stress-shielding effects exerted by scaffolds are mitigated. More

robust and homogeneous mechanical stimulation is possible during tissue development, which is particularly pertinent for engineering the knee meniscus. Sixth, since self-assembled tissue has a continuous ECM, it may be more fully able to remodel itself in response to catabolic exogenous agents such as chondroitinase ABC (C-ABC).

Indeed, self-assembled constructs have been shown to respond well to treatment with exogenous agents [234-236]. A meniscus tissue engineering study using bovine meniscus cells and articular chondrocytes found that treatment with TGF-β1 and C-ABC led to a 196% increase in collagen per wet weight, a 136% increase in compressive instantaneous modulus, a 68% increase in compressive relaxation modulus, a 600% increase in circumferential tensile modulus, and a 500% increase in radial tensile modulus [232]. Circumferential and radial tensile moduli were also significantly different, mirroring prior results indicating anisotropic collagen fiber alignment in scaffoldless meniscus constructs [232, 237]. It is thought that confinement in circular agarose molds during self-assembly may allow for the development of circumferential contractile forces on coalescing neotissue, thus aiding in the development of tissue anisotropy [237].

Mechanical stimulation of scaffold-free and self-assembled tissue has also shown promising results [229, 232, 238]. Self-assembled articular cartilage has been shown to withstand hydrostatic pressures of up to 10 MPa and respond positively by increasing aggregate modulus (96%), Young's modulus (92%), collagen per wet weight (51%) and GAG per wet weight (52%) [235]. A somewhat similar study of scaffold-free porcine chondrocyte constructs demonstrated beneficial responses to direct compression stimulation at strain amplitudes of 5-20% [229]. Following this loading, 200-300% increases in construct stiffness and a 250% increase in Young's modulus was measured [229]. Since the knee meniscus is also loaded in

cyclic direct compression *in vivo* [43, 239] these results are promising for tissue engineering of the meniscus using scaffold-free self-assembly.

It is important to note that while this method is scaffold-free, it is not devoid of the utilization of biomaterials. Agarose hydrogel plays an important role in the self-assembly process as a hydrophobic negative mold used to prevent cell-substrate adhesion during tissue coalescence. Interestingly, it has also been shown that the compliance and surface roughness of this mold can alter the biomechanical properties (strength, stiffness) and even biochemical content (cellularity, collagen I/II, GAG) of self-assembled constructs [240]. It is possible that still other hydrogels and biomaterials may function to significantly modulate the quality of tissue formed from scaffold-free self-assembly.

BIOCHEMICAL STIMULI IN MENISCUS TISSUE ENGINEERING

A large variety of biochemical stimuli have been applied in meniscus tissue engineering investigations. Growth factors are the most prominent biochemical stimuli for tissue engineering the knee meniscus (Table 5). Overall, for meniscus cell proliferation, b-FGF in particular has been seen to elicit a strong response [241-244]. One group studied the ability of nine growth factors (EGF, b-FGF, TGF-α, PDGF-AB, a-FGF, TGF-β1, PDGF-AA, IGF-I, and NGF) to stimulate proliferation of meniscus cells in monolayer over 4 days [241]. Of these nine, b-FGF, PDGF-AB, EGF, and TGF-α encouraged proliferation, with b-FGF inducing the greatest effect [241]. These four growth factors also promoted increased collagen synthesis of meniscus cells [241]. Another study compared monolayer proliferation of meniscus cells from the different tissue regions (inner/middle/outer) [245]. An up to 3-fold increase in DNA synthesis was demonstrated when PDGF-AB, HGF, and BMP-2 were applied to these cultured

cells, while IGF-1 had no such effect [245]. Interestingly, cells from different regions responded differently, with BMP-2 having a slightly stronger effect on cells from the middle zone, and HGF exerting a slightly stronger effect on cells from the inner zone [245]. The effects upon monolayer meniscus cell migration were also examined. PDGF-AB and HGF stimulated migration in cells from all three zones of the meniscus, while EGF, IGF-1, IL-1, and BMP-2 promoted cell migration only in specific zones of the meniscus (outer and inner, middle and inner, outer and middle, and only middle, respectively) [245].

Aside from proliferation and migration, another chief function of growth factors in meniscus tissue engineering is to stimulate matrix synthesis. The TGF-β family, regarded as one of the most important for cartilage tissue engineering [246-248], has repeatedly demonstrated the ability to heighten meniscus cell synthesis of matrix proteins [102, 103, 232]. Since the ECM largely confers the mechanical properties which underlie the primary functions of the knee meniscus, this is particularly salient. An early study demonstrated increased proteoglycan synthesis of meniscus cells in monolayer, explant, and scaffold culture when treated with TGF-β1 [103]. Increased cell proliferation was also observed, in only the monolayer cultures [103]. Additionally, in scaffold and monolayer studies comparing TGF-β1, IGF-1, b-FGF, and PDGF-AB, only TGF-β1 stimulated significant simultaneous production of both collagens and GAGs over controls [244, 249]. TGF-β1 has also been seen to up-regulate the expression and secretion of lubricin, or superficial zone protein (SZP) [250]. This protein is thought to provide essential function to cartilage by aiding in lubrication. By contrast, the same study found that interleukin-1β decreased SZP protein content and gene expression [250]. Finally, TGF-β has also interestingly been shown to inhibit meniscus cell proliferation [241]. This highlights the

proliferation/production interplay in which meniscus cells are preferentially driven to one function or the other.

One potentially important function of growth factors may be to modulate matrix contraction. Both fibroblasts [251] and articular chondrocytes [252] exert local contractile forces on their surrounding matrices. Contiguous tissue constructs may actually benefit from controlled contraction, because ECM compaction and alignment can lead to anisotropy and greater mechanical properties. In fact, inhibition of fibroblast-mediated contraction has been shown to disrupt development of tendon mechanical properties [253]. Too much contraction, however, can render constructs of incorrect geometry [237]. However, the use of controlled contraction as a biophysical means of modulating cartilage development is relatively scarce in the literature. Both TGF-β1 and PDGF have been documented as growth factors involved in encouraging matrix contraction by meniscus cells, fibroblasts, and articular chondrocytes [232, 254-256]. FGF-2 and IGF-1 can also induce articular chondrocyte-mediated contraction of collagen II/GAG gel scaffolds [257]. The continued exploration of this topic may lead to interesting advances in the field.

Phenotype maintenance or cell differentiation to fibrochondrocytes is another vital application of growth factors in meniscus tissue engineering. Relatively little work has been done in this area. However, it has been found that meniscus cell phenotype may be salvaged by exposure to FGF-2 during monolayer expansion [258]. Subsequent 3-D pellet culture of FGF-2 exposed meniscus cells revealed a 200-fold higher expression of collagen II and GAG than controls [258]. Fibrochondrogenic differentiation of human embryonic stem cells has also been performed [121]. CDMP-1 has also been explored in a PGA scaffold modality to enhance fibrochondrogenesis of dermal fibroblasts [259], and has been demonstrated to increase

proteoglycan content and collagen II gene expression [260]. Lastly, exposure to TGF-β1 has also been suggested to push meniscus fibrochondrocytes towards a more chondrocytic phenotype [102]. Since meniscus fibrocartilage is a tissue with varying regions, either similar to or distinct from the hyaline articular cartilage produced by chondrocytes, this is a relevant result for prospective tissue engineers. These varying results demonstrate considerable potential in, and promise for, further investigations of fibrochondrogenic differentiation of cells.

Chondroitinase ABC (C-ABC) is another biochemical stimuli that has been employed in cartilage tissue engineering. This enzyme cleaves chondroitin and dermatan sulfate from proteoglycan chains while leaving collagen fibers unaffected [261, 262]. It has been suggested that a dynamic balance between the swelling pressure caused by proteoglycans and the restraining strength of the collagen network exists [263]. Subsequently, it has been hypothesized that enzymatic depletion of cartilage GAG content (which is afterwards recovered by cellular synthesis) may facilitate increased collagen network alignment and density, leading to heightened tissue tensile properties [232, 264-266]. Indeed, serum-free C-ABC treatment of tissue-engineered articular cartilage (in both self-assembled and agarose scaffold forms) has resulted in increased tensile properties versus untreated controls, as well as recovery of GAG content and compressive stiffness after 2 to 4 wks of culture post-treatment [264-266]. The repeated beneficial results of C-ABC on tissue-engineered articular cartilage motivate its use for tissue engineering meniscus fibrocartilage. Along these lines, self-assembled meniscus constructs (composed of meniscus cells and articular chondrocytes) treated with C-ABC have been seen to display approximate 2 to 3-fold increases in tensile modulus over untreated controls and GAG recovery after 3 wks of culture post-treatment [232]. However, more studies

using C-ABC for meniscus tissue engineering, especially in conjunction with other stimuli, are necessary.

Biochemical stimulus selection is not clear-cut, and the study of multiple agents (especially growth factors) in conjunction necessitates additional investigations. Culture conditions play a non-trivial role in modulating cell responses to biochemical stimulus administration, whether the treated tissue is arranged in monolayer, scaffold, explant, or self-assembled form. The presence of serum in the media of a study is also a critical variable [245, 267]. Futures studies may focus on unconventional growth factors, such as the serum-derived phospholipid agent lysophosphatidic acid (LPA). LPA is naturally present in mammalian sera at concentrations ranging from 1-5 μM [268], and has been studied extensively as an anti-apoptotic factor. Other potent agents may be derived from platelet-rich plasma, which has been shown to increase matrix deposition and proliferation of meniscus cells cultured in monolayer [269]. Finally, although fibrocartilage is a particularly important soft tissue, research into its generation with biochemical stimuli is nascent, and thus future work along these lines may produce significant medical advances. Much remains to be studied concerning biochemical stimuli used in tissue engineering the knee meniscus.

MECHANICAL STIMULATION FOR MENISCUS TISSUE ENGINEERING

Meniscus cells may respond positively to mechanical stimuli by enhancing the fibrocartilage ECM, or negatively by secreting matrix-degrading or inflammatory factors. The mechanical properties of the matrix can be enhanced through three general mechanisms: deposition, alignment, or compaction. To achieve these results, there are several possible methods of stimulating meniscus tissue. These include high and low shear, fluid perfusion, hydrostatic

pressure, direct compression, and even ultrasound. However, most current efforts are centered on hydrostatic pressure and direct compression stimulation.

Explant and engineered tissue can demonstrate varied remodeling responses to hydrostatic pressure. For instance, leporine meniscal explants subjected to cyclic hydrostatic pressure at 1 MPa, 0.5 Hz, for 1 min on/14 min off over 4 hrs, have been shown to upregulate inflammatory factors and matrix degradation proteins [270]. In contrast, leporine meniscus cells seeded in PLLA constructs and stimulated with hydrostatic pressure at 10 MPa statically for 1 hr every 3 days exhibited beneficial responses [271]. In these constructs, collagen and GAG content, as well as compressive properties, were all significantly higher than control or dynamic hydrostatic pressure regimens run at 0.1 or 1 Hz [271]. Furthermore, when combined with TGF-β1, hydrostatic pressure stimulation of leporine meniscal cell-seeded PLLA constructs displayed additive increases in collagen and GAG deposition as well as a synergistic increase in compressive properties [272]. These results demonstrate the various responses meniscus cells may mount in response to hydrostatic pressure.

Direct compression stimulation of the meniscus has also been pursued, although insufficient loading or excessive loading can be detrimental. For example, static and dynamic loading regimens over 24 hrs using direct compression at 0.1 MPa and 0.08-0.16 MPa, respectively, have been shown to decrease mRNA levels of type I collagen, type II collagen, and decorin [273]. Furthermore, under the same regimens, mRNA for ECM-degrading matrix metalloproteinase-1 (MMP-1) and collagenase were both upregulated [273]. Similarly, dynamic compression of porcine meniscus explants (24 hrs, 0.1 MPa, 0.5 Hz) has been demonstrated to upregulate production of nitric oxide, a potent signaling molecule implicated in arthritis and

meniscus degeneration [274]. Thus, the use of incorrect loading regimen parameters can lead to matrix and tissue degradation.

By contrast, certain other loading regimens have shown beneficial effects. Physiological loads on the meniscus *in vivo* may exceed 1000 N [39], and it is believed this compressive loading helps facilitate nutrient-waste exchange in the otherwise transport-limited and avascular meniscus. For example, it has been shown that tensile loading of meniscus cells can suppress the production of inflammatory factors [275]. Further, dynamic compression (2% oscillatory strain, 1 Hz, 1 min on/1 min off duty cycle, 4 hrs per day for 4 days) of meniscus explants has been reported to increase aggrecan expression compared to statically compressed samples [276]. A longer duration loading regimen (0.1 MPa, 0.5 Hz, for 24 hrs) has also been shown to increase protein (68%) and proteoglycan (58%) synthesis in meniscal explants [277]. Dynamic compression has also yielded other positive results in anatomically-shaped alginate scaffolds containing bovine meniscus cells [278]. The investigated loading regimen (7-15% strain, 1 Hz, 1 hr on/1 hr off duty cycle, 3 hrs per day, 3 days per wk for 6 wks) applied to meniscus constructs yielded increases in compressive equilibrium modulus and GAG content after 2 wks, and decreases in these values but increases in collagen content after 6 wks [278]. These results under different loading regimens highlight the varied biosynthetic responses that may occur following mechanical stimulus, and encourage the pursuit of additional research.

Of all of the factors being integrated to achieve successful engineering of the knee meniscus, mechanical stimulation is perhaps the one with the highest ambiguity and largest opportunity for improvement. Interestingly, while shear is generally thought of as detrimental to the chondrocyte phenotype, oscillatory fluid flow has been shown to upregulate calcium signaling and GAG production of meniscus cells in parallel plate flow chambers [279]. The use

of shear and other forces to generate fibrocartilage may yield benefits for meniscus tissue engineering in the future. Due to the large amount of variable parameters (method, time of application, magnitude, duration, and frequency of stimulation) the optimal and most dramatic combination of effects for mechanical stimuli likely remains undiscovered.

CONCLUSIONS AND FUTURE DIRECTIONS

This review has provided an account of current concepts in meniscus pathology and repair, as well as meniscus tissue engineering. Undoubtedly, the need for effective therapies based on tissue engineering approaches is exceedingly high. The driving factors for this are high incidences of meniscal lesions amongst several age groups in the general population and significant deficiencies associated with current repair techniques. Secondary to these factors are degenerative changes in articular cartilage, which lead to osteoarthritis and generate considerable socioeconomic costs for healthcare systems worldwide. Tissue engineering aims to ameliorate these problems by establishing new meniscus repair techniques that, for example, can yield constructs that restore mechanical function by integrating with or replacing the patient's tissue. Apart from its potential clinical benefit, a tissue-engineered meniscus can also be of great use in the study of developmental, regenerative, and degenerative processes in the knee.

Despite considerable diversity amongst current strategies for tissue engineering the meniscus, several important design principles are emerging. In general, these principles relate to a biomimetic approach to generating replacement meniscus tissue by recapitulating biological, structural, and functional features of the native meniscus. First, cells in replacement tissue must possess a similar phenotype to those found in native meniscus. This dictates the presence of a

both fibroblast-like and chondrocyte-like cells. In cases of total meniscus replacement, this may also include vascularization in the outer periphery. Second, the biochemical content in the meniscus (i.e., collagen, GAGs) should closely mirror the regional variation displayed natively. This design principle will follow naturally from the use of cells with appropriate phenotypes. Third, functional anisotropy must be manifest in an engineered meniscus. Functional anisotropy of mechanical properties may in turn be recapitulated from the presence of appropriate ECM content. Taken together, these principles of tissue engineering using biomimicry may guide tissue engineers to generating a fully functional meniscus.

To achieve these goals, several strategies have been proposed, with mixed results. Several cell sources have been studied for meniscus engineering, including autologous, allogeneic, xenogeneic, and stem cells. Yet, amongst these, no specific cell source has been established, although stem cells are particularly promising. Whilst the various categories of biomaterial scaffolds offer different advantages, no approach currently addresses all three fundamental requirements of a successful meniscus tissue replacement (satisfactory mechanics, bioactivity, and logistics). In this field, a scaffoldless self-assembly process utilizing a biomaterial mold is another potentially effective strategy for meniscus tissue engineering that largely fulfills some of the above criteria. However, and perhaps more importantly, it lacks complications associated with scaffolds such as integration, degradation, biocompatibility, and stress shielding. In addition to these approaches, the use of synergistic biochemical and biomechanical stimuli are fundamental to the creation of functional tissue. Thus, based on these advantages, the self-assembly process may provide sufficient flexibility to lead to functional tissue-engineered meniscus constructs.

Even though the existing studies in meniscus tissue engineering show promising results, research needs to progress further. At the basic level, more long-term scaffold and scaffoldless studies aimed at improving mechanical properties and matching them to tissue need to be undertaken. Especially vital is the avoidance of scaffold degradation before mechanically-competent tissue can be formed. In line with this, seeded cells must be encouraged to maintain their phenotype and synthetic capacity in a scaffold. Additionally, the reproducibility of engineered tissue needs to be established. Going a step further, experimental (animal) studies and well-designed prospective, randomized, and controlled clinical trials with long-term quantitative outcome measurement are key to *in vivo* evaluation of research in this field. The outlining of indications and contraindications, the selection of suitable patients for tissue repair with engineered meniscus, and the establishment of specialized surgical techniques are therefore necessary. Moreover, the development of non-invasive assessment procedures for generated tissue, both pre-implantation and post-implantation, is required. Directions for future research should also be guided by minimization of healthcare costs. These essential goals will be pivotal to the potential widespread clinical application of tissue-engineered meniscus. Although the challenge is vast, recent scientific advances suggest that a solution to this as-of-yet intractable problem may be emerging from the collaborative efforts of biomedical engineers, clinicians, and industry leaders.

TABLES AND FIGURES

TABLE 1.1 – COMPRESSIVE PROPERTIES OF THE KNEE MENISCUS.

Study	Species	Location	Aggregate modulus (±SD; MPa)	Permeability (±SD; 10^{-15} m^4 N^{-1} s^{-1})
Sweigart et al. [37]	Human	Medial superior:		
		Anterior	0.15 ± 0.03	1.84 ± 0.64
		Central	0.10 ± 0.03	1.54 ± 0.71
		Posterior	0.11 ± 0.02	2.74 ± 2.49
		Medial Inferior:		
		Anterior	0.16 ± 0.05	1.71 ± 0.48
		Central	0.11 ± 0.04	1.54 ± 0.49
		Posterior	0.09 ± 0.03	1.32 ± 0.61
	Bovine	Medial superior:		
		Anterior	0.21 ± 0.06	6.22 ± 2.55
		Central	0.14 ± 0.05	5.73 ± 6.19
		Posterior	0.11 ± 0.04	4.73 ± 2.56
		Medial Inferior:		
		Anterior	0.16 ± 0.06	5.79 ± 4.31
		Central	0.11 ± 0.03	5.65 ± 4.13
		Posterior	0.13 ± 0.06	5.40 ± 5.36

TABLE 1.2 – TENSILE PROPERTIES OF THE KNEE MENISCUS.

Study	Animal type	Direction	Location	Stiffness (±SD; MPa)
Fithian et al. [38]	Human	Circumferential	Lateral meniscus: *Anterior* *Central* *Posterior* Medial meniscus: *Anterior* *Central* *Posterior*	 159.1 ± 47.4 228.8 ± 51.4 294.1 ± 90.4 159.6 ± 26.2 228.8 ± 51.4 294.1 ± 90.4
Tissakht et al. [280]	Human	Circumferential	Lateral meniscus: *Anterior* *Central* *Posterior* Medial meniscus: *Anterior* *Central* *Posterior*	 124.58 ± 39.51 91.37 ± 23.04 143.73 ± 38.91 106.21 ± 77.95 77.95 ± 25.09 82.36 ± 22.23
		Radial	Lateral meniscus: *Anterior* *Central* *Posterior* Medial meniscus: *Anterior* *Central* *Posterior*	 48.47 ± 25.67 45.86 ± 24.20 29.85 ± 12.77 48.31 ± 24.35 46.20 ± 27.56 32.55 ± 11.27
Lechner et al. [281]	Human	Circumferential	Medial meniscus: *Anterior* *Central* *Posterior*	 141.2 ± 56.7 116.4 ± 47.5 108.4 ± 42.9

TABLE 1.3 – CURRENT RESEARCH FINDINGS ON MENISCUS REPAIR TECHNIQUES (ALTERNATIVES TO MENISCECTOMY) FOR THE AVASCULAR ZONE. ACLT: Anterior cruciate ligament transection.

	Type of study	No. of cases	Mean age (years)	Follow-up time(s) (mo.)	Concurrent ACLT	Type of lesions	Technique	Cases Completely Healed (%)	Evaluation
Arnoczky et al. [189]	Experimental	12	-	6	-	-	Exogenous fibrin clot + suture	100	Histology
Henning et al. [138]	Clinical	153	23	41	Majority	Longitudinal, radial, flap, horizontal split, bucket handle, complex	Exogenous fibrin clot + suture	64	Arthrogram + follow-up arthroscopy
Arnoczky and Warren [14]	Experimental	15	-	2, 5	-	-	Vascular access channels + suture	100	Histology
Vangsness et al.[282]	Experimental	30	-	1, 5	-	-	Neodymium laser + suture	0	Histology
Jitsuiki and Ikuta [283]	Experimental	14	-	1	-	-	Free synovium allograft	Almost 100	Histology
Zhang et al. [132]	Experimental	21	-	1, 2	-	-	Trephination + suture	69	Histology + biomechanical testing
Cisa et al. [284]	Experimental	44	-	12	-	-	Transfer of pedunculated synovial flap	75	Histology
Rubman et al. [52]	Clinical	91	28	18	Majority	-	Arthroscopy + suture	25 (38 partial healing)	Follow up arthroscopy
van Trommel et al. [137]	Clinical	5	20	4, 71	Minority	Radial split	Fibrin clot + suture	60 (4 mos), 100 (71 mos)	Follow up arthroscopy + MRI + clinical examination
Tienen et al. [285]	Experimental	24	-	3, 6	-	Longitudinal	Implantation of a porous polymer in a partial thickness access channel	100	Histology
Uchio et al. [131]	Clinical	48	24	21	Majority	-	Rasping without suturing	71 (21 incomplete healing)	Second look arthroscopy
Papachristou et al. [286]	Clinical	25	20	36	-	Longitudinal	Suture	40	Clinical examination
Pollo et al. [287]	Experimental	10	-	1, 3	-	-	Photoactive laser technique	100	Histology
Petersen et al. [288]	Experimental	18	-	0.5, 1	-	-	Suture coated VEGF/PDLLA	0	Histology
Noyes et al. [289]	Clinical	71	16	18, 51	Majority	Longitudinal, horizontal, radial, complex	Suture	75	Follow up arthroscopy (18 mos) + clinical exam. (51 mos)

TABLE 1.4 – LEADING BIOMATERIALS STRATEGIES FOR MENISCUS TISSUE ENGINEERING. Rated on three primary criteria. Categories were qualitatively rated from one to four stars in mechanics (mechanical properties, geometry, anisotropy, lubrication), bioactivity (cell phenotype, ECM synthesis, immunogenicity, potential for host tissue integration), and logistics (supply, material processability and sterilization, ease of surgical implantation).

Rated Criterion	Synthetic Scaffolds	Hydrogel Scaffolds	ECM Component Scaffolds (e.g., collagen, GAG)	Tissue-Derived Scaffolds (e.g., SIS, decellularized matrix)	Scaffold-Free (e.g., self-assembly)
Mechanics	***	*	***	**	***
Bioactivity	*	**	**	****	****
Logistics	****	****	***	*	**

TABLE 1.5 – INFLUENCE OF SELECTED GROWTH FACTORS ADMINISTERED TO MENISCUS CELLS.

Growth Factor	Effects	Culture Conditions
TGF-β1	↑↓ Proliferation	Monolayer [103, 241, 242]
	↑↑ Collagen Synthesis	Monolayer [249]; Scaffold [242, 244]; Explant [290]; Scaffoldless [232]
	↑↑ GAG/Proteoglycan	Monolayer [103, 249]; Scaffold [103, 244, 291]; Explant [103, 290]; Scaffoldless [232]
	↑ SZP Secretion	Monolayer [250]; Explants [250]
	↑ Contraction	Scaffold [255]
b-FGF	↑↑↑ Proliferation	Monolayer [241-243]; Scaffold [244]
	↑ Collagen Synthesis	Monolayer [241, 243]; Scaffold [244]
	↑ GAG/Proteoglycan	Monolayer [243, 249]; Explants [290]
PDGF-AB	↑↑ Proliferation	Monolayer [241, 245]; Scaffold [292]; Explant [292]
	↑ Collagen Synthesis	Monolayer [241]; Scaffold [242]
	↑ GAG/Proteoglycan	Monolayer [249]; Explant [290]
	↑ Contraction	Scaffold [254]
	↑↑ Migration	Monolayer [245]; Scaffold [292]; Explant [292]
IGF-I	↑ Proliferation	Monolayer [103, 242]; Scaffold [244]
	↑↓ Collagen Synthesis	Monolayer [249]; Scaffold [242]
	↑ GAG/Proteoglycan	Explant [290]
	↑ Migration	Monolayer [245]
EGF	↑ Proliferation	Monolayer [241]
	↑ Collagen Synthesis	Monolayer [241]
	↑ Migration	Monolayer [245]
HGF	↑↑ Proliferation	Monolayer [245]; Scaffold [292]; Explant [292]
	↑↑ Migration	Monolayer [245]; Scaffold [292]; Explant [292]

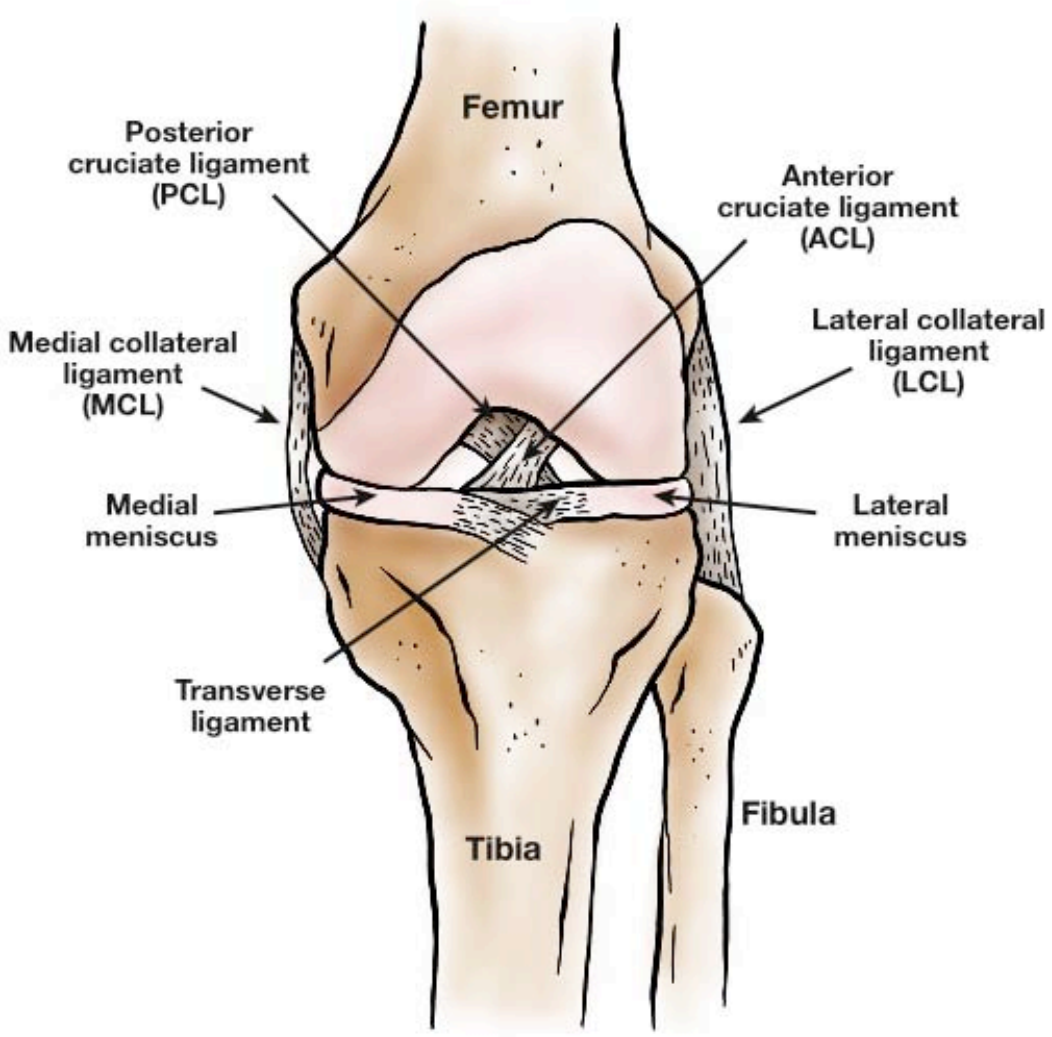

FIGURE 1.1 – ANATOMY OF THE KNEE JOINT: ANTERIOR VIEW. The knee meniscus is situated between the femur and the tibia. Crossing the meniscus are various ligaments, which aid in stabilizing the knee joint.

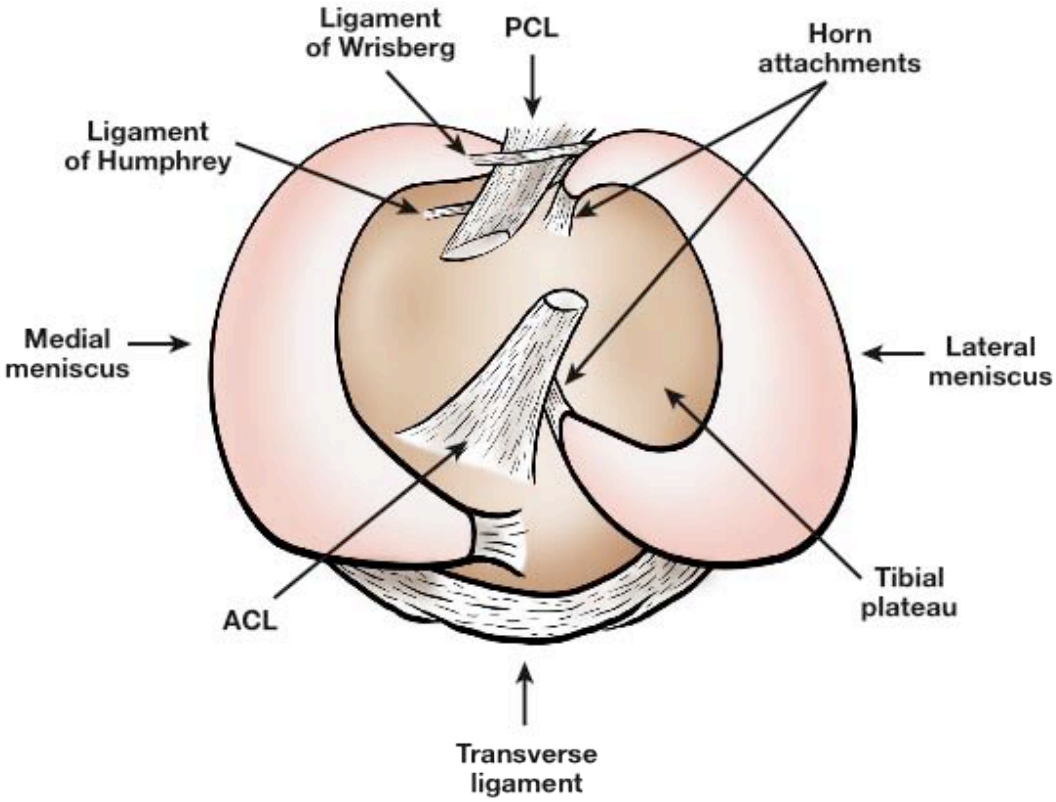

FIGURE 1.2 – ANATOMY OF THE MENISCUS: SUPERIOR VIEW OF THE TIBIAL PLATEAU. This view of the tibial plateau highlights the ligaments of Humphrey and Wrisberg, which attach the meniscus to the femur. The menisci are attached to each other via the transverse ligament. The horn attachments connect the tibial plateau to the meniscus.

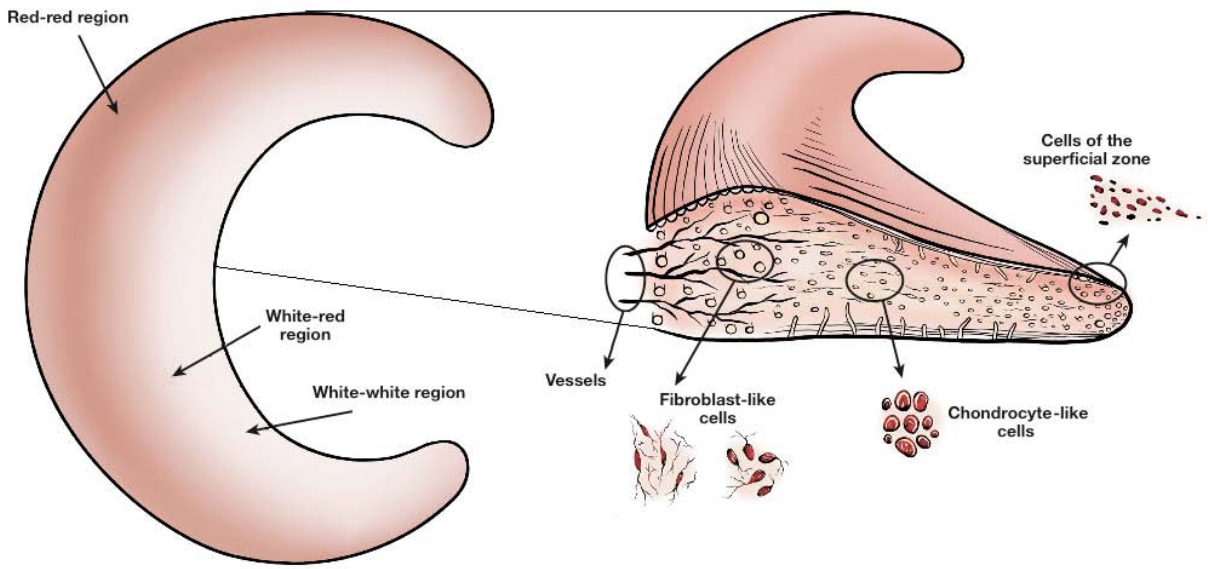

FIGURE 1.3 – REGIONAL VARIATIONS IN VASCULARIZATION AND CELL POPULATIONS OF THE MENISCUS. Left: Though fully vascularized at birth, the blood vessels in the meniscus recede during maturity. In adulthood, the red-red region contains the overwhelming majority of blood vessels. Right: Cells in the outer, vascularized section of the meniscus (red-red region) are spindle-shaped, display cell processes, and are more fibroblast-like in appearance, while cells in the middle section (white-red region) and inner section (white-white region) are more chondrocyte-like, though they are phenotypically distinct from chondrocytes. Cells in the superficial layer of the meniscus are small and round.

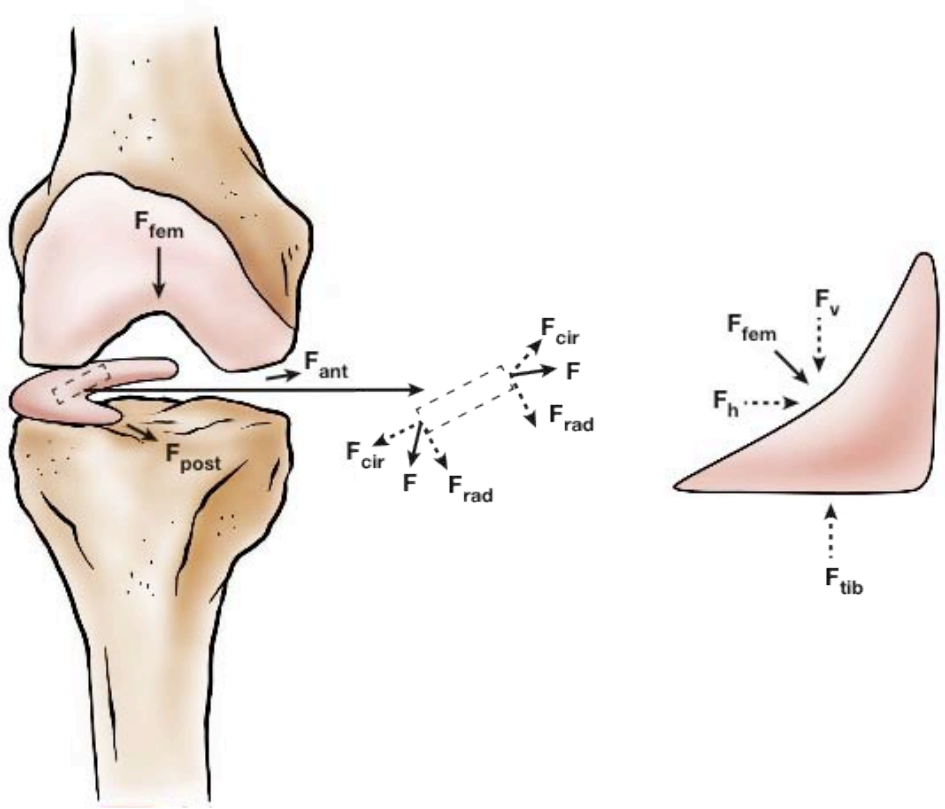

FIGURE 1.4 – HOW FORCE IS TRANSDUCED UPON AND THROUGHOUT THE KNEE MENISCUS. Free body diagram of the forces acting on the knee meniscus during loading (for simplicity, only the lateral meniscus is shown). During everyday activity, the menisci are compressed by the downward force of the femur. Since the meniscus is a wedge, the femoral force is enacted at an angle, and thus a vertical component exists which is countered by the upward force of the tibia. Additionally, a horizontal component of the femoral force exists, which is exerted radially outward on each meniscus. This horizontal force is in turn countered by the anchoring force of the attachments at the posterior and anterior horns of the meniscus. Additionally, as this compression occurs, circumferential stress is created along the meniscus. Therefore, the menisci function by converting compressive loads to circumferential tensile loads. At the same time, shear forces are developed between the collagen fibers within the meniscus while the meniscus is deformed radially.

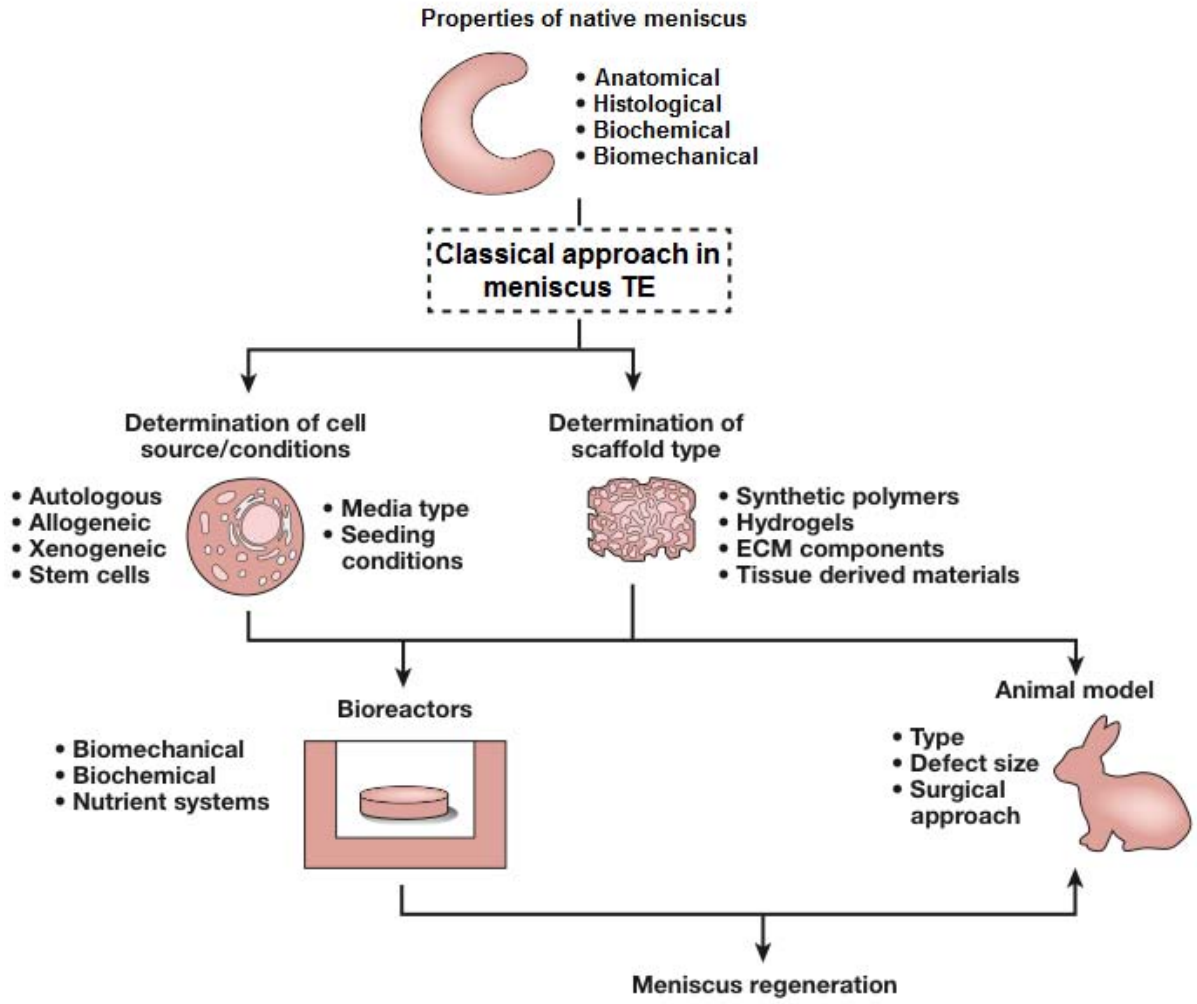

FIGURE 1.5 – THE CLASSICAL, SCAFFOLD-BASED APPROACH FOR MENISCUS TISSUE ENGINEERING. Generation of a functional meniscus requires several key considerations. Characterization of the meniscus is essential for establishing design parameters. Following this, judicious choice of cell type(s), scaffold material(s), and exogenous stimuli must be made. Implantation *in vivo* may be substituted for, or performed subsequent to, bioreactor culture. Using these tools, tissue engineering aims to regenerate or replace the meniscus.

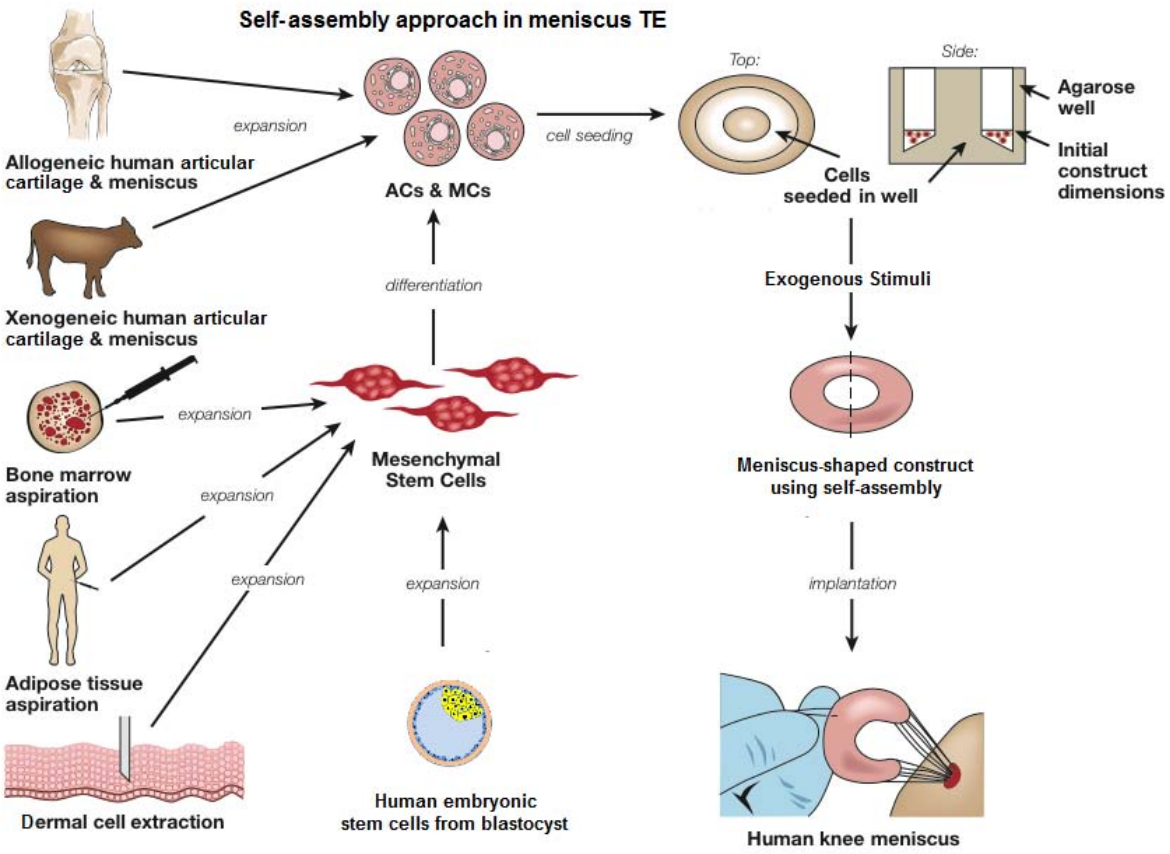

FIGURE 1.6 – THE STRATEGY OF TISSUE SELF-ASSEMBLY FOR MENISCUS TISSUE ENGINEERING. This approach utilizes a hydrogel mold to form completely biologic tissue constructs. Selection of cells is of paramount importance. Following isolation from allogeneic or xenogeneic sources, articular chondrocytes (ACs) and meniscus cells (MCs) are expanded to achieve the high numbers needed for robust tissue engineering. Mesenchymal stem cells, but also potentially embryonic stem cells, are a promising alternative cell source for subsequent differentiation into meniscus cells. Cells are then seeded in high density in a non-adherent biomaterial mold, secreting ECM that coalesces into a continuous tissue over several days. Exogenous stimuli are added during culture to increase the synthetic activity and functional properties of neotissue, which is eventually implanted *in vivo*.

CHAPTER 2 – A COPPER SULFATE AND HYDROXYLYSINE TREATMENT REGIMEN FOR ENHANCING COLLAGEN CROSSLINKING AND BIOMECHANICAL PROPERTIES IN ENGINEERED NEOCARTILAGE

ABSTRACT

The objective of this study was to improve the biomechanical properties of engineered neotissues through promoting the development of collagen crosslinks. It was hypothesized that supplementing medium with copper sulfate and the amino acid hydroxylysine would enhance the activity of lysyl oxidase enzyme to form collagen crosslinks, increasing the strength and integrity of the neotissue. Neocartilage constructs were generated using a scaffoldless, self-assembling process and treated with copper sulfate and hydroxylysine, either alone or in combination, following a two-factor, full factorial study design. Following a 6-week culture period, the biomechanical and biochemical properties of the constructs were measured. Results found copper sulfate to significantly increase pyridinoline (PYR) crosslinks in all copper sulfate-containing groups over controls. When copper sulfate and hydroxylysine were combined, the result was synergistic, with a 10-fold increase in PYR content over controls. This increase in PYR crosslinks manifested in a 3.3-fold significant increase in the tensile properties of the copper sulfate + hydroxylysine group. Additionally, an 123% increase over control values was detected in the copper sulfate group in terms of the aggregate modulus. These data elucidate the

Chapter published as: Makris, E.A., MacBarb, R.F., Responte, D.J., Hu, J.C., & Athanasiou, K.A. A Copper Sulfate and Hydroxylysine Treatment Regimen for Enhancing Collagen Crosslinking and Biomechanical Properties in Engineered Neocartilage. *FASEB journal: official publication of the Federation of American Societies for Experimental Biology*. 27(6): 2421-2430, 2013.

role of copper sulfate and hydroxylysine toward improving the biomechanical properties of neotissues through collagen crosslinking enhancement.

INTRODUCTION

Arthritis is the second most frequent chronic disease in the United States. Currently affecting 46.4 million people and costing the U.S. over $128 billion per annum, the economic burden of this disease is tremendous and growing[344]. The most common form of arthritis, known as osteoarthritis (OA), is characteristic of joint cartilage degeneration[345]. Due to the inability of articular cartilage to self-repair, there are currently no clinical options for treating OA. The ability to generate engineered articular cartilage *in vitro,* therefore, holds much promise as an effective reparative treatment for OA. Many advances have been made in articular cartilage tissue engineering strategies toward developing a biomechanically robust repair tissue able to integrate with the surrounding healthy cartilage. Though much work remains to be done to engineer clinically relevant repair cartilage, tissue engineering approaches offer new hope toward bringing a degenerated joint back to an uncompromised state.

Current tissue engineering approaches for generating articular cartilage typically involve a combination of cells, signals (e.g., growth factors, mechanical stimulation), and scaffolds. Deviating from the typical tissue engineering paradigm, our group has developed a self-assembly method in which we forgo the use of a scaffold. By culturing articular chondrocytes at high densities in 3-dimensional cultures using non-adherent agarose wells, we are able to form robust neocartilage in a manner akin to native cartilage morphogenesis[212, 230, 305]. This process is advantageous in that it is not affected by the inherent problems associated with scaffolds, such as biodegradability, stress-shielding, and hindering of cell-to-cell communication. However, as

with scaffold-based tissue engineering approaches, self-assembled articular cartilage often fails to match the high mechanical strength of native tissue, leaving it incapable of withstanding the complex loading scheme of an articular joint. These inferior properties mainly manifest in the tensile properties of engineered neotissue; targeted efforts to increase the tensile properties of engineered articular cartilage are, therefore, crucial to creating tissues with clinical impact.

The ability of articular joints to withstand high loads is mainly due to the load adsorbing and distributing properties of articular cartilage. With structure and function being intimately linked, a direct tie between mechanical integrity and both extracellular matrix (ECM) composition and structure has been observed. In the case of articular cartilage, the typical structure-function paradigm links the presence of an organized collagen network with the tissue's tensile strength, while compressive stiffness has been related to glycosaminoglycan (GAG) distribution within the tissue[346]. However, recent investigations in both native and engineered articular cartilage have found this paradigm to shift. Such studies have reported that the collagen network significantly affects the compressive properties of articular cartilage[335, 347]. Specifically, a better correlation between the compressive modulus and the collagen content has been described[348]. Similarly, another study examining the correlation between the biomechanical and biochemical properties of superficial zone articular cartilage reported a correlation among the compressive modulus and both collagen and GAG with R^2 values of 0.36 and 0.24, respectively[239]. To explain this finding, it was hypothesized that increased collagen content may decrease the extrafibrillar volume and create a higher effective fixed charge density, which could increase tissue compressive properties[349].

The structure-function relationships related to collagen crosslinking have also been studied, although not as extensively as the effects of GAG and collagen. Pyridinoline (PYR)

crosslinks have been correlated with the tensile properties of native articular cartilage[238]. Likewise, a significant correlation among collagen crosslinks and compressive properties of native articular cartilage has also been reported[348]. Such studies indicate that the specific organization of the collagen architecture, including fiber density, diameter, orientation, and degree of crosslinking, all play a significant role in determining the mechanical integrity of both native and engineered tissues. These additional structure-function relationships will need to be elucidated to fully understand the biomechanics of cartilage.

Although current attempts to increase the tensile properties of engineered articular cartilage frequently focus on collagen content and alignment, increasing interfibrillar collagen crosslinks may provide an additional means to increase the tensile properties of neocartilage. While several investigations have characterized the nature of collagen crosslinking in native tissue, only a few studies have focused on the type, amount, and influence of collagen crosslinking in engineered tissues[350]. For instance, it has been shown that chondrocytes cultured on polyglycolic acid scaffolds or suspended within alginate beads produce collagen crosslinks; however, reported values were far from those of native articular cartilage[351, 352]. Furthermore, another study has demonstrated that collagen networks in engineered cartilage require proper crosslinking to stabilize the matrix and to provide it with mechanical strength[353]. Taken together, these studies illuminate the crucial role of crosslinks in the stabilization and mechanical support of the collagen network within both native and engineered cartilages. Methods must therefore be investigated to induce the formation of collagen crosslinks within engineered neocartilage to generate tissues with functional properties matching those of native tissue.

In native cartilage, the formation of lysine-derived, covalent PYR crosslinks is dependent on the enzyme lysyl oxidase (LOX). To investigate the importance of LOX in articular cartilage, explants were treated with β-aminopropionitrile, a potent inhibitor of extracellular LOX activity. This treatment resulted in disorganization of the collagen architecture within the explants as well as a significant decrease in the biomechanical properties of the tissue[354]. Such work highlights the importance of LOX-mediated collagen crosslinks on the functional integrity of articular cartilage. LOX is a cuproenzyme, meaning its activity is dependent on the presence of copper[12]. Once activated by copper, LOX is able to modify the amino acids lysine and hydroxylysine into PYR crosslinks, the most abundant type of crosslink in native articular cartilage (Fig. 1)[11, 355, 356]. It is important to note that copper sulfate is not a common ingredient in culture mediums, leaving LOX in its inactive form in *in vitro* culture. Therefore, copper sulfate supplementation may be a powerful means to enhance the amount of collagen crosslinks and, therefore, improve the functional properties of engineered tissues.

Previous work on LOX has shown this enzyme to act extracellularly, requiring collagen fibrils in a quarter-staggered array as a substrate to generate crosslinks[357, 358]. Furthermore, the proper aldehyde precursors for LOX must be present in the immature collagen fibrils, including both lysine and hydroxylysine (Fig. 1). While lysine is present as an essential component in culture medium, hydroxylysine can only be formed when the enzyme lysyl hydroxylase catalyzes the conversion of lysine into its hydroxylated form. This is crucial to generate mature PYR crosslinks[11, 355]. Despite its importance in the development of a functionally mature collagen matrix, this essential collagen crosslink precursor is currently not used in cartilage tissue engineering, meriting studies to investigate its potential for increasing interfibrillar collagen crosslinking in engineered articular cartilage.

The overall objective of this study was to enhance collagen crosslinking in engineered articular cartilage to improve the biomechanical properties towards those of native tissue. Articular cartilage constructs were generated using the self-assembly process and supplemented with copper sulfate and hydroxylysine either alone or in combination following a full factorial study design. Overall, it was hypothesized that chondrogenic media supplemented with copper sulfate and hydroxylysine would additively or synergistically enhance the amount of LOX-mediated collagen crosslinks, thus increasing the tensile strength of the engineered neotissue.

MATERIALS AND METHODS

Harvest/isolation/self-assembly

Juvenile bovine knee joints were obtained (Research 87, Boston, MA, USA) and harvested for the articular cartilage. Articular cartilage was minced from the condyles and patellar grove, and digested in a base medium of Dulbecco's Modified Eagle Medium (DMEM) supplemented with 1% penicillin/streptomycin/fungizone (PSF) and 2% collagenase (Worthington, Lakewood, NJ, USA) for 18 hours. Following digestion, chondrocytes were isolated and purified via filtration and centrifugation, and then stored in base medium containing 20% fetal bovine serum and 10% dimethyl sulfoxide in liquid nitrogen until needed for seeding.

For self-assembly, chondrocytes were defrosted, counted, and seeded into 5 mm diameter, 2% agarose wells at 5 million cells/well as previously described[212]. For the first week of culture, constructs were fed 500 µl of chondrogenic medium consisting of DMEM, 1% PSF, 1% non-essential amino acids, 100 nM dexamethasone (Sigma, St. Louis, MO, USA), 1% ITS+ (BD Scientific, Franklin Lakes, NJ, USA), 40 µg/mL L-proline, 50 µg/mL ascorbate-2-phosphate, and 100 µg/mL sodium pyruvate (Fischer Scientific, Pittsburgh, PA, USA). At day

7, the constructs were moved from the agarose molds into non-adherent tissue culture plates. Constructs were fed 1 ml of chondrogenic media until the end of the 6-week culture period.

Treatments

In this study, the effect of both copper sulfate (Sigma-Aldrich, St. Louis, MO, USA) and hydroxylysine (Sigma-Aldrich, St. Louis, MO, USA) on self-assembled neocartilage was investigated. Following a full-factorial study design, constructs were treated with 0.0016 mg/mL copper sulfate and 0.146 mg/ml hydroxylysine either alone or in combination (copper sulfate + hydroxylysine group), or left untreated to serve as controls. Treatments were carried out for the entire culture duration, after which the neotissue was assayed, as described below.

Histology

Portions of constructs were embedded in Histoprep (Fisher Chemical, Vernon Hills, IL, USA) and sliced to 14 μm. After being fixed in chilled formalin, sections were stained with Picrosirius Red for total collagen and Safranin O/Fast Green for GAG.

Biochemistry

The wet and dry (following lyophilization for 2 days) weights of the construct segments designated for biochemical analysis were determined, after which the samples were digested in papain as previously described[229]. A chloramine-T hydroxyproline assay using a SIRCOL collagen assay standard (Accurate Chemical and Scientific Corp., Westbury, NY, USA) was used to assess for total collagen, while GAG content was measured using a dimethylmethylene blue dye-binding assay kit (Biocolor, Newtownabbey, Northern Ireland). DNA content was

determined using a Picogreen Cell Proliferation Assay Kit (Molecular Probes, Eugene, OR, USA).

High performance liquid chromatography (HPLC)

Segments of constructs were digested in 800 µl of 6 N HCl for 18 hours at 100°C prior to drying in a vacuum concentrator. Digested, dried samples were then re-suspended in 50 µl of 10 nmol pyridoxine/ml and 2.4 µmol homoarginine/ml. After a 5-fold dilution with 0.5% HFBA in 10% acetonitrile, 10 µl of each sample was run on the HPLC as previously described in the literature[323]. To quantify the crosslink content, PYR standards (Quidel, San Diego, CA, USA) were used.

Compressive testing

Following a previously established protocol, creep indentation testing was used to evaluate the compressive properties of the engineered neocartilage at the end of 6 weeks[359]. A micrometer was used to measure the thickness of a specimen prior to testing. Samples were then glued to a stainless steel surface and submerged in phosphate buffered saline for 15 minutes to reach equilibrium. Next, a 0.8 mm diameter flat, porous indenter tip was applied to the sample by a 0.7 g mass until the sample crept to equilibrium. Finally, a semi-analytical, semi-numerical, linear biphasic model was used to approximate the aggregate modulus (H_A), permeability, and Poisson's ratio as previously described[359].

Tensile testing

Tensile testing was conducted using an Instron uniaxial testing machine (Model 5565, Canton, MA, USA). After being cut into dog-bone shapes, sample thickness and width were measured via ImageJ software. Samples were then glued at either extremity to paper strips, which were loaded into the Instron grips. A pull to failure test was then run at a strain rate of 1% of the gauge length (measured as the distance between the glued ends of the dog bone) per second until sample failure. The Young's Modulus (E_Y) of the sample was calculated as the slope of the linear portion of the resulting stress vs. strain curve, while the ultimate tensile strength (UTS) was measured as the maximum stress reached during testing.

Statistics

To test the hypothesis that media supplemented with copper sulfate and hydroxylysine would improve the biomechanical properties of engineered articular cartilage, a 1-way ANOVA (n = 6 per group) was used. When the 1-way ANOVA showed significance ($p < 0.05$), a Fisher's *post hoc* test was applied. Data that had a positive interaction on an additive scale and resulted in a combined group that was greater than the addition of the two singular treatments were determined to be synergistic. Data for this study are represented as mean ± standard deviation (SD).

RESULTS

Gross morphology and histology

Table 1 describes the morphological characteristics of the neocartilage (wet weight, water content, thickness, diameter, and cell content). While constructs from all groups displayed uniform diameter, significant differences were detected in terms of their thickness, wet weight,

and water content. Controls presented significantly greater thickness and wet weight over all treated groups. The copper sulfate group displayed lower water content compared to all other groups. When applied alone, hydroxylysine promoted cell proliferation in the engineered tissue. No significant differences were found to exist among groups in terms of neocartilage morphology, with all constructs maintaining a smooth, flat, disc-shaped appearance (Table 1, Fig. 2). Histologically, all constructs stained positive for both collagen and GAG, as displayed in Figure 2.

Biochemistry

Collagen content normalized to construct wet weight (Col/WW) is presented in Figure 3A. The mean ± SD percentages of Col/WW were 1.10 ± 0.14, 0.77 ± 0.08, 0.98 ± 0.24, and 0.75 ± 0.12 for control, hydroxylysine, copper sulfate, and copper sulfate + hydroxylysine, respectively. While Col/WW was significantly decreased in all hydroxylysine-treated groups compared to controls, no significant differences were detected between the copper sulfate group and controls. GAG normalized to construct wet weight (GAG/WW) found the hydroxylysine group to have significantly higher GAG levels than all other groups (Fig. 3B). No significant differences were detected between controls and all copper sulfate-treated groups. The mean ± SD percentages of GAG/WW were 3.2 ± 0.3, 5.4 ± 1.1, 3.1 ± 0.3, and 4.9 ± 1.0 for control, hydroxylysine, copper sulfate, and copper sulfate + hydroxylysine, respectively. However, when GAG was normalized to cell content of the constructs, the hydroxylysine group had significantly lower amount of GAG content per cell, suggesting a decreased synthetic activity of the cells in this group.

HPLC was used to measure the amount of PYR crosslinks formed in the engineered neotissue (Fig. 3). When the amount of PYR crosslinks was normalized to construct wet weight

(PYR/WW), both treatments containing copper sulfate were found to have significantly greater numbers of crosslinks compared to controls (Fig 3C). With a value of 9.9 ± 5.5 nmol/g, the copper sulfate + hydroxylysine treatment resulted in a synergistic 1016% increase over control values, which were measured at 0.9 ± 0.8 nmol/g. The hydroxylysine and copper sulfate groups, on the other hand, were found to have 3.1 ± 1.5 nmol/g and 4.9 ± 0.9 nmol/g, respectively. When the amount of PYR crosslinks was normalized to collagen content of the constructs (PYR/Col), similar trends were detected (Fig. 3D). The mean ± SD values of PYR/Col were 0.08 ± 0.07, 0.39 ± 0.17, 0.49 ± 0.15, and 1.61 ± 0.15 nmol/mg for control, hydroxylysine, copper sulfate, and copper sulfate + hydroxylysine, respectively.

Biomechanics

To understand the influence of copper sulfate and hydroxylysine on the biomechanical properties of engineered articular cartilage, biomechanical testing was conducted (Fig. 4). Creep indentation testing found that all treatments significantly increased the H_A of the engineered neocartilage over controls (Fig. 4A). The mean ± SD of H_A values were 95 ± 41, 146 ± 50, 211 ± 35, and 153 ± 30 kPa for control, hydroxylysine, copper sulfate, and copper sulfate + hydroxylysine, respectively. The copper sulfate group presented the highest H_A and resulted in a 123% significant increase over controls. The mean ± SD permeability values were 3.07 ± 0.83, 4.05 ± 2.77, 4.06 ± 2.66, and 1.99 ± 2.04 × 10^{-15} $m^4/N{\cdot}s$, for control, hydroxylysine, copper sulfate, and copper sulfate + hydroxylysine, respectively, signifying no differences among the groups. Poisson's ratio, on the other hand, was significantly lower in the copper sulfate-treated group. The mean ± SD values were 0.24 ± 0.06, 0.27 ± 0.05, 0.13 ± 0.12, and 0.14 ± 0.11, for control, hydroxylysine, copper sulfate, and copper sulfate + hydroxylysine, respectively.

Tensile testing found that the copper sulfate and copper sulfate + hydroxylysine groups, with values of 1.0 ± 0.2 MPa and 1.3 ± 0.5 MPa, respectively, had significantly greater E_Y values than either the control or hydroxylysine groups (Fig. 4B). Specifically, the copper sulfate + hydroxylysine group presented the highest tensile modulus among all groups, resulting in a significant 3.3-fold increase over controls. No significant differences were detected between the control and hydroxylysine groups, with values of 0.4 ± 0.7 MPa and 0.4 ± 0.1 MPa, respectively. In terms of the UTS, the copper sulfate + hydroxylysine-treated group exhibited a higher value than all other groups (Fig. 4C). Overall, the UTS values of the engineered neotissue were 0.18 ± 0.03, 0.20 ± 0.05, 0.26 ± 0.06, and 0.46 ± 0.15 MPa for the control, hydroxylysine, copper sulfate, and copper sulfate + hydroxylysine, respectively.

DISCUSSION

The purpose of this study was to enhance collagen crosslinking in engineered articular cartilage and therefore improve the tissue's biomechanical properties. To carry out this goal, two agents with important *in vivo* roles in collagen crosslink formation were administered to the engineered tissue: copper sulfate and hydroxylysine. It was hypothesized that supplementing chondrogenic media with both copper sulfate and hydroxylysine would additively or synergistically increase the quantity of LOX-mediated collagen crosslinks in self-assembled articular cartilage, strengthening the collagen network and, thus, improving the tensile properties of the neotissue. The hypothesis was confirmed via a full factorial study design, demonstrating that the treatments enhanced both collagen crosslink content and biomechanical properties. Specifically, the combination of copper sulfate and hydroxylysine synergistically enhanced the PYR crosslinks of the neotissue by 1016% over controls, manifesting in a tensile modulus within this

group that was 3.3-fold larger than that of the control. In terms of the compressive properties, all treatments significantly increased the H_A over controls. The copper sulfate treatment displayed the highest compressive modulus and resulted in an 123% increase over controls. Novel contributions of this study include demonstrating that 1) exogenous application of both copper sulfate and hydroxylysine increase the number of collagen crosslinks in engineered cartilage, 2) these treatments enhance both the tensile and compressive properties of the tissue, and 3) when applied alone, hydroxylysine promotes cell proliferation within the 3-dimensional culture environment provided by self-assembly.

In addition to the novel contributions listed above, the treatments examined in this study resulted in other biochemical and morphological findings, which, when considered together, help explain the most significant findings of this study. For instance, all treated constructs presented with significantly lower thickness and higher pyridinoline content, suggesting that collagen crosslinking prevents expansive cartilage growth *in vitro*[360]. Further, concerning the proliferative effect of hydroxylysine, past work has shown that proliferative activity minimizes the synthetic activity of chondrocytes[361]. This may provide a plausible explanation of why these highly cellular constructs presented with significantly lower collagen and GAG (when normalized to the cell content), greater water content, and concomitantly lower biomechanical properties[272, 362]. It should be noted that no significant differences in cell number were found between control and copper sulfate + hydroxylysine-treated constructs. Possibly, the highly crosslinked collagen network within the combination-treated constructs inhibited the proliferative activity of hydroxylysine due to strong cell-ECM interactions[363]. Another possibility is that with addition of copper sulfate, LOX was activated even further, thus modifying and sequestering the proliferative effect of hydroxylysine. While this mechanism

remains unverified, the benefit of copper curtailing hydroxylysine's proliferative effect is that the combined treated group did not suffer from loss of GAG and collagen when normalized to cell content, unlike the hydroxylysine treatment group. This finding, in combination with the synergistic increase in pyridinoline crosslinks within the copper sulfate + hydroxylysine treated group, may provide an explanation of why the combined treatment resulted in constructs having higher tensile properties than all other treatments.

Copper sulfate was chosen in this study for its potential to enhance collagen crosslinking in engineered tissue based on its principal role in forming LOX-mediated PYR crosslinks *in vivo*. The importance of copper sulfate has been demonstrated in various developmental studies. Such work has linked dietary copper deficiencies in mammals with abnormal skeletal and vascular development[364]. Further, LOX activity has been correlated with dietary copper, indicating that abnormal development is likely due to the inability of LOX to form stabilizing crosslinks in copper-deficient animals[365]. The effect of copper sulfate on cartilage has also been studied *in vitro*. One such study found the addition of copper in the range of 0.001 – 0.034 mg/mL to upregulate collagen synthesis in cultured human articular chondrocytes by approximately 25%, while proteoglycan levels remained unchanged[366]. In a separate study, 0.002 – 0.319 mg/mL copper sulfate was administered to porcine cartilage explants grown *in vitro*. At concentrations of less than 0.016 mg/mL, the copper sulfate was found to have no effect on proteoglycan synthesis. However, at concentrations greater than 0.04 mg/mL, copper sulfate was found to cause a dose-dependent increase of this ECM protein[367]. Together, these studies signify the important effects of copper sulfate for the development of a stabilized collagen matrix in a dose-dependent manner.

While several investigations have taken place showing the important effect of copper sulfate from a developmental standpoint as well as on native cartilage explants and chondrocytes, no studies have thus far investigated the potential for copper sulfate to enhance engineered cartilage. It should be re-emphasized that the basic media formulations used in most cartilage tissue engineering endeavors, such as DMEM, do not contain copper sulfate, limiting LOX-mediated collagen crosslinking. Limited development of crosslinks could affect the biomechanical integrity of the forming collagen network, leading to the relatively low biomechanical properties observed in engineered tissues. Reflecting on past work in which chondrocytes were treated with copper sulfate, the present study supplemented self-assembled articular cartilage with 0.0016 mg/mL copper sulfate. Results found increased levels of collagen crosslinks (444% increase over controls) to correspond with significant, 2.2-fold changes in both the tensile and compressive properties compared to controls. Although this study did not directly assess the activation of LOX by copper sulfate, other studies have amply verified the dependence of LOX on the presence of copper[11, 12, 355]. Overall, the results of this study shed light onto the potential to improve engineered cartilage via the enhancement of PYR collagen crosslinking as promoted by copper sulfate supplementation.

The concentration of copper sulfate used in this study to promote PYR collagen crosslinking did not affect the viability of the cells within the engineered cartilage. Past work has found free circulating copper sulfate ions at physiological concentrations to lead to hydroxyl radical formation via reduction of Cu^{2+} by either superoxides or ascorbic acid, the latter of which is an important media component for engineered tissues[368, 369]. Therefore, when supplemented at too high of a concentration, copper ions can cause cellular toxicity. Results of this study found that the relatively low concentration of copper ions supplemented in the media

did not have a toxic effect on the cells, as the total cell number per construct did not significantly change in those subjected to copper sulfate. These results are similar to those found in a study on engineered arteries, where similar levels of copper sulfate were used with no toxic side effects[370]. Another possible detriment of using copper sulfate is that, in its ionic form, it has been shown to reduce the half-life of ascorbic acid[371]. With ascorbic acid being crucial for stimulating collagen production for *in vitro* tissue culture, decreasing the longevity of ascorbic acid could negatively impact collagen synthesis. Results, however, found that copper sulfate did not significantly change the amount of collagen in the engineered tissue, providing further validation that the amount used in this study is not deleterious to the formation of engineered articular cartilage.

Previously, only one study investigated the effects of copper sulfate on modifying the biochemical and structural properties of engineered tissue. In that case, engineered arteries were supplemented with either 0.2 or 0.4 g copper sulfate/ml for the entire 7-week culture period, or treated with 0.2 g copper sulfate/ml for the first 4 weeks followed by 0.4 g copper sulfate/ml for the remaining 3 weeks of the culture period. Results found the latter regimen of copper sulfate supplementation to increase the number of crosslinks in the tissue to 2.5 mol PYR/mol collagen, compared to 1 mol PYR/mol collagen in tissue treated with 0.2 or 0.4 g copper sulfate/ml supplemented for the entire duration of culture. In spite of the significant crosslink increase, no significant differences in the maximum elastic modulus or burst pressure of the engineered arteries were found[370]. The authors attributed this lack of improvement in tensile properties to the low levels of collagen fibrils present in their tissue[370]. In contrast, the present study showed copper sulfate was able to significantly increase both the number of crosslinks as well as the tensile properties of the tissue. Thus, as previously proposed[231], the tensile strength of a

collagen matrix does not only depend on collagen crosslinks, but also on the interplay within the collagen network among parameters such as fibril density, diameter, and orientation.

In addition to copper sulfate activation of LOX to catalyze the formation of PYR crosslinks, proper incorporation of lysine in both its normal and hydroxylated forms into the collagen fibrils is essential to crosslink formation[372]. Dietary supplementation of radiolabeled hydroxylysine has shown that hydroxylysine is not incorporated into skin collagen, as this amino acid can be readily processed by gut bacteria[373, 374]. In contrast, whether hydroxylysine made directly available to chondrocytes can be incorporated into collagen is currently unknown. With respect to articular cartilage, dietary supplementation versus direct medium addition of chondroitin sulfate can yield profoundly different effects[375-377], and the same might be the case for hydroxylysine. With regards to the incorporation of amino acids in their hydroxylated forms into collagen fibrils, only a limited number of studies currently exist. Exogenously administered hydroxylysine is capable of being incorporated into proteins *in vitro* by prokaryotic microorganisms[378, 379], which share a similar pathway to mammalian cells to generate protein out of amino acids[380]. Work using chick embryos has shown that exogenous hydroxyproline can be incorporated into collagen molecules[381], suggesting that hydroxylysine might likewise be incorporated into collagen in this study.

Although the way chondrocytes use exogenously applied hydroxylysine remains unknown, the present study has found the combination of hydroxylysine and copper sulfate to synergistically increase the PYR content of the neotissue more than 10-fold. Physiologic PYR levels in 1 – 3 week-old bovine articular cartilage have been reported at 95.5 ± 29.4 nmol/g[348]. Should the generated cartilage be implanted, crosslinks within the implant are expected to continue to increase by utilizing the copper that is naturally available *in vivo*. While the

combined treatment promoted a synergistic increase in the PYR content of the neotissue over the individual treatments, a significant, although not synergistic, enhancement was observed in the tensile properties of the constructs of the same group. This suggests that a non-linear correlation may exist between collagen crosslinks and the tensile properties of engineered tissues. There is also the possibility of crosslinks forming between monomeric hydroxylysines outside of the collagen fibers. Future studies will therefore be important to help elucidate how chondrocytes interact with exogenously applied hydroxylysine.

Aside from the physical architecture of the collagen matrix, it has been shown that the ability of LOX to generate collagen crosslinks is dependent on the monomeric or polymeric state of the collagen fibers themselves. LOX activity has been found to be dependent on the molecular chain length of the substrate[382]. Specifically, LOX activity was much higher on intact collagen fibrils than on monomeric collagen. It was suggested that LOX acts on collagen fibril intermediates, binding to and stabilizing growing, as opposed to mature, fibrils. Therefore, it can be seen that recapitulating the *in vivo* formation of collagen fibrils is crucial for enzyme-mediated collagen crosslinking. This suggests that perhaps the way collagen fibrilogenesis occurs *in vitro* does not provide LOX with the intermediate collagen fiber substrate it requires, decreasing its ability to correctly form PYR crosslinks in engineered tissue. Future work toward better understanding collagen matrix formation in engineered tissues and how it compares to that of native tissues may help explain why engineered tissues have comparatively inferior biomechanical properties. Such studies will help provide insight toward developing more mechanically functional collagen networks in engineered tissues which will, in turn, help advance the field toward generating clinically relevant replacement and reparative tissues.

While this study hypothesized that enhanced collagen crosslinking would increase the tensile properties of engineered articular cartilage, results found the copper sulfate treatment to also significantly enhance the compressive properties of the tissue by 123% over control values, as well as over other treated groups. Interestingly, results found the hydroxylysine containing groups to have significantly increased GAG/WW over controls; GAG levels in copper sulfate-treated constructs, however, were not significantly different than controls. This result may at first appear counterintuitive, especially when one considers the structure-function paradigm associated with articular cartilage, that tensile properties are associated with collagen content while compressive properties are linked to GAG content[346]. Although GAG plays an important role in providing articular cartilage with compressive robustness, recent reports have found collagen density and organization also to be important for the compressive properties of this tissue[335, 347, 348]. It has been shown that a better collagen network can more effectively immobilize negatively charged proteoglycans, thus increasing the mechanical stability of the network in both tension and compression[383]. Therefore, with increased collagen crosslinks, it follows that the increased stabilization of the collagen network increases resistance to compressive loading. Additionally, the copper sulfate alone treatment significantly decreased the water content of the engineered neotissue. With no significant differences between the thickness and diameter of the copper sulfate-treated constructs compared to all other groups, this suggests that copper sulfate promotes the development of a denser ECM. This is further corroborated by maintenance of the collagen and GAG content in this group compared to controls. Taken together, copper sulfate appears to yield a functionally superior ECM in engineered neocartilage in terms of construct biomechanical properties. With both tensile and

compressive properties improved, copper sulfate offers much promise as a potent agent toward generating clinically relevant repair cartilage.

An additional finding in this study was that exogenous application of hydroxylysine significantly increased the number of cells per construct, 117% over controls. This finding is pertinent to the field of tissue engineering, as a major problem with clinically relevant cell sources is their limited availability. When working with such cell sources, methods to induce *ex vivo* proliferation are therefore necessary to achieve high enough cell numbers to engineer tissues. Unfortunately, past work has found that passaging and expanding cells in monolayer typically leads to a loss of phenotype[384]. Results of this study suggest that simply adding hydroxylysine to the media of engineered neocartilage significantly increases cell numbers. Although the potential of hydroxylysine, as any chemical agent applied to articular chondrocytes, to affect the phenotype of the cells exists, application of hydroxylysine in the combined group resulted in significantly increased mechanical properties and cartilage-like tissue as also confirmed by histology and biochemistry. Thus, results of this study suggest that hydroxylysine did not alter the chondrogenic phenotype. While future work should be carried out to investigate the effects of hydroxylysine as a potent proliferative agent in different 3-dimensional environments, using other cell types, as well as monitoring cellular phenotype following proliferation, this work promises a new avenue to promote the expansion of cells in 3-dimensional culture. Ultimately, this may be an important step toward solving the limited availability of clinically relevant cell sources for tissue engineering applications.

Making up 50-80% of the dry weight of articular cartilage, collagen fibers act as the main mechanical support structure of cartilage, providing the tissue with the means to effectively distribute and withstand high tensile loading within the joint space[385]. While offering

much promise as an effective remedy for diseased cartilage, engineered cartilage replacements currently do not have the mechanical strength to withstand the high levels of *in vivo* loading. This study focused on a novel approach to enhance the tensile properties of engineered cartilage through reinforcing the collagen network via PYR crosslinks. Using copper sulfate and hydroxylysine, two important agents in the development of such crosslinks, this study found the use of both agents to synergistically enhance the number of PYR crosslinks in the engineered tissue. Further, both copper sulfate and copper sulfate + hydroxylysine treatments significantly enhanced the tensile properties of the tissue. Additionally, all treatments significantly increased the compressive modulus over controls, with the copper sulfate treatment displaying the highest values. Hydroxylysine was also identified as a promising agent to promote cellular proliferation in a 3-dimensional culture environment. Overall, this work speaks to the importance of ensuring proper collagen crosslinking in the generation of robust tissues capable of having a clinical impact. Future work should attempt to understand how hydroxylysine is used by articular chondrocytes, use gene expression assays to investigate whether copper sulfate upregulates LOX expression, as well as focus on understanding how collagen networks are developed in engineered tissues. Together, such work will aid in the quest to generate clinically relevant regenerative tissues.

TABLES AND FIGURES

TABLE 2.1 – ENGINEERED NEOCARTILAGE'S PROPERTIES AT THE END OF A 6-WEEK CULTURE PERIOD. Values marked with different letters within each category are significantly different ($p < 0.05$), with A > B > C.

Group	Wet weight (mg)	Water content (%)	Thickness (mm)	Diameter (mm)	Cells/construct (millions)
Control	51.9 ± 2.7^{A}	86.9 ± 1.9^{A}	1.95 ± 0.34^{A}	5.94 ± 0.12	6.08 ± 3.31^{B}
Hydroxylysine	45.2 ± 1.2^{B}	86.7 ± 1.3^{A}	1.45 ± 0.06^{B}	6.01 ± 0.16	13.2 ± 1.84^{A}
Copper sulfate	29.3 ± 1.8^{C}	83.2 ± 2.2^{B}	1.20 ± 0.08^{B}	5.86 ± 0.21	8.09 ± 2.31^{B}
Copper sulfate + hydroxylysine	28.9 ± 1.1^{C}	86.5 ± 1.3^{A}	1.29 ± 0.11^{B}	6.01 ± 0.17	7.25 ± 4.36^{B}

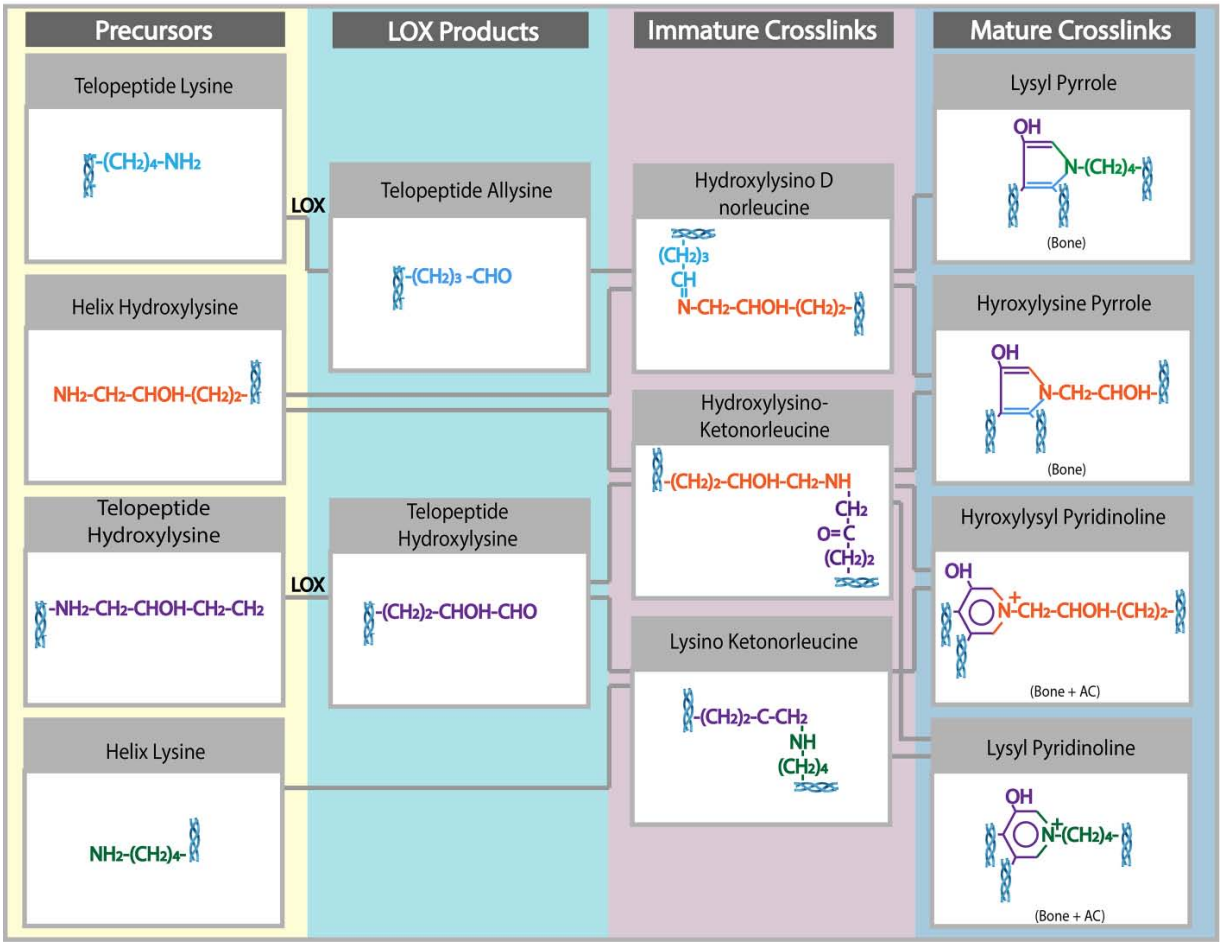

FIGURE 2.1 – MOLECULAR MECHANISM OF LOX-MEDIATED PYR COLLAGEN CROSSLINKING. The molecular pathway of collagen crosslinks in musculoskeletal tissues initiated by the extracellular enzyme LOX. Triple helix and telopeptide lysines are tracked by color, from initial to mature crosslinks. Bone contains both PYR and pyrrole collagen crosslinks, while articular cartilage features only PYR crosslinks. (Adapted from Eyre *et al.*[355]).

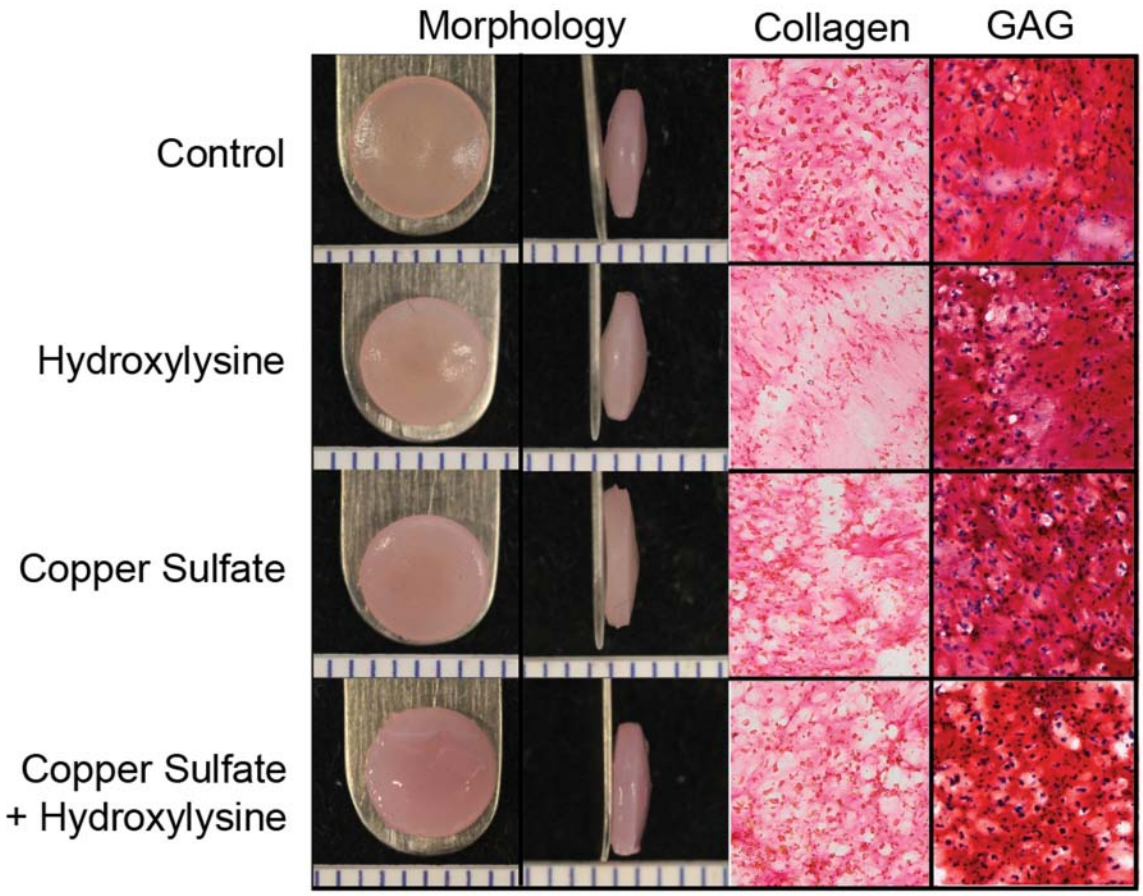

FIGURE 2.2 – GROSS MORPHOLOGY AND HISTOLOGY OF SELF-ASSEMBLED NEOCARTILAGE AT THE END OF THE 6-WEEK CULTURE PERIOD. Both control and treated constructs formed uniform neocartilage without physical abnormalities. Constructs stained positive for Safranin-O/Fast Green staining for GAG and Picrosirius Red staining for collagen in all groups.

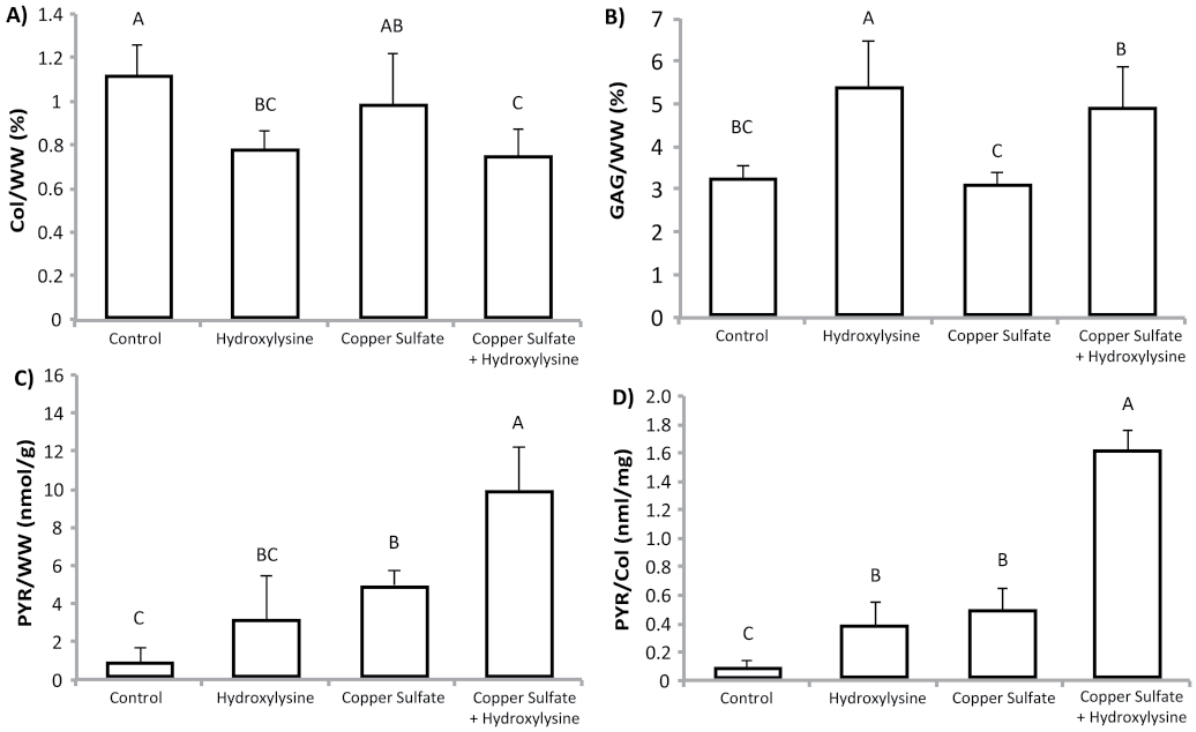

FIGURE 2.3 – BIOCHEMICAL PROPERTIES OF TISSUE-ENGINEERED NEOCARTILAGE. A) Col/WW, B) GAG/WW, C) PYR/WW, and D) PYR/Col. Col/WW was significantly decreased in all hydroxylysine-treated groups compared to controls. No significant differences were detected between the copper sulfate group and controls. In terms of GAG/WW, no significant differences were detected between controls and the copper sulfate-treated groups, while hydroxylysine significantly increased the amount of GAG/WW over controls. HPLC found all copper-sulfate treated groups to have significantly greater amounts of PYR/WW compared to controls, with a synergistic increase measured in the copper sulfate + hydroxylysine group. Similar trends were detected when the amount of PYR crosslinks were normalized to construct collagen content. Bars denote means ± SD, and groups not connected by the same letter are statistically different ($p<0.05$).

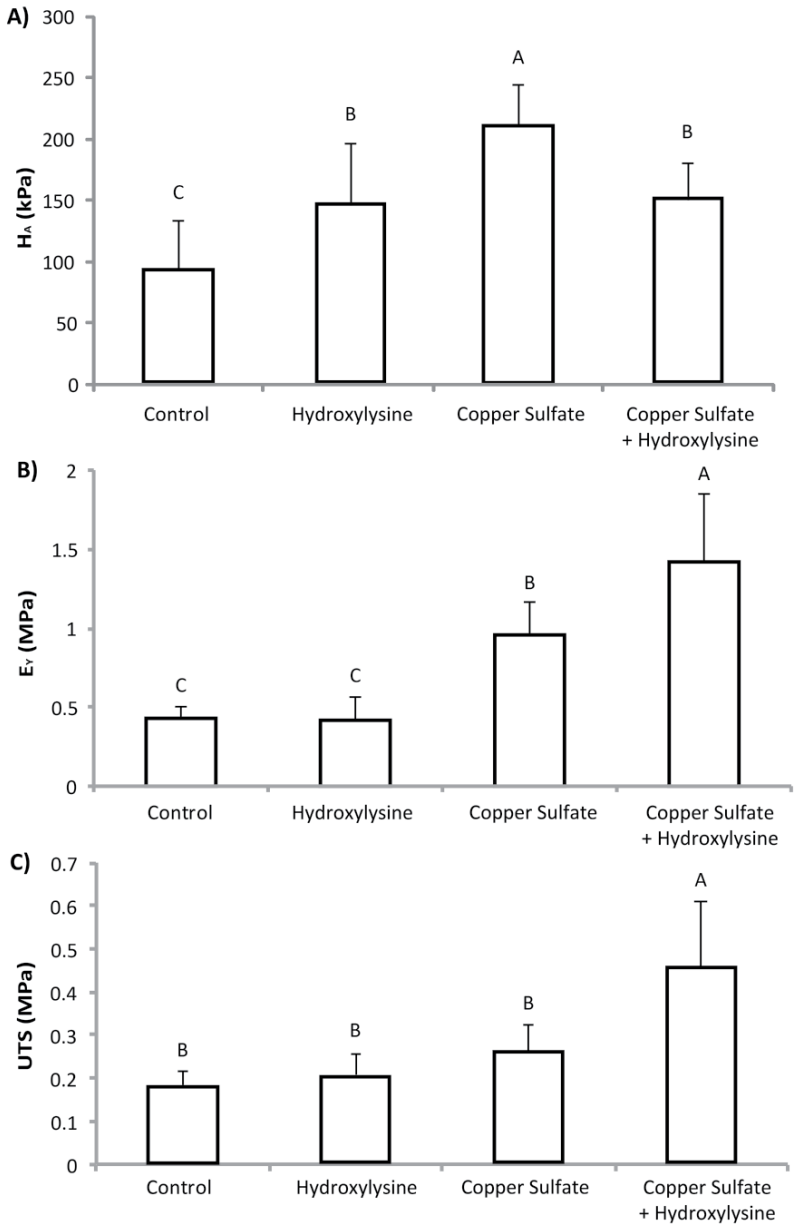

FIGURE 2.4 – BIOMECHANICAL PROPERTIES OF SELF-ASSEMBLED NEOCARTILAGE. A) H_A B) E_Y, and C) UTS. Creep indentation testing found that all treatments significantly increased the compressive modulus of the engineered neocartilage. The copper sulfate group presented the highest H_A and resulted in a 123% significant increase over controls. Both the copper sulfate and copper sulfate + hydroxylysine groups significantly increased the tensile modulus of the constructs over the control and hydroxylysine groups. The copper sulfate + hydroxylysine group presented the highest tensile modulus among all groups, resulting in a significant 3.3-fold increase over controls. Results for the UTS, however, found only the copper sulfate + hydroxylysine group to be significantly higher than all groups. Bars denote means ± SD, and groups not connected by the same letter are statistically different ($p<0.05$).

CHAPTER 3 – HYPOXIA-INDUCED COLLAGEN CROSSLINKING AS A MECHANISM FOR ENHANCING MECHANICAL PROPERTIES OF ENGINEERED ARTICULAR CARTILAGE.

ABSTRACT

Objective: The focus of tissue engineering of neocartilage has traditionally been on enhancing extracellular matrix and thus biomechanical properties. Emphasis has been placed on the enhancement of collagen type and quantity, and, concomitantly, tensile properties. The objective of this study was to improve crosslinking of the collagen network by testing the hypothesis that hypoxia could promote pyridinoline (PYR) crosslinks and, thus, improve neocartilage's tensile properties.

Methods: Chondrocyte expression of lysyl oxidase (LOX), an enzyme responsible for the formation of collagen PYR crosslinks, was first assessed pre- and post- hypoxia application. Then, the mechanical properties of self-assembled neocartilage constructs were measured, after 4 weeks of culture, for groups exposed to 4% O2 at different initiation times and durations, i.e., during the 1st and 3rd weeks, 3rd and 4th weeks, 4th week only, continuously after cell seeding, or never.

Results: Results showed that LOX gene expression was upregulated ~20-fold in chondrocytes in response to hypoxia. Hypoxia applied during the 3rd and 4th weeks significantly

Chapter published as: Makris, E.A., MacBarb, Hu, J.C., & Athanasiou, K.A. Hypoxia-induced collagen crosslinking as a mechanism for enhancing mechanical properties of engineered articular cartilage. In: *Osteoarthritis and Cartilage*. 21(4): 634-641, 2013.

increased PYR crosslinks without affecting collagen content. Excitingly, neocartilage tensile properties were increased ~2-fold. It should be noted that these properties exhibited a distinct temporal dependence to hypoxia exposure, since upregulation of these properties was due to hypoxia applied only during the 3rd and 4th weeks.

Conclusions: These data elucidate the role of hypoxia-mediated upregulation of LOX and subsequent increases in PYR crosslinks in engineered cartilage. These results hold promise toward applying hypoxia at precise time points to promote tensile integrity and direct construct maturation.

INTRODUCTION

Articular cartilage (AC) pathologies, as a result of injury/trauma or age-related degeneration, are a major health problem in the developed world. Osteoarthritis (OA) is undoubtedly the most frequent chronic musculoskeletal disease, limiting the daily activities of the elderly (1). Over the past two decades, progress has been made on the development of therapeutic approaches for the treatment of early stage cartilaginous defects, thus slowing down their progression to OA. However, current therapeutic procedures including washing, shaving and debridement, stem cell stimulation-based procedures and explant grafts have thus far proved to be incapable to effect long-term cartilaginous repair (2). Tissue engineering has the potential to generate tissues by developing a biomechanically competent extracellular matrix (ECM) *in vitro* (3). However, limitations in the development of neotissues that mimic the structural composition and, hence, biomechanical behavior of native tissues present a great challenge in that field (4). Therefore, it is important for technologies to be developed that generate neotissues capable of bearing

physiological loads, and various exogenous stimuli during neocartilage culture have been examined.

In engineering cartilage, hypoxia has been proposed for both stem cells and differentiated chondrocytes. For stem cells, hypoxia has been reported to promote chondro-differentiation (5-7) and to impede hypertrophy (8). Hypoxia inducible factor 1 (HIF-1) has been hypothesized as critical for hypoxic induction of chondrogenesis (8). For engineering articular cartilage, however, hypoxia has shown mixed results. For instance, some studies have suggested that Sox9 expression is largely independent of hypoxia (9), while others have shown that this transcription factor increases with reduced oxygen levels (10). Likewise, extracellular matrix (ECM) components (e.g., aggrecan, collagen type II, proteoglycan 4) have been shown to be upregulated with hypoxia in certain cases (10, 11), while others have shown that cartilaginous ECM production is indifferent to hypoxia (12) or even suppressed by it in certain instances (13, 14). In brief, though the majority of evidence supports hypoxia as an effective method for enhancing engineered cartilage constructs, mechanisms behind such improvements have largely remained elusive. For hypoxia to be used efficiently and reliably in cartilage tissue engineering, a robust mechanistic connection between hypoxia and mechanical properties must be determined.

In the human body, normal oxygen tension, or normoxia, is between 5-13% (15). Oxygen levels lower than 5% are considered hypoxic (16), while the atmospheric oxygen tension of 21% should be considered hyperoxic (17). For differentiated chondrocytes, oxygen tension can be as low as 1–2.5%, thus qualifying cartilage as functioning under a hypoxic environment (14). As a result, oxygen concentration during *in vitro* culture likely needs to be

below 5% to induce significant hypoxia inducible factor 1 (HIF-1) stabilization and its subsequent up-regulation of various matrix-associated genes.

The anisotropic, structural and mechanical properties of articular cartilage, including its well-developed, collagen fiber architecture, determine the functionality and mechanical integrity of the tissue (18). Apart from collagen content and organization, the load-bearing capacity of collagen is related to other ECM components. Two features that directly influence the stiffness of native articular cartilage and determines the maturity of collagen are the type and quantity of collagen crosslinks (19, 20). Thus far, these critical features have not been sufficiently mimicked in the ECM of engineered tissues; lack of progress on this front may be a factor for the current limitations in tissue modulus and strength (19, 21). An opportunity exists in the modulation of collagen crosslinking in engineered neocartilage to enhance tissue structural and functional integrity. While hypoxia has been associated with collagen crosslinking in several other tissues (22-24), its use for inducing crosslinks in engineered cartilage remains unexplored.

In this study, engineered cartilage is formed using a scaffoldless, self-assembling process that removes the potentially confounding effects of scaffolds. The objectives of this study are to examine two hypotheses: 1) that hypoxia (4% oxygen) will enhance the mechanical properties of engineered articular cartilage by mediating collagen crosslinking via LOX, and 2) this specific response to hypoxia is dependent on application time.

MATERIALS AND METHODS

Chondrocyte isolation

Articular cartilage was sterilely harvested from the distal femur of knee joints obtained from 1-week-old calves (Research 87, Boston, MA, USA). Tissue was minced into 1 mm pieces and

digested in 0.2% collagenase type II (Worthington, Lakewood, NJ, USA) for 18 hours in cell culture medium (Dulbecco's modified Eagle's medium (DMEM) with low glucose (1g/L)) (Life Technologies corp., Carlsbad, CA, USA), 10% fetal bovine serum (FBS) (Atlanta Biologicals), 1% non-essential amino acids (NEAA) (Life Technologies corp., Carlsbad, CA, USA), 25 mg of L-ascorbic acid (Sigma-Aldrich, St. Louis, MO, USA), and 1% penicillin/ streptomycin/ fungizone (PSF) (BioWhittaker Inc., Walkersville, MD, USA). After digestion, articular chondrocytes were washed three times in PBS with centrifugation and filtered through a 70-μm filter. Cells then were counted and were frozen at -80°C in culture medium supplemented with 10% FBS and 10% dimethyl sulfoxide (Fischer Scientific, Pittsburgh, PA, USA). Cells were then stored in liquid nitrogen until used.

Construct formation via the self-assembling process

Constructs were generated by seeding articular chondrocytes into cylindrical, non-adherent wells using a technique adapted from previous work (3, 25). A stainless steel mold consisting of 5 mm diameter cylindrical prongs was placed into molten 2% agarose (Life Technologies corp., Carlsbad, CA, USA) in a 48-well plate. The agarose solidified at room temperature, and the mold was removed. Two changes of control medium (DMEM with GlutaMAX (Life Technologies corp., Carlsbad, CA, USA), 100 nM dexamethasone (Sigma-Aldrich, St. Louis, MO, USA), 1% NEAA, 1% PSF, 1% ITS+ premix (BD Scientific, Franklin Lakes, NJ, USA), 50 mg/mL ascorbate-2-phosphate (Sigma-Aldrich, St. Louis, MO, USA), 40 mg/mL L-proline (Sigma-Aldrich, St. Louis, MO, USA), and 100 mg/mL sodium pyruvate (Fischer Scientific, Pittsburgh, PA, USA)) were used to saturate the agarose before cell seeding. Following isolation, articular chondrocytes were thawed within 5 days of freezing. Viability assessed using

trypan blue was >90%. To create each construct, 5.5 million cells in 100 µl control medium were seeded into each gelled, cylindrical agarose well, followed by addition of 400 µl control medium after 4 h. Cells coalesced into free-floating, disc-shaped constructs upon the non-adhesive agarose; t = 1 day was defined as 24 h after seeding. Constructs were cultured in the agarose wells until t = 10 days, at which point they were unconfined transferred to 48-well plates where they were unrestricted by circumferential confinement. Constructs received 500 µl medium change every 24 h and remained in culture until t = 28 days. All culture was at 37 °C and 10% CO_2.

Hypoxia application

Following seeding, constructs were divided into five treatment groups. Constructs in the first group (control) were incubated continuously at 37°C, 5% CO_2, and 21% O_2. Constructs from the other groups were incubated under the same conditions but also treated with 4% O_2 (hypoxia) during the following culture periods: t=1-7 days and 15-21 days (1^{st} and 3^{rd} weeks), t= 8-14 days and 22-28 days (3^{rd} and 4^{th} weeks), t=22-28 days (4^{th} week), and t=1-28 days (continuous hypoxia). Every other day, 500µl of medium was changed. After four weeks of culture, constructs were divided into parts for histological, biochemical, and biomechanical assessments.

Histology

Samples of the neotissue were cryoembedded in Histoprep (Fisher Chemical, Vernon Hills, IL, USA) and sectioned at 14 µm with orientation from top to the bottom of the construct, in all groups. Following sectioning, samples were fixed in formalin for 15 min. Qualitative evaluation

of collagen and GAG content of the samples was performed by using Safranin-O/fast green and Picrocirious red stains as previously described (26). Phenotype maintenance of articular chondrocytes was evaluated with immunohistochemistry (IHC). Briefly, samples were fixed in chilled (4°C) acetone, rehydrated, and stained for collagen type I and II by following protocols provided by Chondrex and Vectastain as previously described (26). Native bovine articular cartilage and patellar tendon were used as positive type II and type I controls, respectively.

Quantitative biochemistry

Biochemical samples were lyophilized, and dry weight was recorded. Subsequently, samples were digested using a pepsin-elastase protocol as previously described (26). Collagen content in the engineered tissue was evaluated using a colorimetric hydroxyproline assay (27).A Blyscan Glycosaminoglycan Assay kit (Biocolor, Newtownabbey, Northern Ireland) was used for sulfated GAG content quantification (28) . Cell content in the engineered tissue was approximated using a Picogreen dsDNA reagent (Molecular Probes, Eugene, OR, USA) for DNA quantification and a conversion factor of 7.7 pg DNA/cell.

High performance liquid chromatography

The abundance of pyridinoline crosslinks in the engineered tissue was quantified using high performance liquid chromatography (HPLC). Portions of the constructs were weighed wet, digested in 400μl 6N HCL and dried in a vacuum concentrator. 50 μL of an aqueous solution containing 10 nmol pyridoxine/mL and 2.4 μmol homoarginine/mL was used for sample re-suspension and then diluted fivefold with an aqueous solution of 0.5% HFBA acetonitrile in 10% acetonitrile. Following this, 10 μL of each sample was injected into a 25 mm C18 column (Shimadzu, Columbia, MD, USA) and eluted using a solvent profile as previously described

(29). A calibration curve was performed using pyridinoline standards (Quidel, San Diego, CA, USA) for crosslink quantification.

Creep indentation testing

Compressive properties were evaluated using creep indentation as previously described (30). Specimens equilibrated in PBS for 15 minutes and then indented to ~15% strain using a flat, porous indenter tip (0.8 mm diameter). The compressive properties of the samples were obtained using a semi-analytical, semi-numeric, linear biphasic model (30).

Tensile testing

Tensile properties were determined using a uniaxial material testing apparatus (Instron Model 5565) and tested as previously described (31, 32). Samples were tested until failure by applying a strain rate of 1% of the gauge length per second. Tensile stiffness and ultimate tensile strength (UTS) were determined based on stress-strain plots.

RT-PCR

Real time PCR analysis was performed to investigate hypoxia-mediated gene expression of the target genes. Dynamic changes in LOX expression can occur during the first 18 hours of a culture's introduction to hypoxia (17, 33). In order to observe LOX expression at steady state, measurements within the short time period immediately after hypoxia exposure were avoided. On the other hand, since LOX-induced crosslink formation can require weeks to mature, it was desirable to assess for LOX expression as early as possible. Thus, hypoxia was applied in 3 wk-engineered neocartilage for two days and the gene expression of lysyl oxidase was quantified as

previously described (17). S18 (housekeeping gene) and lysyl oxidase (LOX) primers were purchased from US Biological. RT was performed by incubating 500 ng of RNA with SuperScript III (Life Technologies corp., Carlsbad, CA, USA) as recommended by the manufacturer. Real-time PCR was done using SYBR Green mastermix and 1 μm primers on a Rotor-gene 3000 real-time PCR machine (Corbett Research, Bath, UK). A 10 min denaturing step was employed, followed by 45 cycles of 95 °C (15 s) and 60 °C (60 s). The take-off cycle (C_T) for each gene of interest (GOI) was compared to the housekeeping gene GAPDH. Relative gene expressions were calculated using the $2^{-\Delta\Delta CT}$ method.

Statistical analysis

All biochemical and mechanical assessments in this study were performed using n = 5 - 8 samples per group. Numerical data are represented as mean ± 95% confidence interval for the mean (95% CI). The presence of outliers was determined using either Grubb's test and/or by noting assaying errors. Prior to performing statistical tests, the data were checked for both normality and equal-variance using Levene's test. To compare among equal treatment groups one-way analysis of variance (ANOVA) was performed using StatView software (StaView inc Cary, Nesbit, MS, USA). If significance was identified, Fisher's post hoc testing was applied. Unequal sample sizes were addressed by nonparametric all-pairs multiple comparisons based on pairwise rankings in the one-way design with the Steel-Dwass procedure. P-values less than 0.05 were considered significant.

RESULTS

Gross morphology and histology

At the end of the culture period the morphological properties and composition of the engineered constructs were assessed via gross inspection and histological evaluation. All constructs presented with similar flat surfaces without abnormalities and no significant differences were detected in morphology among the groups. Table 1 describes morphological characteristics (diameter, thickness, and wet weight) of the constructs. Histology showed that all constructs stained uniformly positive for both GAG and collagen content (Fig. 1). Additionally, IHC showed that neocartilage from all groups stained positive for collagen type II and negatively for collagen type I proving normal articular cartilage phenotype maintenance in all groups (Fig. 1).

Biochemical properties

Growth of the constructs was evaluated through assessment of the amount of collagen, GAG, DNA, and PYR of neotissue at the end of the culture period. Table 2 describes the biochemical characteristics of the constructs. Concerning the GAG content normalized to constructs' wet weight no significant differences were detected among the groups (p=0.718). In terms of the percentage of collagen normalized to construct wet weight (Col/WW), no significant differences were detected among control, and late hypoxia application groups (3rd and 4th weeks, and 4th week group) (p=0.2716 and p=0.9919 respectively). Interestingly, constructs treated with hypoxia at an early stage (1st and 3rd weeks and all weeks groups) presented with significantly lower amount of collagen over control and late treated groups (p=0.004 and p=0.004). Hypoxia applied during 3rd and 4th weeks significantly increased the amount of PYR/WW over controls (34% increase) (p=0.003), while no significant effects were detected on the other applied groups over controls (p=0.4160, p=0.9753, and p=0.9991 for 1st and 3rd weeks, 4th week and continuous groups, respectively) (Table 2). However, when pyridinoline content normalized to constructs'

collagen content (PYR/Col) early application of hypoxia (1st and 3rd weeks, continuous groups) exhibited the highest amount of collagen crosslinks (p<0.001 and p=0.001, respectively) (Table 2). Furthermore, in the 3rd and 4th weeks group the amount of PYR/Col was significantly higher over controls (p=0.0499), while in the 4th week group no significant differences were detected (p=0.4583). Results suggest that early hypoxia treatment, although it significantly decreases collagen synthesis in the engineered tissue, promotes higher pyridinoline crosslinks than when applied late during the self assembling process. The 3rd and 4th weeks hypoxia application group suggests an optimal treatment for promoting collagen crosslinking without affecting the collagen content of the constructs and, thus, enhancing the mechanical properties of the engineered tissue.

Biomechanical properties

To quantify the influence of low oxygen tension applied at different time periods on biomechanics of self-assembled neocartilage, compressive properties represented by the aggregate modulus, permeability and poison's ratio and tensile properties represented by Young's modulus (E_Y) and UTS and were determined. On regards of compression properties no significant difference was detected among the groups (p=0.4017, p=0.1101, and p=0.3124 for aggregate modulus, permeability, and Poisson's ratio, respectively) (Table 3). Low oxygen tension applied during 3rd and 4th weeks of self assembling process significantly increased the tensile stiffness of the constructs over control group (~80% increase) (p<0.0001). Similar trends were observed concerning the UTS of the constructs (Table 3). Enhanced mechanical properties reflected the observed changes in the pyridinoline content.

RT-PCR

Real time PCR was employed to investigate the effects of hypoxia in the engineered neocartilage using the self-assembly method. Application of hypoxia in the neotissue promoted 18-fold increase in the gene expression of lysyl oxidase over controls cultured under normoxic conditions.

DISCUSSION

This is the first study to demonstrate that hypoxia's effect on enhancing engineered cartilage's tensile properties is through collagen crosslinking. Experimental data proved both hypotheses motivating the study, showing 1) hypoxia is a viable method for promoting collagen crosslinking in engineered tissue through LOX gene expression and 2) distinctly different responses can be elicited by this stimulus by manipulating application time and duration. Hypoxia can be restricted to influence only the tensile properties of the constructs, while other neocartilage properties such as gross morphology, collagen and GAG biochemistry, and compressive stiffness remain unaltered. By determining a method wherein hypoxia can be isolated to act only through collagen crosslinks, this study provides a robust method for improving the tensile properties of engineered cartilage that has the potential to be extended to other engineered tissues.

In this study, hypoxia was applied in tissue engineered articular cartilage to enhance crosslinking by promoting gene expression of lysyl oxidase. Low oxygen tension (4% O_2) applied during the 3rd and 4th weeks of self assembly of neocartilage significantly increased the amount of pyridinoline molecules (PYR/WW and PYR/Col) over controls and the other treated groups with concomitant increase in the gene expression of lysyl oxidase (18-fold) over

controls. In contrast, no significant differences were observed among the 3rd and 4th weeks, the 4th week and control groups for collagen, GAG and DNA content per WW and DW. Additionally, hypoxia applied during the 3rd and 4th weeks increased the tensile stiffness of neocartilage by approximately 80% over controls $p<0.0001$). These results demonstrate that application of hypoxia can be directed to promote collagen crosslinking and enhance the tensile properties in engineered cartilage, independently of other biochemical and biomechanical properties.

In contrast, hypoxia applied during times other than the 3rd and 4th weeks did not result in improved properties. At times, these properties were diminished, shedding light onto the mixed results seen in the cartilage engineering literature that employ hypoxia. Specifically, early application of hypoxia (1st and 3rd weeks and continuous application groups) significantly increased the PYR/Col content. This can be explained by the longer time that hypoxia-mediated collagen crosslinking formation was allowed to develop in these groups compared to late application groups. For instance, the characteristic time constants for the formation of immature (difunctional) and mature (trifunctional) pyridinoline crosslinks have been reported to be 1-2 and 7-30 days, respectively (34). However, early hypoxia application had no effect on PYR/WW and significantly decreased the collagen content of neotissue at these groups. Thus, the mechanical properties of neotissue remained unchanged. Biochemical evaluation further showed no significant differences in terms of the number of cells per construct and GAG/WW in these groups; It would, thus, appear that early hypoxia application is actually detrimental to engineering self-assembled cartilage when it is applied during a time previously identified as the collagen synthesis phase (25).

These results are similar to a previous study investigating the effects of 5% and 20% O_2

applied continuously for 2, 4 and 6 weeks in a scaffold-free chondrocyte culture (13). In this study, engineered cartilage from scaffold-free cultured chondrocytes at 20% O_2 produced better ECM than that at 5% O_2. Thus, the present study offers an examination on the conflicting results currently seen with hypoxia; hypoxia applied during the collagen synthesis phase of engineered cartilage can diminish collagen production and therefore adversely affect construct biomechanical properties. This time dependence issue should be further investigated in other cartilage engineering approaches.

In 3-dimensional cultures or engineered tissues, work on studying the effects of different oxygen concentrations might be impaired by poor oxygen diffusion that creates an oxygen gradient within tissue (35). Additionally, HIF-1α protein is very unstable at the environmental oxygen level while its mRNA is not affected by hypoxic conditions (16). This makes it difficult to demonstrate, experimentally, HIF-1α protein increases in response to hypoxia. However, the link between hypoxia, LOX gene expression, and LOX-mediated collagen crosslinking has been explored in many other tissues (17, 23, 25, 36). Specifically, growth of porcine aortic endothelium cells in 0% or 2% oxygen tension resulted in little change in cell numbers or cell protein, but a fall in collagen synthesis and in proline and lysine hydroxylases, as well as a rise in LOX gene expression, were observed (36). Similarly, the crosslink pattern and the gene expression of lysyl hydroxylase 2 (LH2) were investigated using skin cells from systemic scleroderma, cultured under low oxygen tension conditions. Prolonged hypoxia induced a marked increase of the mRNA level of LH2 in relation to collagen I (22). Thus, the use of hypoxia to promote LOX- and LH- mediated collagen crosslinking can be considered as a robust mechanism and this experiment showed not only that hypoxia can be used in engineering cartilage, but that its effects can be isolated to tensile properties only.

Further proof of the robustness of the hypoxia-tensile relationship can be seen in engineering other tissues (17, 35, 37). It has been reported that 7% O_2 applied in human vascular-derived myofibroblasts seeded onto a biodegradable scaffold similarly increases construct properties as seen in this study (37). In another case, 4% O_2 enhanced gene expression of LOX and LH2 (17). It is, thus, conceivable that the use of hypoxia can be translated to other musculoskeletal tissues. The extracellular matrix of native ligaments, tendons, bone, and other musculoskeletal tissues is composed of proteoglycans and fibrillar proteins, such as elastin and collagen. The load-bearing capacity of collagen is, apart from collagen content and organization, highly dependent on collagen crosslinking, which stabilizes the collagen fibrils (38). The *in vitro* formation of these highly important ECM components can be affected by mechanical, biochemical, and environmental stimuli, such as oxygen concentration (37, 39, 40). As with this experiment, hypoxia could potentially improve the mechanical properties of other engineered musculoskeletal tissues through collagen crosslinking enhancement. However, application time for these engineered tissues must be optimized as to restrict its effects on crosslinks only.

Due to HIF-1α's link with other ECM gene expression, this study provides strong support for further development of other hypoxia duty cycles. Specifically, hypoxia may be applied during certain times to encourage proper differentiation, switching to normoxia to induce collagen synthesis, and returning to hypoxia to promote crosslinking. The motivation that underlies such a duty cycle can be found in multiple studies. For stem cells, hypoxia, through HIF-1α overexpression, has been shown to be effective and sufficient in inducing a chondrocytic phenotype on human bone marrow stem cells without use of exogenous growth factors (41). Similar results have been obtained with adipose-derived stem cells (42). While

hypoxia seems beneficial for chondrodifferentation, early application during neocartilage tissue engineering does not result in improved properties as demonstrated by this and prior work (13). Thus, the present study provides strong support for further development of other hypoxia duty cycles, suggesting that, until robust mechanisms can be determined for hypoxia's effects on ECM synthesis, this potent stimulus should only be applied for differentiation and for collagen crosslinking.

Aside from pyridinoline, other cartilage crosslinks such as arginoline and advanced glycation end products (AGEs) might similarly be manipulated to influence neocartilage stiffness. Arginoline makes up for half of the mature cross-links in native cartilage (43) but cannot be measured via HPLC, necessitating future studies on its characterization in engineered tissues. AGEs occur over a time-scale of decades as sugars react with the lysine and arginine residues during aging. Examples of common AGEs include crosslinks, such as pentosidine (44-46), methylglyoxal-lysine dimer (MOLD) (45), and threosidine (47), as well as N^{ε}-(carboxymethyl)lysine (CML) (48) and N^{ε}-(carboxyethyl)lysine (CEL) (49). Though past work has correlated AGEs with stiffening of the collagen matrix (50), AGEs have also been implicated in the progression of age-related cartilage degeneration such as osteoarthritis (51). AGEs may thus be an inferior candidate when compared to pyridinoline and arginoline for enhancing neocartilage mechanical properties.

In this experiment, low oxygen tension (4% O_2) was investigated at various application times during the self-assembling process both to identify optimal regimens for hypoxia application and to elucidate a mechanism through which hypoxia-induced increases in cartilage mechanical properties occur. Hypoxia applied during the collagen synthesis phase resulted in decreased collagen content. However, hypoxia applied later in culture served to induce LOX

expression, crosslink formation, and increased tensile properties. Strong evidence from both this study and a plethora of prior studies suggest that this occurs through the robust mechanism of HIF-1α-induced upregulation of LOX. The results shown here are promising as they show that hypoxia can be used to tissue engineer neocartilage with robust tensile properties. In the future, while one may consider the possibility of employing hypoxia to achieve similar biomechanical improvements in cartilage just showing signs of mechanical degradation, a different regimen will have to be identified for intra-articular regulation of oxygen tension. Additionally, hypoxia may be beneficial for enhancing the mechanical properties of autografts or allografts.

TABLES AND FIGURES

TABLE 3.1 – GROWTH METRICS AND BIOCHEMICAL CONTENT OF 4 WEEKS NEOCARTILAGE CONSTRUCTS. The effects of hypoxia as a function of application time during the self-assembly of articular cartilage (control, 1st & 3rd weeks, 3rd & 4th weeks, 4th week, and continuous hypoxia groups) were examined on gross morphology (diameter, thickness, and wet weight) and biochemical properties (water content and DNA) of 4 weeks neocartilage constructs. Values are mean±95% CI. No significant differences were detected among controls and hypoxia treated groups. See Results section for details. Col=collagen, GAG=glycosaminoglycan, WW=wet weight.

Groups	Diameter (mm) (P = 0.4645)	Thickness (mm) (P = 0.2384)	Wet weight (mg) (P = 0.4566)	Water content (%) (P = 0.7472)	Cell number (millions) (P = 0.2669)
Control	5.21 ± 0.22	1.53 ± 0.11	29.87 ± 4.93	88.75 ± 13.23	3.01 ± 2.86
1st & 3rd weeks	5.17 ± 0.33	1.35 ± 0.25	29.65 ± 8.80	90.50 ± 12.11	4.03 ± 3.26
3rd & 4th weeks	5.11 ± 0.23	1.40 ± 0.22	26.45 ± 2.06	87.46 ± 7.93	4.24 ± 5.22
4th week	5.09 ± 0.33	1.48 ± 0.42	28.30 ± 7.42	87.81 ± 9.52	4.46 ± 4.39
Continuous	5.20 ± 0.24	1.45 ± 0.35	28.09 ± 10.95	88.19 ± 5.43	2.64 ± 2.22

TABLE 3.2 – BIOCHEMICAL PROPERTIES OF SELF ASSEMBLED NEOCARTILAGE. Biochemical properties of the engineered neocartilage as represented by Col/WW, GAG/WW, PYR/WW and PYR/Col. Values are mean±95% CI. See Results section for details. Col=collagen, GAG=glycosaminoglycan. WW=wet weight, PYR=pyridinoline.

Groups	**Collagen/WW (%) (P < 0.0001)**	**GAG/WW (%) (P = 0.718)**	**PYR/WW (nmol/g) (P = 0.0036)**	**PYR/Col (nmol/mg) (P < 0.0001)**
Control	3.03 ± 0.61^{A}	4.39 ± 2.10	4.99 ± 1.86^{B}	0.16 ± 0.030^{D}
1st & 3rd weeks	1.93 ± 1.27^{B}	3.84 ± 3.85	$5.68 \pm 1.00^{A,B}$	0.30 ± 0.169^{A}
3rd & 4th weeks	3.33 ± 1.23^{A}	4.96 ± 3.44	6.63 ± 1.90^{A}	0.20 ± 0.034^{C}
4th week	3.03 ± 1.50^{A}	4.91 ± 3.50	5.19 ± 1.06^{B}	$0.17 \pm 0.105^{C,D}$
Continuous	1.91 ± 0.44^{B}	4.44 ± 2.96	5.08 ± 1.88^{B}	0.26 ± 0.063^{B}

TABLE 3.3 – BIOMECHANICAL PROPERTIES OF THE ENGINEERED NEOCARTILAGE. Compression properties of tissue engineered neocartilage constructs represented by aggregate modulus, permeability and Poison's ratio and tensile properties represented by Young's modulus and ultimate tensile strength (UTS). Values are mean±95% CI. See Results section for details.

Group	Aggregate modulus (MPa) (P = 0.4017)	Permeability (10^{-15} m^4/N's) (P = 0.1101)	Poisson's ratio (P = 0.0773)	Young's modulus (MPa) (P < 0.0001)	UTS (MPa) (P = 0.4600)
Control	0.11 ± 0.06	18.50 ± 15.69	0.09 ± 0.22	0.45 ± 0.23[B,C]	0.07 ± 0.04
1st & 3rd weeks	0.10 ± 0.06	16.85 ± 16.89	0.08 ± 0.02	0.19 ± 0.23[C]	0.11 ± 0.07
3rd & 4th weeks	0.12 ± 0.05	11.62 ± 9.68	0.05 ± 0.11	0.82 ± 0.53[A]	0.06 ± 0.09
4th week	0.13 ± 0.04	16.04 ± 8.70	0.01 ± 0.02	0.53 ± 0.54[A,B]	0.11 ± 0.11
Continuous	0.11 ± 0.06	24.98 ± 28.31	0.06 ± 0.12	0.25 ± 0.19[B,C]	0.18 ± 0.18

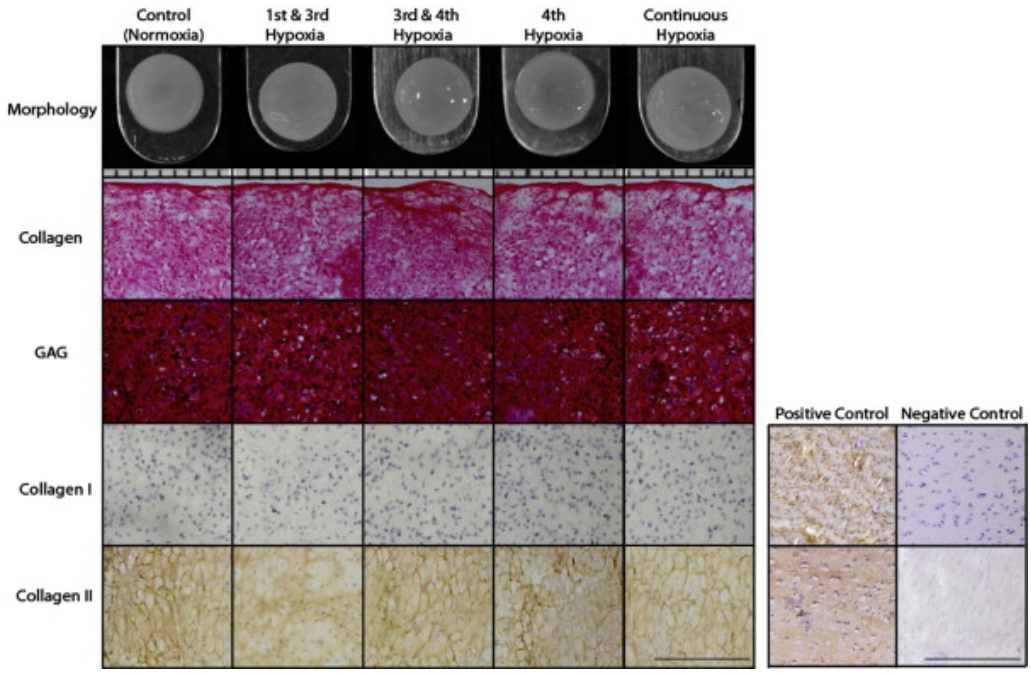

FIGURE 3.1 – GROSS MORPHOLOGY, HISTOLOGY, AND IMMUNOHISTOCHEMISTRY (IHC) OF SELF-ASSEMBLED NEOCARTILAGE. Both controls and hypoxia treated constructs (LOX) formed uniform neocartilage constructs with similar flat surfaces without physical abnormalities. The orientation of cryosectioning was from top to bottom in all groups (14 μm sections). Safranin-O/fast green staining for glycosaminoglycans and Picrosirius Red staining for collagen showed that constructs produced these matrix components uniformly for all groups. IHC illustrated that all groups were positive stained for collagen type II but not for collagen type I, suggesting articular cartilage phenotype.

CHAPTER 4 – IMPROVING THE BIOMECHANICAL PROPERTIES OF MUSCULOSKELETAL TISSUES THROUGH EXOGENOUS AND ENDOGENOUS APPLICATION OF LYSYL OXIDASE

ABSTRACT

The inability to recapitulate native tissue biomechanics, especially tensile properties, hinders progress in regenerative medicine. To address this, strategies have focused on enhancing collagen production. However, manipulating collagen crosslinks, ubiquitous throughout all tissues and conferring mechanical integrity, has been under-investigated. Invoking a mechanism of hypoxia inducing pyridinoline crosslinks via intermediaries such as lysyl oxidase (LOX), a series of studies showed that both native and engineered tissues are enhanced. Hypoxia was shown to enhance 1.4-6.4x pyridinoline crosslinking and concomitantly increase 1.3-2.2x tensile properties of collagen-rich tissues. Exogenous LOX administration enhanced 1.9x tissue biomechanics. Finally, LOX concentration- and time-dependent increases in pyridinoline content (~16x of controls) and tensile properties (~5x of controls) of neotissue were detected, resulting in properties on par with native tissue. LOX pre-treatment of engineered cartilage promoted *in vivo* matrix maturation resulting in an additional increase in tensile properties. Collectively, these results provide the first report of endogenous (hypoxia-mediated) and exogenous LOX applications promoting collagen crosslinking and improving the tensile properties of a spectrum of native and engineered tissues.

Chapter submitted as: Makris, E.A., Responte, D.J., Paschos, N.K., Hu, J.C., & Athanasiou, K.A. Improving the biomechanical properties of musculoskeletal tissues through exogenous and endogenous application of lysyl oxidase. 2014

MANUSCRIPT

Recent efforts have focused on developing *de novo* musculoskeletal tissues such as cartilage, bone, tendons, and ligaments for reparative and regenerative strategies. Tissue engineering has the potential to provide alternative treatment options for musculoskeletal disease and injury by generating neotissue that mimics the complex structure of native tissue[1,2]. Despite recent advances, poor biomechanical properties of engineered tissues limit their potential for clinical application[3,4]. In particular, tensile properties are still not on par with native tissue values, mainly due to the lack of interfibrillar collagen crosslinks[5]. Therefore, it is important that additional treatment modalities be evaluated toward enhancing tensile properties.

Collagen, comprising the major fraction of the extracellular matrix (ECM) of musculoskeletal tissues, accounts for approximately 65-80% of these tissues' respective dry weights[6]. After collagen biosynthesis and triple-helix formation, extracellular modification of lysine and hydroxylisine of the collagen fibers into their aldehyde forms, by the extracellular enzymes lysyl oxidase (LOX) and lysyl hydroxylase (LH), results in covalent crosslink formation between individual collagen molecules (Fig. 1)[7]. These intermolecular collagen crosslinks, pyridinoline and pyrrole, are present in all musculoskeletal tissues such as bone, cartilage, ligaments, and tendons[8]. The crosslinked collagen fibrils non-covalently stabilize the highly hydrated, negatively charged proteoglycans[9]. Articular cartilage features only pyridinoline collagen crosslinks, with the major types including the difunctional (initial/immature) crosslink dehydrodihydroxylysinonorleucine (DDHLNL) and the trifunctional (mature) crosslink hydroxylysylpyridinoline (HP). In ligaments, the most predominant collagen crosslink is dihydroxylysinonorleucine[10], which turns into the mature pyridinoline form, while in tendons and menisci the trifunctional pyridinoline crosslinks, HP

and lysyl PYR, stabilize the fibrillar collagen structure[11]. Despite the differences present in the type of collagen crosslinks in the various musculoskeletal tissue, several studies have highlighted how biomechanical properties of all native musculoskeletal tissues are closely correlated with collagen crosslinking[5,12,13], suggesting the need for recapitulating crosslinking *in vitro* in engineered tissues.

In engineered musculoskeletal tissues, such as cartilage, tendon, ligament, or fibrocartilage there have been only few studies evaluating the extent of collagen crosslinks [14,15] and, more importantly, their influence on tissue tensile and compressive properties. In contrast, many studies have investigated how other ECM components, such as glycosaminoglycans (GAG), collagen, and mineralization, contribute to biomechanical properties[14,16-18]. Such work has yielded variable results, as exemplified by the following: For instance, while it has been suggested that the compressive properties of native articular cartilage are best correlated with the proteoglycan component of the ECM[19], more recent studies have shown a better correlation of the compressive modulus with a combination of both GAG and collagen content[20-22]. For engineered tissues, tensile stiffness has been strongly associated with total collagen content[17] as well as pyridinoline content[23]. Nevertheless, a significant correlation with compressive properties has also been reported with respect to the pyridinoline content of engineered tissues[23]. Clearly, tissue biomechanical properties are dependent on more than merely the quantity of one biochemical component[24]. The unique structural organization, cross-linking and architecture of the collagen network also play equally important roles along with collagen quantity in determining the biomechanical functionality of the tissue.

To the best of our knowledge, there are no studies demonstrating methods for promoting collagen crosslinking in native and engineered tissues. Low oxygen tension, though, has been

shown to have various effects in different tissues[25,26], through a hypoxia-dependent mechanism. This molecular mechanism is based on the critical involvement of hypoxia inducible factor-1 (HIF-1)[27] which is present in articular chondrocytes[28] and in many other cells[29-31]. In diarthrodial joints as well as developmental growth plates, cartilage experiences hypoxic conditions[32]; deletion of HIF-1α results in chondrocyte death along with diminished expression of the CDK inhibitor p57, highlighting the importance of HIF-1α expression for cell survival and growth arrest in this environment[33]. More recently, the critical role of HIF-1α in chondrogenic differentiation of rat mesenchymal stem cells as well as human embryonic stem cells has been identified[34-37]. Low oxygen tension has also been shown to affect the metabolism of articular chondrocytes targeting the production of tissue-specific cartilage ECM proteins[34,38-41]. The manifold role of HIF-1 raises the potential toward promoting cartilage repair through stimulation of HIF-regulated pathways that promote cartilage specific matrix synthesis. Although studies have elucidated the pathway underlying the effects of HIF-mediated signaling on cartilage growth, function, and synthesis, the use of hypoxia to specifically enchance mechanical properties in native and engineered tissues through collagen crosslinking has not been explored.

In the series of studies presented in this manuscript, a variety of musculoskeletal tissues were used to assess collagen crosslinking manipulation in an attempt to promote tissue functional properties *in vitro*. Purposefully targeting collagen crosslinks should be useful for engineering tissues *de novo*, for elucidating disease processes, and for the development of potential novel therapeutic modalities. The first study established the presence of the triptych hypoxia-PYR crosslinking-biomechanics correlation in native cartilage. Figure 2 shows that hypoxia applied to articular cartilage explants enhanced collagen crosslinking by promoting LOX gene

expression, leading to significant improvement of tissue biomechanical properties. Low oxygen tension (2% O_2) application for 4 weeks significantly increased the amount of pyridinoline crosslinks 43% over controls, with a concomitant increase in LOX gene expression (~44-fold) (Fig. 2b and 2c). The tensile stiffness of articular cartilage treated with hypoxia was 238% of control values. No significant differences were observed for collagen, GAG, and DNA content per wet weight (WW) and dry weight (DW) (Table 1), indicating that the increase in properties was directly associated with the formation of crosslinks. By applying the LOX inhibitor β-aminopriopionitrile (BAPN), the effects of hypoxia (increased Young's modulus and PYR/WW) were abolished, reaffirming the proposed mechanism of action. These results demonstrate that application of hypoxia can be directed to promote LOX-mediated pyridinoline collagen crosslinking and to enhance tensile properties in native articular cartilage. Hypoxia increased tensile properties independently of other biochemical and biomechanical properties, making it a good target for further investigation. These data not only call forth new biological questions on the mechanism of action in articular cartilage, but also generate clinical interest in the ability of hypoxia to alter the biomechanical properties of other tissues.

Taking a step further, the second study sought to determine whether hypoxia could effectively enhance the mechanical properties of other musculoskeletal tissues via the same LOX-mediated mechanism. Similarly, low oxygen tension application resulted in significant increases (140-643% of controls) in the tensile properties of a wide spectrum of musculoskeletal tissues, such as the anterior (cranial) cruciate ligament, posterior (caudal) cruciate ligament, patellar tendon, and knee meniscus (Fig. 3a and 3b). As hypothesized, this was shown to occur through hypoxia-induced increases in pyridinoline crosslinks per WW (52-71% increase over control values) and per collagen content (63-117% increase over control values) (Fig. 2c and

2d). These findings were further confirmed with the addition of LOX inhibitor BAPN that resulted in partial ofr full abolishment of the measured differences generated from the application of hypoxia (Young's moduli, PYR/WW, and PYR/Col). Hypoxia leads to increased tensile properties through the up-regulation of HIF-1α[42], which then up-regulates LOX[43], and in turn, catalyzes the formation of pyridinoline crosslinks[44] to result in enhanced tissue biomechanics. This series of events appears to be rather robust, considering the multitude of tissues validated here. In essence, hypoxia was effective in manipulating the tensile properties of a spectrum of tissues through LOX-mediated crosslinking.

Interestingly, the increase of tensile properties in articular cartilage and other collagen-rich tissues was not the only effect of hypoxia; low oxygen tension induced other significant effects (Table 1). Specifically, although hypoxia induced pyridinoline crosslinks in all examined tissues, it decreased the amount of collagen in some tissues, such as the PCL and meniscus. Hypoxia-induced HIF-1α upregulation controls the expression of cartilage specific transcriptional factor SOX-9 that directly regulates the main matrix genes, such as those encoding Col-2a1, aggrecan, Col-9, and LOX[34,41]; Thus, these findings indicate that hypoxia exerts various effects upon ECM components of musculoskeletal tissues in addition to endogenously inducing crosslink formation. Considering the pleiotropic effects of low oxygen tension (e.g., angiogenesis, apoptosis, and chondrogenesis), it would be useful to identify other methods to enhance tensile properties, ideally through exogenous agents.

From the several exogenous agents, which could potentially be used to enhance tissue tensile properties, the most straightforward route is through the exogenous addition of LOX. This enzyme is directly responsible for the formation of pyridinoline crosslinks. Exogenous addition of LOX would potentially bypass side effects caused by hypoxia, HIF-1α, and their

downstream products. Thus, the next series of experiments within the present study employed exogenous LOX administration on both native and engineered tissues. Literature lacks any comparable experience, with only few previous studies just show LOX application in smooth muscle cell monolayer cultures to increase matrix synthesis and pyridinoline content[45]. In the present study, exogenous LOX application at various concentrations applied for 2 weeks on native articular cartilage showed that a LOX concentration of 0.15ng/ml (High LOX) significantly increased pyridinoline crosslink content per WW (204% of control values) and per collagen (250% of control values) (Fig. 4c and 4d). This LOX concentration resulted in tensile stiffness and strength of articular cartilage at 186% and 185% of control values, respectively (Fig 4a and 4b). No significant effects were observed on collagen, GAG, and DNA content of the LOX-treated tissue over controls (Table 1), strongly suggesting that LOX mainly acts on the ECM. Thus, exogenous LOX application appears to provide a simple, yet effective, way to promote matrix maturation and enhance cartilage integrity, and it is anticipated the same will hold true across other collagenous tissues.

To further refine how collagen crosslinks can be controlled *in vitro* during tissue development, the temporal modulation of LOX-induced collagen crosslinking was examined in two phases, using self-assembled neocartilage as a representative model. A Phase I study showed that a LOX concentration of 0.15μg/ml significantly increased the amount of pyridinoline crosslinks in the engineered tissue over controls by 16.2 times (Fig. 5b). More importantly, the tensile properties of the engineered tissue increased to 5.0 times those of the controls (Fig. 5a). A Phase II study, which examined the time dependence of LOX application, showed that early LOX application significantly increased the tensile stiffness of engineered neocartilage over late LOX application. In this case, the tensile stiffness of LOX-treated

neotissue was 5.3 times that of control, with concomitant increases in the amount of pyridinoline crosslinks (16.0 times) (Fig. 5c and 5e). Additionally, both treatments also increased the compressive properties of neotissue (Fig. 5d). Collectively, these results proved the effectiveness of the LOX-mediated pathway on promoting the biomechanical properties of engineered tissues. Specifically, these data demonstrated that effective LOX concentration and application time can direct collagen crosslinking and significantly enhance the tensile properties in a collagen-rich tissue.

Finally, an *in vivo* study was performed to investigate neotissue growth and development post-implantation, since this step is pivotal toward developing *in vitro* tissue engineering strategies that will result in functional replacement tissues. The *in vivo* growth environment is described to be beneficial for engineered tissue maturation, as it potentially provides the neotissue with nutrients, growth factors, and stimuli not applied in the tissue culture, thus enhancing its biochemical and functional properties[18]. Specifically, in this step the potential of using a LOX pre-treatment to further promote *in vivo* maturation of neotissues was explored. To do so, self-assembled neocartilage was first grown *in vitro* for 6 weeks and subjected to the optimal LOX treatment, as identified in the previous series of studies. At this 6-week time point, both LOX-treated and control constructs were implanted subcutaneously into the backs of athymic mice, where they remained for an additional 6 weeks until the mice were sacrificed. In addition, control and LOX-treated tissues were simultaneously grown *in vitro* for the entire 12-week culture duration to compare with those grown *in vivo*.

In vivo culture promoted the maturation of post-translational modifications, collagen fibers, and collagen content. Quantitative evaluation of SEM images revealed that the *in vivo* environment significantly enhanced the fibril density of control neocartilage compared *in vitro*

neotissue. In addition, both *in vitro* and *in vivo* LOX-treated neotissues exhibited significantly enhanced fibril density over *in vitro* control neocartilage (Fig. 5a). In terms of the fibril diameter of the neotissue, no differences were observed among any of the factors (Fig. 5b). The *in vivo* environment significantly increased the amount of PYR/WW in controls over those grown *in vitro* culture, while *in vivo* culture of LOX-treated neotissue increased PYR content per WW by 14-times (Fig. 6c). Furthermore, the *in vivo* growth environment significantly enhanced the amount of collagen content per WW in both control and LOX-treated groups (Fig. 6d); no significant differences, however, were observed in the amount of GAG content per WW among all groups (Fig. 6e). In addition, *in vivo* treatment significantly increased tensile properties compared to *in vitro* culture (Fig. 6a). LOX-treated constructs implanted *in vivo* displayed a 3-fold increase in tensile modulus compared to the *in vitro* control (Fig. 6a). In terms of the compressive properties, the *in vivo* environment again provided a significant benefit in tissue growth over the *in vitro* culture for both control and LOX-treated constructs; however, LOX pre-treatment in the *in vivo* group did not further promote these effects over *in vivo* controls (Fig. 6b). Overall, these results show that *in vitro* LOX pre-treatment of engineered cartilage promotes *in vivo* development of the neotissue, resulting in enhanced matrix maturation and increased tensile properties compared to *in vitro* tissue. This work illustrates the potential of LOX as a potent agent for promoting neotissue maturation, not only *in vitro* but also *in vivo*, suggesting a pivotal role of PYR crosslinks in the pre- and post-implanted tissue.

In the present study, the biomechanical properties of the collagen crosslinked engineered neotissue were not only increased, but also reached values close to those of native articular cartilage. Specifically, under compression, the aggregate modulus of 6-week engineered

neocartilage treated with LOX was 220±47 kPa. For comparison, the aggregate modulus of the corresponding native articular cartilage, tested under the same conditions (thickness, strain), was 280±72 kPa. With the LOX values obtained being approximately 80% of the native tissue's values, the compressive modulus is on par with native tissue values, especially when considering the reported range of compressive modulus of native cartilage (150-380 kPa)[46],. Similarly, under tension, the tensile modulus of the corresponding native, 1-week old, articular cartilage was 5.0±1.9 MPa. Thus, the tensile modulus of the LOX-treated engineered tissue generated in this study (2.3±0.8 MPa) represented approximately 50% of the native tissue's values. Juxtaposing the LOX data against literature values of the native cartilage Young's modulus (4.0-6.0 MPa)[47], one finds that the tensile values obtained in this study using LOX can be up to ~60% of the native tissue's values. Thus, the stiffness indices of the collagen crosslinked engineered tissue reach approximately 38-79% of native tissue's values.

To the best of our knowledge, this is the first study describing a method for promoting collagen crosslinking in both native and engineered tissues. Both endogenous (hypoxia-mediated) and exogenous LOX application enhanced the biomechanical properties of collagen-rich tissues through pyridinoline crosslinking formation. LOX acts using a completely different mechanism than other currently employed stimuli, such as hydrostatic pressure, direct compression, or growth factors, suggesting that LOX could be combined with these stimuli to produce synergistic effects, and, thus, promoting even more the functional properties of neotissue. Biomechanical properties have consistently been a crucial barrier to the translation of tissue engineering technologies; LOX application thus represents an exciting development. Indeed, the FDA guidance document for knee cartilage repair lists the "ability of the implant to withstand expected *in vivo*…loading" as a key success criterion for the pre-clinical evaluation of

repair products. The quantitative increases in tensile properties observed in this study thus illustrate an important step toward producing neotissue that is suitable for pre-clinical work.

The systematic examination of low oxygen tension application on tissue culture and growth pursued in this study provides a novel mechanistic description of HIF1α-mediated pyridinoline collagen crosslinking formation toward enhancing a tissue's biomechanical properties (Fig. 6). This adds to the already known roles of HIF-1α in apoptosis[30], peripheral immune tolerance, tumor angiogenesis[48,37], and cell-mediated inflammation[49,50]. Additionally, hypoxia has been reported to switch the basic translation initiation machinery during protein synthesis[51]. The present study highlights that hypoxia application during tissue culture resulted in HIF-1α-mediated LOX gene expression, as detected by RT-PCR. As previously described, *in vivo* collagen maturation following biosynthesis occurs through extracellular modification of the collagen fibers by LOX and LH endopeptidases; these result in the formation of both immature and mature covalent pyridinoline crosslinks[7,12,52]. Thus, hypoxia-induced signaling promotes the formation of pyridinoline collagen crosslinks and subsequently enhances tensile properties. As a consequence, the low-oxygen modification of the tissue culture environment can conceivably be used not only in the engineering of articular cartilage, but potentially on any collagen-rich tissue where collagen crosslinks likewise play crucial biomechanical roles, such as tendon, ligament, fibrocartilage and skin.

Although the exact molecular pathways of endogenous LOX gene expression and mediation in collagen crosslinking formation in different tissues are not yet fully elucidated and understood, these processes seem to take place at the initial stages of collagen growth and maturation[53]. By employing the self-assembling process that recapitulates features of cartilage morphogenesis[1,2], this study provides additional clues on the role of endogenous LOX

expression and regulation in native cartilage development. For both self-assembled neocartilage and native cartilage during morphogenesis, the initially ubiquitous collagen type VI localizes around the pericellular matrix while collagen type II production rises. Although qualitative data show LOX localization in cartilage during development, quantitative data for LOX expression do not exist, making it difficult to evaluate its developmental role. The present study showed that LOX-induced tensile increases are time-dependent, indicating that endogenous LOX regulation during morphogenesis is timed to correspond with temporal changes in collagen types, eventually resulting in optimized tensile properties. Future studies should shed more light into these important aspects of collagen growth and maturation during *in vivo* morphogenesis and *in vitro* development of engineered tissues.

In orthopedics, grafts and explants intended for implantation or reconstruction are often stored in culture media. However, it is known that the material properties of these grafts deteriorate with time. Serum-supplemented medium causes tissue swelling[54], chondrocyte phenotypic differentiations[55], as well as cellular outgrowth from tissue[56]. Although a chemically-defined serum-free medium has been introduced to specifically avoid these deleterious effects, properties of stored tissues still remain inferior over native tissues' values[57,58]. In the present study we show that chemically-defined serum free media supplemented with LOX results in the maintenance, if not improvement, of graft properties. In addition to the role of collagen crosslinks in a tissue's biomechanical properties, some studies have highlighted how pyridinoline reduces collagen type II catabolism[5,59]. The presence of pyridinoline in the ECM reduces susceptibility to matrix degradation due to metalloproteinase-1 (MMP-1)[5]. In parallel, it has been reported that matrices produced by skin fibroblasts with more pyridinoline crosslinks were less susceptible to MMP-1 degradation[59]. Therefore, promoting

pyridinoline crosslinking in native or engineered tissues through endogenous or exogenous LOX application might be a potential way to prevent degenerative processes in both tissues and neotissues. Thus, In terms of clinical applicability, it may be advisable to consider LOX supplementation during the storage or transport of highly collagenous grafts intended for implantation.

In conclusion, the present series of studies demonstrates that hypoxia-mediated or exogenous LOX application promotes collagen crosslinking and maturation, resulting in concomitant increase in finctional properties of collagen-rich tissues. These findings are clinically applicable in a broad spectrum of collagen-rich tissues, including articular cartilage, tendon, meniscus, and ligament, and could thus offer potent new agents for tissue repair strategies. Additionally, hypoxia or exogenous LOX can be employed to improve or maintain the mechanical properties of transplantation grafts such as osteochondral, meniscal, sinews, and possibly any other highly collagenous tissue. With several growth factors and mechanical stimuli being identified to increase the biochemical content and compressive properties of engineered tissues, but only few methods existing on how tensile properties can be improved, this study represents a major contribution for tissue engineering approaches. Moreover, LOX pre-treatment promotes *in vivo* development and maturation of the neotissue, resulting in further increase in the tensile properties in vivo. Additionally, the ability of LOX to be applied exogenously and to promote tissue maturation may allow for direct *in vivo* applications to treat defects or pathologies such as for example via intra-articular injections. Finally, this study demonstrates the potential for LOX to be combined with other exogenous factors to generate biomimetic tissue implants *in vitro* with biomechanical properties on par with native tissue

values. Overall, results of this study demonstrate that endogenous (hypoxia-mediated) and exogenous LOX application provide exciting new technologies for promoting collagen network maturation and enhancement of the biomechanical properties in both native and engineered tissues.

MATERIALS AND METHODS

Sample preparation

Explants (articular cartilage, anterior (cranial) cruciate ligament (ACL), posterior (caudal) cruciate ligament (PCL), patellar tendon, and medial meniscus) were harvested from the knee joint of 1-week-old calves (Research 87 Inc.). Explants were either analyzed immediately (d=0) or incubated for 24 hours prior to analysis.

Explant culture

To investigate the effect of hypoxia on musculoskeletal tissues, two different types of media were used for explant culture: 1) cell culture medium (DMEM with low glucose (1g/L) (Life Technologies), 10% fetal bovine serum (FBS) (Atlanta Biologicals), 1% non-essential amino acids (NEAA) (Life Technologies), 25 mg of L-ascorbic acid (Sigma-Aldrich), and 1% penicillin/ streptomycin/ fungizone (PSF) (BioWhittaker Inc.)) or 2) cell culture medium supplemented with 0.25mM β-aminopriopionitrile (BAPN), (Sigma-Aldrich). Explants were divided into 4 treatment groups and cultured for 4 weeks: Control, BAPN, Hypoxia, Hypoxia & BAPN. Explants in the Control and BAPN groups were incubated at 37°C, 5% CO_2, and 21% O_2, and hypoxia groups received 2% O_2.

Cell isolation

Articular cartilage, harvested from the distal femur of 1-week-old calves, was digested in 0.2% collagenase type II (Worthington Biochemical Cor.) for 18 hours. Cells were isolated, frozen at -80°C for 24 hours, and stored in liquid nitrogen until needed.

Neocartilage culture

Using the self-assembling process[1,2] chondrocytes were thawed, evaluated using trypan blue, seeded into cylindrical, non-adherent agarose wells as previously described[1,60], and fed with chondrogenic medium[61-63] (DMEM (Life Technologies), 1% non-essential amino acids (Life Technologies), 100 nm dexamethasone (Sigma-Aldrich), 1% ITS + premix (BD Biosciences), 40 mg/mL l-proline (Sigma-Aldrich), 50 mg/mL ascorbate-2-phosphate (Sigma-Aldrich), 100 mg/mL sodium pyruvate (Fisher Scientific), 0.146 mg/ml hydroxylysine (Sigma-Aldrich), 0.0016 mg/ml copper (Sigma-Aldrich), and 1% penicillin/streptomycin/fungizone (Biowhittaker/Cambrex)).

LOX application in native and engineered neocartilage

Articular cartilage explants were fed with chondrogenic medium supplemented with LOX at two concentrations: Low (0.0015μg/ml) and High (0.15μg/ml) during a 2-week culture period. In engineered neocartilage, Phase I investigated the effects of three different LOX concentrations: Low (0.0015μg/ml), Medium (0.015 μg/ml), and High (0.15μg/ml), during a 4-week culture period. LOX-treated groups received LOX medium during t=8-21 days. In Phase II, two LOX treatment windows were evaluated using the concentration identified in Phase I

(i.e., 0.15μg/ml): control, Early LOX (applied t=8-14 days), and Late LOX (applied t=15-21 days) during a 6-week culture period.

Gross morphology

ImageJ was used to determine the diameter and thickness of each sample. The central 3 mm of each construct was used for creep indentation testing[1] while the outer ring was divided for tensile testing, histology, and quantitative biochemistry, as previously described[64].

Histology/ Immunohistochemistry (IHC)

For histology, constructs were cryoembedded at -20°C in HistoPrep™ (Fisher Scientific) and were sectioned at 14 μm. Sections were then fixed in 10% formalin and stained using Safranin-O/fast green or Picrosirius red for GAG and collagen, respectively. For IHC, sections were fixed in 4°C acetone and stained for collagen type I and II, as previously described[65].

Quantitative biochemistry

Samples were weighed, frozen, and lyophilized, and dry weights were recorded. Samples were then digested in phosphate buffer with 5 mm EDTA, 5 mm N-acetyl-cysteine, and 125 μg/mL papain (Sigma-Aldrich) for 18 hours at 65°C. Following digestion of the samples, total collagen was quantified using chloramine-T hydroxyproline assay[66]. Sulfated GAG of articular cartilage and neocartilage was quantified using the Blyscan Glycosaminoglycan Assay (Biocolor), and total number of cells was estimated with a Picogreen DNA Assay (Life Technologies) assuming 7.7 pg DNA per cell, as previously described[64].

Real time PCR

To study hypoxia-induced gene up regulation, real time PCR was employed. Past work has found LOX gene expression to change within 18 hours following exposure to hypoxic conditions [67,68]. Following a 24-hour incubation in normoxic conditions, articular cartilage explants were subjected to hypoxia for an additional 24 hours. Immediately after this exposure to hypoxia, LOX gene expression was measured as previously described [68], using S18 (US Biological) as the housekeeping gene and a LOX primer (US Biological).

High performance liquid chromatography (HPLC)

HPLC samples were digested in 6 N HCl at 100°C for 18 hours. Following digestion, samples were dried using a vacuum concentrator and re-suspended in a solution of 10 nmol pyridoxine/ml and 2.4 μmol homoarginine/ml. Samples were subsequently diluted fivefold with 0.5% HFBA in 10% acetonitrile and analyzed as described previously[69]. Pyridinoline standards (Quidel Corp.) were used to quantify crosslink content.

Creep indentation testing

Compressive properties were evaluated using creep indentation as previously described[70]. Specimens were equilibrated in PBS for 15 minutes and then indented to ~15% strain using a flat, porous indenter tip (0.8 mm diameter). The compressive properties of the samples were obtained using a semi-analytical, semi-numeric, linear biphasic model[70].

Tensile testing

Tensile properties were determined using a uniaxial material testing apparatus (Instron, Model 5565) as previously described[61,63]. Samples were tested until failure by applying a strain rate of 1% of the gauge length per second. Tensile stiffness and ultimate tensile strength (UTS) were determined based on stress-strain plots.

Quantitative evaluation of SEM images using ImageJ

Samples were prepared and evaluated as previously described[18]. To quantify SEM images, ImageJ was used to measure both fibril density and diameter.

Statistical analyses

Data, based on $n = 7$, are represented as means ± standard deviations. Analysis of variance (ANOVA) was used for intergroup comparisons. Tukey's *post hoc* testing was applied if $p<0.05$. For all figures, statistical significance is indicated by bars not sharing the same letters.

TABLES AND FIGURES

TABLE 4.1 – BIOMECHANICAL PROPERTIES AND BIOCHEMICAL CONTENT OF NATIVE AND ENGINEERED TISSUES. Values are mean±95% SD. Tukey's *post hoc* testing was applied if $p<0.05$. Groups not connected by the same letter are significantly different. E_Y=Young's modulus, UTS=ultimate tensile strength, H_A=aggregate modulus, Col=collagen, GAG=glycosaminoglycan, WW=wet weight.

Study	Group	E_Y (MPa)	UTS (MPa)	COL/WW %
Hypoxia in anterior cruciate ligament	d=0	7.3±3.8^{A}	5.0±3.6^{A}	14.4±3.2
	Control	0.9±0.4^{C,D}	0.7±0.4^{D}	13.6±2.9
	BAPN	0.5±0.4^{D}	0.7±1.0^{D}	14.0±4.3
	Hypoxia	2.3±0.7^{B}	2.3±0.7^{B}	13.6±2.0
	Hypoxia & BAPN	1.0±0.8^{C}	1.3±0.6^{C}	12.6±0.9
Hypoxia in posterior cruciate ligament	d=0	12.8±6.0^{A}	12.8±6.0^{A}	16.2±1.7^{A}
	Control	0.5±0.3^{D}	0.5±0.3^{D}	15.0±2.1^{A}
	BAPN	1.0±0.1^{C}	1.2±0.4^{C}	16.1±2.4^{A}
	Hypoxia	1.7±0.9^{B}	1.7±0.9^{C}	13.7±1.3^{B}
	Hypoxia & BAPN	1.4±0.6^{B,C}	4.2±2.5^{B}	13.1±2.4^{B}
Hypoxia in patellar tendon	d=0	23.7±13.3^{A}	13.3±6.5^{A}	15.2±2.1^{A}
	Control	0.7±0.3^{D}	0.7±0.3^{C}	14.2±3.1^{A}
	BAPN	0.7±0.5^{D}	1.0±0.7^{C}	11.2±1.7^{B}
	Hypoxia	4.6±2.3^{B}	2.3±2.0^{B}	15.6±1.2^{A}
	Hypoxia & BAPN	2.0±1.6^{C}	0.8±0.7^{C}	10.4±1.8^{B}
Hypoxia in knee meniscus	d=0	49.5±10.0^{A}	14.6±6.7^{A}	24.1±2.2^{A}
	Control	20.7±2.4^{C}	19.8±3.6^{C}	22.5±3.1^{A}
	BAPN	9.0±4.5^{D}	7.4±3.6^{D}	22.9±1.7^{A}
	Hypoxia	29.0±3.0^{B}	30.0±4.0^{B}	18.9±2.8^{B}
	Hypoxia & BAPN	11.5±2.7^{D}	10.3±2.3^{D}	19.8±3.9^{B}

TABLE 4.1 (CONTINUED)

Study	Group	E_Y (MPa)	UTS (MPa)	H_A (MPa)	COL/WW %	GAG/WW %
Hypoxia in articular cartilage	Control	2.0 ± 1.5^{B}	1.3 ± 1.1^{B}	0.5±0.4	9.1±1.5	5.2±0.8
	BAPN	2.5 ± 1.0^{B}	2.3 ± 0.7^{B}	0.4±0.2	8.2±2.4	5.0±
	Hypoxia	4.6 ± 1.7^{A}	3.0 ± 1.0^{A}	0.4±0.2	9.5±2.1	5.9±1.2
	Hypoxia & BAPN	1.3 ± 1.2^{B}	2.0 ± 0.5^{B}	0.5±0.2	8.1±1.6	5.4±0.5
Exogenous LOX in articular cartilage	d=0	12.7 ± 1.17^{A}	8.4 ± 1.2^{A}	0.7±0.3	13.6 ± 1.4^{A}	8.0±1.0
	Control	6.6 ± 2.4^{B}	2.9 ± 1.7^{C}	0.5±0.3	5.6 ± 2.5^{B}	8.4±0.6
	Low LOX	7.7 ± 2.7^{B}	3.2 ± 1.7^{C}	0.5±0.2	7.5 ± 2.7^{B}	8.4±0.8
	High LOX	12.3 ± 3.4^{A}	5.4 ± 1.5^{B}	0.6±0.2	5.8 ± 2.8^{B}	8.4±0.7
Exogenous LOX in neocartilage (Phase I)	Control	0.4 ± 0.1^{C}	0.2 ± 0.0^{C}	0.1±0.1	1.8±0.2	1.1±0.1
	Low LOX	1.0 ± 0.3^{B}	0.3 ± 0.0^{B}	0.1±0.0	1.6±0.2	1.5±0.4
	Medium LOX	1.14 ± 0.16^{B}	0.3 ± 0.0^{B}	0.1±0.0	1.8±0.2	1.2±0.1
	High LOX	2.17 ± 0.68^{A}	0.5 ± 0.1^{A}	0.1±0.0	1.9±0.3	1.4±0.4
Exogenous LOX in neocartilage (Phase II)	Control	0.4 ± 0.1^{C}	0.2 ± 0.0^{B}	0.1 ± 0.1^{B}	1.7±0.2	1.8±0.2
	Early LOX	2.3 ± 0.8^{A}	0.5 ± 0.1^{A}	0.2 ± 0.0^{A}	1.8±0.2	1.6±0.1
	Late LOX	0.8 ± 0.1^{B}	0.4 ± 0.2^{A}	$0.2\pm0.1^{A,B}$	1.8±0.1	1.7±0.1

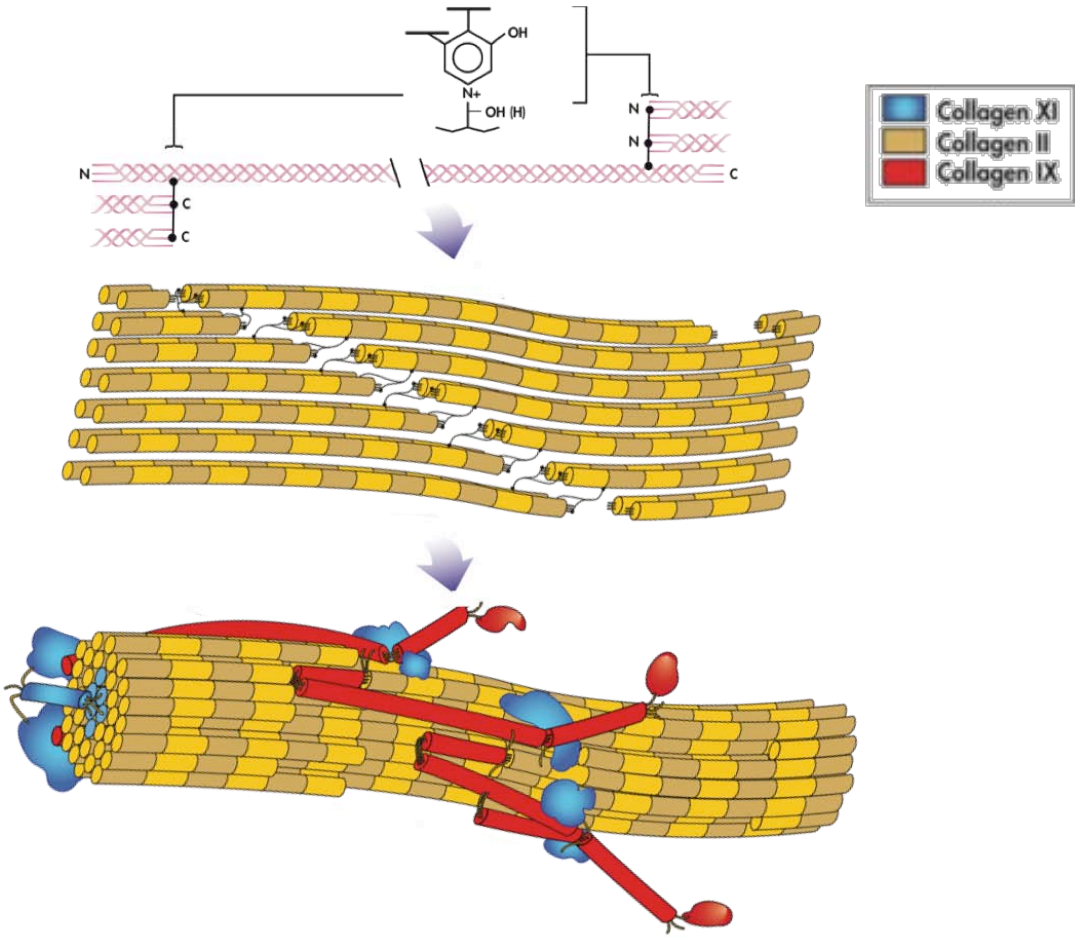

FIGURE 4.1 – HIERARCHICAL ARCHITECTURE OF COLLAGEN FIBRILS. Upper: A heterofibril consisting of collagen types II, IX, and XI is a major component of the extracellular matrix of musculoskeletal tissues. Middle: Each mature (trifunctional) crosslink interconnects three different collagen molecules within the fibril. Lower: Intermolecular pyridinoline crosslinks are found in particular locations due to the specificity of the enzyme lysyl oxidase (Adapted from Eyre et al[71].).

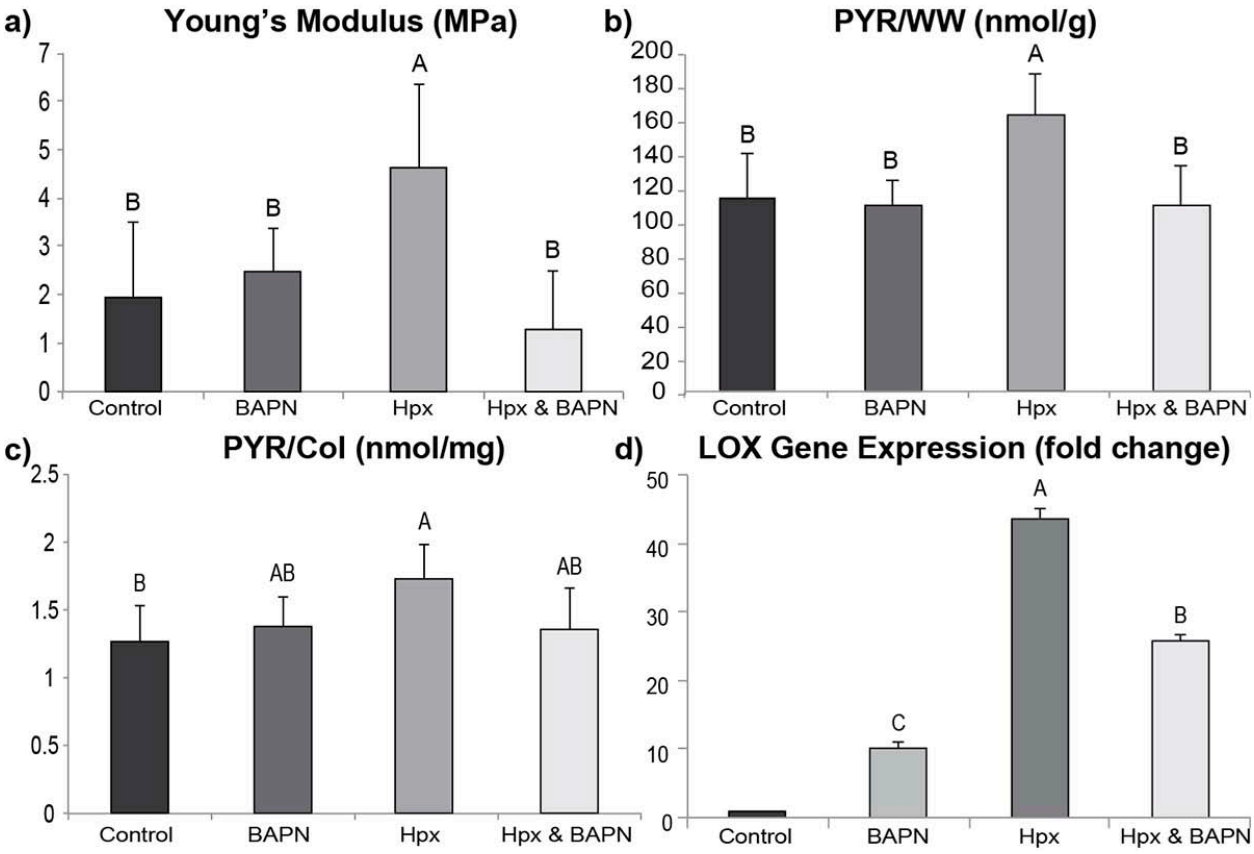

FIGURE 4.2 – BIOMECHANICAL AND BIOCHEMICAL PROPERTIES OF HYPOXIA-TREATED ARTICULAR CARTILAGE. **a**) Tensile stiffness as represented by Young's modulus, **b**) pyridinoline content normalized to tissue wet weight (PYR/WW), **c**) pyridinoline content normalized to tissue collagen content (PYR/Col), and **d**) hypoxia-mediated LOX gene expression as detected by RT-PCR. Results demonstrate that low oxygen tension (2% O_2) application for 4 weeks significantly increased the amount of pyridinoline crosslinks 43% over controls, with concomitant increase in LOX gene expression (~44-fold). Additionally, the tensile stiffness of articular cartilage treated with hypoxia was 238% of control values. Results were further confirmed with the LOX inhibitor β-aminopropionitrile (BAPN), as the measured differences resulting from the application of hypoxia (Young's moduli, PYR/WW, and PYR/Col) were abolished with the addition of BAPN. Bars denote means ± SD, and groups not connected by the same letter are significantly different. PYR=pyridinoline, WW=wet weight, Col=total collagen.

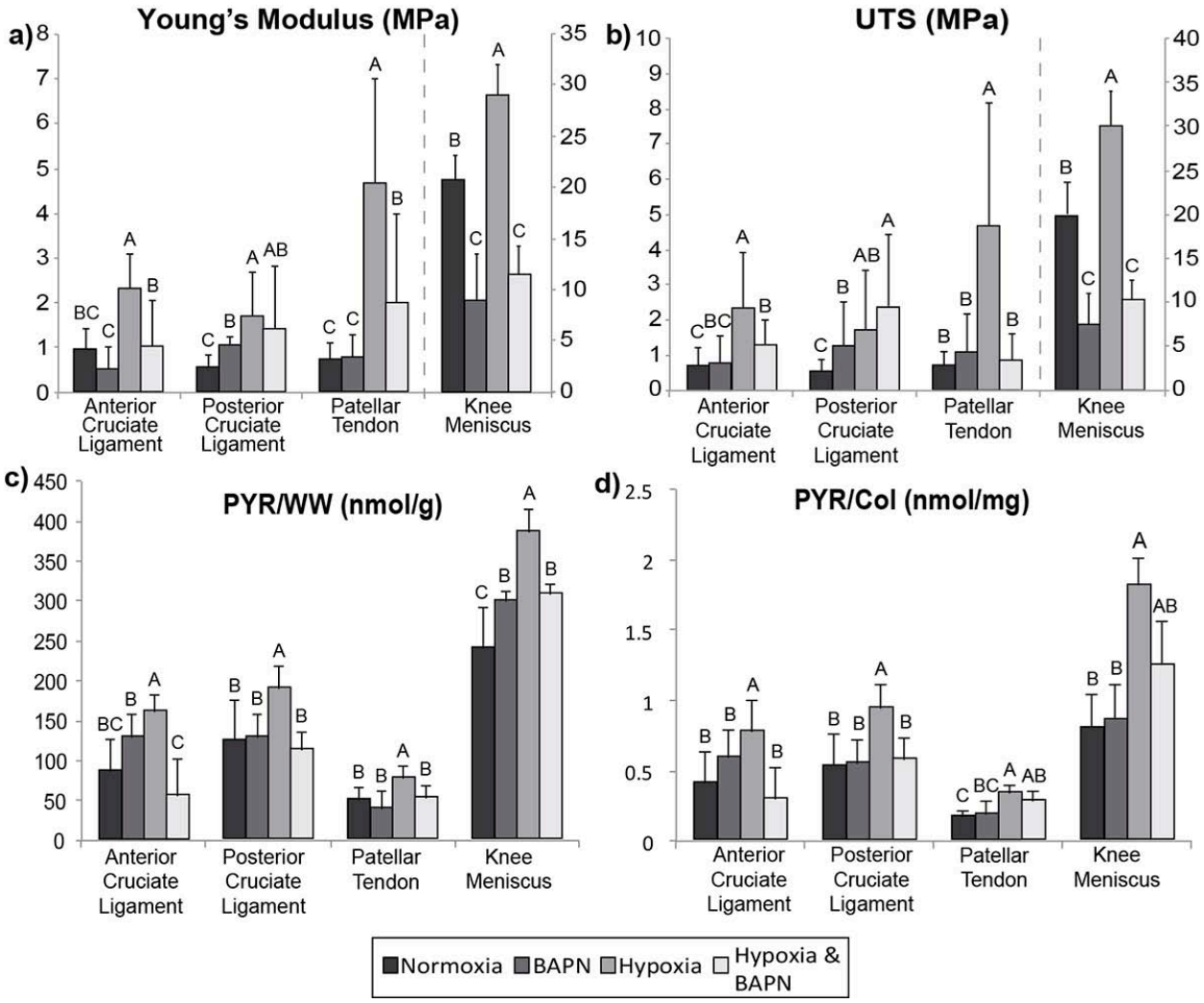

FIGURE 4.3 – BIOMECHANICAL AND BIOCHEMICAL PROPERTIES OF HYPOXIA-TREATED ANTERIOR CRUCIATE LIGAMENT (ACL), POSTERIOR CRUCIATE LIGAMENT (PCL), PATELLAR TENDON, AND KNEE MENISCUS. a) Tensile stiffness as represented by Young's modulus, **b**) ultimate tensile strength (UTS), **c**) pyridinoline content normalized to tissue wet weight (PYR/WW), and **d**) pyridinoline content normalized to tissue collagen content (PYR/Col). Results demonstrate that application of hypoxia can be directed to promote LOX-mediated pyridinoline collagen crosslinking per WW (52-71% increase over control values) and per collagen (63-117% over control values), and to enhance tensile properties in various collagen-rich tissues (140-643% of control values). Results were further confirmed with the LOX inhibitor β-aminopropionitrile (BAPN), as the measured differences resulting from the application of hypoxia were partially or fully abolished with the addition of BAPN. Bars denote means ± SD, and groups not connected by the same letter are significantly different. PYR=pyridinoline, WW=wet weight, Col=total collagen.

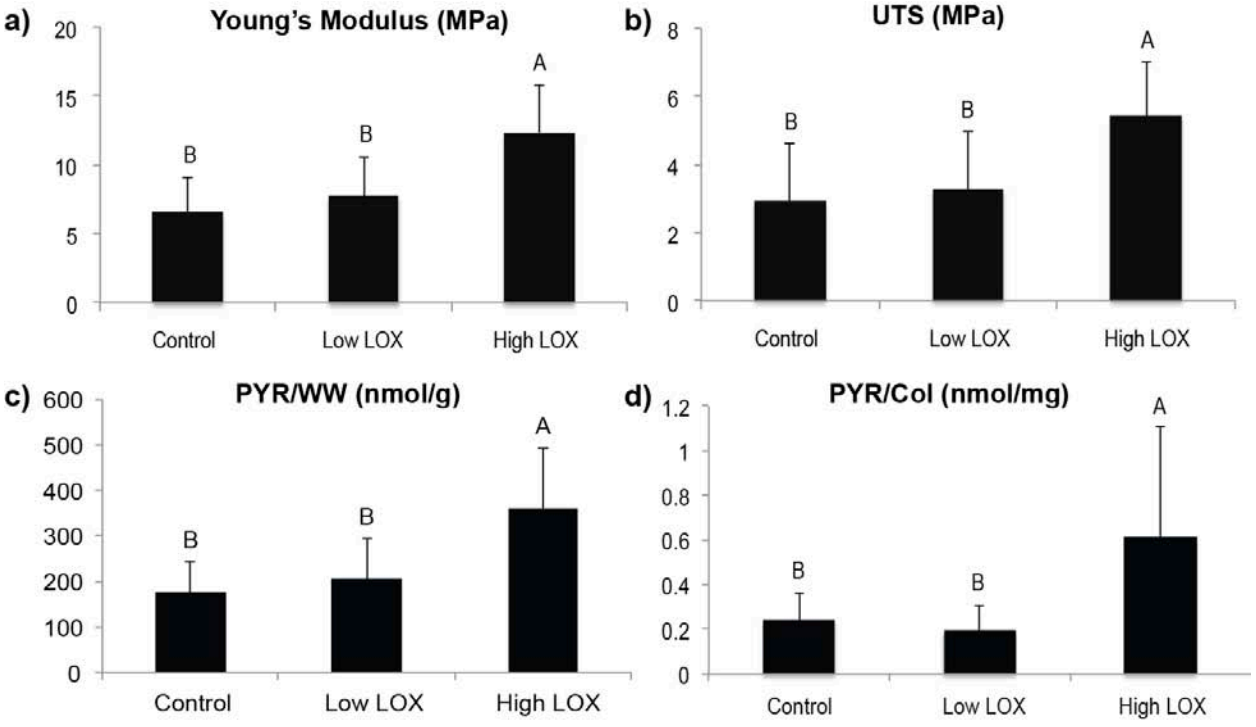

FIGURE 4.4 – BIOMECHANICAL AND BIOCHEMICAL PROPERTIES OF LOX-TREATED ARTICULAR CARTILAGE. **a**) Tensile stiffness as represented by Young's modulus, **b**) ultimate tensile strength (UTS), **c**) pyridinoline content normalized to tissue wet weight (PYR/WW), and **d**) pyridinoline content normalized to tissue collagen content (PYR/Col). Results demonstrate that exogenous LOX application at a concentration of 0.15ng/ml (High LOX) significantly increases the amount of pyridinoline crosslinks over controls, normalized per WW (104% increase) and per collagen (150% increase), and concomitantly enhances the tensile properties of the tissue (86% over controls). Bars denote means ± SD, and groups not connected by the same letter are significantly different. PYR=pyridinoline, WW=wet weight, Col=total collagen.

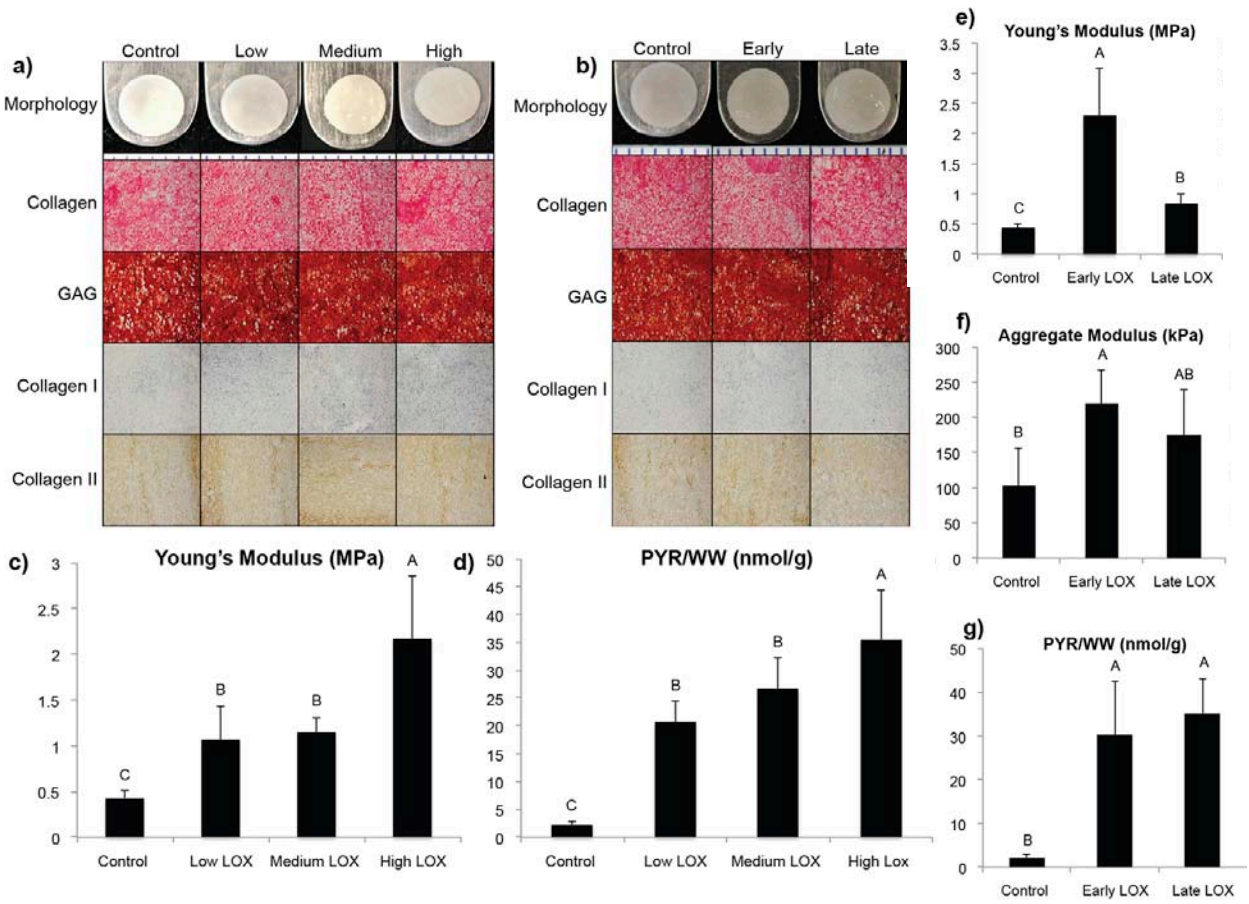

FIGURE 4.5 – PHASE I AND II GROSS MORPHOLOGY, HISTOLOGY, IMMUNOHISTOCHEMISTRY (IHC), BIOMECHANICAL PROPERTIES AND BIOCHEMICAL CONTENT OF LOX-TREATED ENGINEERED NEOCARTILAGE. a-b) Both control and constructs treated with LOX (Phase I and II) formed uniform neocartilage without physical abnormalities. Safranin-O/fast green staining for glycosaminoglycans and Picrosirius Red staining for collagen showed that constructs produced these matrix molecules uniformly for all groups. IHC illustrated that all groups exhibited collagen type II but not collagen type I, suggesting an articular cartilage phenotype. Phase I: **c**) Tensile stiffness as represented by Young's modulus and **d**) pyridinoline content normalized to neotissue wet weight (PYR/WW). Tensile stiffness was significantly enhanced by High LOX treatment (5.0 times over controls). These trends in biomechanical properties were mirrored by the crosslink content, which was 16.2 times greater for the High LOX group over controls. Phase II: **e**) Tensile stiffness as represented by Young's modulus, **f**) compressive modulus, and **g**) pyridinoline content normalized to neotissue wet weight (PYR/WW). Tensile stiffness was 5.3 times greater for the Early LOX group over controls. Pyridinoline content was significantly increased for both Early and Late LOX treatments (16.0 times over controls). Early LOX treatment significantly increased compressive stiffness and Late LOX treatment resulted in an aggregate modulus that was not significantly different from either control or Early LOX groups. Bars denote means ± SD, and groups not connected by the same letter are significantly different. PYR=pyridinoline, WW=wet weight.

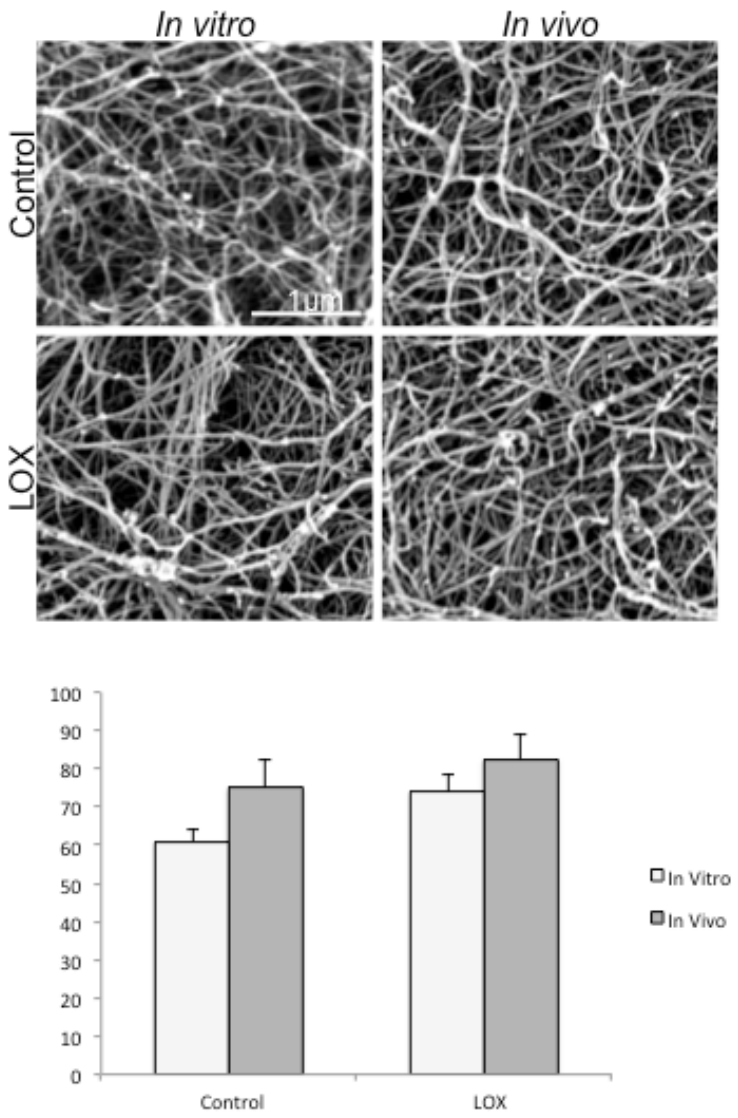

FIGURE 4.6 – SEM IMAGES AT T=12 WEEKS. (a) the *in vivo* environment to significantly enhance the fibril density of control neotissues over those grown in the *in vitro* culture environment. In addition, both *in vitro* and *in vivo* LOX-treated neotissues presented with significantly enhanced fibril density over *in vitro* control neocartilage (b) In terms of the fibril diameter of the neotissue no differences were detected among all groups. Bars labeled with different letters or star exhibit significant differences ($p < 0.05$).

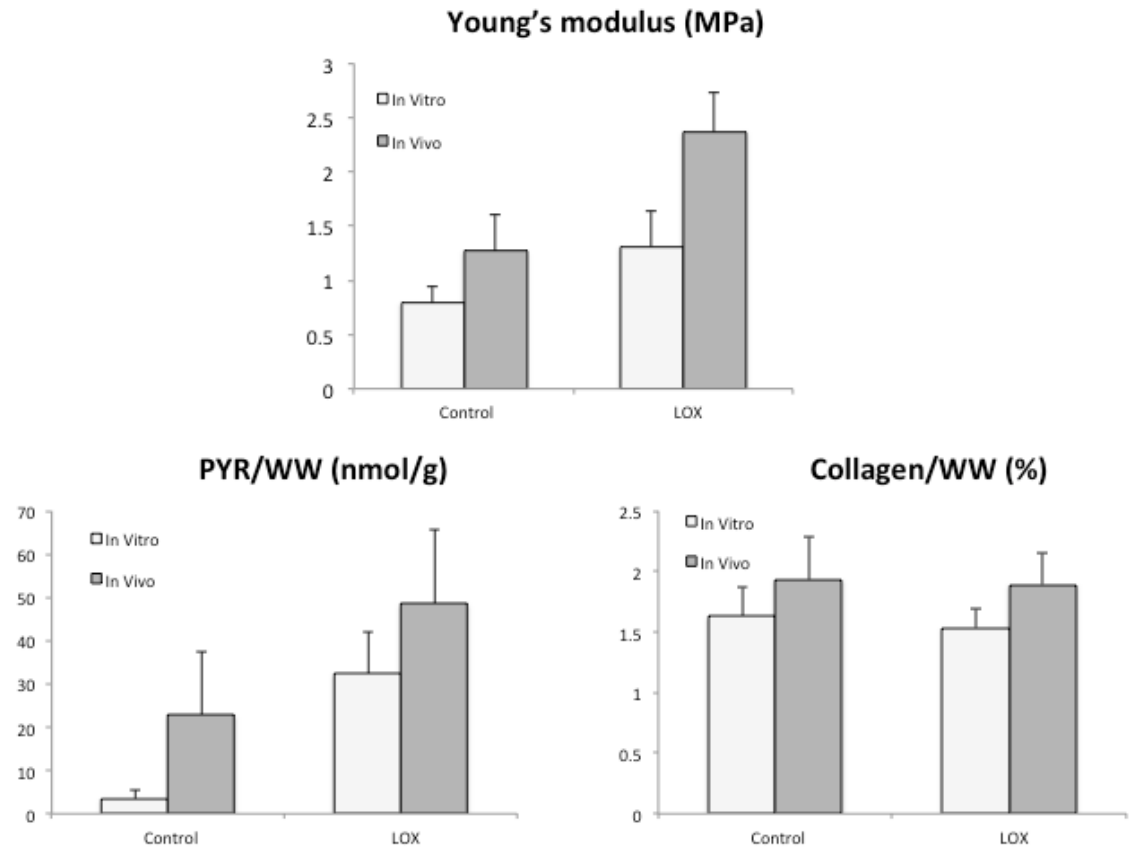

FIGURE 4.7 – PROPERTIES OF NEOCARTILAGE AT T=12 WEEKS AFTER *IN VITRO* CULTURE AND *IN VIVO* GROWTH IN NUDE MICE. Self-assembled articular cartilage was cultured for 6 weeks with LOX treatment applied during weeks 3 and 4. Neocartilage was then implanted in nude mice for additional 6 weeks; neocartilage constructs cultured at the same time *in vitro* as controls (n=6). Biomechanical evaluation revealed (a) *in vivo* implants to have significantly increased tensile modulus over their *in vitro* counterparts, while the *in vivo* grown LOX-treated constructs displayed a significantly increased tensile modulus that was 3-times greater than that of *in vitro* control. (b) The *in vivo* environment provided a significant benefit in tissue's compressive properties over the *in vitro* culture. Biochemical analysis showed (c) the *in vivo* environment to significantly increase the amount of PYR/WW in controls over those grown *in vitro* culture and the i*n vivo* LOX treatment to further promote that increase 14-times the *in vitro* control values. (d) The *in vivo* growth environment significantly enhanced the amount of collagen content per WW in both control and LOX treated groups. (d) No significant differences were observed in the amount of GAG content per WW. Bars labeled with different letters or star exhibit significant differences ($p < 0.05$).

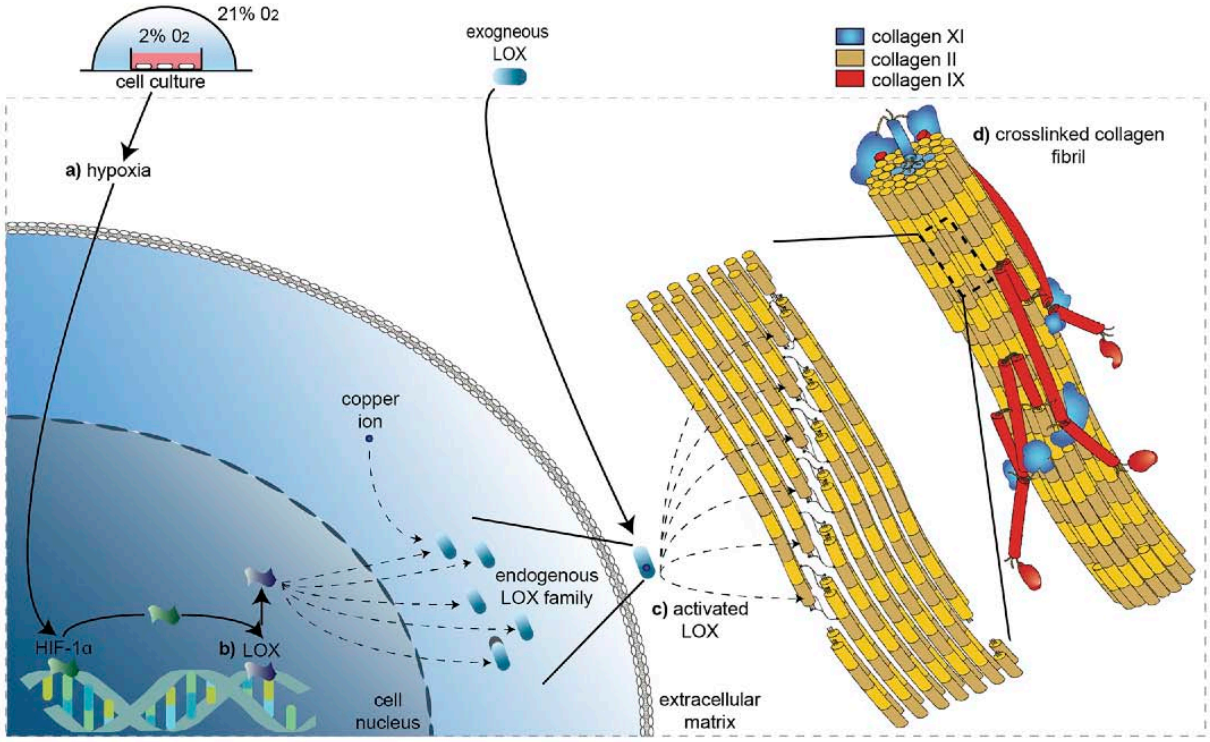

FIGURE 4.8 – A NOVEL MECHANISTIC DESCRIPTION OF HIF-1α-MEDIATED PYRIDINOLINE COLLAGEN CROSSLINKING FORMATION TOWARD ENHANCING BIOMECHANICAL PROPERTIES IN NATIVE AND ENGINEERED COLLAGEN-RICH TISSUES. a) Hypoxia application during tissue culture promotes HIF-1α-mediated endogenous LOX gene expression. **b**) Upregulation of LOX gene expression results in different LOX enzymes belonging in the same family (LOX-1, LOX-2, LOX-3, LOX-4, LOX-propeptide). **c**) Collagen maturation following biosynthesis occurs through extracellular modification of the collagen fibers by LOX, resulting in the formation of covalent pyridinoline crosslinks. Exogenous LOX application can promote the same effects bypassing the side effects of hypoxia. **d**) LOX (endogenous and exogenous)-mediated pyridinoline crosslinking formation enhances tensile properties of tissues and neotissues.

CHAPTER 5 – DIGOXIN AND ATP ENHANCE THE FUNCTIONAL PROPERTIES OF NEOCARTILAGE IMPLANTS THROUGH INTRACELLULAR ION MODULATION

ABSTRACT

Objective: Towards developing engineered cartilage for the treatment of arthritic pathologies, achieving relevant functional properties prior to implantation remains a significant challenge. Digoxin and adenosine triphosphate (ATP) are agents known to modulate intracellular Ca^{2+} signaling, a pathway through which mechanical stimuli acts in maintaining healthy cartilage matrix. The objective of this study is to determine whether these agents can promote matrix production in engineered neocartilage and increase its functional biomechanical properties

Design: Neocartilage constructs were formed by scaffold-free self-assembly of primary bovine articular chondrocytes. Digoxin, ATP, or both agents were added to the culture medium for 1 h/day at days 10-14. At the end of a 4-week culture period, neocartilage properties were assessed for gross morphology, biochemical composition, and biomechanical properties. Ca^{2+} dyes and time-lapse confocal microscopy were used to characterize Ca^{2+} oscillations induced by these agents.

Results: Digoxin and ATP were shown to increase the frequency of intracellular Ca^{2+} oscillations in chondrocytes. In neocartilage constructs, digoxin and ATP increased collagen content by 52-110% over untreated controls, while maintaining proteoglycan content near native

Chapter submitted as: Makris, E.A., Huang, B.J., Hu, J.C., Chen-Izu, Y., & Athanasiou, K.A. Digoxin and ATP enhance the functional properties of neocartilage implants through intracellular ion modulation. 2014

tissue values. Furthermore, digoxin and ATP increased the tensile modulus by 280% and 180%, respectively, while the application of both agents increased the modulus by 380%. The trends in tensile properties were found to correlate with the amount of collagen crosslinking.

Conclusions: This study provides a novel approach toward modulating intracellular calcium signaling in articular chondrocytes to direct neocartilage maturation and increase its functional properties.

INTRODUCTION

Affecting 46.4 million people annually, arthritis is the second most common chronic disease in the United States, creating a tremendous socioeconomic impact (1). Current therapies for cartilage pathologies include disease modifying osteoarthritis drugs, microfracture, cell- and scaffold-based procedures, and allograft transplantation. Although satisfactory short-term outcomes have been achieved with these techniques, they do not offer a permanent solution. Furthermore, the biomechanical properties of engineered tissues still remain far from native tissue values, leaving the neotissue incapable of withstanding the rigorous mechanical environment of articulating joints (2). Therefore, focusing on methods to bring the functional properties of engineered cartilage closer to native articular cartilage is crucial toward developing regenerative treatments.

Mechanical stimulation has been shown to be an important regulator of cartilage function and matrix homeostasis. *In vitro* experiments have shown that stimuli, such as dynamic compression and hydrostatic pressure, can induce chondrocytes to increase collagen and

proteoglycan synthesis (3, 4). These mechanotransduction pathways have been linked to ion channels and changes in intracellular Na^+ and Ca^{2+} concentrations (5, 6). For example, hydrostatic pressure applied to chondrocytes has been shown to inhibit the Na^+/K^+-ATPase and the $Na^+/K^+/2Cl^-$ co-transporter (5) and induce Ca^{2+} transients (7, 8). Micropipette indentation of chondrocytes induce Ca^{2+} transients via opening of stretch-activated Ca^{2+} channels (6). Fluid flow has also been observed to induce immediate Ca^{2+} transients in chondrocytes (9). Therefore, modulation of intracellular ion concentration provides a potentially beneficial tissue engineering strategy that is an alternative to mechanical stimulation.

Digoxin and ATP has been shown to alter intracellular Ca^{2+} through two different pathways. Digoxin's main action has been linked to inhibiting the Na^+/K^+-ATPase and reversing the function of the Na^+/Ca^{2+} exchanger (NCX), thereby raising intracellular Ca^{2+} (10). The rise in intracellular Ca^{2+} also raises Ca^{2+} stores in the endo/sarcoplasmic reticulum. The effects of digoxin on articular chondrocytes have not yet been investigated.

In addition to being a source of energy, ATP also functions as an extracellular signaling molecule, activating cell surface purinergic (P2Y and P2X) receptors for the regulation of various cell functions (11). Activation of P2Y receptors (G-protein coupled receptors) release ER-stored Ca^{2+} via the IP3 pathway, while activation of P2X receptors (ligand-gated ion channels) open the cell to cation (e.g., Na^+, K^+, Ca^{2+}) fluxes (11). Chondrocytes, specifically, have been shown to maintain a level of 2-3 nM ATP in the extracellular medium during *in vitro* culture (12) and express both P2Y and P2X receptor subtypes. During mechanical stimulation, ATP is thought to be release from chondrocytes and induce Ca^{2+} transients in a autocrine/paracrine fashion. Such Ca^{2+} transients are thought to be responsible for the beneficial effects of mechanical stimulation, such as increased matrix production (13-15). Because the

model suggests that mechanical stimuli are transduced to units of extracellular ATP, it is a promising chemical stimulus for cartilage tissue engineering.

In the present study, digoxin and ATP were applied to self-assembled neocartilage constructs to test the hypothesis that these agents will enhance their matrix content and biomechanical properties. A high dose of digoxin (20 μM) was applied to investigate its effect in neotissue; a low dose of digoxin (200 nM) was tested to explore a lower therapeutic dose. A concentration of 250 μM ATP was used, as this dosage had been shown to increase chondrocyte collagen synthesis (16). ATP and digoxin were applied simultaneously under the hypothesis that they will have an additive or synergistic effect. For a positive control, 20 μM ouabain was used, since its beneficial effects on chondrocytes through ion modulation have already been reported (17). Finally, KB-R7943, an inhibitor of the NCX, and suramin, an inhibitor of the P2Y receptor, were used to probe the mechanism of action of digoxin and ATP, respectively. All agents were applied at days 10-14 for 1 h/day, as this treatment window was shown to work best for mechanical and chemical stimuli that similarly alter calcium transients (3).

MATERIALS AND METHODS

Chondrocyte isolation

Superficial and middle/deep zone bovine articular chondrocytes were isolated from the femoral condyle and trochlear groove of calves (Research 87 Inc.), as previously described (3). All tissue engineered cartilage constructs were derived from cells of the same harvest.

Self-assembly of neocartilage constructs and growth

Disk-shaped neocartilage constructs were grown, as previously described (18). Briefly, $5.5x10^6$

chondrocytes were seeded into 5 mm diameter, 2% agarose wells. After 4 h, 400 μL medium was carefully added. 500 μL medium was changed every 24 h until day 10. At day 10, constructs were unconfined from the wells and placed into 6-well plates, where the medium was changed every 48 h. At 4 weeks, constructs were portioned for testing. The medium formulation consisted of DMEM (25 mM glucose with GlutaMAX™, Invitrogen), 100 nM dexamethasone (Sigma), 1% penicillin/streptomycin/fungizone, 1% ITS (BD Biosciences), 1% NEAA (Invitrogen), 100 μg/mL sodium pyruvate (Fischer Scientific), 50 μg/mL ascorbate-2-phosphate (Sigma), 40 μg/mL L-proline (Sigma).

Application of digoxin, ouabain, ATP, KB-R7943, and suramin

At days 10-14, the constructs were treated daily with a low or high concentration of digoxin (200 nM and 20 μM; Sigma), ATP (250 μM; Sigma), ouabain (20 μM; Sigma) or both digoxin (200 nM) and ATP. For the groups involving the use of inhibitors, constructs were first treated with KB-R7943 (10 μM; Tocris Biosciences) or suramin (100 μM; Tocris Biosciences) alone for 30 min. The constructs were then incubated in medium containing both the inhibitor and the respective agent for 1 h. After treatment, constructs were washed for 30 min and returned to normal culture conditions. Stock digoxin was prepared at 20 mM in DMSO (Sigma); KB-R7943 at 20 mM in DMSO; ouabain at 1 mM in PBS; and suramin at 2 mM in culture medium. ATP was freshly prepared in medium before application.

Analysis of growth metrics

Pictures of gross construct morphology were taken and construct total wet weights measured. Each construct was then sectioned into appropriately sized pieces for biochemical and

biomechanical analysis. Water content was calculated with samples used for biochemical analysis.

Histology and immunohistochemistry

Samples were cryosectioned at 16 μm, fixed in formalin, and stained with Safranin O/Fast Green and Picrosirius Red. Collagen II and collagen I immunohistochemistry were conducted, as described previously (19). Briefly, cryosections were fixed in cold acetone and incubated with mouse anti-collagen I (Accurate) and rabbit anti-collagen II (Cedarlane Labs) primary antibodies. The secondary antibodies used were anti-mouse and anti-rabbit IgG antibodies, respectively, from the Vectastain ABC kit. Color was developed using the Vectastain ABC reagents and DAB (Vectastain).

Biochemical analysis

Lyophilized portions of the constructs were digested in papain for 18 h at 60°C. Total collagen content was determined by measuring hydroxyproline content using a chloramine T assay (20). Total sulfated glycosaminoglycan (GAG) content was measured using the Blyscan sGAG assay kit (Accurate). DNA content was measured using the Quant-iT PicoGreen assay kit (Invitrogen) and normalized to cell number using a conversion of 7.7 ng DNA/cell. Pyridinoline crosslinks were measured as previously described (21). Briefly, tissue samples were digested in 800 μL 6 N HCl at 100°C for 18 h, dried with a SpeedVac, re-suspended in 50 μL of a solution containing 10 nmol pyridoxine/mL and 2.4 μmol homoarginine/mL (Sigma) in water, and analyzed under high performance liquid chromatography (HPLC).

Biomechanical analysis

For compressive testing, 3 mm diameter punches were tested with a creep indentation apparatus, as previously described (17). Aggregate modulus, permeability, and Poisson's ratio were calculated using a semianalytical, seminumeric, linear biphasic model and finite element analysis (22). For tensile testing, dog bone-shaped samples were made, photographed, and subjected to uniaxial tension using an Instron (Model 5565). Cross-sectional areas were calculated using the photographs and ImageJ software. The linear region of the stress-strain curve was used to determine the Young's modulus. The ultimate tensile strength (UTS) was determined as the maximum stress reached in the curve.

Ca^{2+} imaging of chondrocytes stimulated with ATP, digoxin, and ATP + digoxin

Chondrocytes were seeded on glass cover slips (No.1, 25 mm x 25 mm) at 70,000 cells/cm^2, cultured overnight, and stained with 2.5 μM Fluo-4/AM (Invitrogen) for 1-2 h in the presence of 0.75 μM Pluronic F-127 (Invitrogen). Coverslips were placed into a custom-built drug perfusion system, which used gravity flow to continuously profuse the cells with fresh solution at a flow rate of ~1.5 mL/min. With an Olympus FV1000 confocal microscope, time-lapse images (6 s/frame) were acquired over 30 min in a field of view containing ~20-30 cells using a 60X water immersion objective (NA1.2, corrected for the thickness of the No.1 glass coverslip). Fluorescence was collected at 488 nm excitation and 505-605 nm emission. During the first 15 min, buffer solution (Tyrode's solution containing 1 mM Ca^{2+}) was perfused over the cells to capture baseline Ca^{2+} activity. During the next 15 min, buffer solution, containing either ATP (250 μM), digoxin (200 nM), or the combined drugs, was perfused over the cells. Using ImageJ software, regions of interest were drawn around each cell, fluorescence values measured, and

Ca^{2+} traces established. Traces were loaded into a Matlab program to count the number of Ca^{2+} oscillations, which were defined as peaks exceeding a threshold of 1.3 times the baseline fluorescence intensity. Frequency of oscillations was defined as the average number of oscillations per cell over 15 min. Each slide represented one sample (n = 4-6).

Statistics

All data sets were analyzed with one-factor ANOVA to determine significance among groups and Fischer's LSD *post hoc* test ($p<0.05$) using StatView software. To test for synergistic or additive effects between digoxin and ATP, the interaction term of a two-factor ANOVA was used, as previously described (23), where the factors assessed were digoxin and ATP. Univariate regression was run to correlate pyridinoline content and tensile modulus.

RESULTS

Gross morphology and histology

At the end of 4 weeks of culture, all self-assembled constructs had smooth surfaces and uniform morphology (Fig. 1) (Table 1). All constructs stained uniformly for GAG and collagen with no gross differences in staining intensity among the groups (Fig. 2A). In addition, neocartilage from all groups stained positively for type II collagen and negatively for type I collagen (Fig. 2A), indicating the formation of hyaline-like cartilage phenotype.

Biochemical properties

Digoxin- and ATP-treated constructs had significantly higher collagen per wet weight (WW) than untreated controls (52-110% increase) (Fig. 2B). In line with previous results (17), ouabain

increased collagen/WW by ~90% over controls. Unexpectedly, the application of inhibitors KB-R7943 and suramin did not abolish the action of digoxin and ATP, suggesting an alternative mechanism of action. These results indicate that digoxin and ATP can increase collagen synthesis in tissue engineered cartilage constructs.

The digoxin (low) and digoxin (low)+ATP group had a significantly higher amount of pyridinoline per collagen (PYR/collagen) than the ouabain, digoxin (high), and ATP groups (Table 1). Consistent with previous results from our group, PYR/collagen for the control group was 1.36 ± 0.24 nmol/mg. Univariate regression analysis revealed that PYR/collagen was statistically correlated to the Young's modulus ($R^2 = 0.70$) (Fig. 4), indicating that the formation of collagen crosslinks was a major contributor to neocartilage biomechanical properties.

All digoxin-treated groups had lower GAG content (GAG/WW) than controls (Table 1). Ouabain and ATP did not affect GAG content. Pre-treatment with the NCX inhibitor KB-R7943 abolished digoxin-induced changes in the GAG content of neotissue. Finally, the number of cells per construct was significantly decreased in the digoxin (high) group compared to controls, while no significant differences were observed in the other groups (Table 1).

Biomechanical properties

Compressive and tensile tests were conducted to determine the biomechanical properties of the self-assembled cartilage constructs. In terms of the tensile properties, digoxin (low), digoxin (high), ATP, and ouabain significantly increased the construct's Young's modulus over untreated controls by 282%, 170%, 148%, and 120%, respectively (Fig. 3A). Combined treatment of digoxin (low) and ATP resulted in the highest increase in tensile modulus (~380% increase over controls). Pre-treatment with the NCX inhibitor KB-R7943 partially inhibited

digoxin-induced effects, while pre-treatment with suramin completely abolished ATP-induced effects. Similar trends were shown in the ultimate tensile strength (UTS) of the constructs (Fig. 3B). In terms of compressive properties, no significant differences were detected among the groups (Table 2). Results here indicate that digoxin and ATP significantly enhanced the tensile properties of the constructs, while their combined treatment resulted in an additive increase.

Ca^{2+} imaging of 2D cultured chondrocytes

Without any stimulation, chondrocytes are known to express a basal level of Ca^{2+} oscillations, a natural signaling process that has been linked to the regulation of matrix production following mechanical stimuli. Addition of digoxin (200 nM) and ATP (250 μM) significantly increased the frequency of intracellular Ca^{2+} oscillations in cultured chondrocytes over basal levels (Fig. 5C). When comparing between drugs, ATP induced a higher frequency of Ca^{2+} oscillations than digoxin, while the combination of drugs induced a frequency similar to ATP alone.

Digoxin and ATP induced Ca^{2+} oscillations of different characteristics (Fig. 5B). Representative traces are shown in Fig. 5B, but it is noted that chondrocyte Ca^{2+} activities were heterogeneous. Digoxin-induced Ca^{2+} transients showed little periodicity, were generally small in amplitude, and had a rolling shape (Fig. 5B, top). Digoxin induced a response in ~60% of the cells, while the other 40% did not show any response to the agent. ATP induced a single, large Ca^{2+} peak immediately after drug application in more than 95% of the cells. This initial peak was followed by trains of periodic oscillations (3-8 peaks) that continued over the next 15 min in ~20% of the cells (Fig. 5B, bottom). In the other ~80% of the cells, only 0-2 peaks were observed immediately after the initial peak, which was then generally followed by inactivity (Fig. 5B, bottom). Digoxin combined with ATP generated Ca^{2+} oscillations that were

characteristically similar to ATP alone. Results here show that digoxin and ATP were able to increase the frequency of Ca^{2+} oscillations in chondrocytes.

DISCUSSION

Tissue engineering holds great potential toward treating articular cartilage defects resulting from trauma or degenerative diseases, such as osteoarthritis. However, current methods to develop neocartilage *in vitro* result in functionally inadequate matrix possessing poor biomechanical properties. To address this problem, mechanical stimuli, such as dynamic compression or hydrostatic pressure, have often been used to increase chondrocyte matrix production (3, 4). Because the mechanotransduction pathway is thought to involve intracellular Ca^{2+} signaling (5-8). the application of Ca^{2+}-modulating agents to tissue engineered cartilage presents an alternative strategy that may achieve similar results to mechanical stimulation.

The results of this study demonstrate that digoxin or ATP can increase the biochemical and biomechanical properties of neocartilage. The application of either digoxin (200 nM and 20 μM) or ATP (250 μM) significantly increased collagen content of neocartilage by ~1.5- to 2-fold over controls and tensile modulus by ~2- to 4-fold over controls. When digoxin (200 nM) and ATP (250 μM) were applied together, they additively increased the tensile modulus by ~5-fold over controls. Thus, this study demonstrates that modulation of intracellular Ca^{2+} in articular chondrocytes via digoxin and ATP is a viable strategy to enhance neocartilage functional properties. These results also further establish the importance of Ca^{2+} signaling pathways in chondrocyte metabolism and matrix homeostasis.

The use of digoxin and ATP was motivated in part by the fact that both are clinically used, albeit for indications not related to cartilage pathologies. Digoxin is a cardiac glycoside

and one of the most prescribed agents for treating heart failure and arrhythmias (24). Digoxin was chosen in light of previous results demonstrating that ouabain (20 μM), a cardiac glycoside similar in structure to digoxin, increased the collagen content (90% increase over controls) and tensile properties (110% increase over controls) of self-assembled neocartilage (17). Digoxin is also an FDA-approved drug, while ouabain remains an experimental drug that is not easily translatable to the clinical setting. ATP was chosen because of its role in the chondrocyte mechanotransduction pathways (13-15, 25). ATP has been injected intravenously in patients as a nutritional supplement (26). Because these agents are effective in increasing neocartilage properties and are currently clinically used, they demonstrate great potential as immediate candidate agents for translational tissue engineering applications.

The 200 nM (low) dose of digoxin was found to have a better effect on construct properties than the 20 μM (high) dose of digoxin. Both doses significantly increased collagen content to similar values (54-73% increase over controls), but the low dose increased the tensile modulus more than the high dose. The lower tensile properties of the digoxin (high) group can be attributed to its lower collagen crosslinking content. It is also possible that the 20 μM dose of digoxin promoted a cytotoxic effect on the cells, as potentially indicated by the lower DNA content. Therefore, 200 nM of digoxin was determined to be an effective dose that enhances both collagen content and tensile properties of neocartilage constructs without having significant adverse effects.

Digoxin, when compared to ouabain, was found to have a more potent effect. Specifically, digoxin (low) significantly increased the Young's modulus by 54% and digoxin (low and high) significantly increased the UTS by ~50% over that of ouabain (20 μM). Given the current data, these differences can be attributed to digoxin's ability to induce more collagen

crosslinks than ouabain. Interestingly, previous reports have reported different mechanisms of action of these drugs. For example, digoxin and ouabain can induce different hemodynamic effects in rats (27), indicating the two drugs may have different cellular effects**.** Digoxin not only affects the Na^+/K^+-ATPase, but may also affect intracellular receptors and transmembrane calcium channels differently than ouabain (28). Although these molecular mechanisms are still under investigation, this study supports that digoxin has a more potent effect over ouabain in enhancing neocartilage properties.

Although digoxin and ATP promoted neocartilage collagen content and tensile properties, these two properties did not correlate as typically expected (29). Previous attempts to correlate mechanical properties with matrix components, such as collagen, GAG, and mineralization, have been met with inconsistent results (21, 29-31). In one study, a significant correlation was found between tensile strength and collagen content of engineered cartilage (32), while another study reported no significant correlation between the Young's modulus and collagen content (30). A tissue's tensile properties most likely arise from the interactions among multiple matrix components. Some of these have received little attention, such as pyridinoline crosslinks within the collagen network. Indeed, in the present study, regression analysis revealed that for the treated groups, tensile properties were found to correlate (R^2=0.70) with the amount of pyridinoline crosslinks normalized to collagen (Fig. 4). Interestingly, the digoxin (low) group exhibited the highest amount of PYR/collagen, showing for the first time that digoxin can increase collagen crosslinks in articular cartilage.

Although the control group contained a higher crosslink to collagen ratio when compared to all treated groups, its tensile properties were lower. This paradox may be explained by the timing of treatment application. In self-assembled neocartilage, collagen content plateaus

roughly at 10 days, which is then followed by tissue maturation (33). Treatment with the agents at days 10-14 may have induced additional collagen synthesis that may not have had sufficient time to form crosslinks, as formation of mature (trifunctional) pyridinoline crosslinks requires 7 to 28 days (34). Therefore, the control group did not exhibit correlation between the Young's modulus and PYR/collagen content as the other groups.

The compressive properties of neocartilage remained indifferent to treatment, despite observed changes in the GAG content. All digoxin-treated groups significantly lowered the GAG content, while ouabain and ATP had no effects on GAG. While most articular cartilage engineering approaches result in relatively low levels of collagen, they are able to attain quantities of GAG on par with native tissue (19). This imbalance in the physiological GAG to collagen ratio has typically resulted in engineered tissues with reasonable compressive properties but very low tensile properties. Therefore, it is of interest to target approaches that increase the collagen content and tensile properties of engineered cartilage without necessarily further enhancing the compressive properties. Intracellular ion modulation with digoxin and ATP provides a method for increasing tensile properties and collagen content independent of affecting the compressive modulus.

Time-lapse confocal microscopy revealed that digoxin and ATP increased the frequency of intracellular Ca^{2+} oscillations in chondrocytes. Effects of digitalis glycosides on Ca^{2+} signaling of non-excitable cells, such as chondrocytes, have not been previously studied. However, in these excitable cells, such as cardiomyocytes, digoxin at high doses has been shown to induce spontaneous release of Ca^{2+} transients from overloaded and unstable intracellular Ca^{2+} stores (35). Therefore, the increased frequency of spontaneous Ca^{2+} oscillations in digoxin-induced chondrocytes may follow a similar mechanism.

ATP has been well known to induce trains of Ca^{2+} oscillations in chondrocytes (36) and in other cell types. In chondrocytes, Ca^{2+} oscillations induced by ATP have been attributed to the activation of P2Y receptors and release of ER-stored Ca^{2+} via the IP3 pathway (37). It is unclear why ATP induces periodic trains of Ca^{2+} oscillations in only a specific proportion of the cells (20%), as reported here and in previous studies (36), but the heterogeneity of the chondrocyte population may be a factor.

Since the two agents additively increased construct tensile properties, it was of interest to see if an explanation could be derived from the level of Ca^{2+} signaling. Because ATP-stimulated chondrocytes exhibited periodic trains of Ca^{2+} oscillations, they appear to behave like excitable cells. With digoxin's known effects on excitable cells, cooperation between ATP and digoxin was hypothesized to manifest in an additive or synergistic increase in Ca^{2+} signaling activity. However, this was not observed when the two agents were combined. Although the additive effects of the agents cannot be explained by the frequency of Ca^{2+} transients, other characteristics of the Ca^{2+} signal yet to be characterized, such as the amplitude of oscillations, may be a contributing factor.

The mechanisms of action of digoxin and ATP were also explored using the inhibitors KB-R7943 and suramin, respectively. KB-R7943 binds to and inhibits the reverse mode of the NCX and has been shown to prevent digoxin-induced rises in intracellular Ca^{2+}. In the present study, addition of KB-R7943 partially abolished digoxin (low)-induced changes in Young's modulus and GAG content but did not abolish digoxin-induced changes in other construct properties. Therefore, digoxin may act by pathways independent of the NCX. Inhibition of the Na^{+}/K^{+}-ATPase may alter cell resting potential, cell swelling, and MAPK activation (38) among

other effects. Interestingly, these cellular changes are also known to occur in chondrocytes during mechanical compression of cartilage (39-41).

Suramin, a reported inhibitor of P2YR, abolished ATP-induced changes in the Young's modulus, but did not affect ATP-induced changes in the collagen content. These results indicate that ATP can act by pathways independent of the P2YR. ATP is known to also bind cell surface P2X receptors, ligand-gated ion channels, which can affect intracellular ion concentrations and cell signaling. In addition, chondrocyte surface ecto-nucleotidases can convert extracellular ATP into adenosine (11), a widely studied extracellular signaling molecular in cartilage biology. Depletion of extracellular adenosine has been shown to promote cartilage degradation (42), indicating a role of adenosine in cartilage matrix homeostasis. Therefore, digoxin and ATP may have multiple effects on the chondrocyte that requires further study. These Ca^{2+}-independent pathways may also contribute to the additive effects seen by digoxin and ATP, which could not be initially explained by the Ca^{2+} signaling characteristics.

In conclusion, the present study supports that modulating intracellular calcium concentration via exogenous application of the chemical agents digoxin and ATP can alter the development of engineered articular cartilage. These agents are chosen to mimic the effects of stimuli involved in mechanotransduction. Application of 200 nM digoxin and 250 μM ATP individually increases the tensile modulus and collagen content of the engineered neocartilage, while their combination results in additive increases in both biochemical and functional properties. Overall, this study provides insight into important aspects of chondrocyte mechanotransduction-like pathways and suggests the use of novel pharmacological agents. Additionally, the ability of these agents to be applied exogenously raises the potential for direct

in vivo applications of these drugs, for example via intra-articular injections, to treat degenerative cartilage pathologies such as osteoarthritis.

TABLES & FIGURES

TABLE 5.1 – GROSS MORPHOLOGY OF NEOTISSUE. Neocartilage wet weight (WW), water content, glycosaminoglycan (GAG) content, cells/construct, and PYR/collagen content at the end of 4 weeks of culture.

Group	Wet Weight (mg)	Water Content (%)	GAG/WW (%)	Cells/ Construct (millions)	PYR/collagen (nmol/mg)
Control	38.5 ± 1.5^{c}	85.1 ± 1.5^{ab}	4.1 ± 0.6^{a}	5.8 ± 0.2^{ab}	1.36 ± 0.24^{a}
Ouabain	32.6 ± 1.0^{d}	87.1 ± 3.2^{a}	4.7 ± 1.2^{a}	5.1 ± 0.6^{bc}	0.83 ± 0.15^{cd}
Digoxin (low)	41.6 ± 3.5^{ab}	84.9 ± 1.6^{ab}	3.5 ± 0.4^{bc}	6.1 ± 0.5^{a}	1.07 ± 0.21^{b}
Digoxin (high)	33.1 ± 3.2^{d}	86.4 ± 2.0^{a}	2.5 ± 0.2^{c}	4.5 ± 0.4^{c}	0.81 ± 0.20^{cd}
ATP	41.7 ± 1.7^{a}	85.0 ± 1.4^{ab}	4.0 ± 0.8^{a}	5.8 ± 0.4^{ab}	0.68 ± 0.11^{d}
Digoxin (low) + ATP	40.0 ± 2.5^{abc}	86.6 ± 1.2^{a}	3.3 ± 0.6^{bc}	5.7 ± 0.7^{ab}	1.06 ± 0.21^{bc}
Digoxin (low) + KB-R7943	38.9 ± 2.5^{bc}	83.5 ± 2.2^{b}	3.9 ± 0.6^{ab}	6.1 ± 0.7^{a}	0.75 ± 0.18^{cd}
ATP + Suramin	40.5 ± 1.7^{abc}	83.3 ± 1.3^{b}	4.2 ± 1.0^{a}	5.5 ± 0.8^{ab}	0.83 ± 0.23^{bcd}

TABLE 5.2 – NEOCARTILAGE COMPRESSIVE PROPERTIES AT THE END OF 4 WEEKS OF CULTURE.

Group	Aggregate Modulus (kPa)	Permeability (10^{-15} $m^4/N \cdot s$)	Poisson Ratio
Control	125±45	46±26[a]	0.12±0.06
Ouabain	111±40	20±12[b]	0.08±0.05
Digoxin (low)	139±49	28±12[ab]	0.10±0.05
Digoxin (high)	120±35	21±14[b]	0.11±0.08
ATP	90±23	29±22[ab]	0.11±0.07
Digoxin (low) + ATP	123±36	17±8[b]	0.14±0.05
Digoxin (low) + KB-R7943	93±36	33±19[ab]	0.09±0.07
ATP + Suramin	123±19	38±22[ab]	0.13±0.10

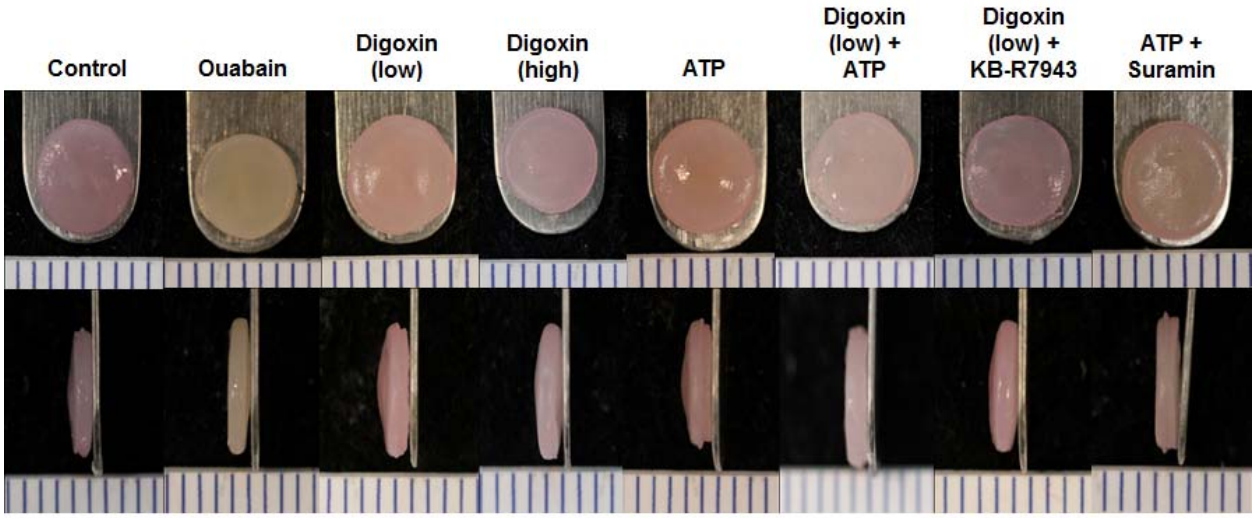

FIGURE 5.1 – REPRESENTATIVE IMAGES OF SELF-ASSEMBLED NEOCARTILAGE CONSTRUCTS FROM EACH GROUP AT THE END OF 4 WEEKS OF CULTURE. All constructs appeared flat and disc-shaped with no gross morphological differences.

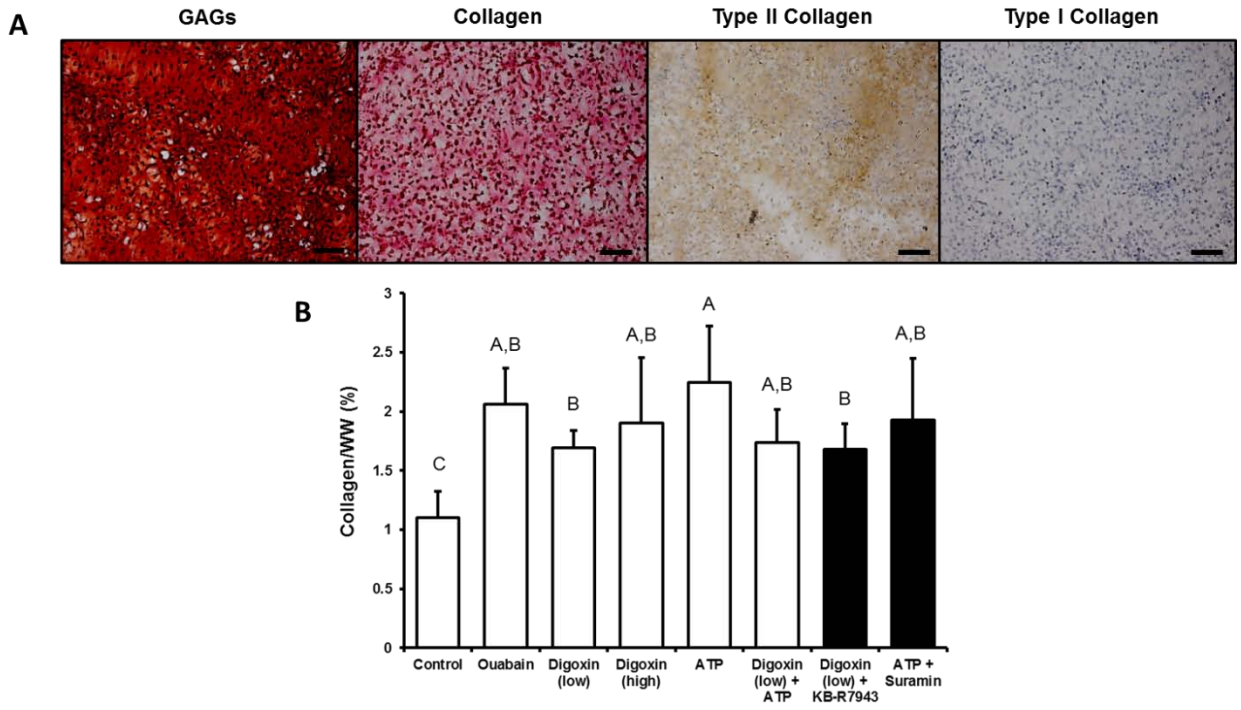

FIGURE 5.2 – NEOCARTILAGE GAG AND COLLAGEN CONTENT AT THE END OF 4 WEEKS OF CULTURE. (A) Histological staining showed the presence of GAGs (Safranin O/Fast Green stain) and total collagen (Picrosirius Red stain) throughout the construct. Immunohistochemistry indicated the presence of type II collagen and the absence of type I collagen. Scale bar: 50 μm. (B) Measurement of the collagen content indicated that all chemical agents increased collagen production over controls.

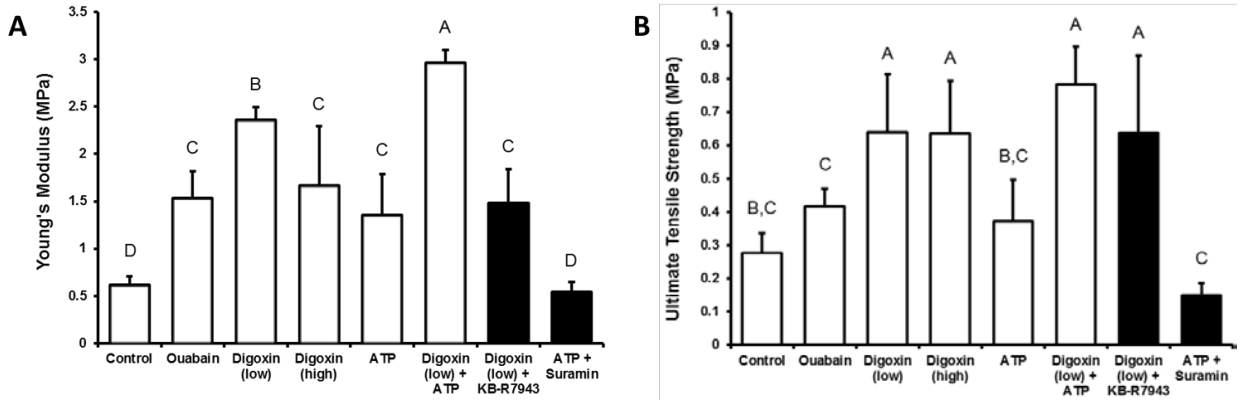

FIGURE 5.3 – NEOCARTILAGE TENSILE PROPERTIES. Neocartilage Young's modulus (A) and UTS (B) after 4 weeks of culture. Digoxin and ATP, either alone or combined, were able to increase the tensile properties of neocartilage compared to controls.

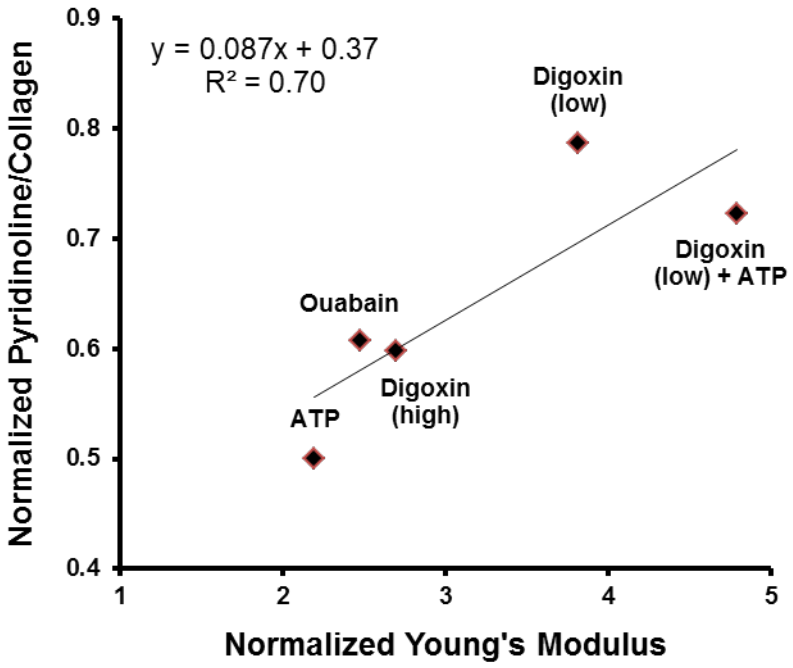

FIGURE 5.4 – RELATIONSHIP BETWEEN PYRIDINOLINE CONTENT AND YOUNG'S MODULUS. PYR/collagen plotted with Young's modulus (both normalized to control) indicated a strong correlation between collagen crosslinks and tensile properties.

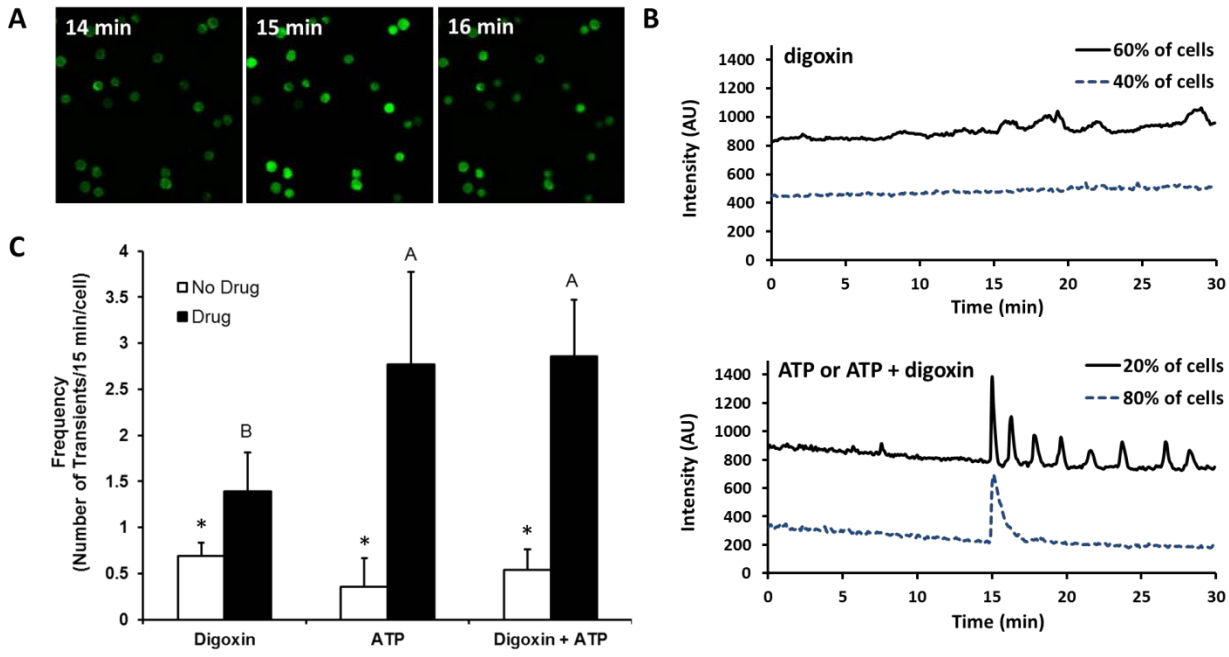

FIGURE 5.5 – INTRACELLULAR Ca^{2+} SIGNALING IN 2D CULTURED ARTICULAR CHONDROCYTES STIMULATED WITH DIGOXIN AND ATP. (A) Representative images of chondrocytes cultured on glass slides showing an increase in intracellular Ca^{2+} upon induction with ATP at 15 min. (B) Representative Ca^{2+} traces induced by each agent. ATP and digoxin+ATP induced similar responses. Traces were shifted on the y-axis for better visualization. Downward drifts were due to photobleaching. (C) All agents increased the frequency of Ca^{2+} oscillations over baseline controls, as determined by a paired t-test (significance denoted by an asterisk). ATP and digoxin+ATP induced more Ca^{2+} oscillations than digoxin alone, as determined by a one-way ANOVA comparing the different drugs (black bars).

CHAPTER 6 – A CHONDROITINASE-ABC AND TGF-β1 TREATMENT REGIMEN FOR ENHANCING THE MECHANICAL PROPERTIES OF TISSUE ENGINEERED FIBROCARTILAGE

ABSTRACT

The development of functionally equivalent fibrocartilage remains elusive despite efforts to engineer tissues such as the knee menisci, intervertebral disc, and TMJ disc. Attempts to engineer these structures often fail to create tissues with mechanical properties on par with native tissue, resulting in constructs unsuitable for clinical applications. The objective of this study was to engineer a spectrum of biomimetic fibrocartilages representative of the distinct functional properties found in native tissues. Using the self-assembly process, different co-cultures of meniscus cells (MCs) and articular chondrocytes (ACs) were seeded into agarose wells and treated with the catabolic agent chondroitinase-ABC (C-ABC) and the anabolic agent transforming growth factor-β1 (TGF-β1) via a two-factor (cell ratio and bioactive treatment), full factorial study design. Application of both C-ABC and TGF-β1 resulted in a beneficial or positive increase in the collagen content of treated constructs compared to controls. Significant increases in both the collagen density and fiber diameter were also seen with this treatment, increasing these values 32% and 15%, respectively, over control values. Mechanical testing found the combined bioactive treatment to synergistically increase the Young's modulus and

Chapter published as: MacBarb, R.F., Makris, E.A., Hu, J.C., & Athanasiou, K.A. A Chondroitinase-ABC and TGF-β1 Treatment Regimen for Enhancing the Mechanical Properties of Tissue-Engineered Fibrocartilage. *Acta Biomaterialia.* 9(1):4626-4634, 2012.

ultimate tensile strength of the engineered fibrocartilages compared to controls, with values thatC-ABC and TGF-β1 interact to develop a denser collagen matrix better able to withstand tensile loading. This study highlights a way to optimize the tensile properties of engineered fibrocartilage using a biochemical and biophysical agent together to create distinct fibrocartilages with functional properties mimicking those of native tissue.

INTRODUCTION

Fibrocartilage is uniquely situated within specific joint spaces of the body to facilitate the distribution of peak loads. Viscoelastic in nature, this tissue is capable of deforming its shape to effectively spread loads across a greater surface area. Found, for example, in the knee, intervertebral, and temporomandibular joints, fibrocartilage is distinctively situated to allow for congruent meshing of the articulating structures within these joint spaces, ensuring smooth, stable articulation and stress absorption[10, 223, 224]. However, fibrocartilage lacks an innate ability to self-repair following disease or injury. With a lack of clinically available treatment options for patients suffering from injured or diseased fibrocartilage, the need for an effective remedy is crucial. Fibrocartilages engineered *in vitro* offer new hope as a long-term treatment option to repair or replace injured or degenerated fibrocartilaginous tissues.

Collagens make up the majority of the extracellular matrix (ECM) of a fibrocartilaginous tissue. Within a specific fibrocartilage, these collagen fibers align with the peak tensile loads in a given joint space, situating the tissue to best distribute complex forces. While fibrocartilages are primarily composed of collagen type I, they also contain lower amounts of collagen type II as well as glycosaminoglycans (GAGs). The levels at which these

main ECM components are found are characteristic of the anatomical location and function. The heterogeneous distribution and organization of ECM result in anisotropic biomechanical properties specific to each fibrocartilage type. Efforts to tissue engineer fibrocartilages able to withstand the mechanical complexity of a joint space must therefore focus on creating a well-developed, collagen-rich matrix.

Capitalizing on chondrocytes' unique ability to form dense, ECM-rich clusters when seeded at high densities, a scaffold-free, self-assembly approach to cartilage tissue engineering has been developed[212]. With primary TMJ disc and intervertebral disc cells presenting as an implausible cell source due to limited cell numbers in the tissue as well as low levels of matrix production *in vitro*, this technology has recently been extended to co-cultures of varying ratios of meniscus cells (MCs) and articular chondrocytes (ACs), allowing for the formation of a spectrum of fibrocartilages[4, 47, 225]. While current efforts to tissue engineer fibrocartilage have succeeded in creating constructs with compressive properties on par with native tissue values, tensile properties have lagged greatly behind[4, 5, 226-228]. This is a significant problem for fibrocartilages, as they function under both compression and tension. For instance, resistance to compression in the knee menisci occurs via tensile, hoop stresses developed in the wedged-shape of this tissue. Likewise, tension-compression is also observed in the TMJ disc[10]. Here, ligaments around the periphery of the disc secure the tissue within in the joint space, and as the condyle translates during jaw opening, it compresses the disc, causing inherent tension much like that of a trampoline[31]. Exogenous stimuli such as TGF-β1 and chondroitinase-ABC (C-ABC) have therefore been investigated to enhance the tensile properties of self-assembled, engineered fibrocartilages[4, 8, 99, 217].

Previous work with C-ABC has shown that this enzyme's temporary depletion of GAG enhances the tensile properties of treated articular cartilage explants[229]. It has also been shown that there is a window of effectiveness for C-ABC's application; applying C-ABC at both t = 2 wk and t = 4 wk of culture is superior to a single treatment at either time point for enhancing the tensile properties of tissue-engineered articular cartilage[8]. In another study, tissue-engineered meniscus cartilage was treated with C-ABC at an earlier time point to determine if treating a more immature matrix would have a greater effect on tissue development, as chondrocytes produce the majority of their matrix during the first week of self-assembly[230]. Results found a single, early application of C-ABC at t = 1 wk to be beneficial in enhancing the tensile properties of the tissue[99].

Recent work has shown concurrent application of C-ABC and TGF-β1 results in further enhancement of the mechanical properties of tissue-engineered cartilage compared to treatment with either agent alone[99, 231]. Application of these two agents on tissue-engineered neocartilage was found to synergistically increase collagen content and additively increase the tissue's tensile strength[231]. In a separate study, engineered meniscus fibrocartilage experienced a 5-fold increase in the radial tensile modulus as well as a 196% increase in collagen content after being treated with both C-ABC and TGF-β1[99]. Through depleting GAG, C-ABC releases GAG fragments, such as hyaluronic acid fragments, into the tissue, and such fragments have been reported to have an anabolic effect on surrounding cells[232]. Microarray analysis of self-assembled articular cartilage treated with C-ABC, however, has found no changes in gene expression as a result of this treatment, suggesting the GAG fragments are being effectively removed from the tissue[231]. Further, inspection of C-ABC treated engineered articular cartilage via scanning electron microscopy (SEM) has found C-ABC to work via a biophysical

mechanism, through altering the physical structure of a collagen network. Microarray analysis work has also found that TGF-β1 promotes chondrocytes to synthesize more ECM through a MAPK biochemical pathway[231]. It was concluded that these bioactive agents are able to collaboratively increase the functional properties of tissue-engineered cartilage because they act via different mechanisms: one being biophysical, the other biochemical. With previous work on enhancing the functional properties of a spectrum of engineered fibrocartilage focused on TGF-β1 alone, it is important to institute both TGF-β1 and C-ABC with the goal of further enhancing the functional properties of such tissues.

The overall objective of this study was to generate biomimetic fibrocartilages representative of the vast array of distinct fibrocartilages found in the body. Given the previous success of engineering such tissues with compressive properties on par with native tissue values, this study emphasized enhancing the tensile properties of engineered fibrocartilage. To capture the heterogeneous nature of the different types of fibrocartilage, a spectrum of fibrocartilaginous tissues was generated using the self-assembly process and optimized using C-ABC and TGF-β1 alone or in combination. Tissues having different ratios of MCs and ACs were created to recapitulate the diversity of collagen type I to collagen type II found in fibrocartilages. After optimizing a C-ABC treatment regimen, tissues were treated with the bioactive agents C-ABC and TGF-β1 using a two-factor, full factorial study design with cell ratio and bioactive treatment as the factors. Overall, it was hypothesized that the combination of C-ABC and TGF-β1 would significantly increase the tensile properties of each of the co-culture constructs without compromising their compressive properties. It was further hypothesized that by increasing the tensile properties, the combined bioactive treatment regimen would generate

co-culture ratio-dependent fibrocartilages having distinct functional properties within the range of native tissue.

MATERIALS AND METHODS

Cell isolation and self-assembly into fibrocartilage constructs

Bovine articular chondrocytes and meniscus cells were harvested from juvenile bovine knee joints (Research 87, Boston, MA). Minced articular cartilage was digested in base medium of Dulbecco's modified Eagle's medium (DMEM) with 1% penicillin/streptomycin/fungizone (PSF), containing 0.2% collagenase (Worthington, Lakewood, NJ) for 18 hours. Minced menisci were digested in base medium containing 0.25% Pronase E (Sigma, St. Louis, MO) for 1 hour prior to 18 hours in 0.2% collagenase-containing base medium. Isolated cells were frozen in base medium containing 20% fetal bovine serum and 10% dimethyl sulfoxide until needed for seeding.

Cells were self-assembled at 50:50 and 75:25 MC:AC co-culture ratios as previously described[4, 212]. Based on preliminary work, a 100:0 MC:AC cell ratio was not used in this study, as neither C-ABC nor TGF-β1 alone or in combination was found to have significant effects on this cell ratio, resulting in constructs with subpar functional properties compared to constructs containing both MCs and ACs. Briefly, MC and AC cell suspensions were seeded into 5 mm diameter, 2% agarose wells at t = 0 hr. By t = 4 hr, the cells had assembled into constructs. Constructs were fed 500 µl of chondrogenic medium consisting of DMEM, 1% PSF, 1% non-essential amino acids, 100 nM dexamethasone (Sigma, St. Louis, MO), 1% ITS+ (BD Scientific, Franklin Lakes, NJ), 40 µg/mL L-proline, 50 µg/mL ascorbate-2-phosphate, and 100 µg/mL sodium pyruvate (Fischer Scientific, Pittsburgh, PA), every day. At t = 1 wk, constructs

were removed from the agarose molds and placed into 48 well plates for the duration of the 5 wk culture period.

Bioactive treatment regimens

Two bioactive agents were investigated in this study: C-ABC (Sigma-Aldrich, St. Louis, MO) and TGF-β1 (PeproTech, Rocky Hill, NJ). Constructs treated with C-ABC received 2 U/mL C-ABC with a 0.05 M acetate activator in chondrogenic medium for 4 hr at 37°C once at t = 7 d and again at t = 21 d. This dual C-ABC treatment was developed in preliminary studies to confirm that this regimen was superior to a single treatment at either time point for enhancing the tensile properties of the tissue-engineered fibrocartilage. In TGF-β1 treated constructs, TGF-β1 was given continuously at 10 ng/ml with every medium change from t = 0 hr to the end of culture[4]. To investigate the interaction of these bioactive agents, treatments consisted of the following: C-ABC alone, TGF-β1 alone, the two bioactive agents combined, or none. At t = 5 wk, each construct was segmented for various assessments, as described below.

Histology and immunohistochemistry (IHC)

Samples were frozen in HistoPrep (Fisher Chemical, Vernon Hills, IL), sectioned at 12 μm, fixed in chilled formalin, and stained with Safranin O/Fast Green and picrosirious red for GAG and total collagen, respectively. For IHC, sections were fixed in chilled acetone, after which endogenous peroxidase was blocked using 3% H_2O_2. Samples were then blocked with horse serum (Vectastain ABC kit, Vector Labs, Burlingame, CA) and incubated with mouse anti-collagen type I (AccurateChemicals, Westbury, NY) or rabbit anti-collagen type II (Cedarlane Labs, Burlington, NC) antibodies. Corresponding 2° antibodies as well as the Vectastain ABC

and DAB solutions were applied as instructed by the Vectastain ABC kit (Vector Labs, Burlingame, CA) for collagen visualization.

Quantitative biochemistry

Sample wet weights were taken after blotting, followed by lyophilization for t = 2 d to determine their dry weights. Samples were then digested in papain as previously described[99]. Total collagen was assessed using a chloramine-T hydroxyproline assay with a SIRCOL collagen assay standard (Accurate Chemical and Scientific Corp.). GAG content was determined using a dimethylmethylene blue (DMMB) dye-binding assay kit (Biocolor, Newtownabbey, Northern Ireland). DNA content was measured using a Picogreen Cell Proliferation Assay Kit (Molecular Probes, Eugene, OR).

Biomechanical testing

Uniaxial, unconfined stress-relaxation compressive testing was applied on 3 mm biopsy punches from the center of the tissue-engineered constructs. Samples were placed in a PBS-filled petri dish and loaded onto the stage of an Instron uniaxial testing machine (Model 5565, Canton, MA). Sample height was determined by applying a 0.02 N tare load. Following pre-conditioning at a 5% strain for 15 cycles at 1 Hz, the sample was compressed at a 1% strain rate per sec to 10%, 20%, and 30% strains. Samples were held at a given strain for 400 sec, which allowed sufficient time for the force vs. time curve of each strain level to equal zero, signifying the sample had fully relaxed. Following this holding time, the next sequential strain level was applied. A Kelvin solid model was used to fit the results of the 20% stress relaxation test and to

calculate the viscoelastic material properties of the samples; this included the relaxation and instantaneous moduli, as well as the viscosity of the tissue.

Uniaxial tensile testing was also conducted using the Instron. Constructs were cut into dog bone shapes and glued onto strips of paper at either extremity. The gauge length was measured between the glued ends. The paper strips holding the sample were loaded into grips, and a pull to failure test was applied at a 1% strain rate per sec. The linear portion of the stress vs. strain curve was used to determine the Young's Modulus of the sample, while the peak of the linear region was taken as the ultimate tensile strength (UTS).

SEM

Samples were dehydrated in increasing ethanol and stored in 100% ethanol at 4°C. Just prior to imaging, samples were further dehydrated using a critical point dryer and sputter-coated with gold. For each sample, three separate locations were imaged using a Philips XL30 TMP SEM, and collagen matrix fiber density and diameter were quantified using ImageJ as previously described[231].

Statistical analysis

To test the hypothesis that the combined bioactive treatment was a significant factor in increasing the functional properties within a given cell ratio, a 1-way ANOVA (n = 8 per group) was used within each cell ratio. Results of the 1-way ANOVA for the 50:50 cell ratio are represented by upper case letters, while those of the 75:25 cell ratio are represented by lower case letters. Separately, to test the hypothesis that the cell ratio and the bioactive treatments were both significant factors in altering construct composition, a 2-way ANOVA (n = 8 per group) was used to analyze the data. When either the 1- or 2-way ANOVA showed significance

($p < 0.05$), a Tukey's HSD *post hoc* test was applied. Data that had a positive interaction on an additive scale and resulted in a combined group that was greater than the addition of the two singular treatments were determined to be synergistic, while those that had a negative interaction on an additive scale but resulted in a combined group that was greater than either treatment alone were determined to be beneficial or positive. Data for this study are represented as mean ± standard deviation with bars or groups marked by the same letter having no significant differences, while those that are marked by different letters are significantly different from one another.

RESULTS

Gross morphology

At t = 5 wk, all constructs maintained a flat, disc-shaped morphology (Fig. 1). However, as the ratio of MCs to Acs increased, construct diameter, thickness, and total wet weight decreased (Table 1). Treated constructs from the 50:50 cell ratio group had significantly lower wet weights, diameters, and thicknesses compared to untreated controls. For example, when treated with both C-ABC and TGF-β1, the wet weight, diameter, and thickness of the 50:50 constructs were decreased by 66%, 24%, and 29%, respectively. Similar, decreasing trends were seen in 75:25 constructs, though TGF-β1 alone significantly increased the wet weight 12% compared to controls within this cell ratio. Further, all bioactive treatments increased the thickness of the 75:25 constructs compared to controls. In terms of construct hydration, combination treated constructs of both cell ratio groups had significantly decreased water content compared to controls or either treatment alone, signifying a denser matrix in the combined treated groups. These results are summarized in Table 1.

Histology and IHC

Overall, collagen and GAG staining were stronger in the 50:50 compared to the 75:25 cell ratio constructs. Staining trends within each cell ratio, however, were similar, with the combined bioactive treatment resulting in more uniform, dense collagen and GAG staining compared to all other treatments for both cell ratios (Fig. 1).

To test whether the cell ratio and bioactive treatment factors had an effect on the collagens being produced within a construct, IHC staining specifically for collagen type I and II was performed (Fig. 1). IHC staining found distinct trends to occur among the bioactive treatment levels within each cell ratio. Collagen type I stained positive in the control treatment within the 50:50 cell ratio group, while 50:50 constructs treated with C-ABC alone or in combination with TGF-β1 had much lighter, diffuse collagen type I staining. The 75:25 cell ratio group had positive collagen type I staining in all bioactive treatment levels, with stronger staining appearing in the combination treated constructs. Collagen type II staining was positive in all treatment levels for each cell ratio. Overall, collagen type II staining was slightly more intense in the 50:50 than the 75:25 cell ratio, particularly within the C-ABC treated and combination treated constructs.

Quantitative biochemistry

The number of cells per construct was significantly decreased with the addition of C-ABC alone or in combination with TGF-β1, while control and TGF-β1 treated constructs were not significantly different from each other. Overall, the 50:50 cell ratio had higher cellularity within the control and TGF-β1 treatments, at approximately 3 million cells/construct, while the 75:25

control and TGF-β1 treatments had approximately 2 million cells/construct. Following treatment with either C-ABC alone or the combination treatment, cell number decreased by 70% in the 50:50 cell ratio and by 32% in the 75:25 cell ratio (Table 1).

Collagen/WW (Fig. 2A) in the 50:50 cell ratio constructs was significantly affected by the various bioactive treatments employed in this study. C-ABC increased collagen/WW 40% over control values, while a 60% increase over controls was measured in TGF-β1 treated constructs. When the two bioactive agents were combined, collagen content was increased by 80% over control constructs. Furthermore, in the combined treatment, the two factors were found to result in a beneficial or positive significant enhancement of the collagen content in the 50:50 cell ratio compared to treatment with either bioactive agent alone. A similar significant effect was observed for collagen/WW in the 75:25 cell ratio, with values increasing 104% in combination treated constructs over controls. Comparison between the two cell ratios found the 50:50 cell ratio factor to have significantly more collagen/WW compared to the 75:25 cell ratio, while the C-ABC + TGF-β1 treatment factor resulted in significantly higher collagen/WW than any other treatment factor across both cell ratios.

GAG/WW (Fig. 2B) was significantly decreased in combination treated 50:50 and 75:25 cell ratios compared to controls. GAG content was significantly greater in the 75:25 cell ratio constructs, ranging from approximately 4 – 6.5%, compared to the 50:50 cell ratio constructs, which ranged from approximately 2 – 5%. Within the bioactive treatment factor, the combined bioactive treatment had significantly less GAG than controls or TGF-β1 treated constructs.

Biomechanics

Biomechanical testing was run to understand the influence of the cell ratio and bioactive treatment factors on the mechanical properties of the engineered fibrocartilages (Table 2). Similar trends in compressive properties were found among all tested strain levels; therefore, only the 20% strain level results are shown to represent these properties. Stress-relaxation, unconfined compression testing at 20% strain found no significant differences among treatments within the 50:50 cell ratio for the relaxation modulus, with values ranging from 95 ± 16 kPa to 125 ± 40 kPa. The relaxation modulus for the combined treated constructs within the 75:25 cell ratio was significantly lower than controls, at 40 ± 14 kPa compared to 57 ± 8 kPa, respectively. Significant differences were observed among treatments within both cell ratios for the instantaneous modulus and viscosity. At a 20% strain, the instantaneous modulus in TGF-β1 alone treated constructs was 5-fold and 2.4-fold higher in the 50:50 and 75:25 cell ratios compared to respective controls, while similar increases were observed in the viscosity. The combination treatment within either cell ratio, however, was not significantly different than corresponding control values, although they trended higher than their respective controls.

Tensile testing showed the most exciting results of this study (Fig. 3). With significant effects in response to bioactive treatments for both the Young's modulus (Fig. 3A) and the UTS (Fig. 3B), results mirrored those observed for the collagen/WW data for each cell ratio. Compared to controls, within the 50:50 cell ratio, C-ABC increased the Young's modulus 226%, while TGF-β1 increased this parameter by an additional 237%. The combined treatment further increased the Young's modulus by an additional 260%. Overall, the combined treatment synergistically increased the Young's modulus 724% compared to controls, from 414 ± 121 kPa in the controls to 3410 ± 706 kPa in the combined treated constructs. In a similar fashion, the UTS in combined treated constructs was 12.7-fold higher than control values in the 50:50 cell

ratio. Within the 75:25 cell ratio, a 208% increase was observed by the combination treatment over controls, reaching a value of 2295 ± 241 kPa in the combination treated constructs, while the UTS in the combined treated constructs was 4.1-fold higher than that of controls. Overall, the combined treatment was found to additively increase the Young's modulus and UTS compared to either treatment applied alone, while the 50:50 cell ratio factor had significantly higher tensile properties than the 75:25 cell ratio factor.

SEM

With the 50:50 cell ratio showing the greatest percent increases among bioactive treatments for the collagen/WW and tensile properties, portions of constructs representative of each treatment within this cell ratio were analyzed via SEM to investigate if the different treatments were altering the matrix. Resulting images were quantified for fiber density and diameter (Fig. 4). Overall, fiber density in the SEM images ranged from 75% to 80%, while fiber diameter ranged from 34 to 50 nm. C-ABC treatment was found to significantly increase the density of the fibers 10.2% over controls, while TGF-β1 alone had no effect on the density. For the diameters, TGF-β1 alone was found to significantly increase the fiber diameter 18.4% over control values, although C-ABC alone decreased fiber diameter 9.3%. Interestingly, when constructs were treated with C-ABC and TGF-β1 in combination, both the fiber diameter and the density increased 31.9% and 15.0%, respectively, compared to controls (Fig. 4). Further, these increases were greater than either treatment alone, signifying a synergistic behavior between these two agents in modifying collagen network organization.

DISCUSSION

This study focused on generating distinct tissue-engineered fibrocartilages by treating different MC:AC co-culture ratios with the bioactive agents C-ABC and TGF-β1. It was hypothesized that the combined use of C-ABC and TGF-β1 would significantly increase the tensile properties of the co-culture ratio constructs without compromising their compressive properties. Through enhancing their tensile properties, it was further hypothesized that the combined bioactive treatment regimen would promote the development of biomimetic fibrocartilages having co-culture ratio-dependent biochemical and biomechanical properties within the range of native tissue. Through a two-factor, full factorial study design, the hypotheses were confirmed: First, the tensile properties of the engineered tissues for both cell ratio groups were significantly enhanced when C-ABC and TGF-β1 stimuli were combined. The compressive properties of the 50:50 cell ratio were also not compromised, unlike the 75:25 cell ratio, which showed a reduction in the relaxation modulus. Second, by enhancing the tensile properties of the co-cultures, overall construct functional properties fell within the range of native tissue properties for both cell ratio groups by the combined bioactive treatment.

Fibrocartilages generated from different seeding ratios of MCs and ACs were found to have distinct functional properties. This can be correlated with each cell type having different synthetic abilities *in vitro*. In culture, MCs have been found to produce lower amounts of ECM components compared to ACs. For example, MCs embedded in agarose were found to synthesize 25% less proteoglycans than ACs in the same system. Furthermore, of this 25%, approximately 54% of the GAGs synthesized by the MCs were lost to the surrounding medium[233]. Medium was not assessed in this experiment as some treatments in this study (i.e., all that contained C-ABC) work by causing ECM components to leach out of the constructs.

Therefore the media of different treatments are incomparable. In a separate study, the genes encoding for the proteoglycans, collagens, and enzymes important for collagen synthesis and degradation were measured. Results found significantly lower expression levels of **α**1(I) procollagen, **α**1(II) procollagen, procollagen-lysine 2-oxoglutarate 5-dioxygenase 1, 2, and 3, and lysyl oxidase genes were measured in freshly isolated MCs than in freshly isolated ACs. Instead, higher expression of the matrix metallopeptidase 13 gene, a member of the matrix metalloproteinase family, was measured in MCs after 18 d of culture in alginate beads[234, 235]. These findings provide much insight as to why MCs alone may not be suitable for producing mechanically sound engineered fibrocartilaginous tissues; without a well-developed matrix, the mechanical integrity of a tissue will be compromised. As shown by this study, incorporating a certain percentage of ACs into co-culture with MCs allows for mechanically robust fibrocartilages having different functional properties to be produced.

The biophysical effect of C-ABC is dependent on its ability to temporarily deplete GAGs, which ultimately allows for the formation of a more functional collagen network with greater tensile strength[231]. Immature cartilage explants were found to experience an imbalance in the normal GAG:collagen ratio when grown *in vitro,* resulting in a loss of tensile properties[236]. A more physiologic GAG:collagen ratio was reinstated following treatment with C-ABC, recovering the loss of tensile properties[229, 236]. Such studies have led researchers to believe that an imbalance between GAG and collagen occurring in *in vitro* cartilage growth induces a pre-stress in the tissue, altering the tissue's mechanical properties. This theory may apply to tissue-engineered fibrocartilages, which tend to have higher than normal GAG levels compared to their native tissue counterparts. This will, in turn, alter the engineered tissue's GAG:collagen ratio, causing an unnatural pre-stress in the developing matrix of the tissue that

may affect its ability to form a mechanically robust matrix. By simultaneously increasing the collagen content while decreasing the GAG content, treatment with C-ABC reinstates a more physiologic GAG:collagen ratio in engineered fibrocartilages. Through significantly decreasing the GAG content and allowing for the development of a more functional collagen network, C-ABC enhanced the tensile properties of the tissue engineered fibrocartilage, as hypothesized.

In addition to generating tissues with a more physiologic GAG:collagen ratio, treatment with C-ABC significantly decreased the cellularity of the engineered fibrocartilage. Previous studies have reported that as cartilage matures *in vivo*, the cellularity of this tissue decreases via apoptosis by more than half the original number[237-239]. The significant decrease in cellularity of the C-ABC engineered fibrocartilage therefore suggests that C-ABC is expediting the maturation of the tissue *in vitro*. Further, a study investigating the cell viability of porcine cartilage explants found that loss of GAG via C-ABC treatment did not cause cell death, suggesting the loss of GAG from the engineered fibrocartilage to not be the cause of the decreased cell number[240]. In a separate study on engineered articular cartilage, while C-ABC was found to suppress cell proliferation in the tissue, treatment produced more mature constructs compared to controls[241]. Although the direct cause for decreased cellularity following treatment with C-ABC remains unknown, the resulting maturation of engineered cartilage and fibrocartilage merits future studies to better understand this beneficial phenomenon.

It is important to note that the purpose of this study was to increase the tensile properties without compromising the compressive properties of the tissue-engineered fibrocartilage. In general, compressive properties of the combined treated constructs were not compromised and fell within the range of native tissue for the TMJ disc, intervertebral disc, and knee menisci[242-244]. The only exception was the C-ABC + TGF-β1 treated 75:25 cell ratio constructs, which had

a significantly lower relaxation modulus than respective controls. The instantaneous modulus and the viscosity values for this group were not significantly lower than the control values, however. This result appears paradoxical when one considers the accepted structure-function relationship of articular cartilage[242-244]. Past studies on articular cartilage have found a strong correlation between GAG content and compressive properties, as well as between collagen content and tensile properties. In this study, as the percentage of MCs increased, the structure-function behavior deviated from what would be expected based on the articular cartilage paradigm. Along with other recent work, this study challenges the existing structure-function paradigm, showing that it does not necessarily hold for fibrocartilage. Instead, tissues containing low GAG levels, such as fibrocartilages, appear to have a more complex mechanism that has more to do with the interplay between collagen and GAGs, as opposed to each component being independently responsible for a specific mechanical property[243, 245]. Studies must therefore be conducted to explain the intricate interaction between ECM structures and the function of fibrocartilaginous tissues; such data will be useful for optimizing design criteria towards creating tissues able to withstand *in vivo* loading.

Results from this study shed some light onto the complexity of the tensile behavior of tissue-engineered fibrocartilages. In this study, C-ABC treatment was found to significantly increase the collagen density of the engineered fibrocartilage via SEM analysis. Biochemical analysis, on the other hand, found the collagen/WW to be significantly increased in a positive or beneficial way within the combined treated group. This corroborates the SEM analysis of collagen density, as higher collagen content will lead to a denser collagen network. Together, these results suggest that increased collagen in the engineered constructs is contributing to the increases in tensile properties in the combined treated group, as GAG significantly decreased

within this same group. Further, various studies concerning the tensile mechanics of native fibrocartilages have correlated higher tensile properties with greater collagen content and density[31, 47, 246-248]. Together, a strong correlation between tensile properties and collagen content and density can be seen in both engineered and native fibrocartilages.

Another parameter affecting the tensile properties of fibrocartilage is collagen fiber diameter. Native tissue studies have found thicker collagen fibers to correspond to areas of higher tensile strength[249]. Collagen fiber diameter has been found to vary in fibrocartilaginous tissues, ranging between 30 – 70 nm in the TMJ disc and between 50 – 100 nm in the annulus fibrosus and the knee menisci[45, 250, 251]. Quantification of fibril diameters within the engineered tissues found them to range between 34 and 50 nm, on par with diameters seen in native TMJ, spine, and knee fibrocartilages. Further, among bioactive treatment levels, the combined bioactive treated constructs had significantly greater fiber diameters than all other treatments. This information provides a mechanistic view for how C-ABC and TGF-β1 alter the developing matrix in engineered fibrocartilage; by increasing collagen fiber diameters, these agents increase the tensile properties of engineered tissue.

The complexity of fibrocartilage is further extended to its anisotropic tensile properties. For instance, the tensile modulus of the annulus fibrosus of the intervertebral disc was found to be 5.6 – 17.4 MPa in the circumferential direction, in contrast to 0.8 MPa in the axial direction[252]. The TMJ disc has also been shown to display anisotropy; both testing direction and location affect the disc's Young's modulus, ranging between 3 and 75 MPa[30, 31]. Tensile stiffness values of the menisci are two to three times higher in the circumferential direction compared to values in the radial direction[253]. Although the anisotropic tensile properties of native fibrocartilages are crucial for their function, such properties were not expected, and

therefore not assessed for, in this study, as the constructs were not subjected to culture gradients or directional forces. However, it is exciting to note that the tensile properties of the engineered fibrocartilages were synergistically enhanced by treatment with both C-ABC and TGF-β1 to reach levels seen in native tissue. The value of the Young's modulus for both the 50:50 and 75:25 cell ratios were 3.5 MPa and 2.5 MPa in the combined treated groups, respectively, exceeding the tensile properties measured for the axial direction of intervertebral discs and within the lower range of values seen for the TMJ disc. It is worth repeating that the collagen fiber diameters measured in the engineered tissues were on par with those measured in these two native fibrocartilages. Further work in engineering anisotropy into these tissues, as well as refining the methods identified here to enhance collagen fiber diameters, density and content, will likely have significant effects in further improving the tensile properties to the levels seen in fibrocartilages such as the knee meniscus.

Recent attempts to induce anisotropic mechanical properties in engineered fibrocartilage have used electrospinning to create aligned nanofiber scaffolds. Most studies have created these scaffolds out of polycaprolactone (PCL), a biocompatible polymer that degrades over a course of 1 – 2 years. When electrospun, this material has produced nanofibers ranging from 1 – 4 μm in diameter, having an average tensile modulus of 10 MPa in the pre-dominant direction of fiber alignment[254]. When seeded with cells, aligned nanofibrous scaffolds have been found to direct neotissue formation according to the pre-determined architecture. Further, the tensile modulus has been found to increase by roughly 40 – 50% in seeded vs. unseeded scaffolds[245, 255]. In one example, annulus fibrosus cells were seeded on electrospun, aligned PCL scaffolds. Uniaxial tensile testing revealed no difference in the tensile modulus in the direction parallel or perpendicular to the pre-dominant fiber direction between t = 1 d and t = 4 wk seeded

constructs. Testing at an oblique, 30° angle with respect to the pre-dominant fiber direction, however, found the tensile modulus to double, from a value of 3 MPa at t = 1 d to 6 MPa at t = 4 wk post-seeding[256]. While electrospinning shows promise as a tool to induce anisotropy, much work needs to be done to fully understand the effects of this process for tissue engineering applications. Nevertheless, it is exciting to know that anisotropy can be engineered into fibrocartilaginous tissues, as shown with electrospinning studies, suggesting that appropriate methodologies need to be designed to capture anisotropy in the self-assembly process.

While this study has not employed methods to align collagen fibers, treatment with both C-ABC and TGF-β1 nonetheless increased the Young's modulus of the engineered fibrocartilage 723% and 208% in the 50:50 and 75:25 co-culture ratios, respectively, compared to controls. Modifying the self-assembly process to induce collagen fiber alignment should be explored to further enhance the mechanical properties of scaffold-free engineered fibrocartilage. One approach may be through generating shape-specific constructs; combined with native loading schemes, these constructs may be prompted to capture the complex arrangement of native collagen fibers. Previous work on self-assembled meniscus constructs, for example, has found that geometric constraint by a meniscus-shaped mold guides collagen fibril alignment, resulting in anisotropic tensile properties[5]. Such efforts will lead to the development of a tissue able to adapt to and survive in the native joint environment.

CONCLUSIONS

This work speaks to the potential of tissue engineering to create tissues to repair or replace fibrocartilage that is unable to heal on its own accord, an important implication considering the current lack of treatment options for degenerated TMJ discs, knee menisci, and intervertebral

discs. Distinct tissue-engineered fibrocartilages with functional properties approaching native tissue were created by treating different MC:AC co-cultures with C-ABC and TGF-β1. SEM analysis showed that these agents together alter the physical structure and organization of the developing collagen network, allowing it to better withstand tensile forces. This alludes to a possible mechanism by which these agents collaboratively augment the collagen network in engineered fibrocartilage. It was found that the engineered fibrocartilages had collagen fibril diameters and tensile properties on par with native tissues. Future work will be focused on subjecting shape-specific, self-assembled constructs to biomechanical stimulation mimicking *in vivo* loading schemes to generate tissues that capture the anisotropy of native fibrocartilages.

TABLES AND FIGURES

TABLE 6.1 – CONSTRUCT PROPERTIES AT T = 5 WK. Values marked with different letters within each category are significantly different ($p < 0.05$), with A > B > C.

Cell Ratio (MC:AC)	Bioactive Treatment	Wet Weight (mg)	Hydration (%)	Diameter (mm)	Thickness (mm)	Cells/Construct (10^6)
50:50	None	30.19 ± 1.49^{A}	87.25 ± 1.45^{A}	6.67 ± 0.10^{A}	0.61 ± 0.08^{A}	3.05 ± 0.40^{A}
	C-ABC	12.38 ± 1.10^{C}	85.47 ± 0.68^{B}	5.61 ± 0.11^{B}	0.33 ± 0.04^{C}	0.94 ± 0.23^{B}
	TGF-β1	17.35 ± 1.25^{B}	84.89 ± 0.66^{B}	5.72 ± 0.18^{B}	0.46 ± 0.05^{B}	3.28 ± 0.30^{A}
	Combined	10.16 ± 0.17^{D}	82.72 ± 0.64^{C}	5.08 ± 0.06^{C}	0.44 ± 0.06^{B}	0.86 ± 0.33^{B}
75:25	None	13.44 ± 0.80^{b}	88.40 ± 2.10^{a}	5.20 ± 0.11^{a}	0.44 ± 0.06^{c}	1.95 ± 0.18^{a}
	C-ABC	8.76 ± 0.16^{c}	86.80 ± 0.92^{ab}	4.68 ± 0.09^{c}	0.47 ± 0.09^{c}	1.33 ± 0.07^{b}
	TGF-β1	15.00 ± 0.52^{a}	86.02 ± 0.82^{b}	4.99 ± 0.10^{b}	0.79 ± 0.04^{a}	2.15 ± 0.41^{a}
	Combined	7.87 ± 0.43^{c}	82.00 ± 1.25^{c}	4.24 ± 0.06^{d}	0.66 ± 0.06^{b}	1.33 ± 0.11^{b}

TABLE 6.2 – CONSTRUCT VISCOELASTIC COMPRESSIVE PROPERTIES AT T = 5 WK. Fibrocartilage was treated with either C-ABC alone, TGF-β1 alone, the two agents combined, or left untreated (control). The relaxation modulus showed no significant differences in the 50:50 constructs, but was significantly decreased in the combined treated 75:25 constructs compared to controls. The instantaneous modulus and viscosity was highest in the TGF-β1 alone treatment for both cell ratios. Values marked with different letters within each category are significantly different ($p < 0.05$), with A > B > C.

Cell Ratio (MC:AC)	Bioactive Treatment	Relaxation Modulus (kPa)	Instantaneous Modulus (kPa)	Viscosity (kPa*s)
50:50	None	52.10 ± 32.8^{A}	190.18 ± 95.0^{C}	7742.06 ± 4695.0^{B}
	C-ABC	71.33 ± 26.5^{A}	650.01 ± 189.8^{B}	14403.08 ± 1682.7^{B}
	TGF-β1	86.10 ± 40.0^{A}	933.70 ± 131.1^{A}	22395.50 ± 3986.2^{A}
	Combined	63.90 ± 10.9^{A}	397.14 ± 112.7^{C}	11072.00 ± 3941.8^{B}
75:25	None	70.40 ± 28.5^{a}	451.58 ± 122.6^{bc}	6833.66 ± 2493.9^{ab}
	C-ABC	51.21 ± 19.1^{ab}	243.32 ± 82.4^{c}	2681.81 ± 1918.6^{c}
	TGF-β1	44.56 ± 10.2^{ab}	748.53 ± 237.7^{a}	7747.91 ± 1876.5^{a}
	Combined	30.02 ± 15.6^{b}	497.48 ± 146.6^{b}	4230.19 ± 1704.8^{bc}

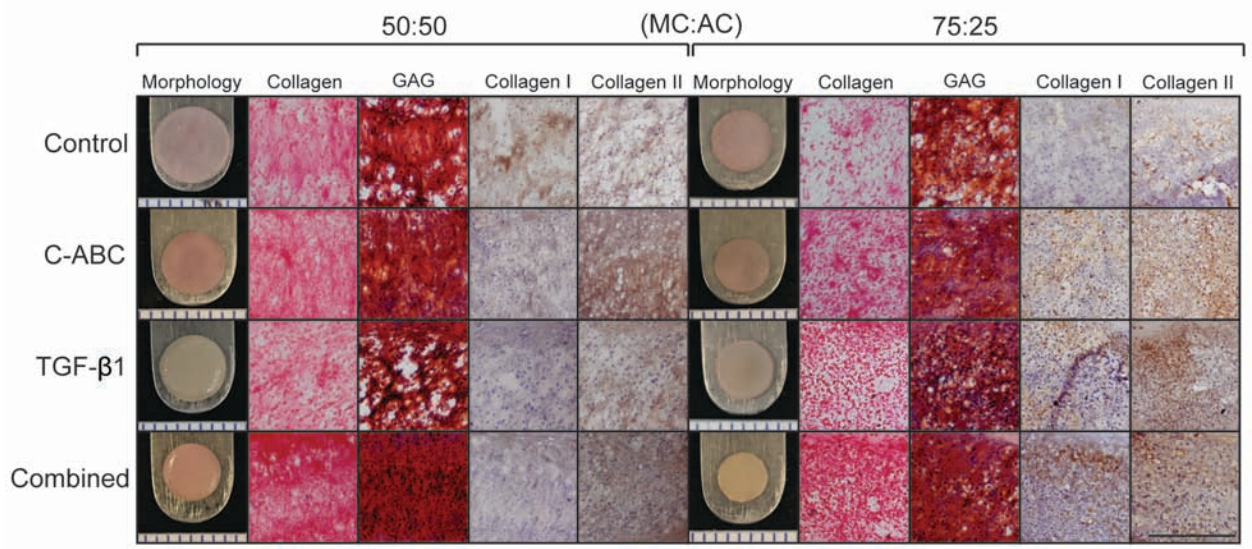

FIGURE 6.1 – GROSS MORPHOLOGY, HISTOLOGY AND IHC OF CONSTRUCTS AT T = 5 WK. Fibrocartilage was treated with either C-ABC alone, TGF-β1 alone, the two agents combined, or left untreated (control). Collagen was stained for using picrosirious red, GAG was stained for using Safranin O/Fast Green, while IHC was used to stain for collagen types I and II. Collagen and GAG staining was stronger in the 50:50 constructs, with the combined treatment producing constructs with the most uniform staining in both cell ratios. IHC staining showed different patterns of collagen types I and II between cell ratios as well as among bioactive treatments within each cell ratio. Scale bar for histology and IHC images is 500 μm and the markings on the morphology images are 1 mm apart.

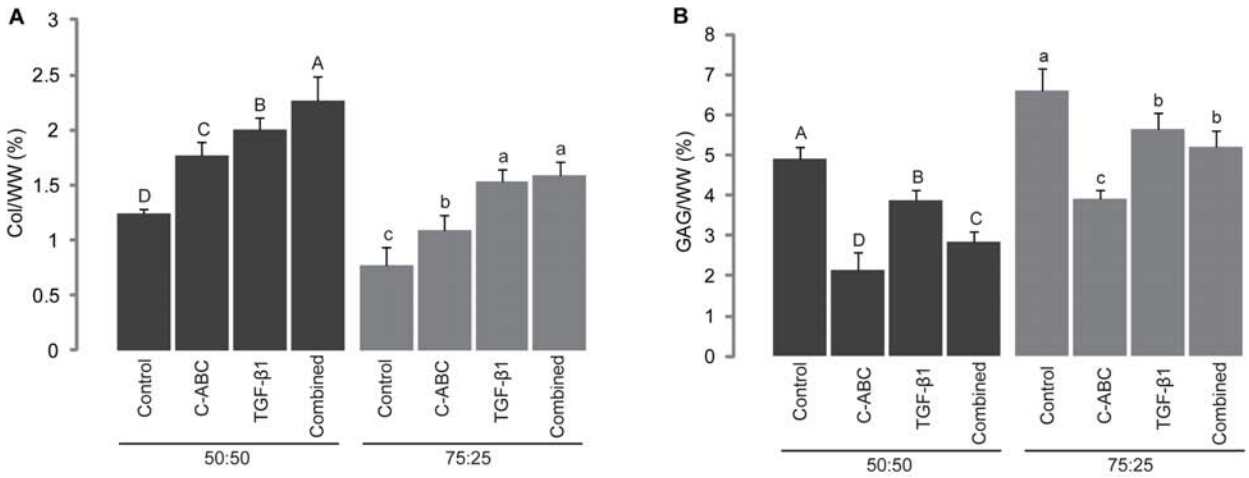

FIGURE 6.2 – BIOCHEMICAL PROPERTIES OF CONSTRUCTS AT T = 5 WK. Fibrocartilage was treated with either C-ABC alone, TGF-β1 alone, the two agents combined, or left untreated (control). Col/WW (A) exhibited significance among bioactive treatments, with constructs from both cell ratios having the greatest collagen content in the combined treatment. C-ABC and TGF-β1 significantly increased the collagen content in the 50:50 constructs in a beneficial or positive manner. Bioactive treatments significantly decreased GAG/WW (B) compared to controls. Bars not connected by the same letter are significantly different ($p < 0.05$).

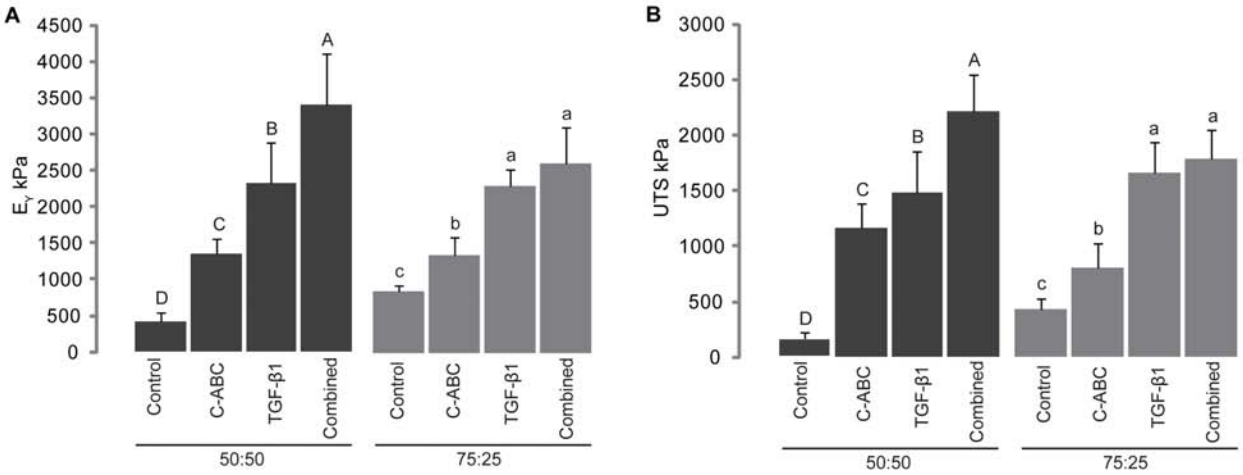

FIGURE 6.3 – **TENSILE PROPERTIES OF CONSTRUCTS AT T = 5 WK**. Fibrocartilage was treated with either C-ABC alone, TGF-β1 alone, the two agents combined, or left untreated (control). The Young's modulus (A) and UTS (B) exhibited significance among bioactive treatments, corresponding to trends in the collagen content (Fig. 2, A). Constructs from both cell ratios had the greatest collagen content and tensile properties with the combined treatment. C-ABC and TGF-β1 together synergistically increased the Young's modulus and UTS of the 50:50 constructs. Bars not connected by the same letter are significantly different ($p < 0.05$).

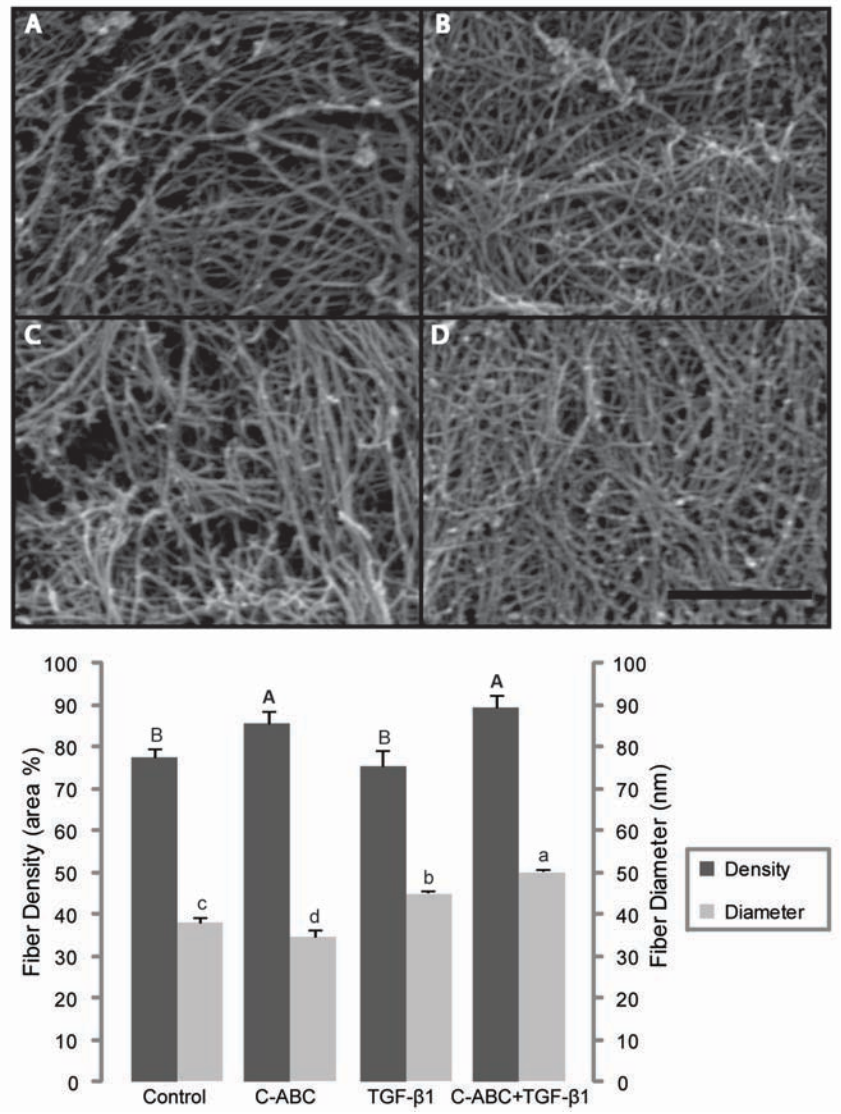

FIGURE 6.4 – SEM ANALYSIS OF 50:50 FIBROCARTILAGE CONSTRUCTS AT T = 5 WK. Includes images of control, C-ABC treated, TGF-β1 treated, and C-ABC + TGF-β1 treated constructs. To measure collagen fibril diameter and density, 3 locations on n = 3 fibrocartilage constructs from each bioactive treatment level were quantified. Results found C-ABC in significantly increase collagen density, while C-ABC + TGF-β1 significantly increased collagen fibril diameter over all other treatments. Bars not connected by the same letter are significantly different ($p < 0.05$). Scale bar is 1 μm.

CHAPTER 7 – STRAIN-INDUCED MATRIX SYNTHESIS AND ORGANIZATION IN SHAPE-SPECIFIC NEOTISSUES

ABSTRACT

Tissue engineered musculoskeletal soft tissues typically lack the appropriate mechanical robustness of their native counterparts, hindering their clinical applicability. With structure and function being intimately linked, efforts to capture the anatomical shape and matrix organization of native tissues are imperative to engineer functionally robust and anisotropic tissues capable of withstanding the biomechanically complex *in vivo* joint environment. The present study sought to tailor the use of passive axial compressive loading to drive matrix synthesis and reorganization within self-assembled, shape-specific fibrocartilaginous constructs, with the goal of developing functionally anisotropic neotissues. Specifically, shape-specific fibrocartilaginous neotissues were subjected to 0, 0.01, 0.05, or 0.1N axial loads early during tissue culture. Results found the 0.1N load to significantly increase both collagen and glycosaminoglycan synthesis by 27% and 67%, respectively, and to concurrently reorganize the matrix by promoting greater matrix alignment, compaction, and collagen crosslinking compared to all other loading levels. These structural enhancements translated into improved functional properties, with the 0.1N load significantly increasing both the relaxation modulus and Young's modulus by 96% and 255%, respectively, over controls. Finite element analysis further revealed the 0.1N uniaxial load to induce multi-axial tensile and compressive strain gradients within the shape-specific neotissues, with maxima of 10.1%, 18.3%, and -21.8% in the XX-, YY- and ZZ-directions, respectively.

Chapter submitted as: MacBarb, R.F., Paschos, N.K., Abeug, R. Makris, E.A., Hu, J.C., & Athanasiou, K.A. Strain-induced Matrix Synthesis and Organization in Shape-Specific Neotissues. *Tissue Engineering Part A.* (November 2013).

This indicates that strains created in different directions in response to a single axis load drove the observed anisotropic functional properties. Together, results of this study suggest that strain thresholds exist within each axis to promote matrix synthesis, alignment, and compaction within the shape-specific neotissues. Tailoring of passive axial loading, thus, presents as a simple, yet effective way to drive *in vitro* matrix development in shape-specific neotissues toward more closely achieving native structural and functional properties.

INTRODUCTION

Musculoskeletal soft tissues support body movement by withstanding complex mechanical loads, with each tissue having morphological and mechanical characteristics specific to its biomechanical role. Failure or degeneration of a single tissue in a diarthrodial joint can lead to functional impairment of the entire joint. Unfortunately, current treatment modalities often fail to fully restore joint functionality[257]. Tissue engineering has therefore garnered increasing interest over the last decade as a means to generate clinically relevant musculoskeletal implants. A potential advantage of this approach is to generate neotissues with specific characteristics that are necessary for withstanding the mechanical complexity of joints. Given that the highly specialized biomechanical roles of musculoskeletal soft tissues are closely related to their matrix organization[191], it has become of critical importance to capture the anisotropic functionality of native tissues during *in vitro* neotissue development.

Mechanical stimulation has shown efficacy in driving the biomechanical characteristics of engineered tissues[297-303]. Natively, musculoskeletal soft tissues are subject to loading during all phases of their lifespan. Importantly, loading is critical to the development, maturation, and

maintenance of their mechanical integrity[273, 275, 282, 304, 305]. Efforts to identify beneficial biomechanical stimuli have focused on determining efficacious loading types (e.g., compressive, tensile, hydrostatic pressure, shear) and regimens (e.g., static versus dynamic, durations, resting periods, magnitudes). While stimuli have been successful in increasing some functional characteristics of engineered tissues, their properties remain far from reaching native tissue values, particularly in an anisotropic manner. It is, therefore, necessary that the effect of loading on neotissue development be more carefully assessed to fine-tune its use toward engineering clinically robust neotissues with anisotropic characteristics necessary to perform their intended biomechanical role.

With structure and function being intimately linked, a key criterion for engineering functionally anisotropic constructs is that they attain a native-like matrix organization. To achieve this goal, several studies have developed anatomically shaped matrix scaffolds made of either natural or synthetic fibers, or even the two combined[306-309]. Such scaffolds, however, have been found to exhibit insufficient biomechanical integrity, particularly in the case of naturally derived fibers[310, 311]. Scaffolds also suffer from biodegradability and biocompatibility issues, as especially seen with synthetic scaffolds[312-314]. Further, it has been suggested that use of any scaffolding material may hinder both cellular communication and responsiveness to external stresses[212]. Such drawbacks have led to the development of a scaffold-free, self-assembling process to cartilage and fibrocartilage tissue engineering[3, 212]. In this method, high densities of cells are seeded into non-adherent wells, where they quickly coalesce and, over time, produce a robust matrix in a manner akin to native morphogenesis[230]. Further, self-assembled neotissue has been readily formed into several complex, clinically relevant shapes, such as the knee meniscus [5] and temporomandibular joint (TMJ) disc[315]. While these anatomically shaped

neotissues have been found to exhibit mechanical properties that are at times on par with native tissues, they still lack the overall anisotropic functionality and biomechanical integrity of their native tissue counterparts.

Mechanical strain has been shown to result in fiber alignment within collagen-rich neotissues[316-319]. For example, engineered vessels subjected to circumferential strain during an 8 wk culture period exhibited highly organized matrices capable of withstanding pressures up to 2000 mmHg (267 kPa)[320]. Similarly, in ligament tissue engineering, axial mechanical strain was found to induce uniaxial collagen alignment and anisotropic functional properties[318]. It has also been shown that self-assembling fibrocartilaginous neotissues around a central post guides development of circumferential collagen fiber organization[5]. Together, such work indicates that mechanical strain can be strategically tailored to promote matrix reorganization toward engineering more functionally robust neotissues.

Recently, the concept of using strain to improve matrix organization has been investigated in self-assembled TMJ disc neotissues. In this study, biconcave neotissues were subjected to a 1g mass (0.01N load) early during development[321]. The significance of this study was that neotissue loaded with 1g had tensile properties trending higher than unweighted controls; however, the 1.1 – 2% strains induced by this load were insufficient to cause detectable changes in collagen organization. This study further found the 1g mass unable to promote the neotissue to capture the anisotropic functional trends of the native TMJ disc. The present study, therefore, aimed to tailor the use of different levels of passive axial compression to trigger region-specific collagen reorganization within self-assembled, TMJ disc-shaped neotissues. Overall, it was hypothesized that a strain threshold exists to drive matrix synthesis and alignment within the biconcave constructs, leading to the development of functionally

anisotropic neotissues.

MATERIALS AND METHODS

Cell isolation

Articular chondrocytes (AC) and meniscus cells (MC) were harvested from juvenile bovine knee joints (Research 87, Boston, MA), as previously described[272]. Isolated cells were frozen in freezing medium comprising Dulbecco's Modified Eagle's Medium (DMEM), 20% fetal bovine serum and 10% dimethyl sulfoxide until cell seeding.

Self-assembly into shape-specific neotissue

Using co-cultures of MC and AC, biconcave, TMJ disc shape-specific constructs were self-assembled as previously described[321]. Briefly, at t = 0 d, 50:50 MC:AC co-culture suspensions were seeded into, shape-specific 2% agarose wells at 12 M cells/well to induce the formation of biconcave neotissues displaying a thin, inner middle zone surrounded by a thicker, outer band region (Fig 1A). Shape-specific agarose top pieces were placed on top of the constructs at t = 3 d to fully confine their geometry; the constructs remained confined for the remainder of culture. Agarose/construct assemblies were placed in 6-well culture plates and fed 6 ml of chondrogenic medium consisting of DMEM, 1% penicillin/streptomycin/fungizone (PSF), 1% non-essential amino acids, 100 nM dexamethasone (Sigma, St. Louis, MO), 1% ITS+ (BD Scientific, Franklin Lakes, NJ), 40 μg ml^{-1} L-proline, 50 μg ml^{-1} ascorbate-2-phosphate, and 100 μg ml^{-1} sodium pyruvate (Fischer Scientific, Pittsburgh, PA), every other day. At t = 5 wk, constructs were removed from culture and analyzed regionally for their properties.

Passive axial compression of shape-specific constructs

The present study imparted axial compressive loading via 4.75 mm diameter, type 304 stainless steel posts machined to weigh 1, 5, or 10g, corresponding to 0.01, 0.05, and 0.1N loads, respectively. Posts were applied to the shape-specific constructs from t = 10 – 14 d based on previous work identifying this time as a critical window in which self-assembled neotissue is most responsive to mechanical stimulation[212, 277]. To ensure proper medium diffusion under the post as well as to maintain the tissue's biconcavity, the posts were positioned perpendicular to top of the shape-specific agarose top pieces, such that they were aligned with the neotissue middle zone.

Quantitative biochemistry and high-performance liquid chromatography (HPLC)

At t = 5 wk, wet weights of samples designated for biochemical analysis were taken, after which samples were lyophilized and their dry weights recorded. Following papain digestion[217], total collagen content was measured using a chloramine-T hydroxyproline assay with a SIRCOL collagen assay standard (Accurate Chemicals, Westbury, NY). A dimethylmethylene blue dye-binding assay kit (Biocolor, Newtownabbey, (UK) was used to measure sulfated glycosaminoglycan (GAG) content. Pyridinoline (PYR) collagen crosslinks were analyzed and quantified via HPLC using PYR standards (Quidel, San Diego, CA), as previously described[322, 323].

Histology and Immunohistochemistry (IHC)

HistoPrep (Fisher Chemical, Vernon Hills, IL) was used to freeze samples, which were sectioned at 12 μm. Slides were then fixed in formalin before being stained with Safranin

O/Fast Green to examine GAG distribution and with Picrosirius Red for total collagen content. Separately, slides were fixed in chilled acetone for collagen type I and II IHC as previously described[272].

Stress-relaxation compressive testing

Neotissue compressive properties were measured via uniaxial unconfined stress-relaxation compression testing[321]. Briefly, 2 mm biopsy punches were taken from both the middle zone and band region of the biconcave neotissue. Following height detection, samples were pre-conditioned for 15 cycles at 5% strain at 1 Hz, after which they were compressed at a strain rate of 1% of the sample height per second to both 10% and 20% strains. Matlab (Mathworks, Natick, MA) was used to the fit the resulting data to a Kelvin solid model to determine both the instantaneous modulus (E_i) and relaxation modulus (E_r).

Uniaxial tensile testing

Neotissue tensile properties were obtained from the middle zone in the X-direction and from the band region in the Y-direction using a uniaxial testing machine (Test Resources, Shakopee, MN)[321]. Dog bone-shaped samples were glued at their extremities to a paper frame, which was clamped into the machine grips. A strain-to-failure test was then run at a 1% of the gauge length (measured as the distance between the glued ends of the paper frame) per second. For each sample, the Young's modulus (E_Y) was calculated as the slope of the linear region of the stress-strain curve, while the ultimate tensile strength (UTS) was determined as the curve's peak.

Finite Element Analysis (FEA)

Three-dimensional, computational models of the biconcave neotissue were developed via Autodesk Inventor (Autodesk, San Rafael, CA). Using ABACUS/CAE (Dassault Systèmes, Vélizy-Villacoublay, France), material properties were set to match estimated t = 10 d functional properties of the neotissue, as previously described[321]. Specifically, the neotissue was modeled using a 4-noded linear tetrahedral mesh consisting of 52,636 elements. The resulting biconcave model was confined in the Z-direction along its bottom surface to represent the axial constraint of the agarose well, while the construct remained free to move in both the X- and Y-directions to mimic the ability of the neotissue to expand and contract in the wells. A linear, elastic model was used to measure the biconcave model's response to each passive axial loading level (1, 5, and 10g) once it had fully relaxed to the respective load. The loads were modeled as a pressure distribution across the middle zone of the top surface of the biconcave model. For each load, the resulting stress, strain, and displacement were displayed as a heat map.

Scanning Electron Microscopy (SEM)

Samples were dehydrated in increasing ethanol and stored in 70% ethanol at 4 ^{o}C. Just prior to imaging, samples were transferred into 100% ethanol, dehydrated in a critical point dryer, and gold sputter-coated. Each sample was imaged in three separate locations within their middle zones using a Philips XL30 TMP scanning electron microscope. To quantify SEM images, ImageJ was used to measure both fibril density and diameter as previously described[231]. Fibril alignment was quantified using the ImageJ plugin OrientationJ[324]. Ten uniformly sized regions of interest were randomly selected from an overlain grid on SEM images of the neotissue middle zones, from which the software then calculated the corresponding alignment in terms of a coherency factor. Six middle zone images were analyzed this way for each loading level. The

coherency factor, which indicates the degree of local orientation, is an index between 0 and 1. A coherency of 1 corresponds to perfectly oriented and aligned fibrils, while a coherency of 0 refers to completely unoriented fibrils.

Statistical Analysis

To determine whether the different passive axial compressive loads resulted in significant changes in neotissue functional and structural properties, a one-way ANOVA (n = 8 per group) was used. If the one-way ANOVA showed significance ($p < 0.05$), a Tukey's HSD *post hoc* test was then applied. All data are represented as mean ± standard deviation (SD), with bars or groups marked by different letters to represent significant differences. For structure-function relationships, significant correlations ($p < 0.05$) were considered strongly positive at R^2 value > 0.5, weakly positive at $0 < R^2 < 0.5$, weakly negative at $-0.5 < R^2 < 0$, or strongly negative at $R^2 < -0.5$.

RESULTS

Gross morphology and growth metrics

While neotissue constructs from all groups maintained the shape-specific biconcavity throughout the entire culture duration, loading level was found to significantly affect construct morphology (Fig. 1B). Specifically, although the major diameter (as measured along the X-axis between the outside edges of the band region) was not altered by any of the loading levels, the minor diameter (as measured along the Y-axis between the outside edges of the band region) of 10g loaded constructs was significantly greater than that of controls. Further, while the band region thickness did not change with the different loads, the middle zone of 10g loaded

constructs was half as thick as the middle zone of controls. In terms of water content, there were no significant differences in whole construct wet weight or band region hydration among groups. The middle zone of the 10g loaded constructs, however, displayed significantly decreased hydration compared to controls.

Quantitative Biochemistry and HPLC

Construct collagen, GAG, and PYR content was measured in both the band and middle zone regions at t = 5 wk (Fig. 2). No significant differences in collagen per wet weight (Col/WW), GAG per wet weight (GAG/WW), PYR per wet weight (PYR/WW), or PYR per collagen content (PYR/Col) were found among the band regions of any of the groups. While no significant differences in collagen or GAG content was detected among control, 1g, or 5g loaded constructs in their respective middle zones, the 10g mass significantly increased both middle zone Col/WW and GAG/WW by 27% and 67%, respectively, over that of controls. Further, both PYR/WW and PYR/Col were found to be significantly greater in the middle zone of 10g loaded constructs, with values 6.8- and 5.2-fold, respectively, those of controls.

Histology and IHC

Representative images of histological and IHC stained middle zone samples are shown in Fig. 3. Corroborating the biochemical results, similar collagen and GAG staining was observed in the middle zone of control, 1g, and 5g loaded constructs, while the 10g mass prompted denser collagen and GAG staining in this region. Collagen I IHC staining became denser with increasing load. Collagen II staining, on the other hand, appeared to slightly decrease in intensity with increasing load.

Stress-relaxation compressive testing

Compressive testing at t = 5 wk found both 10% and 20% strain levels to yield similar trends among the groups; therefore, only the 20% strain level results are presented (Fig. 4A-B). No significant differences in either the E_r or E_i were found among the band regions of any of the constructs or among the middle zone of control, 1g, or 5g loaded constructs. The 10g mass, however, caused a significant increase in both the E_r and E_i in the middle zone by approximately 96% and 145%, respectively, over the middle zone of all other groups.

Uniaxial tensile testing

Similar to compressive results, uniaxial tensile testing revealed no significant differences in the band region of any constructs in terms of either the E_Y or UTS (Fig. 4C-D). In terms of the middle zone, while the 1g loaded constructs trended higher in terms of both the E_Y and UTS compared to controls, the 5g mass prompted a significant increase in the middle zone tensile properties over controls. The 10g loaded constructs, on the other hand, resulted in significantly greater tensile properties in the middle zone compared to all other groups, exhibiting a 255% and 273% increase in the E_Y and UTS, respectively, over those of controls.

FEA

Modeling of the biconcave, engineered neotissue in response to 1, 5, and 10g masses resulted in the development of different strain distributions and magnitudes within the model's middle zone, as seen in Fig. 5. For all loading situations, tensile strains were approximately 1.6x greater in the YY- compared to the XX-direction, while compressive strains were observed only in the

ZZ-direction. Comparing among loads, maximum strains imparted by the 10g mass were 9.2-, 10.1-, and 9.9-fold greater than maximum strains achieved by 1g in the XX-, YY-, and ZZ-directions, respectively. The 5g mass, on the other hand, increased XX-, YY-, and ZZ-maximum strains by 4.6-, 5.1-, and 5.0-fold over respective maxima achieved by the 1g mass in each direction.

SEM

SEM images of construct middle zone regions were quantified for fibril diameter, density, and alignment at t = 5 wk (Fig. 6). Middle zone matrix density was found to be significantly greater in constructs loaded with 10g, with values 1.3-fold those of all other groups. The 10g mass was further found to significantly enhance fibril diameter in the neotissue's middle zone 1.2-fold that of controls. In terms of alignment, fibrillar coherency in the middle zone was found to be significantly greatest in constructs loaded with 10g compared to all other groups, with fibrils aligning predominantly in the Y-direction.

Structure-function relationships

Neotissue middle zone Col/WW, GAG/WW, PYR/Col, collagen fibril alignment, and collagen fibril density were correlated with both the E_r and E_Y values (Fig. 7). All correlations were found to be positive and statistically significant. In terms of the middle zone compressive modulus, strong positive correlations were found with PYR/Col (R^2 = 0.64), GAG/WW (R^2 = 0.53), and collagen fibril density (R^2 = 0.55). Collagen fibril alignment (R^2 = 0.41) and Col/WW (R^2 = 0.44) demonstrated weak positive correlations with the compressive modulus. For the middle zone tensile modulus, the highest strong correlation was with collagen fibril

alignment (R^2 = 0.75), followed by PYR/Col (R^2 = 0.64), and Col/WW (R^2 = 0.54), while weak correlations were found with collagen fibril density (R^2 = 0.42) and GAG/WW (R^2 = 0.42).

DISCUSSION

The objective of this study was to tailor the use of passive axial compression to drive both region-specific matrix synthesis and reorganization toward enhancing the functional properties of shape-specific, engineered fibrocartilage. Results found the 10g mass to fulfill this objective, as it prompted significantly increased structural and functional properties in the biconcave neotissue's middle zone, while the band region remained unaltered, leading to the development of functionally anisotropic constructs. Specifically, in the middle zone, the 10g mass significantly increased both GAG and collagen synthesis, and simultaneously promoted matrix reorganization via significantly increased collagen fibril density, alignment, and crosslinking, by 67%, 27%, 30%, 202%, and 263%, respectively, over all other loading levels. This enhanced matrix content and organization translated into significantly augmented tensile and compressive properties in the middle zone of 10g loaded constructs, which were found to be 3.5-, 3.7-, 2.1-, and 2.3-fold that of controls in terms of the E_Y, UTS, E_r, and E_i, respectively. Further, FEA found the 10g mass to induce different strain gradients within each of the three axes of the neotissue's middle zone, with the XX-strain ranging from 5.7 – 10.1%, the YY-strain ranging from 7.2 – 18.3%, and the ZZ-strain ranging from -16.1 – -21.8%. This suggests that, contrary to the hypothesis that a single strain threshold exists, separate strain thresholds may actually be necessary within the XX-, YY-, and ZZ-directions that together promote matrix synthesis and reorganization within the biconcave neotissue. Additionally, it was also found that 5 d of loading (from t = 10 – 14 d) was sufficient for the region-specific collagen fibril reorganization

to be maintained throughout the remainder of the culture period, when no load was present. Together, these data suggest that exogenous strain applied early during neotissue development can be strategically fine-tuned to control lasting matrix synthesis and reorganization toward achieving improved functional properties in shape-specific neotissues.

Mechanical stimulation via axial loading enhanced the fibril alignment of the fibrocartilaginous neotissues in an anisotropic manner. To understand how load influenced such alignment, FEA was conducted, finding the passive axial load-induced strains to be greatest in the middle zone of the biconcave model. Further, the increasing strain magnitudes and distributions resulting from the increasing loads correlated with SEM results of the middle zone, showing alignment to occur with higher load primarily in the direction of greatest tensile strain: the YY-direction. This is physiologically significant, as the native TMJ disc presents with middle zone matrix alignment in the same direction[192]. In terms of engineered tissues, similar correlations between loading direction and alignment have been observed in collagen gels in response to axial tensile strain[325] and in fibrin gels in response to axial compressive strain[326]. Such work has found increasing loading levels to correspond to increased alignment in the direction of loading. These previous studies, however, examined these effects in neotissues of uniform geometries, resulting in principally either tensile or compressive strains. In the present study, the utility of a biconcave neotissue prompted the translation of a uniaxial load into multi-axial tensile and compressive strains. Thus, unlike previous work, this study was able to promote region-specific alignment within the middle zone of the biconcave construct, leading to the development of functionally anisotropic neotissues.

In addition to driving matrix synthesis and alignment, passive axial compressive loading was also found to promote matrix compaction and collagen crosslinking in the neotissue's

middle zone. Specifically, this compaction and crosslinking was only observed at the 10g loading level, where the neotissue had a significantly thinner and denser middle zone as well as increased PYR/WW and PYR/Col compared to all other groups. Previous work has found fiber alignment and compaction to go hand-in-hand; cell-seeded collagen gels have been found to undergo simultaneous fiber alignment and compaction in response to mechanical strain[327-329]. Further, treatment of cell-seeded collagen gels with either sodium azide, an ATP inhibitor, or cytochalasin D, a cytoskeletal inhibitor, has been found to inhibit such matrix reorganization following mechanical stimulation[330, 331]. Previous work has also correlated increased biomechanical properties in engineered neotissues with increased crosslinks[7, 322], suggesting that the greater functional properties in the middle zone of 10g loaded constructs is likely related to the increased crosslink content in this region. Together, such work indicates that cells, in response to a mechanical input, generate intrinsic traction forces to reorganize randomly oriented collagen fibers by aligning, compacting, and crosslinking them such that they counter the newly loaded environment[328]. This, therefore, suggests that the strain-induced matrix changes observed in the self-assembled neotissue are primarily a cellular mechanotransductive response. In correlating cellular response to strain level, previous work has shown that anisotropic strains of $\geq 5 - 10\%$ are necessary to induce fiber alignment and matrix compaction in cell-seeded collagen gels[325, 326]. Results of the present study suggest that greater strain thresholds may be necessary to induce matrix reorganization in the self-assembled, biconcave neotissues. Specifically, only the 10g mass, which promoted strains in the XX-, YY-, and ZZ-directions in excess of this 5 – 10% range in the neotissue middle zone, was found to align, compact, and crosslink the matrix.

To better understand how the strain-induced matrix reorganization influenced the

functional properties of the biconcave neotissue, structure-function relationships were evaluated. Results of this analysis found significant, positive correlations between both collagen and GAG content with both tensile and compressive properties, respectively. The strongest observed correlations for the tensile modulus was with collagen fibril alignment, PYR/Col, and collagen content. Positive, although weak, correlations were also found between the tensile stiffness modulus and both collagen density and GAG content. Previous work has shown that several types of proteoglycans, including dermatan sulfate and chondroitin sulfate, help regulate collagen fibrillogenesis and aid in microfibril aggregation to form a denser matrix, which may explain the positive correlations between GAG content and the tensile modulus[53, 332, 333]. In terms of the compressive properties, the strongest positive correlations were detected with PYR/Col, GAG content and collagen fibril density, while weak positive correlations were found with both collagen content and alignment. Such findings support recent reports that likewise counter the traditionally accepted structure-function relationships of cartilaginous tissues, which correlated GAG content exclusively with compressive properties and collagen content with tensile properties[242, 334]. Instead, it is now shown that a highly complex and integrated relationship appears to exist that connects not only overall matrix composition, but also its architecture with the functionality of both native and engineered cartilaginous tissues[30, 243, 245, 272, 322, 335]. Gaining a better understanding of the intricate relationship between structure and function in engineered tissues should be the focus of future studies to aid in advancing tissue engineering endeavors.

Previous work has highlighted the physiologic strain levels of cartilaginous tissues. Such work indicates that strains $\leq 20\%$ are within physiologic range for articular cartilage, whereas strains $\geq 40 - 60\%$ are considered extreme and can lead to tissue degradation[336, 337]. Similar

strain levels have been predicted for both the meniscus and TMJ disc; FEA analysis has found tension-compression strain magnitudes in the range of ≥ 20 – 25% to correlate with normal physiologic loading[338, 339]. Based on the present study's FEA analysis, it is predicted that the 10g mass may be close to approaching an upper strain limit for passive axial compression, as maximum compressive strains in the ZZ-direction were found to be 21.8%. It is therefore important that future work determine if higher passive axial loads are potentially more beneficial toward promoting enhanced functional properties in the biconcave neotissues and at which point the axial compression becomes detrimental. It has also been previously shown via single cell studies that there is a "critical strain threshold" at approximately 33% applied axial compressive strain, at which point chondrocytes can no longer fully recover from the applied load[340, 341]. Modeling work has further predicted that bulk tissue strains are approximately 1.5x higher within the microenvironment of the cells within loaded cartilaginous tissues[342, 343]. This prior work, therefore, suggests that the cells within the biconcave constructs may be facing strains approximately 1.5x those applied to the tissue. Thus, future work should also consider the effects of passive axial loading on the cells comprising self-assembled neotissues, which may in turn help to infer upon both the local cellular and tissue level mechanical response of neotissues to axially applied strain.

Overall, this study suggests that passive axial compression, which represents a relatively simple and inexpensive means for inducing mechanical loading, is a promising tool for increasing the functional properties of engineered fibrocartilage. A novel finding of this study is that matrix reorganization in the self-assembled, biconcave neotissues is likely due to the development of anisotropic, tensile-compressive network strains in response to the passive axial load. Additionally, not only is there a dose dependent response to increased mechanical load,

but strain thresholds also appear to exist in different directions above which matrix reorganization, synthesis, and collagen crosslinking become apparent. Future studies should be conducted to determine the effects of passive axial loading on other shape-specific constructs, as this could lead to different strain distributions and, thus, neotissues having differential functional properties. Such work will greatly aid tissue engineers in their quest to drive *in vitro* neotissue development toward capturing the anisotropy and biomechanical complexity of musculoskeletal soft tissues, leading to neotissue implants of clinical relevance.

FIGURES

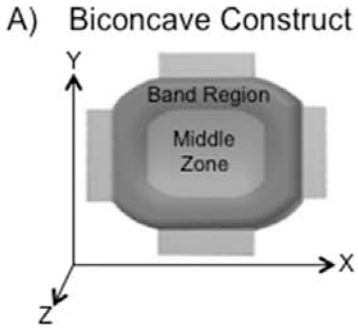

B)

	Control	1g	5g	10g
Gross Morphology	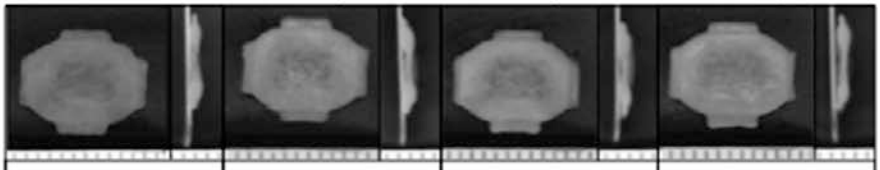			
Major Diameter (mm)	9.4 ± 0.3^{A}	9.4 ± 0.3^{A}	9.2 ± 0.4^{A}	9.2 ± 0.2^{A}
Minor Diameter (mm)	5.3 ± 03^{B}	5.6 ± 0.3^{AB}	5.6 ± 0.3^{AB}	5.9 ± 0.2^{A}
Band Zone Thickness (mm)	0.8 ± 0.1^{A}	0.8 ± 0.1^{A}	0.8 ± 0.1^{A}	0.8 ± 0.1^{A}
Middle Zone Thickness (mm)	0.6 ± 0.2^{A}	0.5 ± 0.1^{AB}	0.5 ± 0.1^{AB}	0.3 ± 0.1^{B}
Band Zone Hydration (%)	92.0 ± 0.7^{A}	90.7 ± 1.4^{A}	91.0 ± 0.5^{A}	90.8 ± 0.5^{A}
Middle Zone Hydration (%)	93.3 ± 1.0^{A}	93.5 ± 0.9^{A}	91.9 ± 1.3^{AB}	91.0 ± 0.8^{B}

FIGURE 7.1 – SCHEMATIC OF BICONCAVE CONSTRUCT AND NEOTISSUE GROSS MORPHOLOGY. Schematic of biconcave construct indicating the band region and middle zone (A). Gross morphology and growth metrics of neotissue at t = 5 wk (B). Shape-specific neotissue was subjected to 1, 5, or 10 g masses, corresponding to 0.01, 0.05, and 0.1 N loads, respectively, from t = 10 – 14 d. Values marked with different letters within each category are significantly different ($p < 0.05$), with A > B > C. Markings on the morphology images are 1 mm apart.

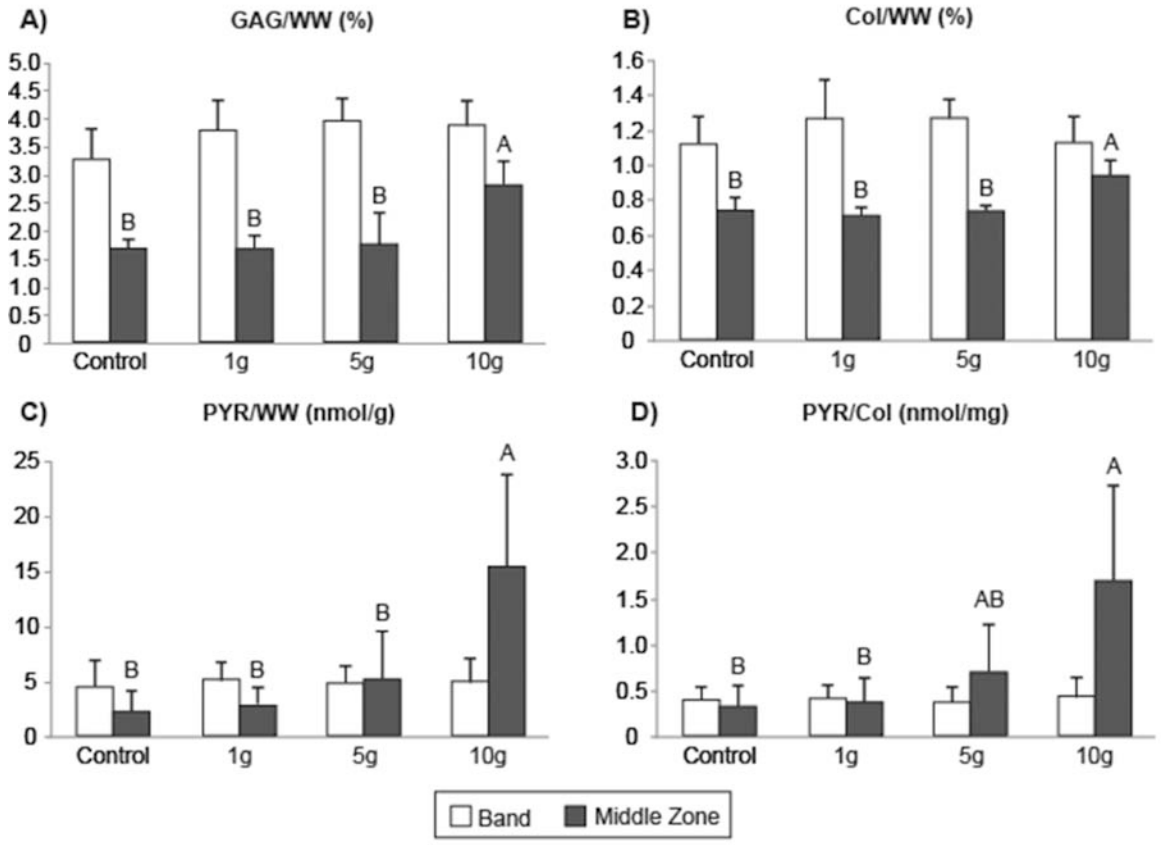

FIGURE 7.2 – GAG/WW, COL/WW, PYR/WW, AND PYR/COL OF NEOTISSUE AT T = 5 WK. Shape-specific neotissue was subjected to 1, 5, or 10 g masses, corresponding to 0.01, 0.05, and 0.1 N loads, respectively, from t = 10 – 14 d. The 10 g mass promoted significant increases in terms of all four parameters (A-D) within the neotissue's middle zone over values achieved in the middle zone of controls; no differences were observed in the neotissue's band region at any loading level. Bars not connected by the same letter are significantly different ($p < 0.05$).

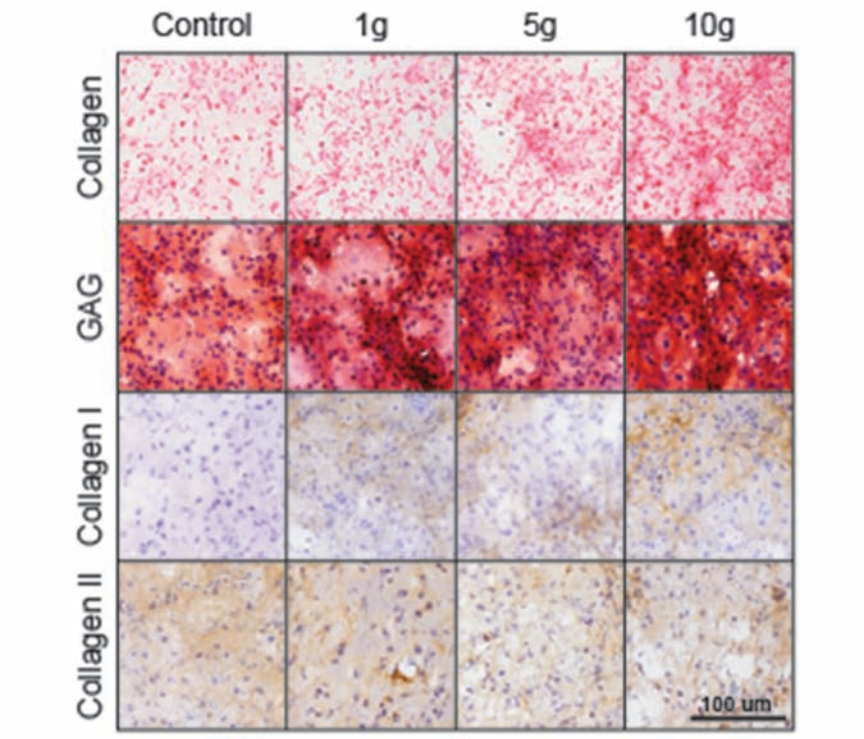

FIGURE 7.3 – HISTOLOGY AND IHC OF THE MIDDLE ZONE OF BICONCAVE NEOTISSUE AT T = 5 WK. Shape-specific neotissue was subjected to 1, 5, or 10 g masses, corresponding to 0.01, 0.05, and 0.1 N loads, respectively, from t = 10 – 14 d. Collagen was stained using Picrosirius Red, GAG was stained using Safranin O/Fast Green, while IHC was used to stain for collagen types I and II. Denser collagen and GAG staining was observed in 10 g loaded constructs compared to all other groups. While Collagen type I staining increased with increasing load, collagen type II staining appeared to slightly decrease with increasing load. Scale bar is 100 μm for both histology and IHC images.

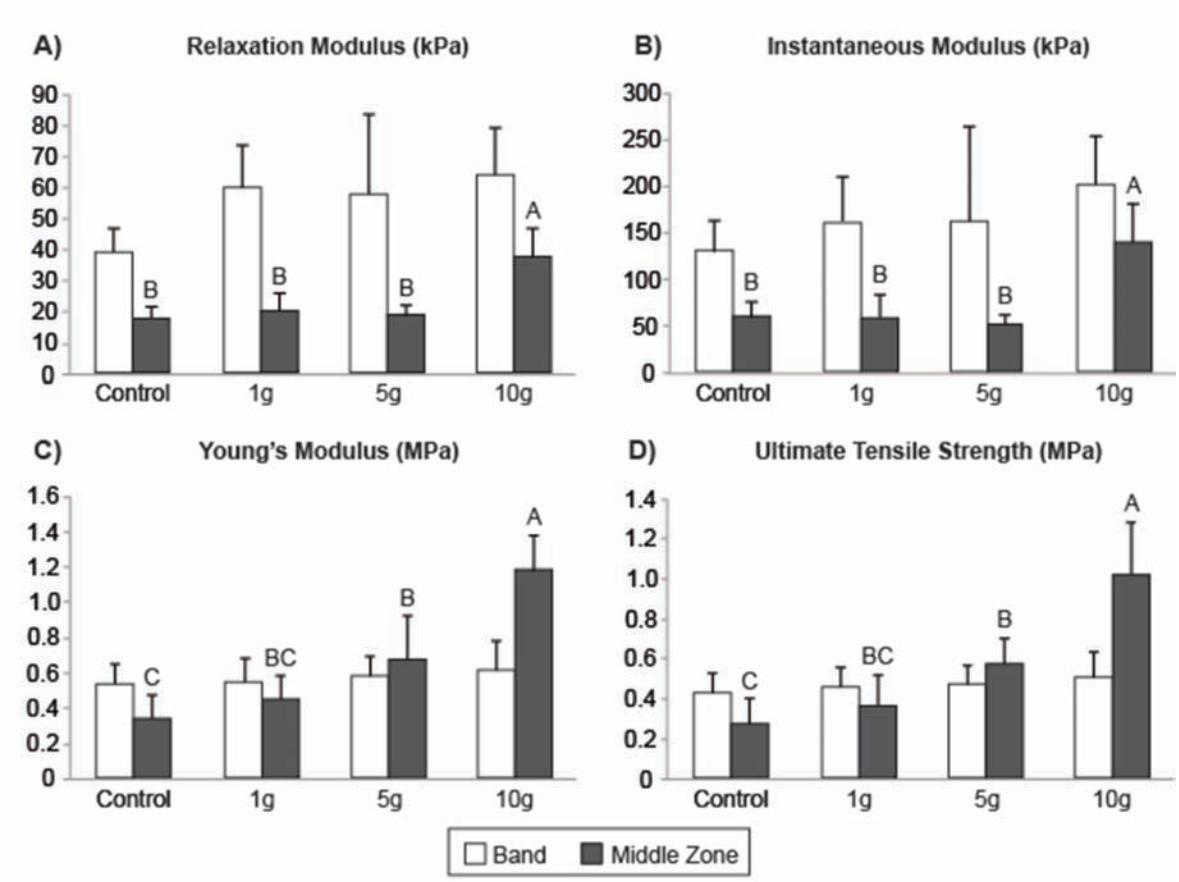

FIGURE 7.4 – RELAXATION MODULUS, INSTANTANEOUS MODULUS, YOUNG'S MODULUS, AND ULTIMATE TENSILE STRENGTH OF BICONCAVE CONSTRUCTS AT T = 5 WK. Shape-specific neotissue was subjected to 1, 5, or 10 g masses, corresponding to 0.01, 0.05, and 0.1 N loads, respectively, from t = 10 – 14 d. The 10 g mass promoted significant increases in terms of all four parameters (A-D) within the neotissue's middle zone over values achieved in the middle zone of controls; no differences were observed in the neotissue's band region at any loading level. Bars not connected by the same letter are significantly different ($p < 0.05$).

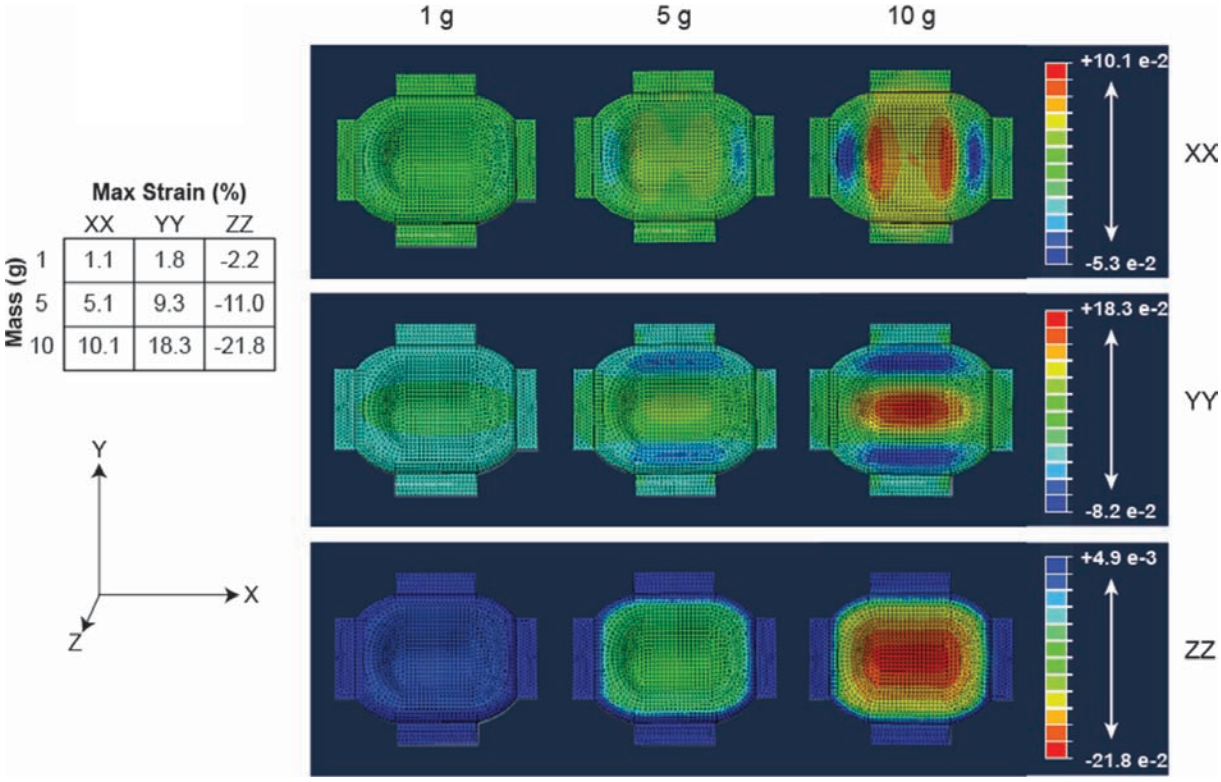

FIGURE 7.5 – RESULTS OF FINITE ELEMENT ANALYSIS. Strain distributions of 3D CAD renderings of biconcave constructs in the XX-, YY-, and ZZ-directions after being subjected to either a 1, 5, or 10 g mass, corresponding to a 0.01, 0.05, and 0.1 N load, respectively. CAD models were developed using a 4-noded linear tetrahedral mesh of 52,636 elements with material properties set to match estimated t = 10 d neotissue functional properties. Nodes at the bottom of the model were constrained in the Z-direction, and the passive axial load was modeled as a pressure distribution across an area of 54 mm^2 on the top surface of the model. Maximum strains induced by each loading level in each axial direction are provided in the table to the left.

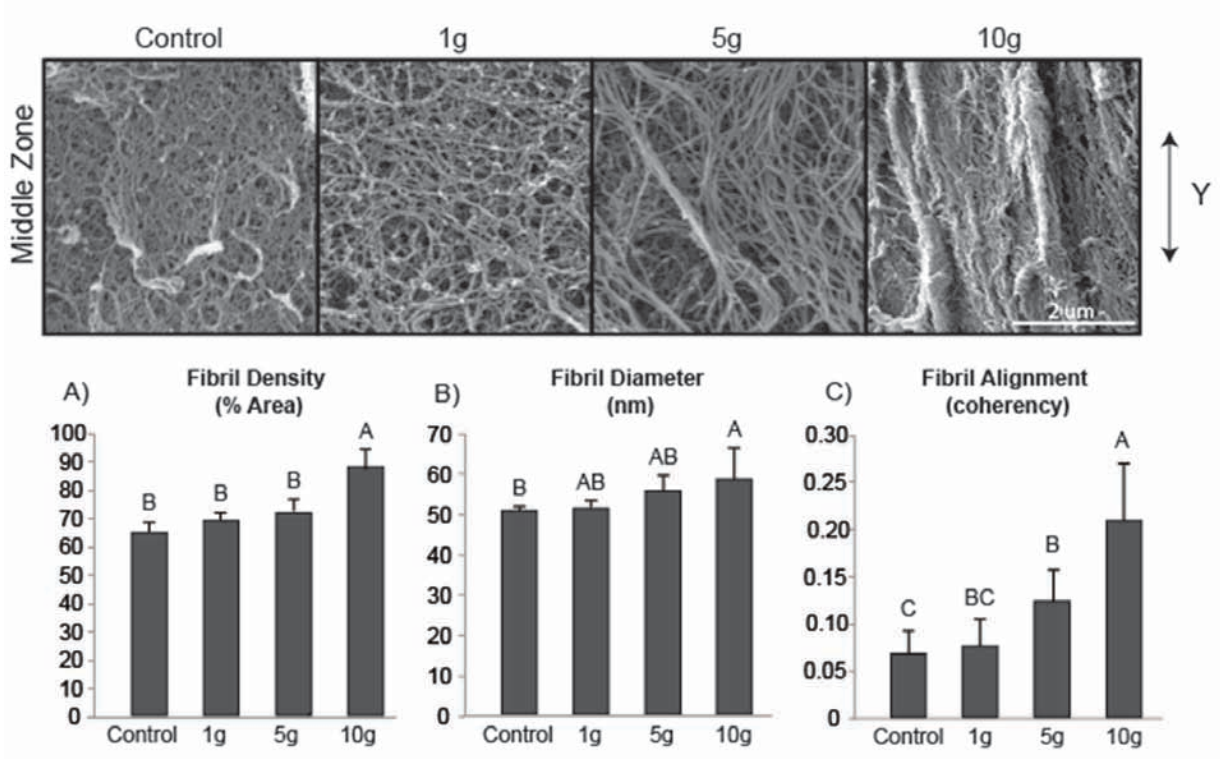

FIGURE 7.6 – SEM IMAGES OF NEOTISSUE MIDDLE ZONE AND MATRIX ANALYSIS. SEM images taken in the middle zone of biconcave constructs at t = 5 wk (top). Shape-specific neotissue was subjected to 1, 5, or 10 g masses, corresponding to 0.01, 0.05, and 0.1 N loads, respectively, from t = 10 – 14 d. Fibril density (A), fibril diameter (B), and fibril alignment (C) were analyzed from SEM images at t = 5 wk. Results found the 10 g mass to promote significant increases in terms of all three parameters (A-C) within the neotissue's middle zone over values achieved in the middle zone of controls. Further, the 10 g mass promoted fibrils to align predominantly in the Y-direction of the construct middle zone. Bars not connected by the same letter are significantly different ($p < 0.05$). Scale bar is 2 μm.

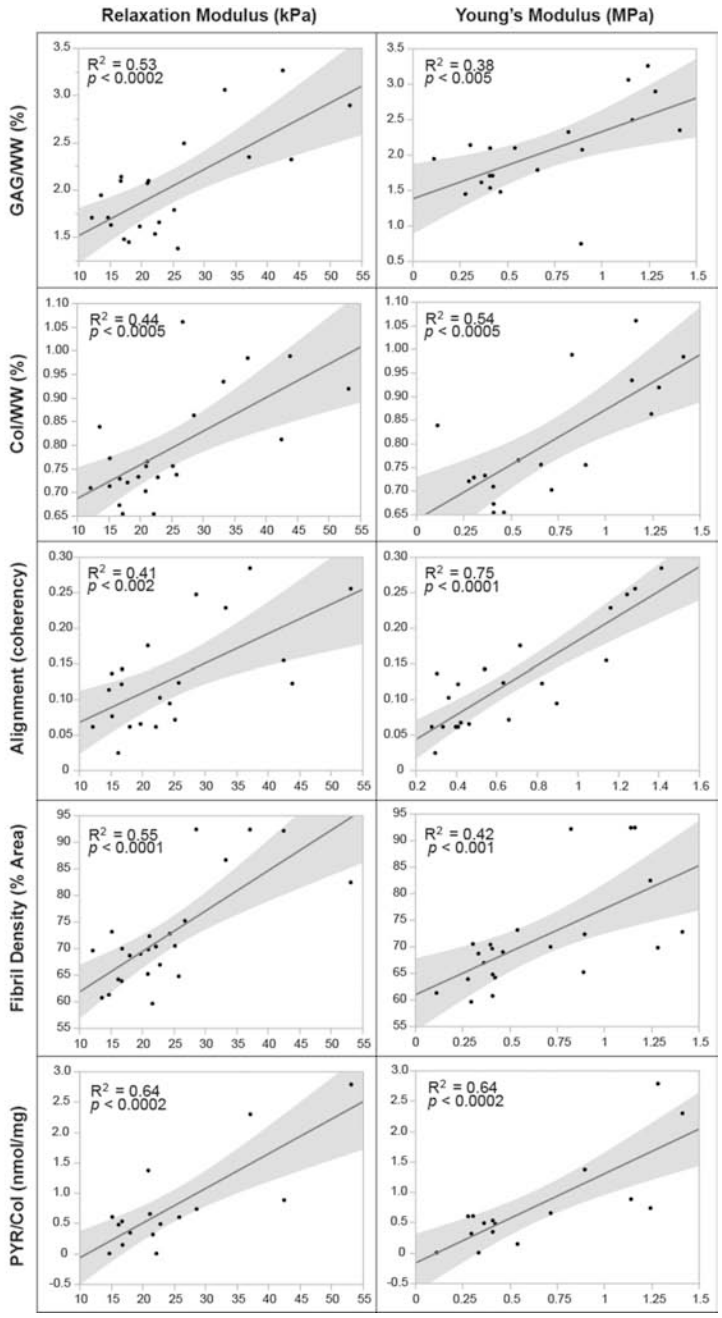

FIGURE 7.7 – STRUCTURE-FUNCTION CORRELATIONS OF NEOTISSUE MIDDLE ZONE PROPERTIES AT T = 5 WK. All correlations were found to be positive and statistically significant ($p < 0.05$). For the middle zone compressive modulus, strong positive correlations ($R^2 > 0.5$) were found with PYR/Col, GAG/WW, and collagen fibril density, while weak positive correlations ($0 < R^2 < 0.5$) were found with collagen fibril alignment and Col/WW. For the middle zone tensile modulus, strong positive correlations were found with collagen fibril alignment, PYR/Col, and Col/WW, while weak positive correlations were found with collagen fibril density and GAG/WW.

CHAPTER 8 – INDUCED COLLAGEN CROSS-LINKS ENHANCE CARTILAGE INTEGRATION

ABSTRACT

Articular cartilage does not integrate due primarily to a scarcity of cross-links and viable cells at the interface. The objective of this study was to test the hypothesis that lysyl-oxidase, a metalloenzyme that forms collagen cross-links, would be effective in improving integration between native-to-native, as well as tissue engineered-to-native cartilage surfaces. To examine these hypotheses, engineered cartilage constructs, synthesized via the self-assembling process, as well as native cartilage, were implanted into native cartilage rings. Both groups were treated with lysyl-oxidase for varying amounts of time. For both groups, lysyl-oxidase application resulted greater apparent stiffness across the cartilage interface 2–2.2 times greater than control. The construct-to-native lysyl-oxidase group also exhibited a statistically significant increase in the apparent strength, here defined at the highest observed peak stress during tensile testing. Histology indicated a narrowing gap at the cartilage interface in lysyl-oxidase treated groups, though this alone is not sufficient to indicate annealing. However, when the morphological and mechanical data are taken together, the longer the duration of lysyl-oxidase treatment, the more integrated the interface appeared. Though further data are needed to confirm the mechanism of action, the enhancement of integration may be due to lysyl-oxidase-induced pyridinoline cross-links. This study demonstrates that lysyl-oxidase is a potent agent for enhancing integration

Chapter published as: Athens, A.A., Makris, E.A., & Hu, J.C. Induced Collagen Cross-Links Enhance Cartilage Integration. *PloS one.* 8(4):e60719, 2013.

between both native-to-native and native-to-engineered cartilages. The fact that interfacial strength increased manifold suggests that cross-linking agents should play a significant role in solving the difficult problem of cartilage integration. Future studies must examine dose, dosing regimen, and cellular responses to lysyl-oxidase to optimize its application.

INTRODUCTION

Because of articular cartilage's lack of inherent healing potential, lesions tend to degenerate to osteoarthritis (OA), a significant problem affecting over a third of adults aged 65 [1]. Currently, there are no cartilage treatments that offer long-term functionality. Mosaicplasty and microfracture require defect site preparation via cartilage removal. Subsequently, the defect is filled by either cartilage plugs or a "super clot" [2]. Autografts and allografts are also options. For these and other procedures success is predicated upon the fill tissue's integration with native cartilage. Various strategies and materials have been proposed to integrate cartilage and bone [3-6]. However, cartilage-to-cartilage integration has proven to be notoriously difficult, even when using tissue engineering approaches [7,8]. To achieve long-term, durable repair, grafts and engineered articular cartilage alike need to be integrated with native cartilage. Without proper integration the implant will fall out of place or degrade rapidly [9], likely due to the high stress concentrations that occur at cartilage interfaces *in vivo*.

The general consensus regarding the main factors that hinder integration are: 1) Cell death, at the wound edge [8] and in surgically prepared defects, leads to metabolically inactive tissue, which prevents cell adhesion and migration to the injury site [10-14]. 2) Cell migration to the wound edge is hindered by the dense collagen network [10-14]; in native cartilage, cells are locked into lacunae and are not observed to migrate [15]. 3) Lack of cross-links between

matrices of native and implant tissues [16,17]. In short, the insufficiency of viable cells at the wound edge prevents synthesis of integrative matrix between the two surfaces to be joined [12-14,18,19], in part by lack of matrix synthesis. Even when viable cells are present, the newly synthesized matrix may not be sufficiently cross-linked to the native tissue. This study aims to overcome all of these factors by supplying viable cells to the interface via engineered neocartilage to mitigate the issues of cell death and lack of cell migration at the wound edge, and by exogenously inducing cross-links.

One way to deliver cells at an interface may be via the use of a construct engineered using the self-assembling process, which is an established method for generating tissue with abundant cells at the construct edge [20]. This method has also generated neocartilage with properties approaching those of native tissue [20]. Maintenance of cartilage with normal functional properties requires sustaining cell density; large areas of cell death would undoubtedly result in biomechanically inferior matrix or none at all [21]. Thus, this study seeks to use tissue engineered constructs created via chondrocyte self-assembly to deliver a higher cell density to the wound edge in order to enhance integration.

Another suggested mechanism for the enhancement of integration is collagen pyridinoline (PYR) cross-links [22]. PYR cross-links have been shown to be a major factor in determining the stiffness of connective tissues. PYR naturally forms within cartilage and other musculoskeletal tissues during development and aging via the enzyme lysyl oxidase (LOX), a metalloenzyme that converts amine side-chains of lysine and hydroxylysine into aldehydes. *In vivo*, LOX is most active at sites of growing fibrils [1]. A potential method for inducing collagen cross-linking across cartilage interfaces is thus the exogenous application of this enzyme. Since LOX is a small-sized molecule, at roughly ~50kDa, and since cross-link

formation occurs over several weeks, exogenous LOX can be applied to *in vitro* cultures on a continuous basis to ensure full penetration via diffusion and to allow sufficient time for cross-link formation. By employing LOX, one would expect the formation of "anchoring" sites, composed of PYR cross-links in the collagen network of the engineered tissue as well as of the native tissue, to bridge the two tissues together. Thus, LOX application combined with the delivery of high cell numbers to the wound edge are expected to promote tissue integration.

Using the self-assembling process, the objective of this study was to determine whether LOX can alter the integration of native-to-construct and native-to-native tissue systems through two experiments. It was hypothesized that application of LOX would enhance integration, as evidenced through tensile measurements. The first experiment sought to examine whether LOX would promote integration between native cartilage and neocartilage and to determine time and duration of application. The second experiment sought to determine whether the results from the first experiment can be replicated in a native-to-native cartilage system.

MATERIALS AND METHODS

Chondrocyte self-assembly

Articular cartilage was harvested from distal femura of one-week old male calves (Research 87 Inc., Boston, MA) less than 36hr after sacrifice. Following harvest, the tissue was digested in 0.2% collagenase type II (Worthington, Lakewood, NJ) in culture medium for 24hr as previously described [23]. Culture medium formulation is as follows: DMEM with 4.5 mg/mL glucose and L-glutamine, 100 nM dexamethasone, 1% fungizone, 1% penicillin/streptomycin, 1% ITS+, 50 μg/mL ascorbate-2-phosphate, 40 μg/mL L-proline, and 100 μg/mL sodium pyruvate. Cell viability was assessed using trypan blue exclusion, and cells were frozen at -80°C

using DMEM containing 20% fetal bovine serum (Atlanta Biologicals, Lawrenceville, GA) and 10% dimethyl sulfoxide until use. To reduce animal variability, cells from four animals were pooled together for cell seeding.

Self-assembly of constructs

Cylindrical, non-adherent, agarose wells were prepared by placing 5mm diameter stainless steel posts in 48 well plates filled with 1 ml of 2%, molten agarose, as previously described [24]. After the agarose gelled, posts were removed. The resultant wells were saturated with two exchanges of medium. After thawing, cells were counted, viability was assessed using trypan blue exclusion, and cells were seeded into the agarose wells at a concentration of 5.5 million/100 μl medium. After 4hr, an additional 400 μl of medium was added per well. Constructs were cultured at 10% CO_2, 37°C, in a humidified incubator for a total of t=28d (t=1d defined as 24hr post seeding). Medium was changed daily (500 μl).

Tissue integration

To examine the study's hypotheses, two separate, but concurrent, experiments were conducted. First, the use of LOX was examined for the construct-to-native interface. At t=28d, engineered constructs were removed from culture and prepared for integration with native articular cartilage. The t=28d culture time was chosen to coincide with prior work in self-assembled cartilage and with other cartilage tissue engineering efforts. Bovine articular cartilage explants, measuring 6mm x 1mm, were harvested using biopsy punches. A concentric, 4 mm diameter defect was punched from the explant. From the engineered constructs, 4 mm diameter biopsies were obtained and press-fitted into the defect in the explant (Fig. 1). To ensure that all

constructs were in firm contact with the explants, cyanoacrylate was applied; a penetration depth of 25 μm (~2.5% of thickness) and degradation within the culture period were verified using histology. These constructs/explant assemblies were cultured for an additional 14d, at which point they were removed for assessments. The second experiment consisted of explants instead of constructs. Native-to-native tissue assemblies were formed using the same geometry as described above.

Collagen cross-linking via lysyl oxidase

The LOX medium contained a concentration of 0.15 μg/ml LOX (GenWay Biotech, Inc., San Diego, CA). This concentration is based a pilot study in which three concentrations, 0.0015, 0.015, and 0.15 μg/ml of LOX, were examined. The results showed that only 0.15 μg/ml of LOX improved pyridinoline content over the culture duration employed; at this concentration, neither the collagen nor glycosaminoglycan per wet weight was altered when LOX was applied to either native or engineered cartilage separately. For the construct-to-native study, four groups were examined: The control (Group A) consisted of construct/explant assemblies maintained in culture medium only. Group B was treated with the LOX medium during t=15-28d. Group C was treated during t=29-35d. Group D was treated during t=15-35d. These groups were chosen to examine LOX treatment prior (Group B), after (Group C), or throughout (Group D) integration with the native tissue. Assemblies were assessed at t=42d to allow for a total of 14d of integration time. For the native-to-native study, two groups were examined. The control group was allowed to integrate for 14d in culture medium, while the LOX Group was maintained in a LOX medium during the same time.

Histology

Frozen sections were collected at 14 μm on positively charged slides to promote maximal adherence. These were fixed in 10% neutral buffered formalin and dehydrated through ascending alcohol percentages (50%, 60%, 70%, 80%, 90%, 95%, 100%) to minimize dehydration artifacts. Picrosirius red was used to demonstrate collagen distribution, as previously described [20].

Biochemistry

Total collagen was assessed using a hydroxyproline assay, and glycosaminoglycan content was measured using a Blyscan kit, both as previously described [20].

Tensile testing

Assemblies were cut into strips 1mm wide. Thickness and width were verified photographically using ImageJ (National Institutes of Health, Bethesda, MD). Specimens were glued onto test strips separated by a pre-defined spacing of 1mm, and the strips were clamped and exposed to constant uniaxial strain of 1% of the 1mm spacing per second until failure using a uniaxial materials testing machine (Instron 5565). Force-deformation data were collected and then normalized with respect to the cross-sectional area and initial spacing length of the specimens. From this, an apparent “stiffness” was derived by calculating the slope of the linear region of the graph. The ultimate tensile apparent strength (UTS) was defined as the maximum stress attained by the specimen before failure.

Statistical analysis

Based on prior data used to determine LOX concentration, application time, and effects on cellular activity, a power analysis was performed to determine an n=6 required to discern differences in tensile properties at $p<0.05$. Data were compiled as mean±standard deviation and analyzed using a single factor ANOVA. If the F-test was statistically significant, a Tukey's *post hoc* test was employed to identify significant groups. Significance was defined as $p<0.05$.

RESULTS

Integration of engineered constructs to native articular cartilage

For all treatment durations, LOX-treated construct-to-native assemblies displayed better integration as compared to controls using gross morphology, histology, and biomechanical evaluations. Prior to histological processing, the assemblies were evaluated straight from culture for gross morphology. Although LOX addition increased the stiffness of the assemblies, it did not affect the size and dimensions of the samples. Grossly, gaps were seen between the construct and native tissue in 33% of the controls (Fig. 2). Gaps were not seen for any of the LOX-treated specimens. Similarly, histological evaluation showed gaps in the controls, while LOX-treated samples showed construct adherence to the native tissue. Tensile testing across the integration interface showed significantly higher apparent stiffnesses when LOX was applied during t=15-35d (Group D) (1.6±0.6 MPa, versus control values of 0.7±0.2 MPa (Fig. 3, top). Significantly higher apparent strength values were observed for both Groups B and D (0.42±0.07 MPa and 0.39±0.06 MPa, respectively), where LOX was applied before formation of the construct-to-native assembly (Fig. 3, bottom). Control and Group C values were 0.23±0.08 MPa and 0.28±0.1 MPa. No significant differences were detected in the GAG/ww or collagen/ww among the construct or the explant portions of the assemblies. Specifically, no

significant differences were detected in the GAG/ww content among the constructs (4.5±1.4%, 2.9±1.4%, 3.1±0.5%, and 4.5±0.6% for Groups A-D, respectively) or among the explant rings (8.6±1.1%, 10.9±1.9%, 9.6±01.2%, and 10.5±2.8% for Groups A-D, respectively). Additionally, no significant differences were detected in the collagen/ww content among the constructs (5.4±2.2%, 5.7±1.7%, 5.7±0.7%, and 7.2±3.1% for Groups A-D, respectively) or among the explant rings (5.6±3%, 10.6±7.5%, 6.2±3%, and 10.5±3.2% for Groups A-D, respectively).

Integration between native cartilage tissues

Qualitatively, the only difference between control and LOX-treated native-to-native assemblies was seen by histology (Fig. 4). The apparent stiffness of the LOX-treated group was more than twice that of the control (1.5±1.1 MPa versus 0.7±0.4 MPa), though neither this property nor the apparent strength were statistically significant (Fig. 5). GAG and collagen content were not different between the two groups.

DISCUSSION

Motivated by the as-of-yet unsolved issue of cartilage integration, the objective of this study was to examine the hypothesis that LOX would induce cartilage integration. This enzyme naturally occurs in cartilage and promotes PYR cross-links in collagen, thereby holding potential for strengthening cartilage-to-cartilage interfaces. The hypothesis was proven to be correct as evidenced by the biomechanical and histological data. At the dosage applied, this naturally occurring enzyme did not alter cellular response with respect to collagen and GAG production. Engineered tissues, formed using a self-assembling process, were integrated to

native tissue explants by applying LOX to a ring-and-implant assembly (Fig. 1). Additionally, LOX was applied to native-to-native cartilage interfaces to examine whether this novel integration method can also be applicable to cases where there is not an abundance of cells at the wound edge. The results showed that cartilage integration can be enhanced if the interface is stocked with metabolically active cells and cross-links simultaneously. Enhanced interfacial properties were observed for construct-to-native but not for the native-to-native case. Group D, which was treated with LOX for the longest period of time, had statistically higher tensile properties than did the other three groups. Group D had approximately 2.2 times the tensile strength of controls. This was confirmed with morphological and histological data. The results of this study are significant for both current and prospective cartilage regeneration and repair methods.

It is worth noting that, despite the lack of any significant differences in the collagen and GAG content in either the construct or explant groups, there were significant LOX-induced increases in interface biomechanics. The fact that interfacial mechanical properties (apparent stiffness and apparent strength) increased significantly, in the absence of increases in the main ECM components, suggests that cross-links play a central role in integration. Unfortunately, a relationship between the strength of the interface and the number of cross-links at the interface cannot be directly assessed. This is because the interface cannot be isolated without adjacent tissues that, too, contain cross-links. It is, therefore, difficult to ascertain the fraction of cross-links belonging to the interface alone. The mechanism of LOX-induced collagen cross-linking is well-established [22] and a strong candidate for explaining the results obtained in this study, though this was not directly proven here. Future studies may consider techniques such as time-resolved fluorescence spectroscopy [25] to quantify PYR at the interface.

It was observed during tensile testing that samples always broke at the interface, indicating that the interface is not as strong as either neocartilage or native cartilage. The mechanical property of the interface is, thus, due to newly synthesized matrix that has had relatively little time to develop cross-links in contrast to the rest of the tissues. It is known that LOX-induced PYR formation requires 7 to 30 days [26], which may also explain why increased apparent strength was observed only for groups whose LOX treatment was initiated 28d prior to tensile assessment. In these cases, PYR cross-link precursors were allowed to accumulate within the constructs prior to their being press-fitted into the native tissue, at which time these precursors readily bridged the construct and native tissue together by maturing into cross-links. In terms of native-to-native interfaces, in future studies it may be prudent to consider longer durations of LOX application

It is worthy to note that, for the timescale applied, diffusion of LOX should not be a bottleneck to its effectiveness. LOX is a relatively small molecule of ~50kDa. For comparison, BMP-1 is 30kDa, and the diffusion coefficient of 40 kDa dextran has been determined to be ~60μm^2/s) [27]. However, LOX may require time to act before it promotes integration since it can take weeks to complete the final PYR product. This can be seen with Group C, which consists of LOX applied at t=25-39d only. This treatment did not result in significant increases in tensile properties. It is unclear whether this is due 1) to the short duration of LOX application or 2) to the late initiation of application. These two variables should be examined in a future study at greater detail. For example, a variety of initiation and culture times can be examined, extending the total time of culture up to 8 weeks to identify the "ceiling" of effectiveness. Once this saturation level has been determined, one can then optimize not only the time of initial application, but also the total duration of application.

Aside from the dependence on *in vitro* culture time [28], cytokines present *in vivo* can also influence integration. A study examined the effects of steroid hormones in bovine cartilage that is lacking a known inhibitor to integration, interleukin-1β. An increase of ~50 kPa in mechanical integration was seen [29], as compared to the 700 kPa obtained in this study for the native-to-native controls. Also, it has also been shown that, without the assistance of exogenous agents, strength of half that which is seen in intact cartilage can be achieved in an equine model for chondrocyte transplantation [30]. It is worth noting that, in the present study, by delivering cells to the interface in concert with LOX, integration strength can be increased to 1.6 MPa (Group D). Given that chondrocyte transplantation is a current therapy that, similar to the self-assembled constructs employed in this study, delivers metabolic cells to the wound edge, it is conceivable for LOX to assist this clinical procedure. Of course, additional studies on 1) optimal dosing time, 2) cross-linker concentration, and 3) activity profile as related to not only the chondrocytes but also other cell types surrounding cartilage would need to be completed to ensure safety and efficacy, prior to deploying this technique clinically.

A major component of articular cartilage ECM is the electronegative aggrecan. This electric charge is an obstacle to integration because the similar charges in two pieces of tissue would cause them to repel [7]. Further studies need to be completed to fully understand the role which aggrecan's electronegativity plays in blocking integration. Future studies might also include the combination of LOX with other bioactive agents that are known to influence cartilage behavior. Already, transforming growth factor β1 (TFG-β1) has shown efficacy when combined with a biomaterial [31], and it would be interesting to examine how LOX can assist this case. TFG-β1 may work in synergism with LOX, the cytokine and enzyme working in tandem to effect greater collagen production and cross-linking.

It should be mentioned that, for this study, LOX concentration was based on a pilot study that examined LOX on native and engineered cartilages separately (described in "Materials and Methods"). Following this study's exciting results, it may be prudent to conduct a systematic examination of various LOX concentrations to identify a minimum, yet effective, concentration between 0.015 and 0.15 μg/ml that enhances interfacial stiffness and strength to the levels of the engineered or native cartilages, or even for other tissues where cross-linking plays important functional roles. For instance, integrating engineered knee meniscus to native knee meniscus has shown dependence on maturation state [32], and therefore the extent of collagen cross-links, and LOX may be used similarly for this tissue. Finding this minimum dose will be significant in not only reducing cost but also in mitigating any potential for this enzyme to interfere with other cellular processes, despite this being a naturally-occurring enzyme. Already, it has been shown here that LOX does not interfere with chondrocyte metabolism with respect to collagen and GAG synthesis, but, for its use *in vivo*, the effects of LOX on other cells may need to be elucidated prior to conducting animal studies with this enzyme. A similar process would allow the identification of an optimal LOX concentration for maximizing the native-to-native integration strength; this will be immensely useful from a clinical perspective, once the safety and efficacy of exogenous LOX has been shown.

While other cross-linkers such as ribose, glutaraldehyde, genipin, and methylglyoxal have all been investigated in conjunction with engineered articular cartilage [33,34], these agents have all been shown to alter cellular activity. Some of these agents are even cytotoxic and thus preclude their use with live cells in influencing integration. Furthermore, unnatural cross-linkers such as glutaraldehyde have been shown to elicit a foreign body giant cell reaction [35], in contrast to LOX, which is found naturally in multiple musculoskeletal tissues. This

study demonstrates that LOX is a potent agent for enhancing integration between native and tissue engineered cartilage. It also paves the way for the use of LOX in improving native cartilage integration. These results could potentially be used to solve the problem of large cartilage defects by allowing tissue engineered cartilage implants to be integrated into the surrounding tissue.

FIGURES

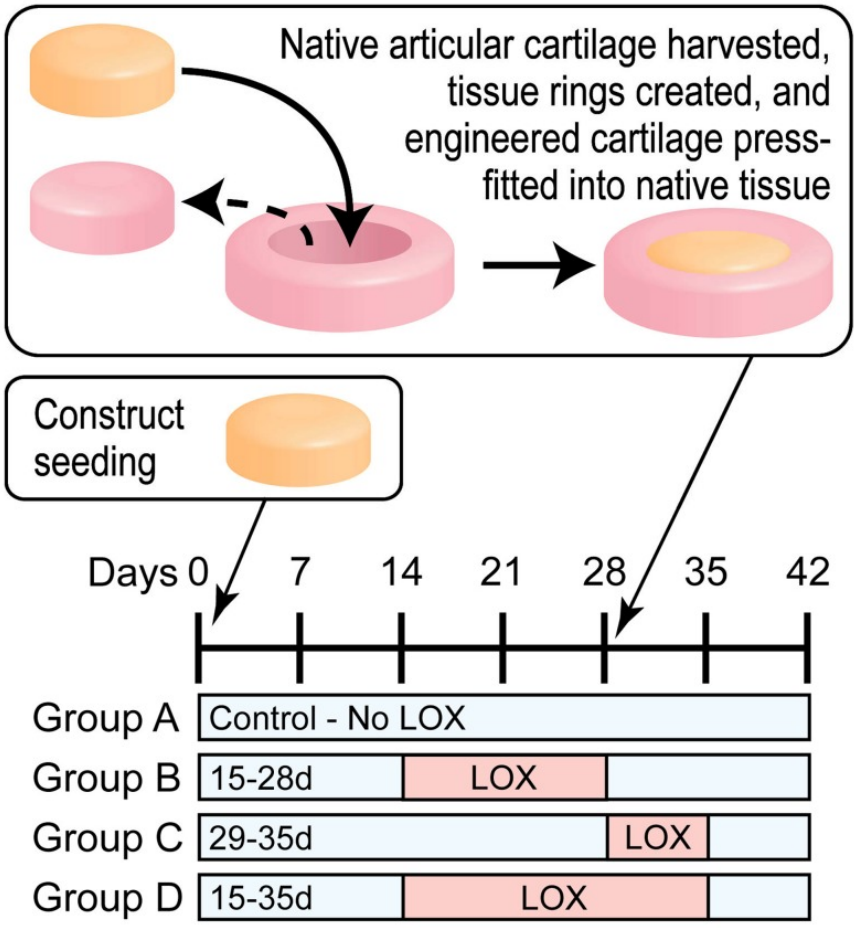

FIGURE 8.1 – SCHEMATIC OF THE EXPERIMENT EXAMINING INTEGRATION OF TISSUE ENGINEERED CARTILAGE TO NATIVE CARTILAGE. For Group B, LOX was applied during construct formation, t = 15–28 d. For Group C, LOX was applied after forming the construct-to-native assemblies, t = 29–35 d. For Group D, LOX was applied both before and after the formation of the construct-to-native assemblies, t = 15–35 d.

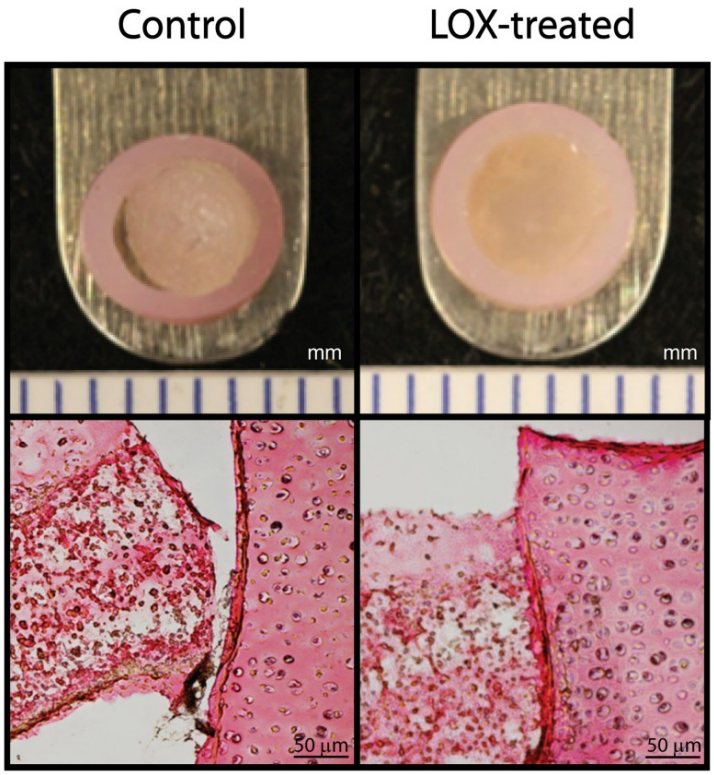

FIGURE 8.2 – GROSS MORPHOLOGY AND HISTOLOGY OF CONSTRUCTS/EXPLANT ASSEMBLIES. Straight from culture, most controls resembled LOX-treated samples, though gaps were seen in one-third of the controls (upper left panel). None of the LOX-treated samples displayed gaps that were grossly visible; a representative sample (Group D) is shown (upper right). Gaps in the controls were also seen after histological processing using picrosirius red (lower left) versus LOX-treated samples (lower right, Group D).

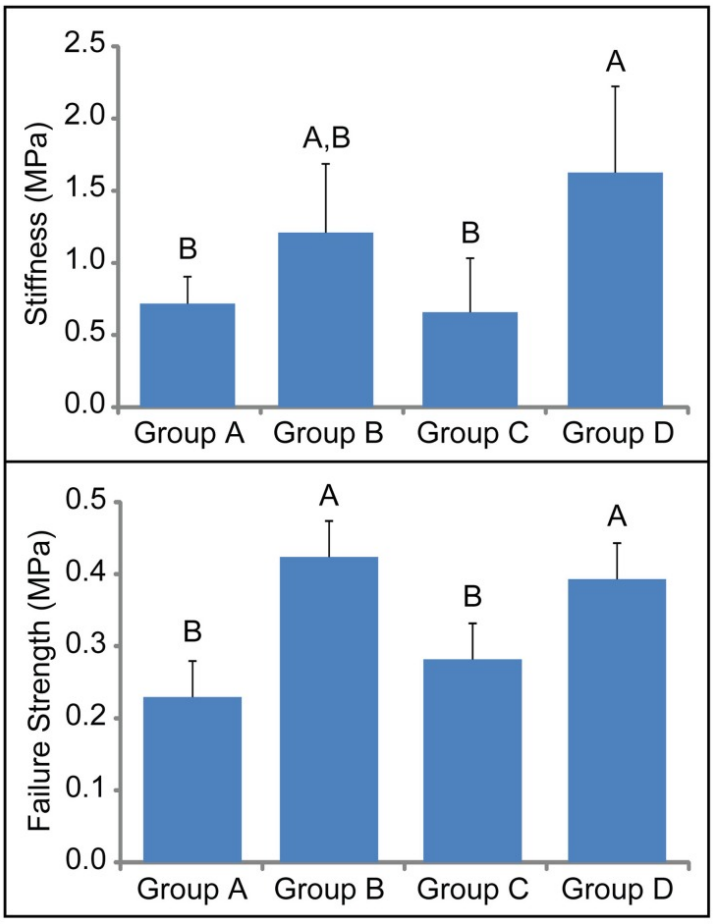

FIGURE 8.3 – TENSILE MECHANICAL DATA OF CONSTRUCT/EXPLANT INTERFACE. Significantly higher apparent stiffness (top) was seen when LOX was applied during t = 15–35 d (Group D) than controls (Group A). Significantly higher apparent strength was obtained across the integration interface when engineered cartilage was treated with LOX before being press-fitted into the native cartilage (bottom). Bars with different letters are significantly different ($p<0.05$).

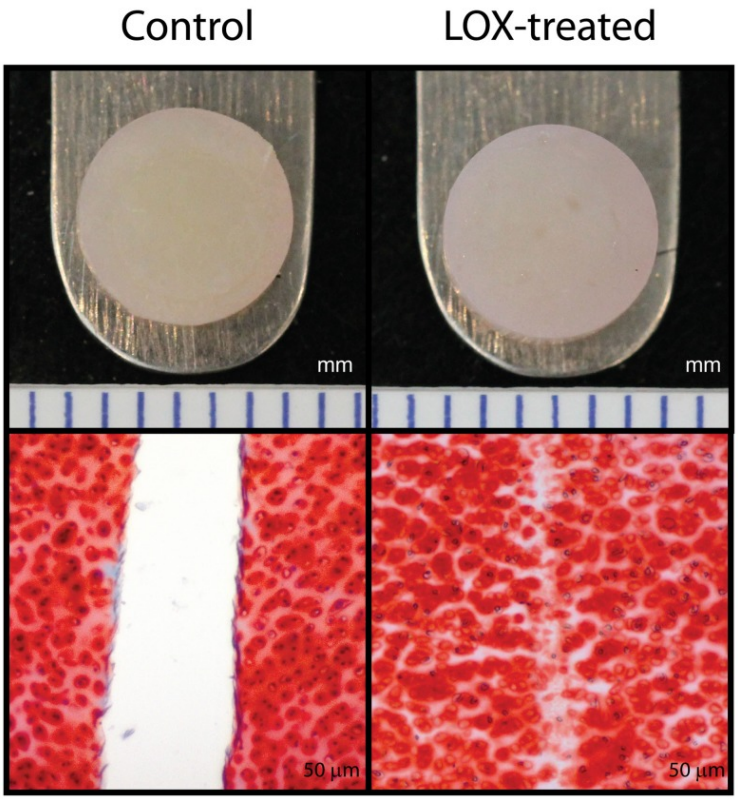

FIGURE 8.4 – GROSS MORPHOLOGY AND HISTOLOGY OF EXPLANT/EXPLANT ASSEMBLIES. Neither control nor LOX-treated native-to-native assemblies displayed grossly visible gaps when removed from culture (top row). However, gaps can be seen after histological processing using picrosirius red in the control group, unlike the LOX-treated group (bottom).

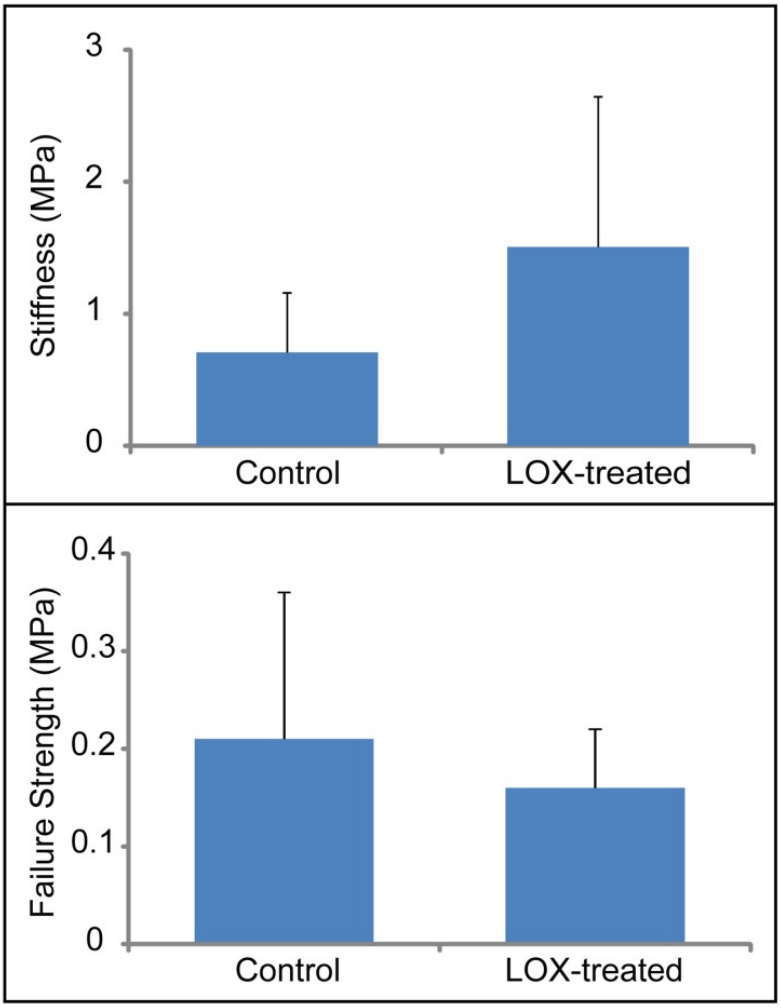

FIGURE 8.5 – TENSILE MECHANICAL DATA OF EXPLANT/EXPLANT INTERFACE. No differences in apparent stiffness (top) or apparent strength (bottom) were seen when LOX was applied to native-to-native integration.

CHAPTER 9 – ENGINEERING FUNCTIONAL NEOTISSUES WITH *IN VIVO* INTEGRATION POTENTIAL FOR REPAIRING FIBROCARTILAGE DEFECTS

ABSTRACT

Patients suffering from damaged or diseased fibrocartilages currently have no effective long-term treatment options. Existing clinical options, such as autografts, allografts, or scaffold-based neotissues, are greatly hindered by their low biomechanical properties and their inability to integrate with healthy native tissue. The present study sought to develop novel methods to enhance the biomechanical integrity of engineered implants as well as to address the two pivotal factors that currently inhibit fibrocartilage integration: 1) low native tissue cellularity, and 2) the lack of collagen crosslinks at the native-to-implant interface. Specifically, highly cellularized, scaffold-free neofibrocartilage implants were subjected to a novel combination of stimuli, including the biophysical agent chondroitinase-ABC, the biochemical agent transforming growth factor-β1, and the enzyme responsible for collagen crosslinking, lysyl oxidase. Combined use of these agents drove *in vitro* neofibrocartilage matrix maturation toward synergistically enhanced Young's modulus and ultimate tensile strength values, which were increased 245% and 186%, respectively, over controls. Furthermore, an *in vitro* fibrocartilage defect model found this treatment regimen to significantly increase the integration tensile properties between neofibrocartilage and native tissue. Translating this technology to an *in vivo* fibrocartilage defect

To be submitted as: Makris, E.A.* & MacBarb, R.F.*, Paschos, N.K., Hu, J.C., & Athanasiou, K.A. Engineering Functional Neotissues with *In Vivo* Integration Potential for Repairing Fibrocartilage Defects. *Proceedings of the National Academy of Sciences of the United States of America*. (December 2014). *indicates co-first author

model found this combination pre-treatment to prime the neofibrocartilage for significantly enhanced integration potential *in vivo*, with interfacial tensile stiffness and strength 730% and 745% greater, respectively, than values achieved during *in vitro* integration. Together, these studies demonstrate that this novel combination of exogenous agents promotes biomechanically robust self-assembled neofibrocartilage implants capable of generating integration interfaces with functional properties on par with intact native fibrocartilage.

SIGNIFICANCE STATEMENT

Damaged or diseased fibrocartilages, such as the knee menisci, intervertebral discs, and ligaments, are unable to self-repair, necessitating clinical management. Unfortunately, current treatment options only provide short-term pain relief. While tissue engineering of replacement fibrocartilages offers much promise as a long-term reparative therapy, their insufficient mechanical robustness and inability to effectively bond to native healthy tissue surrounding the defect hinders their clinical applicability. The present study, therefore, investigated the potential of a combination of novel agents to promote integration of mechanically robust engineered fibrocartilage upon implantation. Results of this work shed light onto the possibility of novel methods to engineer clinically relevant fibrocartilage implants capable of self-bonding to adjacent tissue.

INTRODUCTION

Collagen-rich, fibrocartilaginous musculoskeletal soft tissues, such as the knee menisci, intervertebral discs, temporomandibular joint (TMJ) discs, tendons, and ligaments, lack an intrinsic ability to self-repair following disease- or injury-induced degradation. As such,

different fibrocartilage repair techniques have been developed, which typically utilize either autograft or allograft tissue, or scaffold-based neotissues. However, such approaches are hindered by their inability to successfully integrate with host tissue upon implantation[386, 387]. Proper integration is critical to graft success, as it ensures that the implant remains stabilized and is, therefore, able to competently function *in vivo*[388, 389]. With the insufficiency of current grafts, tissue engineering of neofibrocartilage implants that mimic the complex structures of native tissues holds great potential as a long-term clinical solution for acute fibrocartilage injuries and chronic degenerative pathologies[257]. Toward engineering such implants, it is imperative that they are able to withstand the high mechanical loads of joints, and perhaps even more importantly, are strategically engineered to promote integration with the host tissue upon implantation. Without these critical features, they, like current grafts, will likely fail. Thus, it is critical that novel treatment modalities are developed that specifically target 1) the maturation and extracellular matrix (ECM) organization, and 2) the integration potential of engineered fibrocartilage implants.

There are several factors that may either directly or indirectly impede proper fibrocartilage integration[389]. The four most commonly addressed factors include: 1) the avascularity of the host tissue[390], 2) cell death at the periphery of the defect[391], 3) hindrance of cellular migration due to a dense collagen matrix at the wound edge[392], and 4) the lack of stabilizing collagen crosslinks at the native-to-implant interface[393]. Together, these factors result in a metabolically inactive wound edge that limits both matrix synthesis and crosslink formation, hindering integration with any type of implant[394]. Various methods have been developed in an attempt to overcome the yet unresolved hurdle of integration. For instance, biological tissue adhesives have been used at the integration interface[395, 396], as well as

enzymatic degradation to temporarily reduce the amount of negatively charged proteoglycans at surfaces of the graft and host tissues[397, 398]. While such methods have had a beneficial effect toward encouraging integration, a highly stable, biomechanically robust integration interface, able to withstand the complex distribution of forces within joints, has yet to be achieved. Thus, efforts to enhance the integration potential of neofibrocartilage implants must be established to ensure successful outcomes following implantation.

A self-assembling process has been developed to generate highly cellularized and metabolically active neotissues[212], which may aid in integration upon implantation. Specifically, seeding high-density co-cultures of meniscus cells (MC) and articular chondrocytes (AC) into non-adherent agarose wells promotes the development of neofibrocartilage in a manner akin to native morphogenesis[3, 230]. Past work has identified several exogenous factors to enhance the overall functional properties of self-assembled neotissue, including the bioactive agent transforming growth factor-β1 (TGF-β1) and the biophysical agent chondroitinase-ABC (C-ABC)[4, 99]. While combined use of these factors has been found to enhance neotissue functional properties through increased collagen content, density, and fibril diameter[272, 315], their tensile properties remain inferior to those of native tissue. Thus, efforts to further promote *in vitro* tissue maturation in addition to enhancing their integration potential are necessary to generate mechanically robust neofibrocartilage implants able to withstand the high *in vivo* loads of joints.

Promoting collagen crosslinking in neofibrocartilages may provide a viable solution toward furthering *in vitro* maturation as well as facilitating *in vivo* integration with the host tissue. Natively, lysine-derived, covalent pyridinoline (PYR) crosslinks have been shown to be instrumental to development of a mechanically robust collagen matrix[7]. Such crosslinks are formed via the enzyme lysyl oxidase (LOX), which turns amino acid precursors (lysine and

hydroxylysine) into mature PYR crosslinks over time[11-13]. Capitalizing on the potential of promoting the formation of PYR crosslinks, this study employed a novel combination of stimuli consisting of exogenous LOX, C-ABC, and TGF-β1 to enhance the tensile properties of self-assembled neofibrocartilage implants as well as effect and stabilize their integration with native tissue. This study was conducted in three Phases: The objective of Phase 1 was to promote *in vitro* maturation of engineered fibrocartilage. Phase 2 sought to foster the integration between native and self-assembled fibrocartilages *in vitro*. Finally, Phase 3 investigated the potential of a LOX+C-ABC+TGF-β1 pre-treatment to prime neofibrocartilage for enhanced integration *in vivo*. Overall, it was hypothesized that through collagen enhancement and PYR crosslink formation, combined treatment of LOX+C-ABC+TGF-β1 would 1) induce time-dependent maturation and enhance the tensile properties of the neofibrocartilage constructs, 2) promote *in vitro* integration between engineered and native fibrocartilages, and 3) carry over an effect into the *in vivo* environment to further promote such integration.

RESULTS

Phase 1: In vitro *maturation of engineered fibrocartilage*

The first phase of this study employed a two-factor, full factorial study design, which included a treatment factor (control, LOX, C-ABC+TGF-β1, and LOX+C-ABC+TGF-β1) and a culture duration factor (t = 6 or 12 wk). At both t = 6 and 12 wk, self-assembled neofibrocartilage constructs were analyzed biochemically, biomechanically, and via scanning electron microscopy (SEM) to test the ability of these factors to promote neotissue maturation and tensile property enhancement. All constructs presented with flat, uniform morphology at both t = 6 and 12 wk (Fig. 1A-B), with C-ABC+TGF-β1 and LOX+C-ABC+TGF-β1 constructs having significantly decreased wet weights, hydrations, diameters, and thicknesses compared to

controls at each respective time point (Table 1). Histologically, collagen staining was more dense and uniform in C-ABC+TGF-β1 and LOX+C-ABC+TGF-β1 groups, while glycosaminoglycan (GAG) staining was denser in control and LOX groups at t = 6 wk. Similar results were observed histologically at t = 12 wk; however, GAG staining appeared to increase in both control and LOX groups at this time (Fig. 1A-B).

Biochemical analysis found significantly greater collagen per wet weight (Col/WW) in C-ABC+TGF-β1- and LOX+C-ABC+TGF-β1-treated constructs at both t = 6 and 12 wk compared to LOX and control constructs. Specifically, at t = 6 wk, the LOX+C-ABC+TGF-β1 group exhibited a 180% increase in Col/WW over controls, and at t = 12 wk, a 228% increase over controls was observed in this group (Fig. 2A). In terms of collagen crosslinks, PYR per wet weight (PYR/WW) was found to be significantly greater in both LOX and LOX+C-ABC+TGF-β1 treated constructs at t = 6 wk, with values 1.9- and 2.7-fold those of respective 6 wk controls. By t = 12 wk, the LOX+C-ABC+TGF-β1-treated constructs exhibited significantly greater PYR/WW over all other groups, with a value 3.8-fold those of 12 wk controls (Fig. 2B). GAG per wet weight (GAG/WW), on the other hand, was found to be significantly greater in control and LOX groups compared to C-ABC+TGF-β1 and LOX+C-ABC+TGF-β1 groups at both the 6 and 12 wk time points (Table 1).

Uniaxial tensile testing at t = 6 wk found the LOX+C-ABC+TGF-β1 treatment to synergistically increase both the Young's modulus (E_Y) and ultimate tensile strength (UTS) 202% and 121%, respectively, over 6 wk controls (Fig. 2C-D). These synergistic enhancements were also observed in t = 12 wk constructs, finding the LOX+C-ABC+TGF-β1-treated neofibrocartilage to have E_Y and UTS values 245% and 186%, respectively, over 12 wk controls. Results further found the 12 wk time point to be a significant factor toward enhancing

neotissue tensile properties. Stress-relaxation unconfined compressive testing found both the relaxation modulus (E_r) and instantaneous modulus (E_i) to be significantly greater in LOX constructs compared to all other groups at at t = 6 wk (Table 1). By t = 12 wk, both control and LOX groups presented with greater E_r and E_i values compared to C-ABC+TGF-β1 and LOX+C-ABC+TGF-β1 constructs.

Neofibrocartilage constructs were imaged via SEM to investigate the effects of the two factors on *in vitro* matrix development and organization (Fig. 1A-B). Results found 6 wk constructs treated with LOX+C-ABC+TGF-β1 to have a denser collagen matrix displaying bundling of fibrils into fibers compared to control constructs, which appeared less dense and with no sign of bundling. By t = 12 wk, while the control matrix remained relatively unaltered, the bundling of fibrils into densely packed and organized fibers was even more evident in LOX+C-ABC+TGF-β1-treated constructs. Quantitative analysis of the SEM images at both 6 and 12 wk found C-ABC+TGF-β1 and LOX+C-ABC+TGF-β1 constructs to have significantly enhanced collagen fibril densities over controls. The LOX+C-ABC+TGF-β1 treatment was further found to significantly increase the collagen fibril diameter by 92% over controls at the 6 wk time point; by the 12 wk time point, these increases were found to be synergistic, with values increased by 104% over 12 wk controls. (Fig. 1C-D). Further, the 12 wk time point was again found to be a significant factor toward promoting maturation of the neofibrocartilage matrix in terms of significantly increasing both the fibril density and diameter.

Phase 2:* In vitro *integration of native and engineered fibrocartilage

The second phase of this study sought to promote integration between native and engineered fibrocartilages via an *in vitro* model of integration. Briefly, 3 mm diameter punches of 6-wk-old

neofibrocartilage were press-fit into same size defects in native fibrocartilage explant rings, forming engineered-to-native assemblies (Fig. 3A). Prior to assembly formation, neofibrocartilage was subjected to the same four treatments from Phase 1; the only exception being that LOX was applied both pre- and post-assembly formation to further aid in promoting integration (Fig. 3B). Native-to-native assemblies were also created to determine the ability of LOX to promote integration between native fibrocartilages. Following 6 wk of *in vitro* integration, the integration interface of engineered-to-native and native-to-native assemblies were analyzed histologically and biomechanically.

Histological evaluation of the integration interface found both LOX and LOX+C-ABC+TGF-β1 treatments to promote fusion of the interface in engineered-to-native assemblies; control and C-ABC+TGF-β1-treated assemblies, however, showed little to no integration (Fig. 4A). This was also shown biomechanically: both LOX and LOX+C-ABC+TGF-β1 treatments significantly enhanced the integration interface tensile stiffness and strength in engineered-to-native assemblies over controls or C-ABC+TGF-β1-treated constructs (Fig. 4B-C). Specifically, the E_Y and UTS of the integration interface in LOX-treated assembles were 2.2- and 2.4-fold respectively, those of controls. Similarly, LOX+C-ABC+TGF-β1-treated assembles presented with integration interface E_Y and UTS values that were 2.2- and 2.6-fold, respectively, those of controls. In terms of the native-to-native assemblies, histological evaluation showed little to no integration in either control or LOX-treated groups, which was further confirmed biomechanically (Fig. 4D-F). Results further revealed the integration interface in LOX-treated engineered-to-native assembles to have ~7.5-fold greater tensile stiffness and strength compared to those of LOX-treated native-to-native assemblies.

Phase 3:* In vivo *integration of native and engineered fibrocartilage

Previous work has shown that the nutrient rich subcutaneous environment promotes *in vivo* neotissue maturation[231, 399, 400]. The objectives of Phase 3, therefore, were 1) to investigate whether subcutaneous implantation of engineered-to-native assemblies into the backs of nude mice would help to further fortify the integration interface area, and 2) if this fortification could be enhanced via use of the LOX+C-ABC+TGF-β1 pre-treatment established in Phase 2. All treatments in the third phase were administered to neofibrocartilage during the first 6 wk of culture, prior to formation of the engineered-to-native assemblies (at t = 42 d) and subcutaneous implantation (at t = 43 d). Specifically, a single vs. double application of LOX, in addition to C-ABC and TGF-β1, was administered to neofibrocartilage implants to investigate whether a 2nd LOX application, just prior to formation of the engineered-to-native assemblies, would further reinforce the integration interface *in vivo* (Fig. 3A,C). Six wk post-surgery, the mice were humanely sacrificed, and the tissue assemblies were harvested and analyzed histologically and biomechanically.

Histological evaluation of the engineered-to-native assemblies post-sacrifice revealed untreated assemblies to be partially integrated; both the single and double LOX treatments, however, were found to promote more complete fusion of the integration interface. Further, the neofibrocartilage in the double LOX-treated assemblies presented with denser collagen staining compared to the engineered tissue in single LOX-treated assemblies (Fig. 5A). Biomechanical testing found both LOX treatments to significantly increase the tensile stiffness and strength of the integration interface compared to untreated assemblies (Fig. 5B-C). Specifically, the E_Y and UTS of the integration interface in single LOX-treated assemblies were 3.3- and 3.2-fold, respectively, those of controls. The double LOX treatment, on the other hand, increased the E_Y

and UTS of the integration interface 4.3- and 4.7-fold control values, respectively. Analysis was also conducted to compare the *in vitro* integration results of Phase 2 with the *in vivo* results of Phase 3 (Fig. 5D-E). A two-tailed, paired Student's *t*-test revealed the *in vivo* double LOX treatment to promote significantly enhanced E_Y and UTS values that were 304% and 230% greater, respectively, than those achieved in combination-treated constructs *in vitro.* In comparing the E_Y and UTS of the integration interface of *in vivo* double LOX-treated assemblies to *in vitro* control assemblies revealed 730% and 745% significant increases, respectively, in the combination-treated *in vivo* assemblies over *in vitro* controls. No significant differences, however, were observed between *in vitro* and *in vivo* controls. Further, two-way ANOVA analysis found both the LOX+C-ABC+TGF-β1 pre-treatment as well as the *in vivo* subcutaneous environment to be significant factors toward enhancing the integration interface stiffness and strength in fibrocartilaginous engineered-to-native assemblies.

DISCUSSION

In light of the current insufficiencies of fibrocartilage implants, this study sought to enhance the biomechanical integrity of neofibrocartilage as well as to facilitate and stabilize their integration with native tissue. This goal was addressed via a novel combination of stimuli: LOX, C-ABC, and TGF-β1. Innovative aspects of this study include finding that the LOX+C-ABC+TGF-β1 treatment 1) enhances the tensile properties of self-assembled fibrocartilage via time-dependent maturation of the neotissue's ECM, and 2) promotes integration between engineered and native tissues. With only LOX- and LOX+C-ABC+TGF-β1-treated assemblies showing significantly improved integration over controls, this study demonstrates that LOX is a potent agent for enhancing integration between native-to-implant surfaces, confirming the pivotal role of PYR

crosslinks at the integration interface. Furthermore, this work shows, for the first time, that a pre-treatment carries over an effect into an *in vivo* model toward achieving functional integration. Specifically, results found neofibrocartilage implants pre-treated with LOX+C-ABC+TGF-β1 to have a significantly stiffer and stronger integration interface with native tissue following *in vivo* implantation over untreated controls. Methods used in this study were able to address the two most cumbersome factors that currently hinder integration, including cell death at the wound edge and the lack of collagen crosslinks at the integration interface. Thus, using self-assembled neofibrocartilage implants allows for implantation of highly cellular, metabolically active implants that, when treated with LOX+C-ABC+TGF-β1, are primed for enhanced integration potential following implantation toward achieving values on par with intact native fibrocartilage.

Phase 1 of this study established that longer culture duration promotes a more biomechanically robust matrix in LOX+C-ABC+TGF-β1-treated constructs. Specifically, the LOX+C-ABC+TGF-β1 treatment was found to synergistically enhance the neotissue's tensile properties by 202% over controls at 6 wk and by an additional 43% by 12 wk. While the 12 wk time point was found to be a significant factor toward enhancing neotissue tensile properties, it was not a significant factor toward enhancing collagen content. Previous work has shown that as highly collagenous native tissues develop and mature, the density and diameters of their collagen fibrils increase, along with increased fibrillar bundling and matrix compaction; together, these structural modifications translate to a matrix capable of withstanding greater tensile loading[294-296]. Similarly, the present study found the 12 wk time point to be a significant factor toward increasing the collagen fibril diameter and density in LOX+C-ABC+TGF-β1-treated constructs, as well as to promote distinct collagen bundling. Thus, results indicate that,

over time, the LOX+C-ABC+TGF-β1 treatment promotes *in vitro* neofibrocartilage maturation similar to the maturation observed during native tissue morphogenesis, resulting in a neofibrocartilage construct with greater tensile properties.

Concurrent with the observed matrix modifications, neofibrocartilage constructs treated with LOX+C-ABC+TGF-β1 also experienced increased intermolecular collagen crosslink content. While no significant difference in crosslink content was observed between LOX- and LOX+C-ABC+TGF-β1-treated constructs at t = 6 wk, by t = 12 wk, the crosslink content in combination-treated constructs was significantly increased over all other groups. It has been shown that LOX-mediated PYR collagen crosslinks take ~7 – 30 d to fully mature[13]. While no significant differences were observed in PYR content in 6 wk vs. 12 wk time points, it is, therefore, likely that the longer culture duration allowed for the development of more mature PYR crosslinks to form. Previous work has indicated that it is specifically the mature crosslinks that are correlated with the tensile robustness of native fibrocartilaginous tissues[401, 402]. With more time for the crosslinks to mature *in vitro*, constructs receiving LOX and grown to 12 wk were better suited to withstand tensile loads. By combining LOX with C-ABC+TGF-β1, therefore, neofibrocartilage grown to 12 wk had the benefits of all three agents, including 1) increased collagen content as a result of TGF-β1, 2) a compacted collagen matrix having greater fibril diameters as a result of C-ABC, and 3) more mature PYR crosslinks that aided in the bundling of fibrils into more mechanically robust fibers. Thus, results indicate that the increased tensile properties are directly related to matrix maturation, organization, and crosslinking, showing combined use of these three agents to be a potent regimen to promote matrix maturation and enhanced neotissue biomechanical integrity over time (Fig. 6).

One can consider several exogenous agents that could potentially be used to enhance neotissue collagen crosslinking and, concomitantly, their functional properties. Hypoxia application in neocartilage has been proven to promote HIF-1- and LOX-mediated PYR crosslinking[7]. Similarly, copper application in neotissues has been shown to enhance collagen crosslink formation and biomechanical properties[322]. These more traditional systems for enhancing crosslink formation, however, are associated with deleterious side effects; for example, copper application and the downstream products of hypoxia and HIF-1α decrease collagen synthesis in neotissues[7, 322]. The present study, therefore, found an exogenous LOX treatment to provide a simple and direct, yet effective, way to promote neofibrocartilage integrity by enhancing PYR crosslinking without affecting collagen content. Further, when combined with C-ABC and TGF-β1, enhanced PYR content via exogenous LOX application synergistically increased the tensile properties of self-assembled neofibrocartilage constructs.

In applying the treatments investigated in Phase I to an *in vitro* model of integration, results of Phase II found LOX to promote integration between neofibrocartilage and native tissue. Specifically, the integration interface stiffness and strength were significantly increased an average of 114% and 148%, respectively, in engineered-to-native assemblies treated with either LOX alone or with LOX+C-ABC+TGF-β1. The finding that the LOX+C-ABC+TGF-β1 treatment regimen did not promote integration any further than LOX alone suggests that LOX is the crucial factor contributing to the enhanced integration potential of neofibrocartilage. This indicates that increased PYR collagen crosslinks is critical to the formation of a more robust integration interface. Previous work has found β-aminopropionitrile, an agent that irreversibly inhibits LOX activity, thus blocking collagen crosslink formation, to inhibit integration between cartilage explants[403], further showing the importance of crosslinks at the integration interface.

Thus, results of the present study show that using exogenous LOX to upregulate PYR crosslink formation not only aids in promoting maturation of the neotissue along with C-ABC and TGF-β1, but is also integral to facilitating and stabilizing the integration interface between engineered implants and native tissue (Fig. 6).

As a part of Phase II, native-to-native assemblies were also treated with LOX for 1 wk following assembly formation, followed by an additional 5 wk of *in vitro* culture. While LOX treatment doubled the tensile stiffness of the interface of native-to-native assemblies compared to untreated native-to-native controls, the effect of LOX was 7.5-fold more potent toward enhancing the tensile properties of engineered-to-native assemblies. Natively, collagen crosslinks in fibrocartilaginous tissues remain in an unstable, immature, reducible form during early development; however, as the tissue matures, these reducible crosslinks are converted into more stable, mature, non-reducible PYR crosslinks[404]. Thus, the low cellularity and highly dense, mature crosslink-stabilized matrix likely inhibited exogenous LOX from having much effect at promoting integration in native-to-native assemblies[391, 394]. This suggests that the high cellularity, immature collagen matrix, and high collagen crosslinking potential of the self-assembled constructs enabled the neofibrocartilage to better respond to LOX, resulting in the formation of PYR crosslinks at the integration interface. Overtime in culture, therefore, the metabolically active integration interface in engineered-to-native assemblies matured to produce significantly stronger bonding than in the metabolically inactive native-to-native assemblies.

The final phase of this work found that pre-treating self-assembled fibrocartilage implants with a double LOX application in addition to C-ABC+TGF-β1 carried over a significant effect into the *in vivo* environment, resulting in further promoting integration

between native and engineered fibrocartilage. Specifically, this treatment increased the integration interface E_Y and UTS by 4.3- and 4.7-fold, respectively, values achieved in untreated implanted assemblies. Further, when compared to integration values achieved using the same treatment *in vitro*, the *in vivo* environment was found to improve the integration interface tensile stiffness and strength by 304% and 230%, respectively. These significant enhancements are likely attributable to the nutrient rich environment and mechanical stresses placed on the engineered-to-native assemblies in the subcutaneous environment[231, 399, 400]. However, because no significant differences were found between the integration properties of *in vitro* and *in vivo* control assemblies, the 4.1-fold significant enhancement in the integration properties of LOX+C-ABC+TGF-β1-treated *in vivo* compared to *in vitro* engineered-to-native assemblies indicates the subcutaneous environment had a more potent effect in the pre-treated neofibrocartilage. Thus, the pre-treatment likely primed the implant to better respond to the *in vivo* environment, further accelerating its maturation and, hence, interfacial integration with native tissue (Fig. 6). This speaks to the potential for LOX+C-ABC+TGF-β1-treated neofibrocartilage implants to further mature and form even more stable integration interfaces given longer *in vivo* culture time. Future work must therefore investigate the effects of this treatment toward promoting long-term integration in functional defect sites *in vivo*.

While a plethora of work exists on repairing defects in various fibrocartilaginous tissues, ranging from *in vitro*, to *in vivo*, and clinical work, integration has mainly been treated as an auxiliary portion of these studies. As a result, most of the literature on fibrocartilage repair provides only qualitative means to examine possible integration, such as histological and magnetic resonance imaging techniques[266, 405-414]. The present study, however, highlights the necessity for conducting mechanical characterization of the integration interface. As shown in

the present study, although an implant may appear highly integrated in certain areas with the surrounding native tissue via histological assessment, mechanical integrity of the integration interface may be substantially weak (such as seen in the *in vivo* engineered-to-native control assemblies). Treated engineered-to-native assemblies, which appeared similar, although more uniformly integrated, compared to controls via histology, had significantly stronger integration interfaces. Thus, it is imperative that future studies investigating fibrocartilage repair techniques include mechanical testing of the integration interface as one of the key success criteria for engineered repair tissues. This metric will provide an additional means toward the goal of engineering mechanically robust and stable repair tissues suitable for long-term clinical applications.

Of the few studies that have mechanically characterized the integration interface in fibrocartilaginous repair models[415, 416], only one study has utilized a pull-to-failure test similar to the test used in the present study. This study generated electrospun nanofibrous scaffolds containing entrapped collagenase, with the goal of locally controlling matrix degradation at the meniscus wound interface to enhance native-to-native tissue repair. Results found the integration interface tensile strength to trend higher in defects containing the collagenase-releasing scaffold compared to empty defects or those containing non-collagenase-releasing scaffolds following 50 d of *in vitro* culture, with the integration interface tensile strength of the best group averaging at 13.5 kPa[417]. The present study similarly found the integration interface tensile strength to trend higher in LOX-treated native-to-native assemblies, with a value of 25.9 kPa. Use of the LOX+C-ABC+TGF-β1 and the highly cellular neotissue in engineered-to-native assemblies, however, resulted in integration E_Y values of 240 kPa following *in vitro* culture, which were further promoted following *in vivo* culture to 890 kPa. In comparing the

achieved integration interface tensile modulus to those of intact fibrocartilaginous tissues, results of the *in vivo* portion of this study indicate that the integration interface in assemblies containing LOX+C-ABC+TGF-β1-treated neofibrocartilage was ~100% of the tensile modulus of intact intervertebral disc anulus fibrosus tissue in the axial direction[252], ~28% of intact native TMJ disc middle zone tissue in the mediolateral direction[80], and ~18% of intact native meniscal tissue in the radial direction[253]. Thus, results indicate this combination treatment significantly improves the integration robustness of engineered fibrocartilage implants to values on par with those of intact native tissue.

In summary, this study addresses the current insufficiencies of fibrocartilage implants, namely their subpar biomechanical integrity and, more importantly, their inability to integrate with native tissue upon implantation. Specifically, this study shows that a novel LOX+C-ABC+TGF-β1 pre-treatment synergistically enhances the biomechanical functionality and primes the integration of highly cellularized, metabolically active, self-assembled fibrocartilage implants. By addressing two of the most difficult factors that currently inhibit integration, the tensile properties of the integration interface achieved *in vivo* were on par with values of intact native fibrocartilage. Methods developed in this study are translatable toward addressing defects in a wide variety of fibrocartilaginous tissues. Future work will be focused on adapting these methods toward further promoting the functional properties and integration potential of neofibrocartilage in site-specific, large animal fibrocartilage defect models.

MATERIALS AND METHODS

Neofibrocartilage culture & integration

Juvenile bovine AC and MC were isolated and self-assembled at a 50:50 ratio, as previously described[272]. For Phase 1, constructs were grown and analyzed at t = 6 and 12 wk. For Phases 2

and 3, integration was investigated by press-fitting 3 mm diameter punches of 6-wk-old neofibrocartilage into donut-shaped, 6 mm outer x 3 mm inner diameter native fibrocartilage explants (porcine-derived mandibular disc fibrocartilage), which were cultured for an additional 6 wk either *in vitro* or *in vivo* (Fig. 3). Native-to-native assemblies were likewise created for Phase 2. For both the *in vitro* and *in vivo* integration phases, the integration interface was analyzed at t = 12 wk. To ensure the constructs remained in place, 1 µl of biodegradable cyanoacrylate was applied to the interface at one specific location of both engineered-to-native and native-to-native assemblies, penetrating ~ 2.5% of the thickness of the tissue. Although histology verified the glue to fully degrade prior to testing, all analysis was conducted opposite where the cyanoacrylate glue was administered to ensure any enhancements observed in integration were not related to the affects of the tissue glue.

Treatments

This study employed a novel combination of treatments, including LOX, C-ABC, and TGF-β1. For Phase 1, LOX was applied continuously at 0.15 ng/ml from t = 7 – 21 d[6], C-ABC was applied at 2 U/ml for 4 hrs at t = 7 d and t = 21 d[272], while TGF-β1 was applied at 10 ng/ml for the entire culture duration[4]. The same four treatments were used in Phase 2; the only difference being that LOX was applied two times, from t = 7 – 21 d and again from t = 35 – 49 d. In Phase 3, the three treatment levels were: control, single LOX (from t = 7 – 21 d) + C-ABC+TGF-β1, and double LOX (from t = 7 – 21 d and t = 35 – 42 d) + C-ABC+TGF-β1. All treatments in Phase 3 were administered prior to engineered-to-native assembly formation and *in vivo* implantation.

Histology

Segments of constructs from Phase 1, as well as of the integration interface from assemblies of Phases 2 and 3, were cyroembedded and sectioned at 14 μm. Following formalin fixation, slides were stained with either Picrosirius Red for total collagen or Safranin-O/Fast Green for GAG, as previously described[272].

Biochemistry & HPLC

Construct segments were weighed before and after lyophilization, and then digested in papain as previously described[99]. Total collagen content was measured via a chloramine-T hydroxyproline assay using a SIRCOL standard (Accurate Chemical and Scientific Corp., Westbury, NY). GAG content was measured using a dimethylmethylene blue dye-binding assay kit (Biocolor, Newtownabbey, Northern Ireland). Pyridinoline (PYR) collagen crosslink content was analyzed via HPLC using PYR standards (Quidel, San Diego, CA), as previously described[322, 323].

Mechanical testing

An Instron uniaxial testing machine (Model 5565, Canton, MA) was used to measure unconfined, stress-relaxation data of the neotissue from Phase 1, which were fit to a Kelvin solid model to obtain the neotissue's viscoelastic properties at both t = 6 and 12 wk. Specifically, both E_r and the E_i were calculated, as previously described[272]. For tensile testing, dog-bone-shaped samples from Phase 1, and 1 mm wide strips containing the integration interfaces from Phases 2 and 3, were cut, glued to a paper frame at either extremity, and loaded into the grips of a uniaxial testing machine (Test Resources, Shakopee, MN). A pull-to-failure test was then conducted, from which the E_Y and UTS were obtained, as previously described[272].

SEM

Following ethanol dehydration, Phase 1 neotissue samples were critically point dried and gold sputter coated. A Philips XL30 TMP SEM was used to image three separate locations on each sample. ImageJ was used to quantify the collagen fibril density and diameter of each image, as previously described[231].

In vivo *implantation*

Nine male athymic mice, 6–8 weeks in age, were obtained in accordance with the Animal Use and Care Administrative Advisory Committee, University of California, Davis. Mice were anesthetized under general anesthesia, after which a 3 mm incision was made, and two subcutaneous pouches were created on either side of the incision, one on each side of the thorax. Each pouch received one engineered-to-native assembly, such that no mouse received two assemblies from the same treatment group (control, single LOX+C-ABC+TGF-β1, or double LOX+C-ABC+TGF-β1). The incision was then closed using staples; 6 wk post-surgery, the mice were humanely sacrificed, and the tissue harvested and analyzed.

Statistics

For Phase 1, a one-way ANOVA (n = 6 per group) was used to test the hypothesis that a LOX+C-ABC+TGF-β1 treatment regimen would enhance the *in vitro* maturation and tensile properties of the neofibrocartilage. Separately, to test the hypothesis that treatments and culture durations were both significant factors in promoting neotissue enhancement, a two-way ANOVA (n = 6 per group) was also used to analyze the data from Phase 1. Data that had a

positive interaction on an additive scale and resulted in a combined group that was greater than the addition of the two singular treatments were determined to be synergistic. For Phases 2 and 3, one-way ANOVAs (n = 6 per group) were used to determine the effect of the novel treatment regimen on enhancing the tensile properties of the integration interface. Upon finding significance ($p < 0.05$), a Tukey's HSD *post hoc* test was applied for all Phases. To compare between Phase 2 and Phase 3 results, two-way ANOVA and Student's *t*-test analyses were used. Data from all phases are represented as mean ± standard deviation.

TABLE 9.1 – PHASE 1 NEOTISSUE GROSS MORPHOLOGICAL AND COMPRESSIVE PROPERTIES AT T = 6 AND 12 WK. Values are provided for t = 6 wk (top) and t = 12 wk (bottom). Values marked with different letters within each category are significantly different ($p < 0.05$), $n = 6$ per group, with A > B > C.

6 wk constructs	Wet weight (mg)	Hydration (%)	Diameter (mm)	Thickness (mm)	GAG/WW (%)	E_r (kPa)	E_i (kPa)
Control	13.54 ± 0.39^{A}	87.48 ± 1.32^{A}	5.49 ± 0.04^{A}	0.61 ± 0.06^{A}	5.97 ± 0.41^{A}	42.59 ± 2.49^{B}	228.66 ± 59.92^{B}
LOX	12.75 ± 0.36^{A}	86.18 ± 1.25^{A}	5.53 ± 0.10^{A}	0.48 ± 0.07^{B}	6.89 ± 0.81^{A}	75.74 ± 47.98^{A}	652.17 ± 218.19^{A}
C-ABC + TGF-β1	6.75 ± 0.17^{B}	81.95 ± 2.75^{B}	4.55 ± 0.07^{B}	0.42 ± 0.05^{C}	2.94 ± 0.42^{B}	14.18 ± 2.90^{C}	240.67 ± 67.42^{B}
LOX + C-ABC + TGF-β1	6.51 ± 0.23^{B}	80.45 ± 3.88^{B}	4.55 ± 0.03^{B}	0.42 ± 0.03^{C}	1.83 ± 0.48^{C}	14.26 ± 5.11^{C}	230.01 ± 87.84^{B}

12 wk constructs	Wet weight (mg)	Hydration (%)	Diameter (mm)	Thickness (mm)	GAG/WW (%)	E_r (kPa)	E_i (kPa)
Control	22.76 ± 1.99^{A}	84.19 ± 1.54^{A}	6.22 ± 0.09^{A}	0.70 ± 0.14^{B}	11.00 ± 1.28^{A}	220.24 ± 51.01^{A}	443.62 ± 231.04^{AB}
LOX	21.08 ± 1.24^{A}	83.29 ± 2.20^{A}	5.89 ± 0.08^{A}	0.74 ± 0.03^{A}	10.30 ± 1.08^{A}	268.21 ± 117.19^{A}	823.72 ± 178.73^{A}
C-ABC + TGF-β1	7.68 ± 1.73^{B}	81.73 ± 1.06^{B}	4.51 ± 0.14^{B}	0.49 ± 0.05^{C}	2.59 ± 1.21^{B}	19.92 ± 9.54^{B}	277.66 ± 115.61^{B}
LOX + C-ABC + TGF-β1	6.32 ± 0.15^{B}	80.16 ± 0.70^{B}	4.58 ± 0.01^{B}	0.48 ± 0.03^{C}	0.65 ± 0.56^{C}	7.23 ± 8.88^{B}	120.77 ± 38.51^{C}

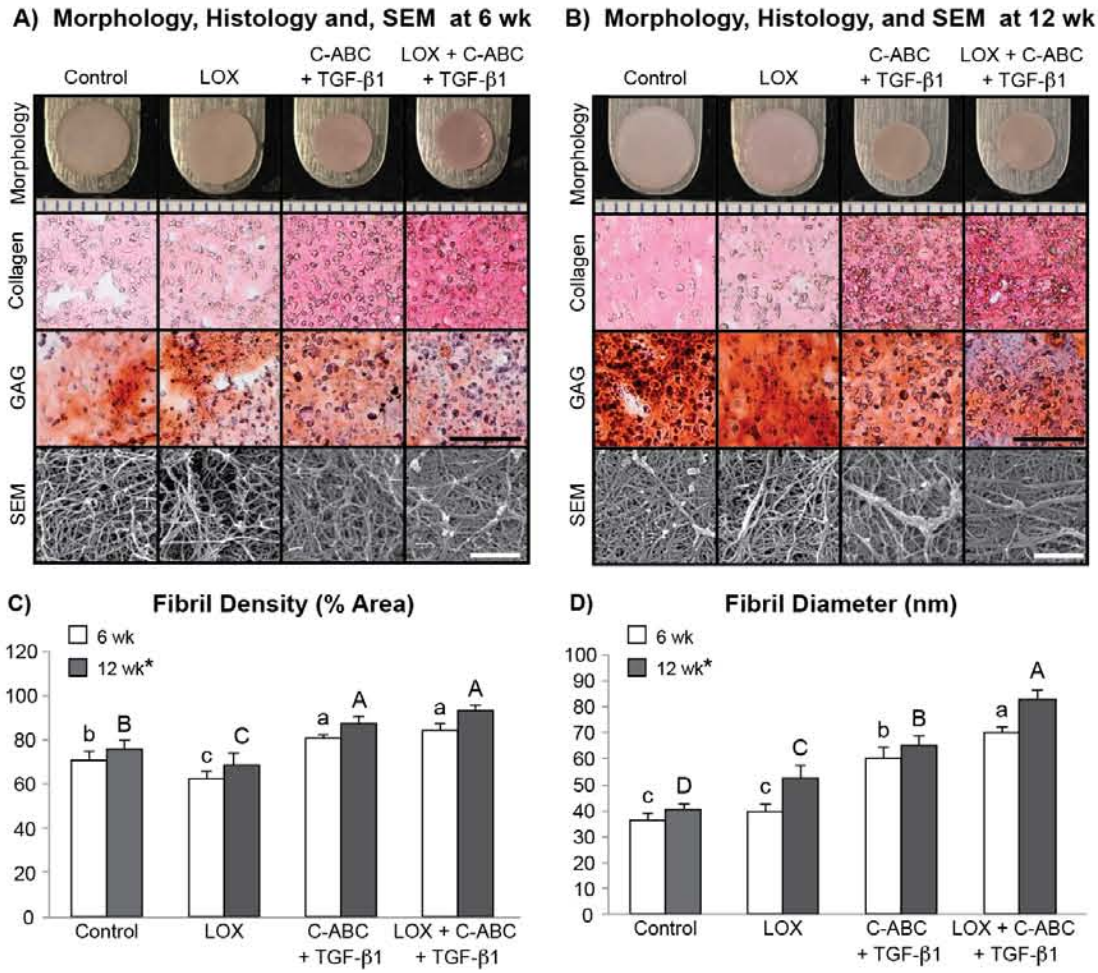

FIGURE 9.1 – PHASE 1 NEOTISSUE GROSS MORPHOLOGY, HISTOLOGY, AND SEM AT T = 6 AND 12 WK. (*A and B*) Gross morphology (markings on ruler = 1 mm), Picrosirius Red for collagen and Safranin O/Fast Green for sulfated glycosaminoglycans (GAG) stained sections (scale bar = 100 μm), and representative scanning electron microscopy (SEM) images (scale bar = 1 μm) of untreated, LOX, C-ABC+TGF-β1, and LOX+C-ABC+TGF-β1 neofibrocartilage at t = 6 wk (*A*) and t = 12 wk (*B*). Collagen fibril density (*C*) and diameter (*D*) quantified from SEM images, bars not connected by the same letter are significantly different ($p < 0.05$), lower case letters denote significant differences for 6 wk constructs, upper case letters denote significant differences for 12 wk constructs, $n = 6$ per group, mean ± SD.

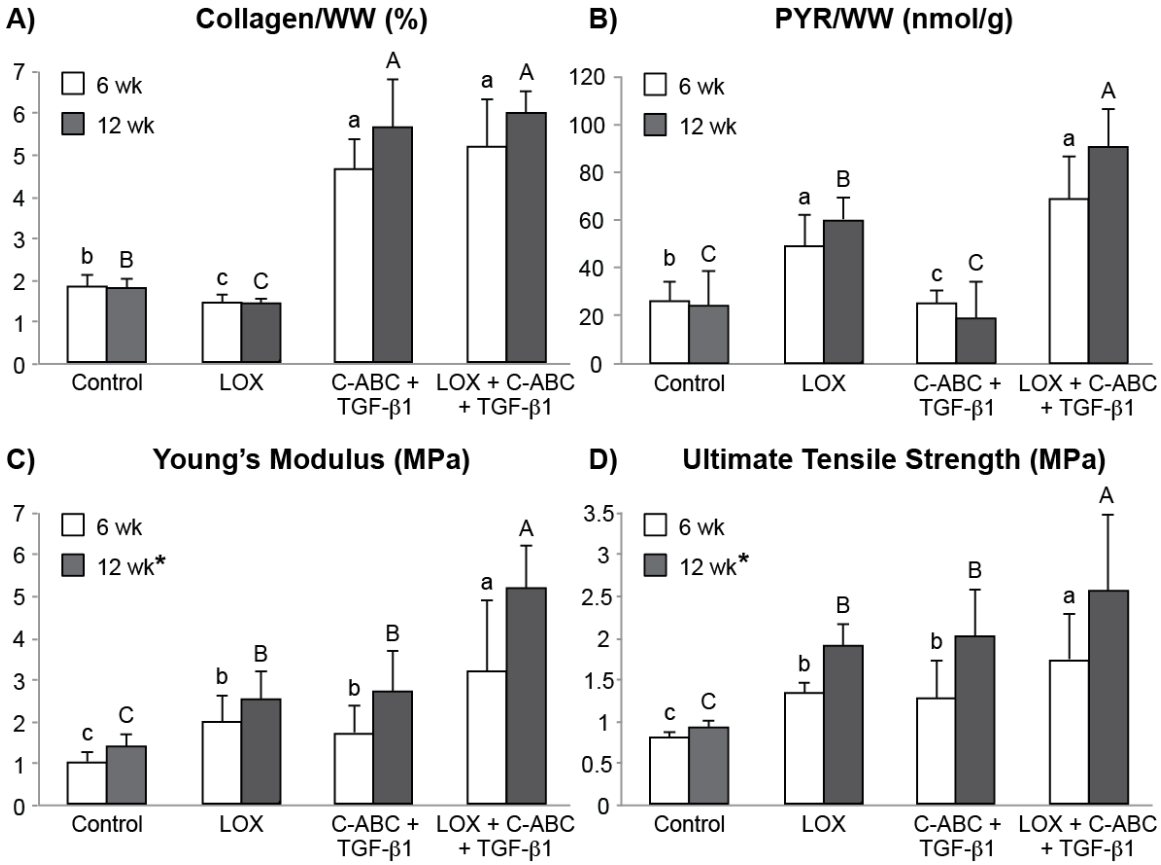

FIGURE 9.2 – PHASE 1 NEOTISSUE FUNCTIONAL PROPERTIES AT T = 6 AND 12 WK. Collagen content per construct wet weight (*A*), pyridinoline content per construct wet weight (*B*), Young's modulus (*C*), and ultimate tensile strength (*D*) of untreated, LOX, C-ABC+TGF-β1, and LOX+C-ABC+TGF-β1 neofibrocartilage at t = 6 and 12 wk. Bars not connected by the same letter are significantly different ($p < 0.05$), lower case letters denote significant differences for 6 wk constructs, upper case letters denote significant differences for 12 wk constructs, $n = 6$ per group, mean ± SD.

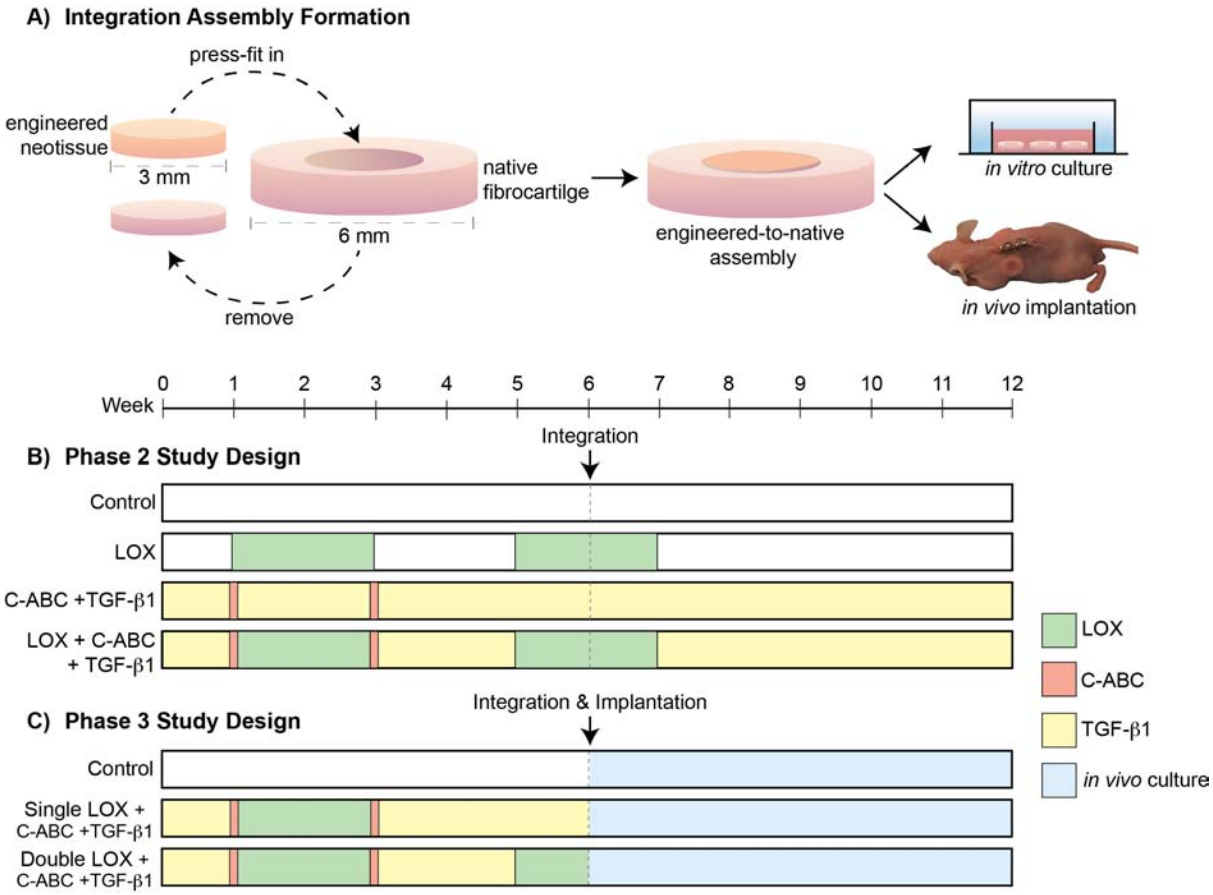

FIGURE 9.3 – PHASE 2 AND 3 EXPERIMENTAL DESIGNS. A fibrocartilage defect model was formed by press fitting 3 mm punches of 6-wk-old neofibrocartilage into same-size native fibrocartilage defects and grown either *in vitro* or *in vivo* for an additional 6 wk (*A*). Control (none), LOX, C-ABC+TGF-β1, or LOX+C-ABC+TGF-β1 pre-treatments were applied to neofibrocartilage prior to integration assembly formation and *in vitro* culture in Phase 2 (*B*). Control (none), single LOX+C-ABC+TGF-β1, or double LOX+C-ABC+TGF-β1 pre-treatments were applied to neofibrocartilage prior to integration assembly formation and *in vivo* culture in the backs of athymic mice in Phase 3 (*C*).

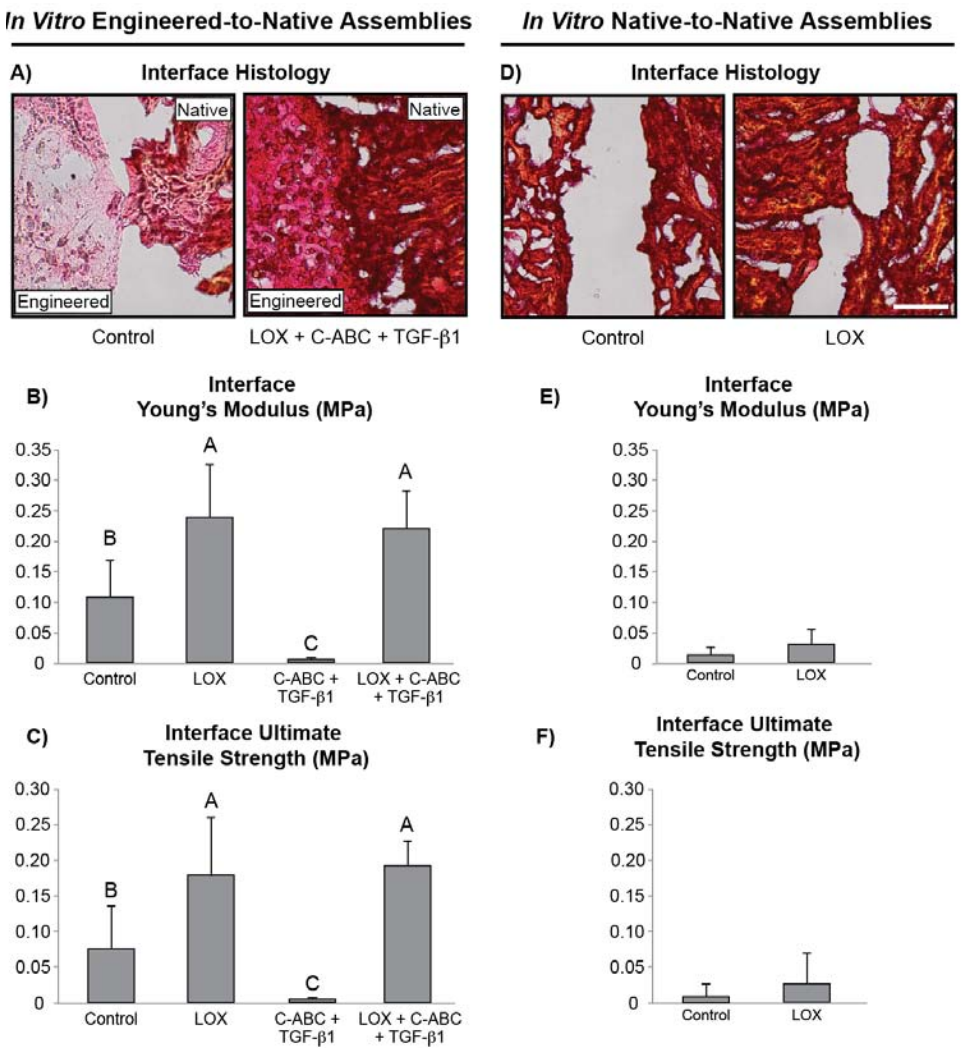

FIGURE 9.4 – PHASE 2 *IN VITRO* INTEGRATION INTERFACE HISTOLOGY AND TENSILE PROPERTIES. Picrosirius Red (for collagen) stained integration interface sections for control and LOX+C-ABC+TGF-β1 pre-treated engineered-to-native assemblies (*A*) (scale bar = 100 μm). Interface Young's modulus (*B*) and ultimate tensile strength (*C*) of control, LOX, C-ABC+TGF-β1, and LOX+C-ABC+TGF-β1 pre-treated engineered-to-native assemblies. Picrosirius Red (for collagen) stained integration interface sections for control and LOX-treated native-to-native assemblies (*D*) (scale bar = 100 μm). Interface Young's modulus (*E*) and ultimate tensile strength (*F*) of control and LOX treated native-to-native assemblies. Bars not connected by the same letter are significantly different ($p < 0.05$), $n = 6$ per group, mean ± SD.

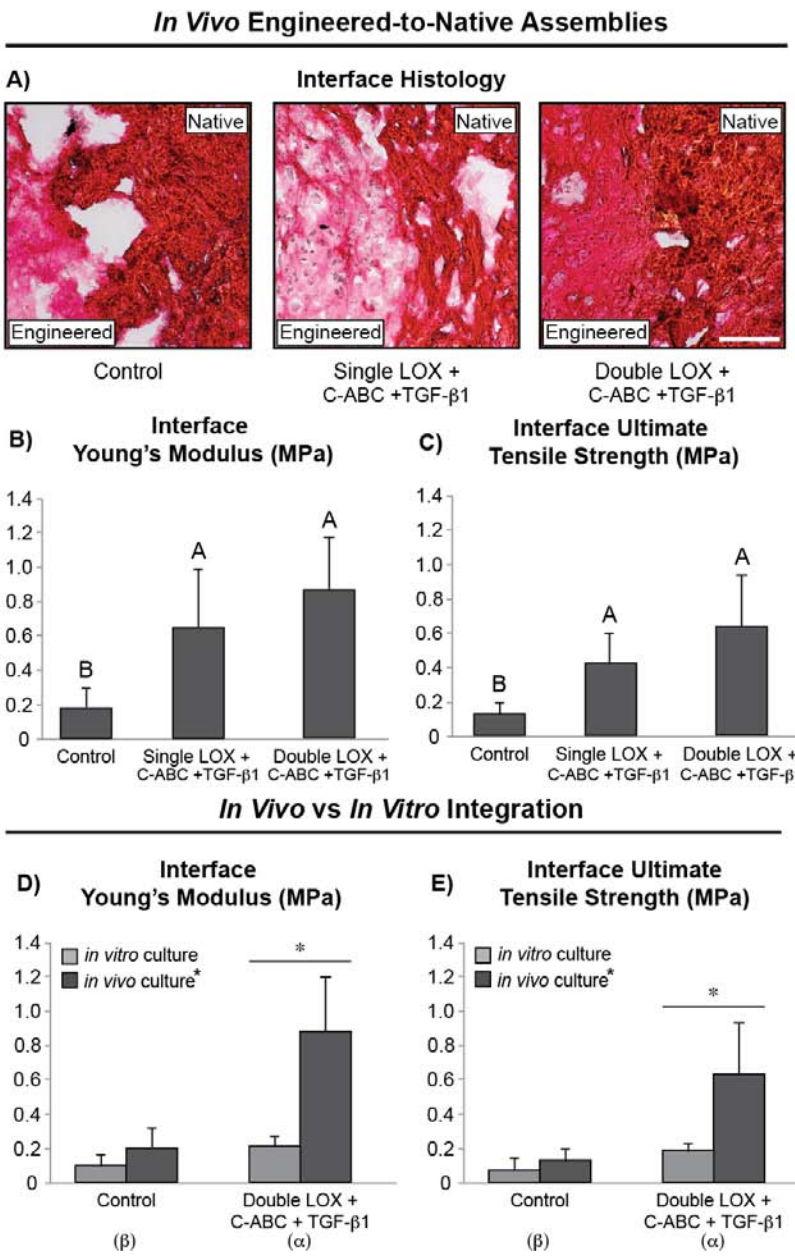

FIGURE 9.5 – PHASE 3 *IN VIVO* INTEGRATION INTERFACE HISTOLOGY AND TENSILE PROPERTIES; COMPARISON WITH PHASE 2 *IN VITRO* RESULTS. Picrosirius Red (for collagen) stained integration interface sections (*A*) (scale bar = 100 μm), interface Young's modulus (*B*), and ultimate tensile strength (*C*) of control, single LOX+C-ABC+TGF-β1, and double LOX+C-ABC+TGF-β1 pre-treated engineered-to-native assemblies. Bars not connected by the same letter are significantly different ($p < 0.05$), $n = 6$ per group, mean ± SD. Comparison between Phase 2 (*in* vitro) and Phase 3 (*in vivo*) results for interface Young's modulus (*D*) and ultimate tensile strength (*E*). Asterix represents significance between *in vitro* and *in vivo* results, and Greek letters represent significance between control and LOX+C-ABC+TGF-β1 treatment following 2-way ANOVA analysis, $n = 6$ per group, mean ± SD.

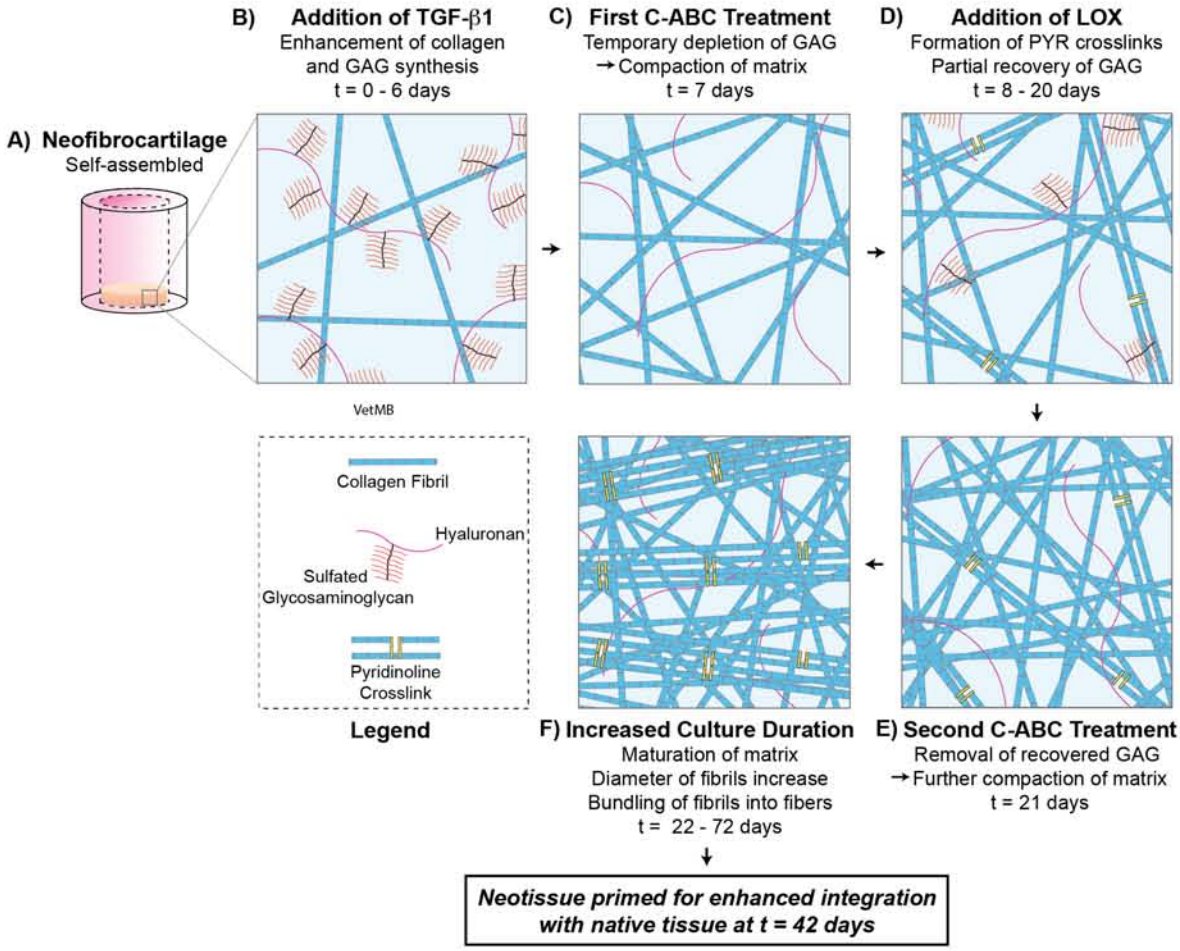

FIGURE 9.6 – NEOFIBROCARTILAGE MATRIX MATURATION, ORGANIZATION, AND CROSSLINKING FOLLOWING LOX+C-ABC+TGF-β1 PRE-TREATMENT. Following self-assembly of neofibrocartilage (*A*), neotissue is grown in the presence of TGF-β1 starting at t = 0 days (*B*), promoting matrix synthesis. The first C-ABC treatment at t = 7 days (*C*) temporarily depletes glycosaminoglycan (GAG) content and compacts the matrix. LOX is added from t = 8 to 20 days (*D*), resulting in pyridinoline (PYR) crosslink formation, while GAG partially recovers. The second C-ABC treatment at t = 21 days (*E)* removes any recovered GAG, furthering compacting the matrix. Increased *in vitro* culture duration of the neotissue to t = 72 days results in matrix maturation and bundling of fibrils into fibers (*F*). Together, these treatments, in addition to a second LOX treatment (Phases 2 and 3), prime the neofibrocartilage matrix for enhanced integration potential with native tissue by t = 42 days.

CHAPTER 10 – TOPOGRAPHICAL VARIATIONS IN BIOMECHANICAL AND BIOCHEMICAL PROPERTIES IN THE ANKLE JOINT: DISPARITIES THAT EXPLAIN THE PATHOGENESIS OF CHONDRAL LESIONS

ABSTRACT

Introduction: The incidence of chondral lesions in the talar dome is remarkably higher compared to other locations of the ankle joint. The purpose of this study was to identify differences in the biomechanical and biochemical properties among the articulating surfaces of the ankle joint, in both native tissue and engineered neotissue, generated using chondrocytes from these locations.

Methods: The biomechanical and biochemical properties of the different topographies within the ankle joint (tibial plafond, talar dome, and distal fibula) were evaluated in native tissue explants. Femoral condyle tissue was used as control. Chondrocytes from the same locations were used to form neocartilage constructs via tissue engineering. The functional properties of the neocartilage constructs were analyzed in comparison to native tissue values.

Results: Articular cartilage harvested from tibial plafond, distal fibula, talar dome, and femoral condyles exhibited Young's modulus values of 4.8, 3.8, 1.7, and 4.0 MPa, respectively. In addition, the compressive properties of the corresponding tissues were measured to be 370, 242, 255, and 274 kPa, respectively. Tibial plafond exhibited 3-fold higher tensile properties and 2-fold higher compressive properties compared to its articulating talar dome; the same disparity was observed in engineered neocartilage. Similar trends were detected in biochemical data for

Chapter submitted as: Makris, E.A., Paschos, N.K., & Athanasiou, K.A. Topographical variations in biomechanical and biochemical properties in the ankle joint: Disparities that explain the pathogenesis of chondral lesions. 2013

both native and engineered tissues.

Conclusions: Cartilage properties of the various topographic locations within the ankle joint are significantly different. In particular, the opposing articulating surfaces of the ankle joint have significantly different biomechanical and biochemical properties. The incompatibility observed between tibial plafond and talar dome cartilage and cells could explain the increased occurrence of chondral lesions in the talus.

Clinical Relevance: Therapeutic modalities need to consider the exact topographic source of the cells or cartilage grafts used. Further, the formation of neocartilage constructs represents a promising tool for the treatment of these lesions.

INTRODUCTION

The ankle joint represents an increasingly common site for various chondral and osteochondral disorders. The incidence of chondral lesions located in the talus is believed to be significantly higher than typically reported, with the majority of such lesions occurring in young and active individuals as a result of ankle injury or fracture [1-4]. These lesions are severely debilitating as a result of both cartilage and bone degeneration and, eventually, lead to the development of osteoarthritis. Interestingly, most of the articular cartilage lesions reported in the ankle joint involve the talus and, more specifically, the talar dome. In contrast, the tibial plafond represents an uncommon site of chondral lesions, with a ratio of 1 to 14-20 lesions of the talus [5,6]. The difference in chondral lesions between these two opposing cartilage surfaces in the ankle is surprising, especially when considering examples from the knee and hip joint, where cartilage lesions occur in a more comparable rate among the different articulating surfaces of the joint [7,8].

The prevalence of cartilage lesions and degenerative changes is dramatically lower in the ankle joint in comparison to the knee [9,10]. Little is known regarding the pathogenic mechanisms responsible for this difference. A few reports describe the anatomical and biomechanical differences among the cartilage comprising different joints, which could be responsible for the disparity in the prevalence of osteoarthritis [11,12] Significant topographical variations in the cartilage material properties have been described that may be related to the increased risk of degeneration [13]. In addition, variations in the biochemical properties of the extracellular matrix (ECM) and the metabolic activity of the chondrocytes between the ankle and the knee joint have been reported [14,15]. This suggests that biomechanical and biological factors may be involved in the pathogenesis of chondral lesions. However, a comparison of the biomechanical and biological characteristics of cartilage in the opposing articulating surfaces of the ankle joint, in relation to the knee, has yet to be performed.

Several treatment modalities have been used for the management of chondral lesions at the ankle joint. Unfortunately, treatment, especially in young patients, is particularly challenging; unsatisfactory outcomes are commonly reported, on account of the inability to repair the articular cartilage damage and restore normal joint function [2,16,17]. Tissue engineering opens a new field in the management of ankle lesions by developing tissues that can replace the damaged cartilage [18,19]. A technique for the development of engineered scaffold-free neocartilage has been described [20]. The self-assembling approach for neocartilage development is considered a representative model of native tissue morphogenesis, maturation, and maintenance [21]. Furthermore, such neotissues recapitulate the morphological structure and organization of native tissues and, thus, present as a model that imitates the fundamental *in vivo* biological processes [20,22]. Self-assembly has been successful in engineering neocartilage tissue

that exhibits biomechanical and functional properties that approach those of native tissue, representing a promising future treatment approach [22]. As such, self-assembled neotissues are considered a suitable model for studying chondrocyte behavior during cartilage development, maturation, and, importantly, during tissue regeneration.

The aim of the present study was twofold: 1) to identify potential differences in the biomechanical properties among the different articulating surfaces of the ankle joint and 2) if topographical differences are identified, to investigate the biological differences between cells from the opposing surfaces using self-assembled neocartilage tissue generated using chondrocytes from different topographical locations of the ankle joint. Explants and tissue engineered constructs from femoral condyles were used as a control. Our hypothesis was that native articular cartilage from different locations in the ankle joint and engineered neotissue formed using cells corresponding to these different locations would exhibit dissimilar biomechanical and biological properties, that would correlate with the respective incidence of chondral lesions reported at these locations.

MATERIALS AND METHODS

Chondrocyte isolation and construct formation

Articular cartilage explants were harvested from different topographical locations of bovine knee and ankle joints using 5mm punches and assayed to investigate the native, location-dependent biomechanical and biochemical properties (Figure 1). For construct formation, chondrocytes were isolated as previously described [23]. Briefly, tissue from the tibial plafond, distal fibula and talar dome (femoral condyle was used as a control) was minced into 1 mm pieces, followed by digestion in 0.2% collagenase type II (Worthington, Lakewood, NJ, USA)

for 18 h as previously described [20,23]. The digestion took place in cell culture medium made of Dulbecco's modified Eagle's medium (DMEM) (Life Technologies corp., Carlsbad, CA, USA) containing low glucose (1 g/L), 10% fetal bovine serum (FBS) (Atlanta Biologicals), 1% non-essential amino acids (NEAA) (Life Technologies corp., Carlsbad, CA, USA), 25 mg of l-ascorbic acid (Sigma–Aldrich, St. Louis, MO, USA), and 1% penicillin/streptomycin/fungizone (PSF) (BioWhittaker Inc., Walkersville, MD, USA). After the tissue had fully digested, the articular chondrocytes were washed three times in DMEM, including centrifugation and filtration through a 70-μm filter. Cells were then counted, and 4.5 million cells from each location were seeded into 2% agarose wells to form neotissue constructs (n=7 per group) [20]. Constructs were fed 500 μl chondrogenic medium, consisting of DMEM, 1% PSF, 1% NEAA, 100 nM dexamethasone (Sigma-Aldrich, St. Louis, MO, USA), 1% ITS+ (BD Scientific, Franklin Lakes, NJ, USA), 40 μg/ml L-proline, 50 μg/ml ascorbate-2-phosphate, and 100 μg/ml sodium pyruvate (Fisher Scientific, Pittsburgh, PA, USA) daily until t = 10 d. At this time point, the constructs were unconfined from the agarose and transferred to 48 well plates, where they were fed 1 ml chondrogenic medium every other day until the end of culture at week 4.

Histology

Histologic evaluation of the tissue was performed as previously described [24]. Samples were cryoembedded and sectioned at 14 μm. Histology samples were fixed in formalin and then stained with Safranin-O/fast green and Picrosirius Red for glycosaminoglycan (GAG) and collagen staining, respectively.

Quantitative biochemistry

Samples were frozen at −20°C for 24 h and then lyophilized to determine their dry weights. Subsequently, a pepsin digestion protocol was used to digest each sample [24]. A Blyscan Glycosaminoglycan DMMB Assay kit (Accurate Chemical and Scientific Corp.) was used to quantify sulfated GAG content. Collagen abundance was determined using a chloramine-T hydroxyproline assay using a SIRCOL collagen standard.

High Performance Liquid Chromatography (HPLC)

Both native and engineered neotissue samples were digested in 800 µl of 6 N HCL at 100°C for 18 h, after which they were dried in a vacuum concentrator. Next, samples were suspended in 50 µl of 10 µM pyridoxine and 2.4 mM homoarginine, and then diluted 5x in 0.5% heptafluorobutyric acid in 10% acetonitrile. For HPLC, 10 µl of each sample was used as previously described (CITE), using PYR standards (Quidel, San Diego, CA, USA) to quantify the cross-link content.

Biomechanical testing

Samples were tested for tensile and compressive properties. For tensile testing, a uniaxial material testing system (Instron Model 5565) was used to apply uniaxial tension to dog-bone shaped samples created using a dermal punch [24]. Samples were glued into paper frames and loaded into the machine grips. The gauge length was measured as the distance between the glued ends of the dog-boned samples. Upon loading, a pull-to-failure test was run at a 1% gauge length per second until failure. The slope of the linear portion of each stress-strain curve was reported as the Young's modulus (E_Y), while the peak of the curve was recorded as the ultimate tensile strength (UTS). For compressive testing, a creep indentation apparatus was used [25].

Samples were tested as previously described [24] using a semi-analytical, semi-numeric, biphasic model [26] and finite element optimization [13] to yield each sample's aggregate modulus, permeability, and Poisson's Ratio. In addition, a correlation between engineered neotissue properties with potential pathogenic mechanisms involved in osteochondral lesion formation was performed.

Statistical analysis

All quantitative assessments in this study were performed using n=7. To compare among different groups one-way analysis of variance (ANOVA) was performed using JMP9 software (SAS institute, Cary, North Carolina, USA). If significance was identified ($p < 0.05$), a Tukey's HSD post hoc test was applied. For positive correlations in regression analysis, a strong correlation was considered present when $1>R^2>0.5$, and a weak when $0.5>R^2>0$. In respect, a strong negative correlation was set at $-1<R^2<-0.5$, and a weak negative correlation at $0>R^2>-0.5$.

RESULTS

Gross Morphology and Histology

No significant differences were observed in the macroscopic appearance between cartilage explants taken from different topographical locations. At the end of a 4-week culture period, chondrocytes from all topographical locations formed disc-shaped constructs, having flat surfaces and no macroscopic deformities. In terms of the growth metrics of neocartilage (Table 1), neotissue from the talar dome had approximately 50% increased thickness compared to all other groups. The increased water content and wet weight reflect this difference. Neocartilage

formed from cells of the tibial plafond, on the other hand, presented with significantly increased diameter. Histological evaluation of the neotissue was consistent among all groups (Figure 2).

Biochemical analysis

Collagen GAG, and pyridinoline content of native cartilage from different topographical locations of the ankle joint were evaluated. In terms of collagen content of native tissue, the tibial plafond cartilage exhibited 3-fold increase in collagen content normalized to tissue wet weight (Col/WW), in comparison to the talus cartilage, that exhibited the lowest amount of collagen; no significant differences were observed between distal femur and fibula cartilage. Regarding the GAG content of the tissues, tibial plafond cartilage presented with the highest amount of GAG per wet weight (CAG/WW), while no significant differences were observed among the other groups (Figure 3). In regards to amount of pyridinoline crosslinks per wet weight (PYR/WW) and per collagen, no significant differences were detected among groups.

Similar trends were observed in the neocartilage constructs formed using cells from the corresponding locations. Specifically, tibial plafond neocartilage presented with the highest amount of collagen per wet weight (Col/WW) among all groups, while the talus constructs presented the lowest Col/WW ratio. No significant differences were detected between the femur and fibula constructs' collagen content. In terms of the GAG content of the neotissue, tibial plafond constructs synthesized the highest GAG/WW, approximately 50% increase, compared to the other groups, where no significant differences were observed among them. Evaluation of the pyridinoline content of neotissues revealed tibial plafond neocartilage to exhibit the highest amount of pyridinoline per WW among all groups. However, no significant differences were observed among groups with regards to pyridinoline content per collagen. Finally a positive

correlation was detected between pyridinoline content and tensile modulus of neotissues (Figure 4).

Biomechanical analysis

Biomechanical evaluation of the native articular cartilage compared the functional properties of the tissue harvested from different topographical locations of the ankle joint and the distal femur. Tensile testing revealed the tibial plafond cartilage to exhibit the highest E_Y and UTS over the other regions, while talus cartilage presented with the lowest properties. Specifically, tensile strength was 3.2 MPa, 2.4 MPa, 1.0 MPa and 2.3 MPa for the tibial plafond, distal fibula, talar dome and femoral condyles respectively. No significant differences were observed between distal femur and distal fibula cartilage tensile properties. In terms of the compressive properties, tibial plafond cartilage presented with a significantly higher aggregate modulus and permeability, comparatively; no significant differences were observed among the other groups (Figure 3).

Similar trends were observed when evaluating the biomechanical properties of neotissue formed using cells from different topographical locations of the ankle joint and distal femur. Tibial plafond neotissue presented with significantly higher compressive moduli compared to all groups; no significant differences were observed among the other groups. In terms of the tensile properties, tibial neocartilage yielded the highest E_Y and UTS, while no significant differences were observed among other groups (Figure 4). Specifically, tibial plafond constructs exhibited 300% more tensile strength and 170% more compressive moduli compared to the talar dome.

DISCUSSION

The present study demonstrates that the biomechanical and biochemical properties of different topographic locations within the ankle joint exhibit significant variations. Specifically, tibial plafond articular cartilage exhibited significantly higher tensile properties in comparison to all other articular surfaces of the ankle joint. More importantly, the opposing articulating surfaces were found to have significantly different biomechanical and biochemical properties, predisposing the talar dome cartilage to degenerative pathologies. Talar dome cartilage showed 3-times lower tensile modulus and strength compared to tibial plafond cartilage. The compressive properties were also higher in native tibial plafond compared to all other topographic areas. The disparity of both tensile and compressive properties of opposing cartilage surfaces, which could potentially lead to degenerative changes of the biomechanically inferior articular surface, explains the increased occurrence of chondral lesions in the talus.

In addition to the mismatches detected in native cartilage, the findings of this study highlight the dissimilar biological behavior of cells isolated from different topographic regions within the ankle joint, as evaluated biomechanically, biochemically and histologically. To assess cellular response, the self-assembling process was used, as it has been shown to recapitulate the fundamental *in vivo* biological processes of articular cartilage generation and development. The biomechanical properties of the neocartilage followed the same pattern with native tissue. For instance, constructs made of chondrocytes from tibial plafond demonstrated 4-times higher tensile properties compared to constructs engineered from talar dome chondrocytes. The compressive properties of the tibial plafond neotissue were 2-times higher than those formed from talar dome cells. A strong positive correlation was detected between the biomechanical properties and biochemical profile of the neocartilage. The amount of collagen

and GAG produced from tibial plafond cells was remarkably higher compared to other locations. The use of the self-assembling process towards neocartilage generation confirmed that the cells of the different topographies within the ankle joint exhibit differences in their synthetic and metabolic activity. Results of the present study imply that the biological response to injury or other pathology of the different topographic areas may likewise vary. Ankle chondrocytes of the talar dome may exhibit a significantly lower potential to respond to injury and lower healing capacity in comparison to chondrocytes of the opposing tibial plafond. Different biological behavior at the cellular level might be an additional pathogenic mechanism that explains the increased incidence of chondral lesions to the talar dome compared to the tibial plafond.

Ankle and knee are remarkably different joints, in terms of their anatomic features, prevalence of chondral lesions, and chondrocyte characteristics, with the ankle joint exhibiting significantly lower susceptibility to osteoarthritis [9]. Factors that could potentially explain the dramatically different prevalence of degenerative changes between the two joints are the different biomechanical properties of articular cartilage between these joints [11,13], differences in collagen and GAG content of the tissues [14], variances in the thickness of the four zones of cartilage, [10] and different metabolic activity [15] of articular chondrocytes. Further, differences between ankle and knee chondrocytes in their response to catabolic stimuli have been previously identified and described [10]. Findings of this study are in accordance with previous reports, confirming the disparity in biomechanical properties and biochemical content between knee and ankle articular cartilage. In addition, the biological response of the knee and ankle chondrocytes was different. The present findings are inadequate to explain the difference in the

prevalence in osteoarthritis between the knee and the ankle joints. However, these results help to shed more light in the potential mechanisms being responsible for this difference.

The use of autologous chondrocytes and cartilaginous grafts is continuously increasing for the treatment of chondral lesions in the ankle joint. For instance, autologous chondrocyte implantation for the treatment of lesions located on the talus is gaining interest [27,28]. Traditionally, the cells were isolated from the ipsilateral knee joint. Some studies suggested the use of talus chondrocytes [29,30], based on the lower incidence of osteoarthritis in the ankle joint. Similarly, talar allografts have been used for large osteochondral defects of the talus [31,32]. Even though, the efficiency of these procedures still needs to be evaluated with large randomized controlled trials, a potential limitation for the use of ankle chondrocytes was the potential loss of these favorable properties when expanded in monolayer culture [33]. Also, there is no consensus in the literature regarding the proteoglycan and collagen synthesis characteristics between ankle and knee chondrocytes [12,14,15,33]. Based on the finding of this study, chondrocytes from the tibial plafond produced higher amounts of collagen and GAG and also had a superior capacity for generating new tissue, compared to those isolated from the femur. In contrast, chondrocytes isolated from the talar dome appeared to have worse biomechanical properties and biological profile compared to femur chondrocytes. The tensile and compressive properties of the native femoral cartilage were inferior only to those of the tibial plafond, with the talus exhibiting significantly lower biomechanical properties. As a consequence, the idea of using ankle chondrocytes or allografts for these repairs could be beneficial only when tibial plafond chondrocytes or grafts are used. Further research is required in order to identify the characteristics of chondrocytes and cartilage tissue in different topographic locations,

suggesting that current therapeutic modalities need to consider the exact topographic source of the cells or cartilage grafts used.

An interesting finding of this study is the comparatively large differences in tensile properties between the talar dome and tibial plafond, in contrast to the much smaller in terms of their compressive properties. Specifically, tibial plafond cartilage demonstrates a 3-fold difference in tensile moduli and strength in comparison to the talar dome in native and engineered tissue. In contrast, talar dome exhibits only 50-60% less compressive modulus in native and engineered tissue. Currently, degeneration of cartilage is correlated with repetitive compressive forces. However, various reports indicate that cartilage is more prone to injuries during shear loading of the joint [34]. Excessive shear strain causes abundant collagen fibril strain that has been shown to correspond accurately with areas of collagen destruction leading to cartilage damage [35]. The present study demonstrated an important disparity between tibial plafond and talus to withstand tensile forces, indicating the presence of a complex pathogenic mechanism responsible for cartilage degeneration. Future research should focus on evaluating the role of tensile loading in the development of chondral lesions and degenerative osteoarthritis.

To the best of our knowledge, this is the first study to use chondrocytes from the tibial plafond and other ankle locations to engineer articular cartilage without the use of scaffolds. Tissue engineering represents a promising technique for developing neocartilage that could be used in the treatment of chondral and osteochondral lesions. Different mechanical and biochemical stimuli can be combined to enhance the functional properties of the engineered tissue on par with native tissue values [23,36-38]. In the present study, native tibial plafond exhibited significantly better properties in comparison to all other locations of the ankle joint.

The measured differences of tibial plafond articular cartilage were also mirrored in the biomechanical and biochemical properties of neocartilage constructs generated using tibial plafond cells. These results may suggest that cells from a specific topographic source need to be tailored for use in particular indications.

LIMITATIONS

One limitation of the present study is the fact that the biomechanical and biochemical properties were evaluated in an *in vitro* model. It remains to be seen whether these *in vitro* results would be reflected into *in vivo* findings. Similarly, in order to evaluate cellular behavior, no *in vivo* studies were employed as the *in vitro* model of self-assembling process was used. However, this model has been shown as representative of the processes of tissue development and maturation.

CONCLUSIONS

Cartilage properties of the various topographic locations within the ankle joint are significantly different. In particular, the opposing articulating surfaces of the ankle joint have significantly different biomechanical and biochemical properties. The incompatibility observed between tibial plafond and talar dome cartilage and cells could explain the increased occurrence of chondral lesions in the talus.

TABLES AND FIGURES

TABLE 10.1 – GROWTH METRICS OF THE NEOCARTILAGE AT 4 WEEKS OF CULTURE.

Jaw Region	Col/WW (%)	GAG/WW (%)	Tissue Hydration (%)
Upper Rostral	5.9 ± 0.7^{A}	11.5 ± 3.4^{A}	83.7 ± 2.4^{C}
Upper Middle	4.0 ± 0.9^{AB}	10.1 ± 0.8^{A}	85.1 ± 1.9^{BC}
Upper Caudal	4.4 ± 1.3^{AB}	8.7 ± 1.5^{AB}	86.7 ± 1.6^{B}
Lower Rostral	4.1 ± 1.6^{AB}	7.1 ± 2.1^{B}	87.4 ± 0.6^{AB}
Lower Middle	2.7 ± 1.9^{B}	5.9 ± 2.8^{B}	88.9 ± 2.0^{A}
Lower Caudal	2.9 ± 1.1^{B}	12.4 ± 2.6^{A}	87.7 ± 0.1^{AB}

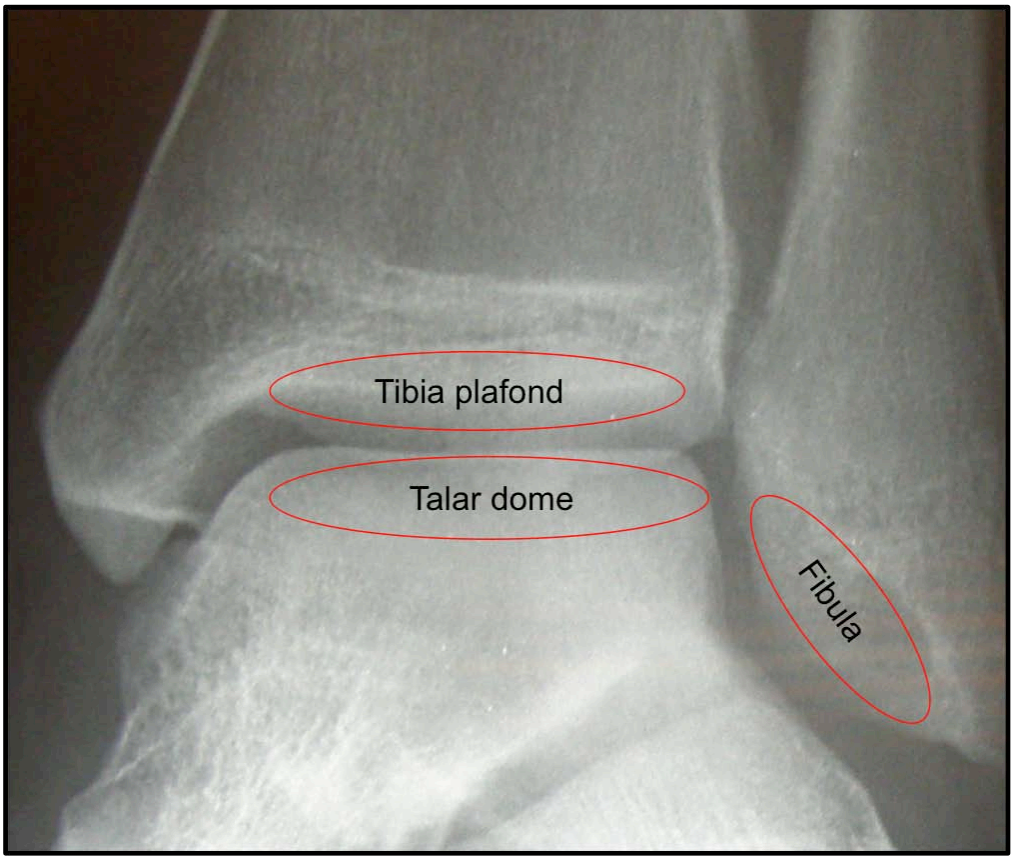

FIGURE 10.1 – TOPOGRAPHIC LOCATIONS OF THE ANKLE JOINT USED FOR ARTICULAR CARTILAGE EXPLANT AND CHONDROCYTE HARVESTING.

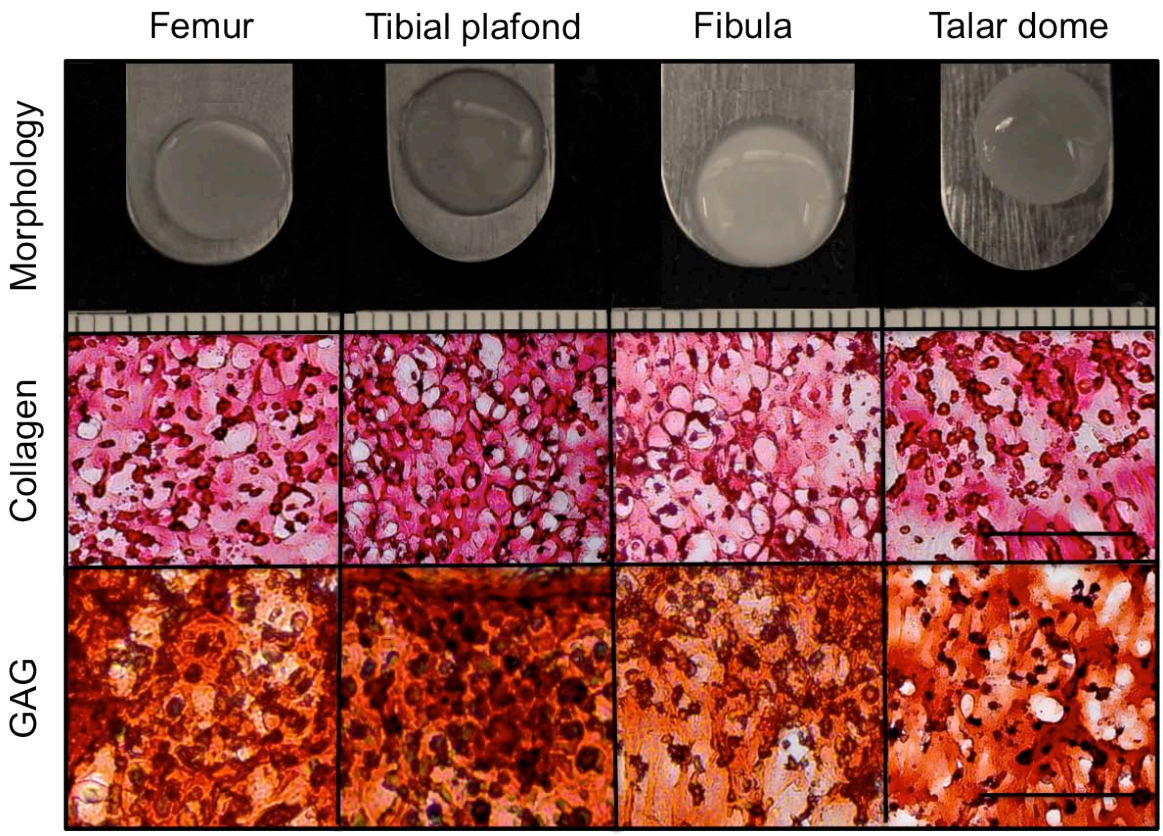

FIGURE 10.2 – GROSS MORPHOLOGY/HISTOLOGY OF NEOCARTILAGE ENGINEERED CONSTRUCTS. Picrosirius red staining for collagen and Safranin-O/fast green staining for GAGs. Histology scale bar represents 100μm.

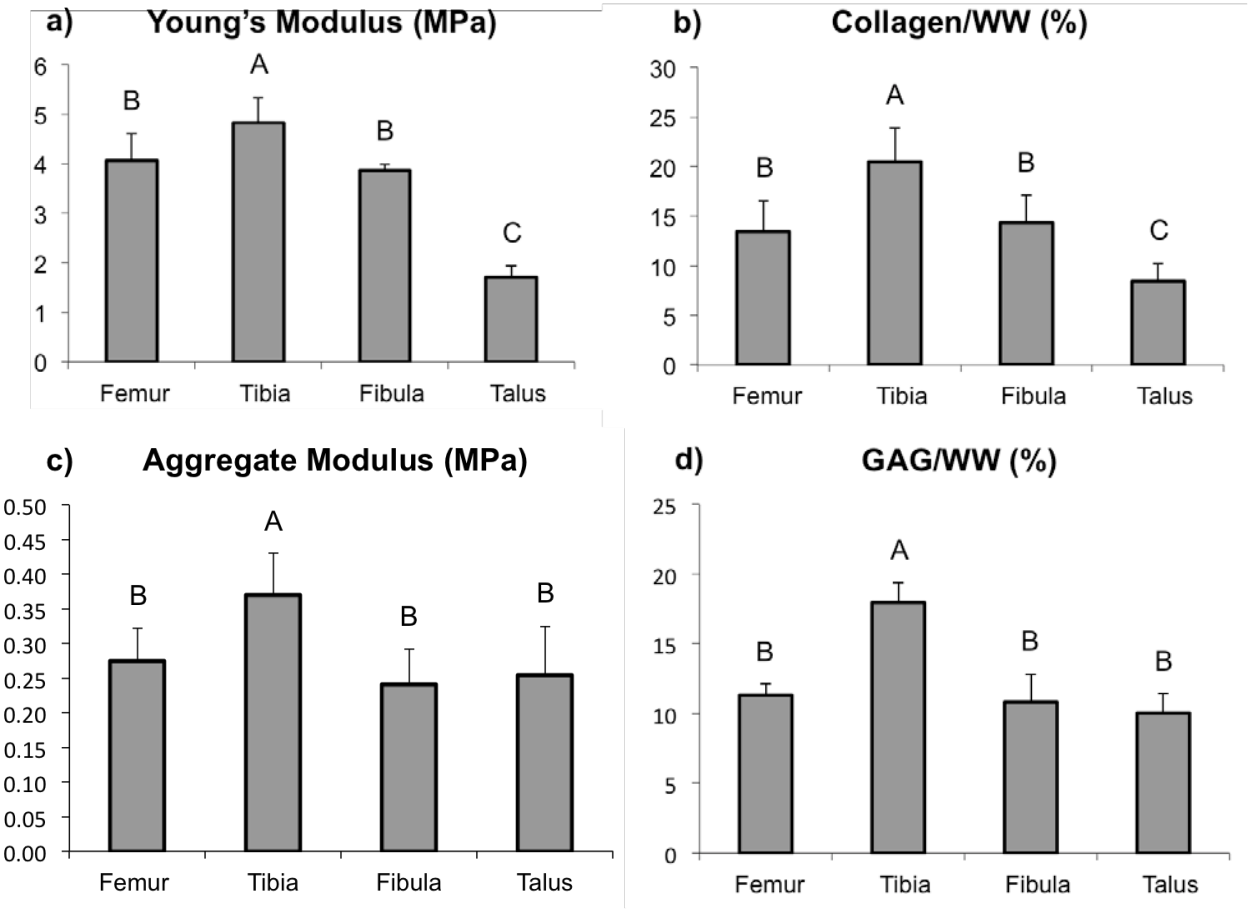

FIGURE 10.3 – BIOMECHANICAL AND BIOCHEMICAL PROPERTIES OF NATIVE CARTILAGE FROM DIFFERENT TOPOGRAPHICAL LOCATIONS OF THE ANKLE JOINT. Femoral condyle explants were used as control.

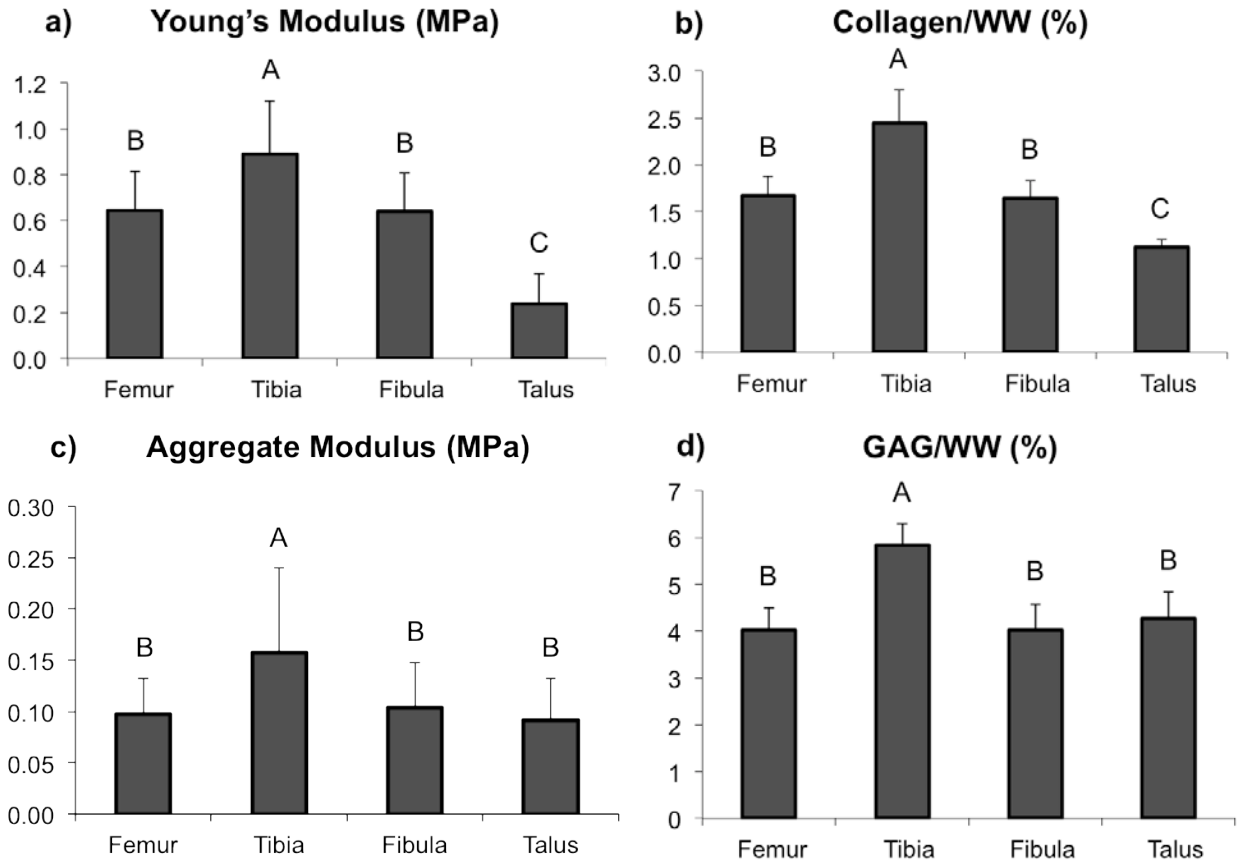

FIGURE 10.4 – BIOMECHANICAL AND BIOCHEMICAL PROPERTIES OF NEOCARTILAGE ENGINEERED USING CHONDROCYTES FROM THE DIFFERENT TOPOGRAPHIC LOCATIONS OF THE ANKLE JOINT. Femoral condyle chondrocytes were used as control.

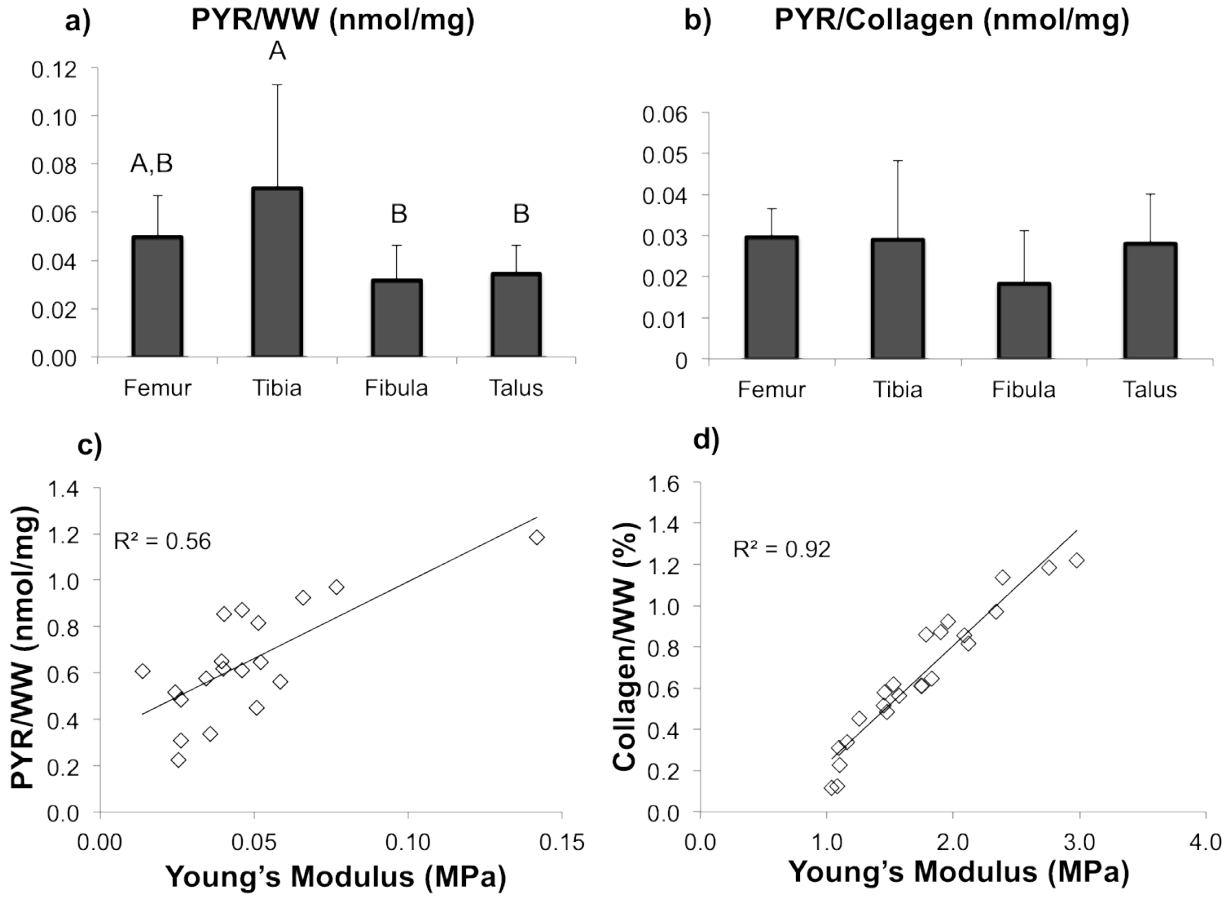

FIGURE 10.5 – PYRIDINOLINE CONTENT PER WET WEIGHT AND PER COLLAGEN IN THE DIFFERENT TOPOGRAPHIC LOCATIONS WITHIN THE ANKLE JOINT. A positive correlation was detected between pyridinoline content and tensile modulus of neocartilage as well as between collagen content and tensile modulus.

CONCLUSIONS

The cartilages of the knee joint are critical to proper function; thus, patients suffering from cartilage degradation are subject to severe pain and restricted mobility, leading to a decreased quality of life. As outlined in the Introduction and Chapter 1, current treatment modalities are insufficient for repairing damaged articular cartilage and the knee meniscus, necessitate novel and effective technologies to help patients suffering from degenerated cartilage. This thesis presented a series of studies describing several new and exciting technologies that have the potential to generate clinically relevant, tissue engineered replacement tissues that are applicable to any collagen-rich tissue of the body. In particular, these studies focused on promoting the *in vitro* development of neotissues that take on the structure-function relationships of their native tissue counterparts such that they may be able to both adapt to and integrate with the native joint environment upon implantation.

The first study (Chapter 2) investigated the potential of promoting the pyridinoline (PYR) collagen crosslink content in engineered tissues via exogenous application of the crosslink precursors hydroxylysine and copper. Furthermore, this study addressed whether enhanced PYR collagen crosslinking in engineered musculoskeletal soft tissues would, in turn, enhance their mechanical properties. Results of this study found simultaneous application of exogenous hydroxylysine and copper sulfate to synergistically increase the amount of PYR collagen crosslink content in the self-assembled constructs. Further, this increased PYR crosslink content resulted in significantly increased compressive and tensile properties. Thus, data from Chapter 6 found exogenous application of collagen crosslink precursors to enhance

PYR crosslink formation in engineered constructs, thereby improving their biomechanical properties.

In Chapter 3, hypoxia was used as an alternative means to induce PYR crosslink content and, therefore, the biomechanical properties of engineered cartilage. This method was found to upregulate the LOX gene expression 20-fold in chondrocytes compared to those cultured under normoxia. Further, hypoxia applied at both the 3rd and 4th weeks of neotissue culture significantly increased the PYR content without compromising collagen content. Furthermore, this regimen correlated with a 2-fold increase in the neocartilage tensile properties. Together, results from this study suggest that hypoxia applied within specific time windows can be beneficial for enhancing the functional properties of neocartilage toward directly promote neotissue maturation.

Chapter 4 of this thesis took the results of Chapters 2 and 3 a step further by investigating the effects of enhanced PYR crosslink content via hypoxia application on a spectrum of collagen-rich native tissues. Results found hypoxia capable of enhancing the PYR content of this spectrum of tissues by 1.4 – 6.4-fold that of tissues cultured under normoxic conditions, corresponding to a significant increase in the tensile properties of these cultured in hypoxic vs. normoxic conditions. Further, this study for the first time established a novel treatment as a means to further enhance the PYR content and functional properties of engineered cartilage via direct application of exogenous lysyl oxidase (LOX). Specifically, LOX was found to increase the PYR content 16-fold that of controls, resulting in neotissue with tensile properties 5x greater than control tissue. Thus, this chapter entails the first study to report endogenous (hypoxia-mediated) and exogenous (direct LOX-mediated) methods to

promote collagen crosslink content and concomitantly improve the tensile properties of a spectrum of native and engineered tissues.

The next chapter of this thesis (Chapter 5) focused on enhancing neomatrix production in engineered articular cartilage via modulation of intracellular Ca^{2+} signaling. To do so, digoxin and adenosine triphosphate (ATP), two agents known to modulate intracellular Ca^{2+} signaling, were investigated. Results found the frequency of Ca^{2+} oscillations to increase in chondrocytes treated with digoxin and ATP. These increase Ca^{2+} oscillations translated into increased collagen content and tensile properties, with the greatest increases observed in neotissue treated with both agents simultaneously. Results of this study highlight the potential of modulating intracellular Ca^{2+} signaling as a means to enhance the functionality of engineered tissues.

Chapter 6 of this thesis focused on a novel treatment regimen consisting of chondroitinase-ABC (C-ABC) and transforming growth factor-β1 (TGF-β1) treatment toward enhancing matrix synthesis and the mechanical properties of engineered fibrocartilage. Results found application of both C-ABC and TGF-β1 to enhance neofibrocartilage collagen content, collagen fibril density, and collagen fibril diameter compared to controls. Further, mechanical testing revealed this combined bioactive treatment regimen to synergistically increase the Young's modulus and ultimate tensile strength of the neotissue, with values reaching the lower spectrum of those measured in native tissues. Thus, Chapter 6 informed upon the use of a bioactive agent regimen comprising a dual C-ABC treatment at 1 and 3 weeks and continuous TGF-β1 application to develop a more functional collagen matrix capable of withstanding greater tensile loading.

Chapter 7 tailored the use of passive axial compressive loading to drive matrix synthesis

and reorganization within shape-specific neotissues. Subjecting biconcave constructs to 1, 5, or 10g masses early during tissue culture found the 10g mass to significantly increase both collagen and GAG synthesis in the neotissue middle zone. Matrix alignment, compaction, and enhanced PYR collagen crosslinking were also observed in the neotissue's middle zone at the 10g loading level. Regional mechanical testing further revealed the matrix synthesis and reorganization prompted by the 10g mass to result in significantly enhanced compressive and tensile properties in the neotissue's middle zone. These results are likely attributable to the multi-axial tensile and compressive strain gradients achieved in the shape-specific neotissues subjected to the 10g mass, which induced physiologically relevant strain levels previously shown to elicit a mechanotransductive response by chondrocytes. Thus, Chapter 6 indicated the potential of passive axial loading as a simple, yet effective, tool to drive *in vitro* matrix development in shape-specific neotissues toward more closely achieving the structural and functional properties of the native fibrocartilage.

Chapter 8 investigated the potential of LOX to promote integration between native and engineered tissues via enhanced collagen crosslink content. Results found the tensile properties of the integration interface to be 2 – 2.2-fold greater in assemblies treated with LOX compared to those left untreated. Histologically, the assemblies treated with LOX were found to have noticeably more uniform integration compared to controls. Thus, this study for the first time demonstrated the potential for LOX to be used to induce *in vitro* integration between native and engineered articular cartilage via the upregulation of PYR crosslinks at the native-to-engineered interface.

The promising results of Chapter 8 prompted investigation of a means to enhance the *in vitro* maturation and integration potential of neofibrocartilage via a novel combination of

stimuli, including exogenous application of C-ABC, TGF-β1, and LOX in Chapter 9. Combined use of these agents was found to drive *in vitro* neofibrocartilage matrix maturation toward significantly increased collagen and PYR content as well as enhanced collagen fibril density and diameter. These matrix modifications resulted in synergistically enhanced tensile properties approaching native fibrocartilage values. Further, allowing the combination-treated neotissue to grow for 12 weeks *in vitro*, as opposed to 6 weeks, found the longer culture duration to be a significant factor toward enhancing neofibrocartilage tensile properties, with values 2-fold higher than those achieved in any other study of this thesis. While the *in vitro* fibrocartilage defect model showed this treatment regimen to promote integration between neofibrocartilage and native tissue, results of the *in vivo* fibrocartilage defect model found this pre-treatment to significantly increase the integration interface tensile stiffness and strength over values achieved *in vitro*. Further, the values achieved at the integration interface *in vivo* were found to be similar to the tensile properties of intact native fibrocartilage. Thus, results of Chapter 9 demonstrated the tremendous potential of a LOX+C-ABC+TGF-β1 pre-treatment to develop biomechanically robust neofibrocartilage implants with physiologically significant integration potential.

The final chapter of this thesis focused on establishing superior primary cell sources for engineered articular cartilage. For this study, chondrocytes from different locations in the ankle joint were compared against primary articular chondrocytes of the knee joint. Results found articular cartilage harvest from the tibial plafond, distal fibula, talar dome, and femoral condyles to have varying biomechanical properties, with the tibial plafond cartilage exhibiting 3-fold greater tensile properties and 2-fold greater compressive properties compared to the talar dome; similar trends were observed in neocartilage self-assembled from cells of the respective sources. Results of this study suggest that the cartilages of the ankle joint have location-specific

properties, and suggests that cells from the tibial plafond present as a more promising cell source than from any other location of the ankle joint in terms of generating mechanically robust replacement tissues.

Overall, the work presented in this series of studies demonstrate a plethora of novel treatment modalities that have the potential to aid in the development of functional neotissues. By addressing two of the most critical short comings of current repair tissues (including their insufficient mechanical properties and inability to effectively integrate with native tissue upon implantation), this thesis speaks to the potential of engineering clinically robust, collagen-rich neotissues to repair and/or replace those damaged by injury or disease. Moving forward, studies should take place that synthesize the various findings of this thesis to aid in further promoting both the maturation and integration potential of engineered articular cartilage and fibrocartilage. Further, studies should take place in site-specific animal defect models to better test the ability of these treatments to provide clinically-relevant solutions. In line with these efforts, studies must be conducted to determine more stringent measures of the biomechanical and biochemical properties of engineered tissues, as well as methods to non-invasively measure the functional properties of tissues following implantation. Furthermore, improved indications for cartilage and fibrocartilage replacement and advanced minimally-invasive surgical techniques will help bring such technologies forward. Together, such efforts will provide a great leap forward toward the next generation of engineered cartilage and fibrocartilage therapies, finally providing patients with robust treatment modalities.

REFERENCES

1. Wilkes, C.H. Internal derangements of the temporomandibular joint. Pathological variations. *Arch Otolaryngol Head Neck Surg* **115**, 469-477 (1989).

2. Detamore, M.S., Athanasiou, K.A. & Mao, J. A call to action for bioengineers and dental professionals: Directives for the future of TMJ bioengineering. *Annals of Biomedical Engineering* **35**, 1301-1311 (2007).

3. Hoben, G.M., Hu, J.C., James, R.A. & Athanasiou, K.A. Self-assembly of fibrochondrocytes and chondrocytes for tissue engineering of the knee meniscus. *Tissue engineering* **13**, 939-946 (2007).

4. Kalpakci, K.N., Kim, E.J. & Athanasiou, K.A. Assessment of growth factor treatment on fibrochondrocyte and chondrocyte co-cultures for TMJ fibrocartilage engineering. *Acta biomaterialia* **7**, 1710-1718 (2011).

5. Aufderheide, A.C. & Athanasiou, K.A. Assessment of a bovine co-culture, scaffold-free method for growing meniscus-shaped constructs. *Tissue Eng* **13**, 2195-2205 (2007).

6. Athens, A.A., Makris, E.A. & Hu, J.C. Induced collagen cross-links enhance cartilage integration. *PloS one* **8**, e60719 (2013).

7. Makris, E.A., Hu, J.C. & Athanasiou, K.A. Hypoxia-induced collagen crosslinking as a mechanism for enhancing mechanical properties of engineered articular cartilage. *Osteoarthritis and cartilage / OARS, Osteoarthritis Research Society* **21**, 634-641 (2013).

8. Natoli, R.M., Revell, C.M. & Athanasiou, K.A. Chondroitinase ABC treatment results in greater tensile properties of self-assembled tissue-engineered articular cartilage. *Tissue engineering. Part A* **15**, 3119-3128 (2009).

9. Elder, B.D. & Athanasiou, K.A. Effects of temporal hydrostatic pressure on tissue-engineered bovine articular cartilage constructs. *Tissue engineering. Part A* **15**, 1151-1158 (2009).

10. Tanaka, E. & van Eijden, T. Biomechanical behavior of the temporomandibular joint disc. *Crit Rev Oral Biol Med* **14**, 138-150 (2003).

11. Mechanic, G., Gallop, P.M. & Tanzer, M.L. The nature of crosslinking in collagens from mineralized tissues. *Biochemical and biophysical research communications* **45**, 644-653 (1971).

12. Wang, S.X. et al. A crosslinked cofactor in lysyl oxidase: redox function for amino acid side chains. *Science* **273**, 1078-1084 (1996).

13. Ahsan, T., Harwood, F., McGowan, K.B., Amiel, D. & Sah, R.L. Kinetics of collagen crosslinking in adult bovine articular cartilage. *Osteoarthritis and cartilage / OARS, Osteoarthritis Research Society* **13**, 709-715 (2005).

14. Wroe, S., Huber, D.R., Lowry, M., McHenry, C., Moreno, K., Clausen, P., Ferrara, T.L., Cunningham, E., Dean, M.N., & Summers, A.P. Three-dimensional computer analysis of white shark jaw mechanics: how hard can a great white bite? *Journal of Zoology* **276**, 336-342 (2008).

15. Athanasiou, K.A. (Morgan & Claypool Publishers, [San Rafael, Calif.]; 2009).

16. Gray, R.J., Davies, S.J. & Quayle, A.A. A clinical approach to temporomandibular disorders. 5. A clinical approach to treatment. *Br Dent J* **177**, 101-106 (1994).

17. Solberg, W.K., Woo, M.W. & Houston, J.B. Prevalence of mandibular dysfunction in young adults. *J Am Dent Assoc* **98**, 25-34 (1979).

18. Conti, P.C., dos Santos, C.N., Kogawa, E.M., de Castro Ferreira Conti, A.C. & de Araujo Cdos, R. The treatment of painful temporomandibular joint clicking with oral splints: a randomized clinical trial. *J Am Dent Assoc* **137**, 1108-1114 (2006).

19. Dao, T.T. & Lavigne, G.J. Oral splints: the crutches for temporomandibular disorders and bruxism? *Crit Rev Oral Biol Med* **9**, 345-361 (1998).

20. Nicolakis, P. et al. Effectiveness of exercise therapy in patients with myofascial pain dysfunction syndrome. *J Oral Rehabil* **29**, 362-368 (2002).

21. Al-Belasy, F.A. & Dolwick, M.F. Arthrocentesis for the treatment of temporomandibular joint closed lock: a review article. *Int J Oral Maxillofac Surg* **36**, 773-782 (2007).

22. Ingawale, S. & Goswami, T. Temporomandibular joint: disorders, treatments, and biomechanics. *Ann Biomed Eng* **37**, 976-996 (2009).

23. Miloro, M. & Henriksen, B. Discectomy as the primary surgical option for internal derangement of the temporomandibular joint. *J Oral Maxillofac Surg* **68**, 782-789 (2010).

24. Guarda-Nardini, L., Manfredini, D. & Ferronato, G. Temporomandibular joint total replacement prosthesis: current knowledge and considerations for the future. *Int J Oral Maxillofac Surg* **37**, 103-110 (2008).

25. Bell, W.E. Clinical management of temporomandibular disorders. (Year Book Medical Publishers, Chicago, Ill.; 1982).

26. Blaustein, D.I. & Heffez, L.B. Arthroscopic atlas of the temporomandibular joint. (Lea & Febiger, Philadelphia; 1990).

27. Kuroda, S. et al. Biomechanical and biochemical characteristics of the mandibular condylar cartilage. *Osteoarthritis Cartilage* **17**, 1408-1415 (2009).

28. Singh, M. & Detamore, M.S. Biomechanical properties of the mandibular condylar cartilage and their relevance to the TMJ disc. *Journal of Biomechanics* **42**, 405-417 (2009).

29. Luder, H.U., Leblond, C.P. & von der Mark, K. Cellular stages in cartilage formation as revealed by morphometry, radioautography and type II collagen immunostaining of the mandibular condyle from weanling rats. *Am J Anat* **182**, 197-214 (1988).

30. Allen, K.D. & Athanasiou, K.A. A surface-regional and freeze-thaw characterization of the porcine temporomandibular joint disc. *Ann Biomed Eng* **33**, 951-962 (2005).

31. Allen, K.D. & Athanasiou, K.A. Viscoelastic characterization of the porcine temporomandibular joint disc under unconfined compression. *J Biomech* **39**, 312-322 (2006).

32. Okeson, J.P. Fundamentals of occlusion and temporomandibular disorders. (Mosby, St. Louis; 1985).

33. Friedman, M.H. & Weisberg, J. Temporomandibular joint disorders : diagnosis and treatment. (Quintessence Pub. Co., Chicago; 1985).

34. Bakke, M., Michler, L., Han, K. & Moller, E. Clinical significance of isometric bite force versus electrical activity in temporal and masseter muscles. *Scand J Dent Res* **97**, 539-551 (1989).

35. Detamore, M.S. et al. Cell type and distribution in the porcine temporomandibular joint disc. *J Oral Maxillofac Surg* **64**, 243-248 (2006).

36. Detamore, M.S. et al. Quantitative analysis and comparative regional investigation of the extracellular matrix of the porcine temporomandibular joint disc. *Matrix biology : journal of the International Society for Matrix Biology* **24**, 45-57 (2005).

37. Nakano, T. & Scott, P.G. Changes in the chemical composition of the bovine temporomandibular joint disc with age. *Arch Oral Biol* **41**, 845-853 (1996).

38. Gage, J.P., Shaw, R.M. & Moloney, F.B. Collagen type in dysfunctional temporomandibular joint disks. *J Prosthet Dent* **74**, 517-520 (1995).

39. Nakano, T. & Scott, P.G. A quantitative chemical study of glycosaminoglycans in the articular disc of the bovine temporomandibular joint. *Arch Oral Biol* **34**, 749-757 (1989).

40. Carvalho, R.S., Yen, E.H. & Suga, D.M. The effect of growth on collagen and glycosaminoglycans in the articular disc of the rat temporomandibular joint. *Arch Oral Biol* **38**, 457-466 (1993).

41. Landesberg, R., Takeuchi, E. & Puzas, J.E. Cellular, biochemical and molecular characterization of the bovine temporomandibular joint disc. *Arch Oral Biol* **41**, 761-767 (1996).

42. Milam, S.B., Klebe, R.J., Triplett, R.G. & Herbert, D. Characterization of the extracellular matrix of the primate temporomandibular joint. *J Oral Maxillofac Surg* **49**, 381-391 (1991).

43. Minarelli, A.M. & Liberti, E.A. A microscopic survey of the human temporomandibular joint disc. *J Oral Rehabil* **24**, 835-840 (1997).

44. Berkovitz, B.K. & Pacy, J. Ultrastructure of the human intra-articular disc of the temporomandibular joint. *Eur J Orthod* **24**, 151-158 (2002).

45. Berkovitz, B.K. & Robertshaw, H. Ultrastructural quantification of collagen in the articular disc of the temporomandibular joint of the rabbit. *Arch Oral Biol* **38**, 91-95 (1993).

46. Berkovitz, B.K. Collagen crimping in the intra-articular disc and articular surfaces of the human temporomandibular joint. *Arch Oral Biol* **45**, 749-756 (2000).

47. Almarza, A.J., Bean, A.C., Baggett, L.S. & Athanasiou, K.A. Biochemical analysis of the porcine temporomandibular joint disc. *Br J Oral Maxillofac Surg* **44**, 124-128 (2006).

48. Merrilees, M.J. & Flint, M.H. Ultrastructural study of tension and pressure zones in a rabbit flexor tendon. *Am J Anat* **157**, 87-106 (1980).

49. Keith, D.A. Elastin in the bovine mandibular joint. *Arch Oral Biol* **24**, 211-215 (1979).

50. Gross, A., Bumann, A. & Hoffmeister, B. Elastic fibers in the human temporo-mandibular joint disc. *Int J Oral Maxillofac Surg* **28**, 464-468 (1999).

51. Mah, J. Histochemistry of the foetal human temporomandibular joint articular disc. *Eur J Orthod* **26**, 359-365 (2004).

52. Allen, K.D. & Athanasiou, K.A. Viscoelastic characterization of the porcine temporomandibular joint disc under unconfined compression. *Journal of Biomechanics* **39**, 312-322 (2006).

53. Scott, J.E., Orford, C.R. & Hughes, E.W. Proteoglycan-collagen arrangements in developing rat tail tendon. An electron microscopical and biochemical investigation. *The Biochemical journal* **195**, 573-581 (1981).

54. Kalpakci, K.N., Willard, V.P., Wong, M.E. & Athanasiou, K.A. An Interspecies Comparison of the Temporomandibular Joint Disc. *Journal of Dental Research* **90**, 193-198 (2011).

55. Kopp, S., Carlsson, G.E., Hansson, T. & Oberg, T. Degenerative disease in the temporomandibular, metatarsophalangeal and sternoclavicular joints. An autopsy study. *Acta Odontol Scand* **34**, 23-32 (1976).

56. de Bont, L.G., Boering, G., Havinga, P. & Liem, R.S. Spatial arrangement of collagen fibrils in the articular cartilage of the mandibular condyle: a light microscopic and scanning electron microscopic study. *J Oral Maxillofac Surg* **42**, 306-313 (1984).

57. Shibata, S. et al. Ultrastructural observation on matrix fibers in the condylar cartilage of the adult rat mandible. *Bull Tokyo Med Dent Univ* **38**, 53-61 (1991).

58. Teramoto, M., Kaneko, S., Shibata, S., Yanagishita, M. & Soma, K. Effect of compressive forces on extracellular matrix in rat mandibular condylar cartilage. *J Bone Miner Metab* **21**, 276-286 (2003).

59. Mizoguchi, I. et al. An immunohistochemical study of regional differences in the distribution of type I and type II collagens in rat mandibular condylar cartilage. *Arch Oral Biol* **41**, 863-869 (1996).

60. Delatte, M., Von den Hoff, J.W., van Rheden, R.E. & Kuijpers-Jagtman, A.M. Primary and secondary cartilages of the neonatal rat: the femoral head and the mandibular condyle. *Eur J Oral Sci* **112**, 156-162 (2004).

61. Luder, H.U. & Schroeder, H.E. Light and electron microscopic morphology of the temporomandibular joint in growing and mature crab-eating monkeys (Macaca fascicularis): the condylar calcified cartilage. *Anat Embryol (Berl)* **185**, 189-199 (1992).

62. Singh, M. & Detamore, M.S. Tensile properties of the mandibular condylar cartilage. *J Biomech Eng* **130**, 011009 (2008).

63. Appleton, J. The ultrastructure of the articular tissue of the mandibular condyle in the rat. *Arch Oral Biol* **20**, 823-826 (1975).

64. Roth, S., Muller, K., Fischer, D.C. & Dannhauer, K.H. Specific properties of the extracellular chondroitin sulphate proteoglycans in the mandibular condylar growth centre in pigs. *Arch Oral Biol* **42**, 63-76 (1997).

65. Mao, J.J., Rahemtulla, F. & Scott, P.G. Proteoglycan expression in the rat temporomandibular joint in response to unilateral bite raise. *J Dent Res* **77**, 1520-1528 (1998).

66. Kim, K.W., Wong, M.E., Helfrick, J.F., Thomas, J.B. & Athanasiou, K.A. Biomechanical tissue characterization of the superior joint space of the porcine temporomandibular joint. *Ann Biomed Eng* **31**, 924-930 (2003).

67. Beek, M., Koolstra, J.H., van Ruijven, L.J. & van Eijden, T.M. Three-dimensional finite element analysis of the cartilaginous structures in the human temporomandibular joint. *J Dent Res* **80**, 1913-1918 (2001).

68. Hylander, W.L. Experimental analysis of temporomandibular joint reaction force in macaques. *Am J Phys Anthropol* **51**, 433-456 (1979).

69. Herring, S.W. & Liu, Z.J. Loading of the temporomandibular joint: anatomical and in vivo evidence from the bones. *Cells Tissues Organs* **169**, 193-200 (2001).

70. Cristofolini, L., McNamara, B.P., Freddi, A. & Viceconti, M. In vitro measured strains in the loaded femur: quantification of experimental error *J. Strain Anal. Eng. Des.* **32**, 193-200 (1997).

71. Hohl, T.H. & Tucek, W.H. Measurement of condylar loading forces by instrumented prosthesis in the baboon. *J Maxillofac Surg* **10**, 1-7 (1982).

72. Yatabe, M., Zwijnenburg, A., Megens, C.C. & Naeije, M. Movements of the mandibular condyle kinematic center during jaw opening and closing. *J Dent Res* **76**, 714-719 (1997).

73. Nitzan, Y., Wexler, H.M. & Finegold, S.M. Inactivation of anaerobic bacteria by various photosensitized porphyrins or by hemin. *Curr Microbiol* **29**, 125-131 (1994).

74. Dolwick, M.F., Katzberg, R.W. & Helms, C.A. Internal derangements of the temporomandibular joint: fact or fiction? *J Prosthet Dent* **49**, 415-418 (1983).

75. Dogan, F. & Celebi, M.S. Real-time deformation simulation of non-linear viscoelastic soft tissues. *Simulation-Transactions of the Society for Modeling and Simulation International* **87**, 179-187 (2011).

76. Hu, K., Radhakrishnan, P., Patel, R.V. & Mao, J.J. Regional structural and viscoelastic properties of fibrocartilage upon dynamic nanoindentation of the articular condyle. *J Struct Biol* **136**, 46-52 (2001).

77. Kuboki, T., Shinoda, M., Orsini, M.G. & Yamashita, A. Viscoelastic properties of the pig temporomandibular joint articular soft tissues of the condyle and disc. *J Dent Res* **76**, 1760-1769 (1997).

78. Yao, H., Kuo, J., Zhang, L.X. & Bacroc, T. The region-dependent biphasic viscoelastic properties of human temporomandibular joint discs under confined compression. *Journal of Biomechanics* **43**, 1316-1321 (2010).

79. Yuya, P.A., Amborn, E.K., Beatty, M.W. & Turner, J.A. Evaluating anisotropic properties in the porcine temporomandibular joint disc using nanoindentation. *Ann Biomed Eng* **38**, 2428-2437 (2010).

80. Beatty, M.W., Bruno, M.J., Iwasaki, L.R. & Nickel, J.C. Strain rate dependent orthotropic properties of pristine and impulsively loaded porcine temporomandibular joint disk. *Journal of biomedical materials research* **57**, 25-34 (2001).

81. Detamore, M.S. & Athanasiou, K.A. Tensile properties of the porcine temporomandibular joint disc. *J Biomech Eng* **125**, 558-565 (2003).

82. Beatty, M.W., Nickel, J.C., Iwasaki, L.R. & Leiker, M. Mechanical response of the porcine temporomandibular joint disc to an impact event and repeated tensile loading. *J Orofac Pain* **17**, 160-166 (2003).

83. Martin, R.B., Burr, D.B. & Sharkey, N.A. Skeletal tissue mechanics. (Springer, New York; 1998).

84. Beatty, M.W., Hohl, R.H., Nickel, J.C., Iwasaki, L.R. & Pidaparti, R.M. Mode I and Mode III fractures in intermediate zone of full-thickness porcine temporomandibular joint discs. *Ann Biomed Eng* **36**, 801-812 (2008).

85. Tanaka, E. et al. Dynamic shear behavior of mandibular condylar cartilage is dependent on testing direction. *Journal of Biomechanics* **41**, 1119-1123 (2008).

86. Tanaka, E. et al. Biomechanical response of condylar cartilage-on-bone to dynamic shear. *J Biomed Mater Res A* **85**, 127-132 (2008).

87. Kang, H. et al. [Tensile mechanics of mandibular condylar cartilage]. *Hua Xi Kou Qiang Yi Xue Za Zhi* **18**, 85-87 (2000).

88. Patel, R.V. & Mao, J.J. Microstructural and elastic properties of the extracellular matrices of the superficial zone of neonatal articular cartilage by atomic force microscopy. *Front Biosci* **8**, a18-25 (2003).

89. Tanaka, E. et al. Dynamic compressive properties of the mandibular condylar cartilage. *J Dent Res* **85**, 571-575 (2006).

90. Mak, A.F., Lai, W.M. & Mow, V.C. Biphasic indentation of articular cartilage--I. Theoretical analysis. *Journal of Biomechanics* **20**, 703-714 (1987).

91. Mow, V.C., Gibbs, M.C., Lai, W.M., Zhu, W.B. & Athanasiou, K.A. Biphasic indentation of articular cartilage--II. A numerical algorithm and an experimental study. *Journal of Biomechanics* **22**, 853-861 (1989).

92. Chen, J., Akyuz, U., Xu, L. & Pidaparti, R.M. Stress analysis of the human temporomandibular joint. *Med Eng Phys* **20**, 565-572 (1998).

93. Mori, H. et al. Three-dimensional finite element analysis of cartilaginous tissues in human temporomandibular joint during prolonged clenching. *Arch Oral Biol* **55**, 879-886 (2010).

94. Tanaka, E. et al. Three-dimensional finite element analysis of human temporomandibular joint with and without disc displacement during jaw opening. *Med Eng Phys* **26**, 503-511 (2004).

95. Tanaka, E. et al. Stress analysis in the TMJ during jaw opening by use of a three-dimensional finite element model based on magnetic resonance images. *Int J Oral Maxillofac Surg* **30**, 421-430 (2001).

96. Perez Del Palomar, A. & Doblare, M. Finite element analysis of the temporomandibular joint during lateral excursions of the mandible. *Journal of Biomechanics* **39**, 2153-2163 (2006).

97. Tuijt, M., Koolstra, J.H., Lobbezoo, F. & Naeije, M. Differences in loading of the temporomandibular joint during opening and closing of the jaw. *Journal of Biomechanics* **43**, 1048-1054 (2010).

98. Gunja, N.J., Huey, D.J., James, R.A. & Athanasiou, K.A. Effects of agarose mould compliance and surface roughness on self-assembled meniscus-shaped constructs. *Journal of tissue engineering and regenerative medicine* **3**, 521-530 (2009).

99. Huey, D.J. & Athanasiou, K.A. Maturational growth of self-assembled, functional menisci as a result of TGF-beta1 and enzymatic chondroitinase-ABC stimulation. *Biomaterials* **32**, 2052-2058 (2011).

100. Johns, D.E., Wong, M.E. & Athanasiou, K.A. Clinically relevant cell sources for TMJ disc engineering. *J Dent Res* **87**, 548-552 (2008).

101. Baek, R.M. & Song, Y.T. Overgrowth of a costochondral graft in reconstruction of the temporomandibular joint. *Scand J Plast Reconstr Surg Hand Surg* **40**, 179-185 (2006).

102. Wang, L. & Detamore, M.S. Tissue engineering the mandibular condyle. *Tissue Eng* **13**, 1955-1971 (2007).

103. Zarb, G.A. & Carlsson, G.E. Temporomandibular disorders: osteoarthritis. *J Orofac Pain* **13**, 295-306 (1999).

104. Laskin, D.M., Greenfield, W. & Gale, E. (American Dental Association, Chicago; 1983).

105. Tanaka, E., Detamore, M.S. & Mercuri, L.G. Degenerative disorders of the temporomandibular joint: etiology, diagnosis, and treatment. *J Dent Res* **87**, 296-307 (2008).

106. Carlsson, G.E. & LeResche, L. in Temporomandibular disorders and related pain conditions. (eds. B.J. Sessle, P. Bryant & R. Dionne) 497-506 (IASP Press, Seattle; 1995).

107. Carlsson, G.E. Epidemiology and treatment need for temporomandibular disorders. *J Orofac Pain* **13**, 232-237 (1999).

108. Martins-Junior, R.L., Palma, A.J., Marquardt, E.J., Gondin, T.M. & Kerber Fde, C. Temporomandibular disorders: a report of 124 patients. *J Contemp Dent Pract* **11**, 071-078 (2010).

109. Goncalves, D.A., Dal Fabbro, A.L., Campos, J.A., Bigal, M.E. & Speciali, J.G. Symptoms of temporomandibular disorders in the population: an epidemiological study. *J Orofac Pain* **24**, 270-278 (2010).

110. Warren, M.P. & Fried, J.L. Temporomandibular disorders and hormones in women. *Cells Tissues Organs* **169**, 187-192 (2001).

111. van Loon, J.P., de Bont, L.G., Stegenga, B., Spijkervet, F.K. & Verkerke, G.J. Groningen temporomandibular joint prosthesis. Development and first clinical application. *Int J Oral Maxillofac Surg* **31**, 44-52 (2002).

112. Farrar, W.B. & McCarty, W.L., Jr. The TMJ dilemma. *J Ala Dent Assoc* **63**, 19-26 (1979).

113. Bertram, S. et al. Diagnosing TMJ internal derangement and osteoarthritis with magnetic resonance imaging. *J Am Dent Assoc* **132**, 753-761 (2001).

114. Brooks, S.L., Westesson, P.L., Eriksson, L., Hansson, L.G. & Barsotti, J.B. Prevalence of osseous changes in the temporomandibular joint of asymptomatic persons without internal derangement. *Oral Surg Oral Med Oral Pathol* **73**, 118-122 (1992).

115. de Bont, L.G., Boering, G., Liem, R.S., Eulderink, F. & Westesson, P.L. Osteoarthritis and internal derangement of the temporomandibular joint: a light microscopic study. *J Oral Maxillofac Surg* **44**, 634-643 (1986).

116. Moffett, B.C., Jr., Johnson, L.C., McCabe, J.B. & Askew, H.C. Articular Remodeling in the Adult Human Temporomandibular Joint. *Am J Anat* **115**, 119-141 (1964).

117. Arnett, G.W., Milam, S.B. & Gottesman, L. Progressive mandibular retrusion-idiopathic condylar resorption. Part II. *Am J Orthod Dentofacial Orthop* **110**, 117-127 (1996).

118. Arnett, G.W., Milam, S.B. & Gottesman, L. Progressive mandibular retrusion--idiopathic condylar resorption. Part I. *Am J Orthod Dentofacial Orthop* **110**, 8-15 (1996).

119. Kai, S., Kai, H., Tabata, O., Shiratsuchi, Y. & Ohishi, M. Long-term outcomes of nonsurgical treatment in nonreducing anteriorly displaced disk of the temporomandibular joint. *Oral Surg Oral Med Oral Pathol Oral Radiol Endod* **85**, 258-267 (1998).

120. Ogus, H. The mandibular joint: internal rearrangement. *Br J Oral Maxillofac Surg* **25**, 218-226 (1987).

121. Sharawy, M., Ali, A.M. & Choi, W.S. Experimental induction of anterior disk displacement of the rabbit craniomandibular joint: an immuno-electron microscopic study of collagen and proteoglycan occurrence in the condylar cartilage. *J Oral Pathol Med* **32**, 176-184 (2003).

122. Ogus, H. The mandibular joint: internal rearrangement. *British Journal of Oral and Maxillofacial Surgery* **25**, 218-226 (1987).

123. Imai, H., Sakamoto, I., Yoda, T. & Yamashita, Y. A model for internal derangement and osteoarthritis of the temporomandibular joint with experimental traction of the mandibular ramus in rabbit. *Oral Dis* **7**, 185-191 (2001).

124. Stegenga, B., de Bont, L.G. & Boering, G. Osteoarthrosis as the cause of craniomandibular pain and dysfunction: a unifying concept. *J Oral Maxillofac Surg* **47**, 249-256 (1989).

125. Nitzan, D.W. The process of lubrication impairment and its involvement in temporomandibular joint disc displacement: a theoretical concept. *J Oral Maxillofac Surg* **59**, 36-45 (2001).

126. Imai, H., Sakamoto, I., Yoda, T. & Yamashita, Y. A model for internal derangement and osteoarthritis of the temporomandibular joint with experimental traction of the mandibular ramus in rabbit. *Oral diseases* **7**, 185-191 (2001).

127. Stegenga, B., de Bont, L.G. & Boering, G. Osteoarthrosis as the cause of craniomandibular pain and dysfunction: a unifying concept. *Journal of Oral and Maxillofacial Surgery* **47**, 249-256 (1989).

128. Petersson, A. What you can and cannot see in TMJ imaging - an overview related to the RDC/TMD diagnostic system. *J Oral Rehabil* **37**, 771-778 (2010).

129. Ahmad, M. et al. Research diagnostic criteria for temporomandibular disorders (RDC/TMD): development of image analysis criteria and examiner reliability for image analysis. *Oral Surg Oral Med Oral Pathol Oral Radiol Endod* **107**, 844-860 (2009).

130. McNeely, M.L., Armijo Olivo, S. & Magee, D.J. A systematic review of the effectiveness of physical therapy interventions for temporomandibular disorders. *Phys Ther* **86**, 710-725 (2006).

131. Gray, R.J., Quayle, A.A., Hall, C.A. & Schofield, M.A. Physiotherapy in the treatment of temporomandibular joint disorders: a comparative study of four treatment methods. *Br Dent J* **176**, 257-261 (1994).

132. Treacy, K. Awareness/relaxation training and transcutaneous electrical neural stimulation in the treatment of bruxism. *J Oral Rehabil* **26**, 280-287 (1999).

133. Rocabado, M. The importance of soft tissue mechanics in stability and instability of the cervical spine: a functional diagnosis for treatment planning. *Cranio* **5**, 130-138 (1987).

134. Fricton, J.R. Management of masticatory myofascial pain. *Semin Orthod* **1**, 229-243 (1995).

135. Manjanna, K.M., Shivakumar, B. & Pramod Kumar, T.M. Microencapsulation: an acclaimed novel drug-delivery system for NSAIDs in arthritis. *Crit Rev Ther Drug Carrier Syst* **27**, 509-545 (2010).

136. Dionne, R.A. Pharmacologic treatments for temporomandibular disorders *Oral Surg. Oral Med. Oral Pathol. Oral Radiol. Endod.* **83**, 134-142 (1997).

137. Dimitroulis, G., Gremillion, H.A., Dolwick, M.F. & Walter, J.H. Temporomandibular disorders. 2. Non-surgical treatment. *Aust Dent J* **40**, 372-376 (1995).

138. Laskin, D.M., Greene, C.S. & Hylander, W.L. Temporomandibular disorders: an evidence-based approach to diagnosis and treatment. (Quintessence Pub., 2008).

139. Mountziaris, P.M., Kramer, P.R. & Mikos, A.G. Emerging intra-articular drug delivery systems for the temporomandibular joint. *Methods* **47**, 134-140 (2009).

140. Holmlund, A., Hellsing, G. & Bang, G. Arthroscopy of the rabbit temporomandibular joint. *International Journal of Oral and Maxillofacial Surgery* **15**, 170-175 (1986).

141. Nitzan, D.W. & Price, A. The use of arthrocentesis for the treatment of osteoarthritic temporomandibular joints. *J Oral Maxillofac Surg* **59**, 1154-1159; discussion 1160 (2001).

142. Laskin, D.M. in TMDs an evidenc-based approach to diagnosis and treatment., Vol. 1. (eds. D.M. Laskin, C.S. Greene & W.L. Hylander) 476 (Quintessence Publishing Co, Hanover Park; 2006).

143. Holmlund, A., Hellsing, G. & Bang, G. Arthroscopy of the rabbit temporomandibular joint. *Int J Oral Maxillofac Surg* **15**, 170-175 (1986).

144. Holmlund, A. Diagnostic TMJ arthroscopy. *Oral Surg Oral Diagn* **3**, 13-18 (1992).

145. Dolwick, M.F. The role of temporomandibular joint surgery in the treatment of patients with internal derangement. *Oral Surgery, Oral Medicine, Oral Pathology, Oral Radiology, and Endodontology* **83**, 150-155 (1997).

146. Dolwick, M.F. & Dimitroulis, G. Is there a role for temporomandibular joint surgery? *Br J Oral Maxillofac Surg* **32**, 307-313 (1994).

147. Dolwick, M.F. The role of temporomandibular joint surgery in the treatment of patients with internal derangement. *Oral Surg Oral Med Oral Pathol Oral Radiol Endod* **83**, 150-155 (1997).

148. Bjornland, T. & Larheim, T.A. Discectomy of the temporomandibular joint: 3-year follow-up as a predictor of the 10-year outcome. *J Oral Maxillofac Surg* **61**, 55-60 (2003).

149. Eriksson, L. & Westesson, P.L. Discectomy as an effective treatment for painful temporomandibular joint internal derangement: a 5-year clinical and radiographic follow-up. *J Oral Maxillofac Surg* **59**, 750-758; discussion 758-759 (2001).

150. Wolford, L.M. Factors to consider in joint prosthesis systems. *Proceedings (Baylor University. Medical Center)* **19**, 232 (2006).

151. Takaku, S. & Toyoda, T. Long-term evaluation of discectomy of the temporomandibular joint. *J Oral Maxillofac Surg* **52**, 722-726; discussion 727-728 (1994).

152. Dimitroulis, G. Condylar Morphology After Temporomandibular Joint Discectomy With Interpositional Abdominal Dermis-Fat Graft. *Journal of Oral and Maxillofacial Surgery* **69**, 439-446 (2011).

153. Henry, C.H. & Wolford, L.M. Treatment outcomes for temporomandibular joint reconstruction after Proplast-Teflon implant failure. *J Oral Maxillofac Surg* **51**, 352-358; discussion 359-360 (1993).

154. Wolford, L.M. Factors to consider in joint prosthesis systems. *Proc (Bayl Univ Med Cent)* **19**, 232-238 (2006).

155. Dimitroulis, G. Condylar morphology after temporomandibular joint discectomy with interpositional abdominal dermis-fat graft. *J Oral Maxillofac Surg* **69**, 439-446 (2011).

156. McLeod, N.M., Saeed, N.R. & Hensher, R. Internal derangement of the temporomandibular joint treated by discectomy and hemi-arthroplasty with a Christensen fossa-eminence prosthesis. *Br J Oral Maxillofac Surg* **39**, 63-66 (2001).

157. Troulis, M.J., Tayebaty, F.T., Papadaki, M., Williams, W.B. & Kaban, L.B. Condylectomy and costochondral graft reconstruction for treatment of active idiopathic condylar resorption. *J Oral Maxillofac Surg* **66**, 65-72 (2008).

158. Qiu, Y.T., Yang, C. & Chen, M.J. Endoscopically assisted reconstruction of the mandibular condyle with a costochondral graft through a modified preauricular approach. *Br J Oral Maxillofac Surg* **48**, 443-447 (2010).

159. Wang, Y.L., Yang, C., Qiu, Y.T., Chen, M.J. & Zhang, S.Y. [The clinical application of arthroscope-assisted reconstruction of the mandibular condyle with costochondral graft]. *Hua Xi Kou Qiang Yi Xue Za Zhi* **26**, 534-536, 540 (2008).

160. Wong, M.E., Allen, K.D. & Athanasiou, K.A. in Tissue Engineering and Artificial Organs. (ed. J.D. Brozino) (CRC Press, Boca Raton; 2006).

161. Alhadlaq, A. et al. Adult stem cell driven genesis of human-shaped articular condyle. *Ann Biomed Eng* **32**, 911-923 (2004).

162. Alhadlaq, A. & Mao, J.J. Tissue-engineered osteochondral constructs in the shape of an articular condyle. *J Bone Joint Surg Am* **87**, 936-944 (2005).

163. Schek, R.M., Taboas, J.M., Hollister, S.J. & Krebsbach, P.H. Tissue engineering osteochondral implants for temporomandibular joint repair. *Orthod Craniofac Res* **8**, 313-319 (2005).

164. Schek, R.M., Taboas, J.M., Segvich, S.J., Hollister, S.J. & Krebsbach, P.H. Engineered osteochondral grafts using biphasic composite solid free-form fabricated scaffolds. *Tissue Eng* **10**, 1376-1385 (2004).

165. Teramoto, M., Kaneko, S., Shibata, S., Yanagishita, M. & Soma, K. Effect of compressive forces on extracellular matrix in rat mandibular condylar cartilage. *Journal of bone and mineral metabolism* **21**, 276-286 (2003).

166. Hansson, T., Oberg, T., Carlsson, G.E. & Kopp, S. Thickness of the soft tissue layers and the articular disk in the temporomandibular joint. *Acta Odontol Scand* **35**, 77-83 (1977).

167. Wang, L., Lazebnik, M. & Detamore, M.S. Hyaline cartilage cells outperform mandibular condylar cartilage cells in a TMJ fibrocartilage tissue engineering application. *Osteoarthritis Cartilage* **17**, 346-353 (2009).

168. Klinge, R.F. The structure of the mandibular condyle in the monkey (Macaca mulatta). *Micron* **27**, 381-387 (1996).

169. Tanaka, E. et al. Dynamic shear behavior of mandibular condylar cartilage is dependent on testing direction. *J Biomech* **41**, 1119-1123 (2008).

170. Lu, X.L., Mow, V.C. & Guo, X.E. Proteoglycans and mechanical behavior of condylar cartilage. *J Dent Res* **88**, 244-248 (2009).

171. Singh, M. & Detamore, M.S. Stress relaxation behavior of mandibular condylar cartilage under high-strain compression. *J Biomech Eng* **131**, 061008 (2009).

172. Takigawa, M. et al. Studies on chondrocytes from mandibular condylar cartilage, nasal septal cartilage, and spheno-occipital synchondrosis in culture. I. Morphology, growth, glycosaminoglycan synthesis, and responsiveness to bovine parathyroid hormone (1-34). *J Dent Res* **63**, 19-22 (1984).

173. Tsubai, T., Higashi, Y. & Scott, J.E. The effect of epidermal growth factor on the fetal rabbit mandibular condyle and isolated condylar fibroblasts. *Arch Oral Biol* **45**, 507-515 (2000).

174. Bailey, M.M., Wang, L., Bode, C.J., Mitchell, K.E. & Detamore, M.S. A comparison of human umbilical cord matrix stem cells and temporomandibular joint condylar chondrocytes for tissue engineering temporomandibular joint condylar cartilage. *Tissue Eng* **13**, 2003-2010 (2007).

175. Williams, J.M. et al. Bone tissue engineering using polycaprolactone scaffolds fabricated via selective laser sintering. *Biomaterials* **26**, 4817-4827 (2005).

176. Darling, E.M. & Athanasiou, K.A. Articular cartilage bioreactors and bioprocesses. *Tissue Eng* **9**, 9-26 (2003).

177. Nicodemus, G.D., Villanueva, I. & Bryant, S.J. Mechanical stimulation of TMJ condylar chondrocytes encapsulated in PEG hydrogels. *J Biomed Mater Res A* **83**, 323-331 (2007).

178. Jiao, Y., Wang, D. & Han, W.L. [Effects of various growth factors on human mandibular condylar cartilage cell proliferation]. *Zhonghua Kou Qiang Yi Xue Za Zhi* **35**, 346-349 (2000).

179. Delatte, M.L., Von den Hoff, J.W., Nottet, S.J., De Clerck, H.J. & Kuijpers-Jagtman, A.M. Growth regulation of the rat mandibular condyle and femoral head by transforming growth factor-{beta}1, fibroblast growth factor-2 and insulin-like growth factor-I. *Eur J Orthod* **27**, 17-26 (2005).

180. Delatte, M., Von den Hoff, J.W., Maltha, J.C. & Kuijpers-Jagtman, A.M. Growth stimulation of mandibular condyles and femoral heads of newborn rats by IGF-I. *Arch Oral Biol* **49**, 165-175 (2004).

181. Maor, G., Hochberg, Z. & Silbermann, M. Insulin-like growth factor I accelerates proliferation and differentiation of cartilage progenitor cells in cultures of neonatal mandibular condyles. *Acta Endocrinol (Copenh)* **128**, 56-64 (1993).

182. Copray, J.C., Brouwer, N., Prins, A.P. & Jansen, H.W. Effects of polypeptide growth factors on mandibular condylar cartilage of the rat in vitro. *J Biol Buccale* **16**, 109-117 (1988).

183. Song, J., Luo, S. & Fan, Y. [Effects of static tension-stress and TGF-beta 1 on proliferation of mandibular condylar chondrocytes]. *Hua Xi Kou Qiang Yi Xue Za Zhi* **21**, 61-63, 73 (2003).

184. Rees, L. The structure and function of the mandibular joint. *Br Dent J* **96** (1954).

185. Dolwick, M. in Internal Derangements of the Temporomandibular Joint (ed. K.R. Helms CA, Dolwick MF) 1-14 (Radiology Research and Education Foundation, San Francisco; 1983).

186. Piette, E. Anatomy of the human temporomandibular joint. An updated comprehensive review. *Acta Stomatol Belg* **90**, 103-127 (1993).

187. Werner, J.A., Tillmann, B. & Schleicher, A. Functional anatomy of the temporomandibular joint. A morphologic study on human autopsy material. *Anat Embryol (Berl)* **183**, 89-95 (1991).

188. Kalpakci, K.N., Willard, V.P., Wong, M.E. & Athanasiou, K.A. An interspecies comparison of the temporomandibular joint disc. *J Dent Res* **90**, 193-198 (2011).

189. Mills, D.K., Fiandaca, D.J. & Scapino, R.P. Morphologic, microscopic, and immunohistochemical investigation into the function of the primate TMJ disc. *J Orofac Pain* **8** (1994).

190. Sindelar, B.J., Evanko, S.P., Alonzo, T., Herring, S.W. & Wight, T. Effects of intraoral splint wear on proteoglycans in the temporomandibular joint disc. *Arch Biochem Biophys* **379**, 64-70 (2000).

191. Almarza, A.J. & Athanasiou, K.A. Design characteristics for the tissue engineering of cartilaginous tissues. *Ann Biomed Eng* **32**, 2-17 (2004).

192. Scapino, R.P., Obrez, A. & Greising, D. Organization and function of the collagen fiber system in the human temporomandibular joint disk and its attachments. *Cells, tissues, organs* **182**, 201-225 (2006).

193. Scapino, R.P., Canham, P.B., Finlay, H.M. & Mills, D.K. The behaviour of collagen fibres in stress relaxation and stress distribution in the jaw-joint disc of rabbits. *Arch Oral Biol* **41**, 1039-1052 (1996).

194. de Bont, L.G., Liem, R.S., Havinga, P. & Boering, G. Fibrous component of the temporomandibular joint disk. *Cranio* **3**, 368-373 (1985).

195. Hirschmann, P.N. & Shuttleworth, C.A. The collagen composition of the mandibular joint of the foetal calf. *Arch Oral Biol* **21**, 771-773 (1976).

196. Ali, A.M. & Sharawy, M.M. An immunohistochemical study of collagen types III, VI and IX in rabbit craniomandibular joint tissues following surgical induction of anterior disk displacement. *J Oral Pathol Med* **25**, 78-85 (1996).

197. O'Dell, N.L., Starcher, B.C., Wilson, J.T., Pennington, C.B. & Jones, G.A. Morphological and biochemical evidence for elastic fibres in the Syrian hamster temporomandibular joint disc. *Arch Oral Biol* **35**, 807-811 (1990).

198. Christensen, L. Elastic tissue in the temporomandibular disc of miniature swine. *J Oral Rehabil* **2**, 373-377 (1975).

199. Axelsson, S., Holmlund, A. & Hjerpe, A. Glycosaminoglycans in normal and osteoarthrotic human temporomandibular joint disks. *Acta Odontol Scand* **50**, 113-119 (1992).

200. Beek, M., Aarnts, M.P., Koolstra, J.H., Feilzer, A.J. & van Eijden, T.M. Dynamic properties of the human temporomandibular joint disc. *J Dent Res* **80**, 876-880 (2001).

201. Thomas, M., Grande, D. & Haug, R.H. Development of an in vitro temporomandibular joint cartilage analog. *J Oral Maxillofac Surg* **49**, 854-856; discussion 857 (1991).

202. Springer, I.N., Fleiner, B., Jepsen, S. & Acil, Y. Culture of cells gained from temporomandibular joint cartilage on non-absorbable scaffolds. *Biomaterials* **22**, 2569-2577 (2001).

203. Puelacher, W.C. et al. Temporomandibular joint disc replacement made by tissue-engineered growth of cartilage. *J Oral Maxillofac Surg* **52**, 1172-1177; discussion 1177-1178 (1994).

204. Girdler, N.M. In vitro synthesis and characterization of a cartilaginous meniscus grown from isolated temporomandibular chondroprogenitor cells. *Scand J Rheumatol* **27**, 446-453 (1998).

205. Anderson, D.E. & Athanasiou, K.A. Passaged goat costal chondrocytes provide a feasible cell source for temporomandibular joint tissue engineering. *Ann Biomed Eng* **36**, 1992-2001 (2008).

206. Anderson, D.E. & Athanasiou, K.A. A comparison of primary and passaged chondrocytes for use in engineering the temporomandibular joint. *Arch Oral Biol* **54**, 138-145 (2009).

207. Johns, D.E. & Athanasiou, K.A. Growth factor effects on costal chondrocytes for tissue engineering fibrocartilage. *Cell Tissue Res* **333**, 439-447 (2008).

208. Almarza, A.J. & Athanasiou, K.A. Seeding techniques and scaffolding choice for tissue engineering of the temporomandibular joint disk. *Tissue Eng* **10**, 1787-1795 (2004).

209. Allen, K.D. & Athanasiou, K.A. Scaffold and growth factor selection in temporomandibular joint disc engineering. *J Dent Res* **87**, 180-185 (2008).

210. Grande, D.A., Halberstadt, C., Naughton, G., Schwartz, R. & Manji, R. Evaluation of matrix scaffolds for tissue engineering of articular cartilage grafts. *J Biomed Mater Res* **34**, 211-220 (1997).

211. Lumpkins, S.B., Pierre, N. & McFetridge, P.S. A mechanical evaluation of three decellularization methods in the design of a xenogeneic scaffold for tissue engineering the temporomandibular joint disc. *Acta Biomater* **4**, 808-816 (2008).

212. Hu, J.C. & Athanasiou, K.A. A self-assembling process in articular cartilage tissue engineering. *Tissue engineering* **12**, 969-979 (2006).

213. Elder, B.D. & Athanasiou, K.A. Systematic assessment of growth factor treatment on biochemical and biomechanical properties of engineered articular cartilage constructs. *Osteoarthritis Cartilage* **17**, 114-123 (2009).

214. Elder, B.D. & Athanasiou, K.A. Synergistic and additive effects of hydrostatic pressure and growth factors on tissue formation. *PLoS One* **3**, e2341 (2008).

215. Detamore, M.S. & Athanasiou, K.A. Effects of growth factors on temporomandibular joint disc cells. *Arch Oral Biol* **49**, 577-583 (2004).

216. Detamore, M.S. & Athanasiou, K.A. Evaluation of three growth factors for TMJ disc tissue engineering. *Ann Biomed Eng* **33**, 383-390 (2005).

217. Natoli, R.M., Responte, D.J., Lu, B.Y. & Athanasiou, K.A. Effects of multiple chondroitinase ABC applications on tissue engineered articular cartilage. *J Orthop Res* **27**, 949-956 (2009).

218. Almarza, A.J. & Athanasiou, K.A. Effects of initial cell seeding density for the tissue engineering of the temporomandibular joint disc. *Ann Biomed Eng* **33**, 943-950 (2005).

219. Revell, C.M., Reynolds, C.E. & Athanasiou, K.A. Effects of initial cell seeding in self assembly of articular cartilage. *Ann Biomed Eng* **36**, 1441-1448 (2008).

220. Roth, T.E., Goldberg, J.S. & Behrents, R.G. Synovial fluid pressure determination in the temporomandibular joint. *Oral Surg Oral Med Oral Pathol* **57**, 583-588 (1984).

221. Almarza, A.J. & Athanasiou, K.A. Effects of hydrostatic pressure on TMJ disc cells. *Tissue Eng* **12**, 1285-1294 (2006).

222. Detamore, M.S. & Athanasiou, K.A. Use of a Rotating Bioreactor toward Tissue Engineering the Temporomandibular Joint Disc. *Tissue Eng* **11**, 1188-1197 (2005).

223. Proctor, C.S., Schmidt, M.B., Whipple, R.R., Kelly, M.A. & Mow, V.C. Material properties of the normal medial bovine meniscus. *J Orthop Res* **7**, 771-782 (1989).

224. Ellingson, A.M. & Nuckley, D.J. Intervertebral disc viscoelastic parameters and residual mechanics spatially quantified using a hybrid confined/in situ indentation method. *J Biomech* **45**, 491-496 (2012).

225. Acosta, F.L., Jr. et al. Porcine intervertebral disc repair using allogeneic juvenile articular chondrocytes or mesenchymal stem cells. *Tissue Eng Part A* **17**, 3045-3055 (2011).

226. Ballyns, J.J., Wright, T.M. & Bonassar, L.J. Effect of media mixing on ECM assembly and mechanical properties of anatomically-shaped tissue engineered meniscus. *Biomaterials* **31**, 6756-6763 (2010).

227. Mandal, B.B., Park, S.H., Gil, E.S. & Kaplan, D.L. Multilayered silk scaffolds for meniscus tissue engineering. *Biomaterials* **32**, 639-651 (2011).

228. Wan, Y., Feng, G., Shen, F.H., Laurencin, C.T. & Li, X. Biphasic scaffold for annulus fibrosus tissue regeneration. *Biomaterials* **29**, 643-652 (2008).

229. Asanbaeva, A., Masuda, K., Thonar, E.J., Klisch, S.M. & Sah, R.L. Mechanisms of cartilage growth: modulation of balance between proteoglycan and collagen in vitro using chondroitinase ABC. *Arthritis Rheum* **56**, 188-198 (2007).

230. Ofek, G. et al. Matrix development in self-assembly of articular cartilage. *PloS one* **3**, e2795 (2008).

231. Responte, D.J., Arzi, B., Natoli, R.M., Hu, J.C. & Athanasiou, K.A. Mechanisms underlying the synergistic enhancement of self-assembled neocartilage treated with chondroitinase-ABC and TGF-beta1. *Biomaterials* **33**, 3187-3194 (2012).

232. Masters, K.S., Shah, D.N., Leinwand, L.A. & Anseth, K.S. Crosslinked hyaluronan scaffolds as a biologically active carrier for valvular interstitial cells. *Biomaterials* **26**, 2517-2525 (2005).

233. Wilson, C.G., Nishimuta, J.F. & Levenston, M.E. Chondrocytes and meniscal fibrochondrocytes differentially process aggrecan during de novo extracellular matrix assembly. *Tissue Eng Part A* **15**, 1513-1522 (2009).

234. Vonk, L.A. et al. Caprine articular, meniscus and intervertebral disc cartilage: an integral analysis of collagen network and chondrocytes. *Matrix Biol* **29**, 209-218 (2010).

235. Freije, J.M. et al. Molecular cloning and expression of collagenase-3, a novel human matrix metalloproteinase produced by breast carcinomas. *J Biol Chem* **269**, 16766-16773 (1994).

236. Williamson, A.K., Masuda, K., Thonar, E.J. & Sah, R.L. Growth of immature articular cartilage in vitro: correlated variation in tensile biomechanical and collagen network properties. *Tissue Eng* **9**, 625-634 (2003).

237. Williams, G.M., Klisch, S.M. & Sah, R.L. Bioengineering cartilage growth, maturation, and form. *Pediatr Res* **63**, 527-534 (2008).

238. Williamson, A.K., Chen, A.C., Masuda, K., Thonar, E.J. & Sah, R.L. Tensile mechanical properties of bovine articular cartilage: variations with growth and relationships to collagen network components. *J Orthop Res* **21**, 872-880 (2003).

239. Williamson, A.K., Chen, A.C. & Sah, R.L. Compressive properties and function-composition relationships of developing bovine articular cartilage. *J Orthop Res* **19**, 1113-1121 (2001).

240. Otsuki, S. et al. The effect of glycosaminoglycan loss on chondrocyte viability: a study on porcine cartilage explants. *Arthritis Rheum* **58**, 1076-1085 (2008).

241. Bian, L. et al. Influence of temporary chondroitinase ABC-induced glycosaminoglycan suppression on maturation of tissue-engineered cartilage. *Tissue Eng Part A* **15**, 2065-2072 (2009).

242. Chia, H.N. & Hull, M.L. Compressive moduli of the human medial meniscus in the axial and radial directions at equilibrium and at a physiological strain rate. *Journal of orthopaedic research : official publication of the Orthopaedic Research Society* **26**, 951-956 (2008).

243. Willard, V.P., Kalpakci, K.N., Reimer, A.J. & Athanasiou, K.A. The regional contribution of glycosaminoglycans to temporomandibular joint disc compressive properties. *J Biomech Eng* **134**, 011011 (2012).

244. Recuerda, M., Cote, S.P., Villemure, I. & Preie, D. Influence of experimental protocols on the mechanical properties of the intervertebral disc in unconfined compression. *J Biomech Eng* **133**, 071006 (2011).

245. Nerurkar, N.L., Han, W., Mauck, R.L. & Elliott, D.M. Homologous structure-function relationships between native fibrocartilage and tissue engineered from MSC-seeded nanofibrous scaffolds. *Biomaterials* **32**, 461-468 (2011).

246. Ambard, D. & Cherblanc, F. Mechanical behavior of annulus fibrosus: a microstructural model of fibers reorientation. *Ann Biomed Eng* **37**, 2256-2265 (2009).

247. Petersen, W. & Tillmann, B. Collagenous fibril texture of the human knee joint menisci. *Anat Embryol (Berl)* **197**, 317-324 (1998).

248. Fithian, D.C., Kelly, M.A. & Mow, V.C. Material properties and structure-function relationships in the menisci. *Clin Orthop Relat Res*, 19-31 (1990).

249. Hedlund, H., Mengarelli-Widholm, S., Reinholt, F.P. & Svensson, O. Stereologic studies on collagen in bovine articular cartilage. *APMIS* **101**, 133-140 (1993).

250. Iatridis, J.C., MaClean, J.J. & Ryan, D.A. Mechanical damage to the intervertebral disc annulus fibrosus subjected to tensile loading. *J Biomech* **38**, 557-565 (2005).

251. Shibuya, S. Meniscus transplantation using a cryopreserved allograft. Histological and ultrastructural study of the transplanted meniscus. *J Orthop Sci* **4**, 135-141 (1999).

252. Elliott, D.M. & Setton, L.A. Anisotropic and inhomogeneous tensile behavior of the human anulus fibrosus: experimental measurement and material model predictions. *Journal of biomechanical engineering* **123**, 256-263 (2001).

253. Tissakht, M. & Ahmed, A.M. Tensile stress-strain characteristics of the human meniscal material. *Journal of biomechanics* **28**, 411-422 (1995).

254. Koepsell, L. et al. Tissue engineering of annulus fibrosus using electrospun fibrous scaffolds with aligned polycaprolactone fibers. *J Biomed Mater Res A* **99**, 564-575 (2011).

255. Baker, B.M., Nathan, A.S., Gee, A.O. & Mauck, R.L. The influence of an aligned nanofibrous topography on human mesenchymal stem cell fibrochondrogenesis. *Biomaterials* **31**, 6190-6200 (2010).

256. Nerurkar, N.L., Elliott, D.M. & Mauck, R.L. Mechanics of oriented electrospun nanofibrous scaffolds for annulus fibrosus tissue engineering. *J Orthop Res* **25**, 1018-1028 (2007).

257. Huey, D.J., Hu, J.C. & Athanasiou, K.A. Unlike bone, cartilage regeneration remains elusive. *Science* **338**, 917-921 (2012).

258. Ben-Yishay, A., Grande, D.A., Schwartz, R.E., Menche, D. & Pitman, M.D. Repair of articular cartilage defects with collagen-chondrocyte allografts. *Tissue engineering* **1**, 119-133 (1995).

259. Lee, C.H. et al. Regeneration of the articular surface of the rabbit synovial joint by cell homing: a proof of concept study. *Lancet* **376**, 440-448 (2010).

260. Makris, E.A., Macbarb, R.F., Responte, D.J., Hu, J.C. & Athanasiou, K.A. A copper sulfate and hydroxylysine treatment regimen for enhancing collagen cross-linking and biomechanical properties in engineered neocartilage. *FASEB journal : official publication of the Federation of American Societies for Experimental Biology* (2013).

261. Woodfield, T.B. et al. Rapid prototyping of anatomically shaped, tissue-engineered implants for restoring congruent articulating surfaces in small joints. *Cell proliferation* **42**, 485-497 (2009).

262. Xie, J. et al. Articular cartilage tissue engineering based on a mechano-active scaffold made of poly(L-lactide-co-epsilon-caprolactone): In vivo performance in adult rabbits. *Journal of biomedical materials research. Part B, Applied biomaterials* **94**, 80-88 (2010).

263. Ballyns, J.J. et al. Image-guided tissue engineering of anatomically shaped implants via MRI and micro-CT using injection molding. *Tissue engineering. Part A* **14**, 1195-1202 (2008).

264. Blanquer, S.B., Sharifi, S. & Grijpma, D.W. Development of poly(trimethylene carbonate) network implants for annulus fibrosus tissue engineering. *Journal of applied biomaterials & functional materials* **10**, 177-184 (2013).

265. Brown, B.N. et al. Inductive, scaffold-based, regenerative medicine approach to reconstruction of the temporomandibular joint disk. *Journal of oral and maxillofacial surgery : official journal of the American Association of Oral and Maxillofacial Surgeons* **70**, 2656-2668 (2012).

266. Brown, B.N. et al. Extracellular matrix as an inductive template for temporomandibular joint meniscus reconstruction: a pilot study. *Journal of oral and maxillofacial surgery :*

official journal of the American Association of Oral and Maxillofacial Surgeons **69**, e488-505 (2011).

267. Kang, S.W. et al. Regeneration of whole meniscus using meniscal cells and polymer scaffolds in a rabbit total meniscectomy model. *Journal of biomedical materials research. Part A* **78**, 659-671 (2006).

268. Pan, Y. et al. Cells scaffold complex for Intervertebral disc Anulus Fibrosus tissue engineering: in vitro culture and product analysis. *Molecular biology reports* **39**, 8581-8594 (2012).

269. Baker, B.M. & Mauck, R.L. The effect of nanofiber alignment on the maturation of engineered meniscus constructs. *Biomaterials* **28**, 1967-1977 (2007).

270. Courtney, T., Sacks, M.S., Stankus, J., Guan, J. & Wagner, W.R. Design and analysis of tissue engineering scaffolds that mimic soft tissue mechanical anisotropy. *Biomaterials* **27**, 3631-3638 (2006).

271. Lee, C.H. et al. Nanofiber alignment and direction of mechanical strain affect the ECM production of human ACL fibroblast. *Biomaterials* **26**, 1261-1270 (2005).

272. MacBarb, R.F., Makris, E.A., Hu, J.C. & Athanasiou, K.A. A chondroitinase-ABC and TGF-beta1 treatment regimen for enhancing the mechanical properties of tissue-engineered fibrocartilage. *Acta biomaterialia* **9**, 4626-4634 (2013).

273. Meller, R. et al. Postnatal maturation of tendon, cruciate ligament, meniscus and articular cartilage: a histological study in sheep. *Annals of anatomy = Anatomischer Anzeiger : official organ of the Anatomische Gesellschaft* **191**, 575-585 (2009).

274. Mikic, B., Isenstein, A.L. & Chhabra, A. Mechanical modulation of cartilage structure and function during embryogenesis in the chick. *Annals of biomedical engineering* **32**, 18-25 (2004).

275. Roddy, K.A., Prendergast, P.J. & Murphy, P. Mechanical influences on morphogenesis of the knee joint revealed through morphological, molecular and computational analysis of immobilised embryos. *PloS one* **6**, e17526 (2011).

276. Hu, J.C. & Athanasiou, K.A. The effects of intermittent hydrostatic pressure on self-assembled articular cartilage constructs. *Tissue engineering* **12**, 1337-1344 (2006).

277. Huey, D.J. & Athanasiou, K.A. Tension-compression loading with chemical stimulation results in additive increases to functional properties of anatomic meniscal constructs. *PloS one* **6**, e27857 (2011).

278. Elder, B.D. & Athanasiou, K.A. Effects of confinement on the mechanical properties of self-assembled articular cartilage constructs in the direction orthogonal to the confinement surface. *Journal of orthopaedic research : official publication of the Orthopaedic Research Society* **26**, 238-246 (2008).

279. Van der Linden, E.J., Burdi, A.R. & de Jongh, H.J. Critical periods in the prenatal morphogenesis of the human lateral pterygoid muscle, the mandibular condyle, the articular disk, and medial articular capsule. *American journal of orthodontics and dentofacial orthopedics : official publication of the American Association of Orthodontists, its constituent societies, and the American Board of Orthodontics* **91**, 22-28 (1987).

280. Radlanski, R.J., Lieck, S. & Bontschev, N.E. Development of the human temporomandibular joint. Computer-aided 3D-reconstructions. *European journal of oral sciences* **107**, 25-34 (1999).

281. Humphrey, T. The development of mouth opening and related reflexes involving the oral area of human fetuses. *The Alabama journal of medical sciences* **5**, 126-157 (1968).

282. Radlanski, R.J. & Renz, H. Genes, forces, and forms: mechanical aspects of prenatal craniofacial development. *Developmental dynamics : an official publication of the American Association of Anatomists* **235**, 1219-1229 (2006).

283. Deschner, J., Rath-Deschner, B. & Agarwal, S. Regulation of matrix metalloproteinase expression by dynamic tensile strain in rat fibrochondrocytes. *Osteoarthritis and cartilage / OARS, Osteoarthritis Research Society* **14**, 264-272 (2006).

284. Ferretti, M. et al. Dynamic biophysical strain modulates proinflammatory gene induction in meniscal fibrochondrocytes. *American journal of physiology. Cell physiology* **290**, C1610-1615 (2006).

285. Gilbert, H.T., Hoyland, J.A., Freemont, A.J. & Millward-Sadler, S.J. The involvement of interleukin-1 and interleukin-4 in the response of human annulus fibrosus cells to cyclic tensile strain: an altered mechanotransduction pathway with degeneration. *Arthritis research & therapy* **13**, R8 (2011).

286. Le Maitre, C.L. et al. Altered integrin mechanotransduction in human nucleus pulposus cells derived from degenerated discs. *Arthritis and rheumatism* **60**, 460-469 (2009).

287. Armstrong, C.G., Lai, W.M. & Mow, V.C. An analysis of the unconfined compression of articular cartilage. *Journal of biomechanical engineering* **106**, 165-173 (1984).

288. Gray, M.L., Pizzanelli, A.M., Grodzinsky, A.J. & Lee, R.C. Mechanical and physiochemical determinants of the chondrocyte biosynthetic response. *Journal of orthopaedic research : official publication of the Orthopaedic Research Society* **6**, 777-792 (1988).

289. Ragan, P.M. et al. Chondrocyte extracellular matrix synthesis and turnover are influenced by static compression in a new alginate disk culture system. *Archives of biochemistry and biophysics* **383**, 256-264 (2000).

290. Davisson, T., Kunig, S., Chen, A., Sah, R. & Ratcliffe, A. Static and dynamic compression modulate matrix metabolism in tissue engineered cartilage. *Journal of orthopaedic research : official publication of the Orthopaedic Research Society* **20**, 842-848 (2002).

291. Imler, S.M., Doshi, A.N. & Levenston, M.E. Combined effects of growth factors and static mechanical compression on meniscus explant biosynthesis. *Osteoarthritis and cartilage / OARS, Osteoarthritis Research Society* **12**, 736-744 (2004).

292. Fan, J.C. & Waldman, S.D. The effect of intermittent static biaxial tensile strains on tissue engineered cartilage. *Annals of biomedical engineering* **38**, 1672-1682 (2010).

293. Sanchez-Adams, J. & Athanasiou, K.A. Biomechanics of meniscus cells: regional variation and comparison to articular chondrocytes and ligament cells. *Biomechanics and modeling in mechanobiology* **11**, 1047-1056 (2012).

294. Ahn, H.J. et al. Age-related changes in the microarchitecture of collagen fibrils in the articular disc of the rat temporomandibular joint. *Archives of histology and cytology* **70**, 175-181 (2007).

295. Diamant, J., Keller, A., Baer, E., Litt, M. & Arridge, R.G. Collagen; ultrastructure and its relation to mechanical properties as a function of ageing. *Proceedings of the Royal Society of London. Series B, Containing papers of a Biological character. Royal Society* **180**, 293-315 (1972).

296. Parry, D.A. The molecular and fibrillar structure of collagen and its relationship to the mechanical properties of connective tissue. *Biophysical chemistry* **29**, 195-209 (1988).

297. Buschmann, M.D., Gluzband, Y.A., Grodzinsky, A.J. & Hunziker, E.B. Mechanical compression modulates matrix biosynthesis in chondrocyte/agarose culture. *Journal of cell science* **108** 1497-1508 (1995).

298. Hung, C.T., Mauck, R.L., Wang, C.C., Lima, E.G. & Ateshian, G.A. A paradigm for functional tissue engineering of articular cartilage via applied physiologic deformational loading. *Annals of biomedical engineering* **32**, 35-49 (2004).

299. Hunter, C.J., Imler, S.M., Malaviya, P., Nerem, R.M. & Levenston, M.E. Mechanical compression alters gene expression and extracellular matrix synthesis by chondrocytes cultured in collagen I gels. *Biomaterials* **23**, 1249-1259 (2002).

300. Vanderploeg, E.J., Imler, S.M., Brodkin, K.R., Garcia, A.J. & Levenston, M.E. Oscillatory tension differentially modulates matrix metabolism and cytoskeletal organization in chondrocytes and fibrochondrocytes. *Journal of biomechanics* **37**, 1941-1952 (2004).

301. Ballyns, J.J. & Bonassar, L.J. Dynamic compressive loading of image-guided tissue engineered meniscal constructs. *Journal of biomechanics* **44**, 509-516 (2011).

302. Zhou, J. & Niklason, L.E. Microfluidic artificial "vessels" for dynamic mechanical stimulation of mesenchymal stem cells. *Integrative biology : quantitative biosciences from nano to macro* **4**, 1487-1497 (2012).

303. Teh, T.K., Toh, S.L. & Goh, J.C. Aligned fibrous scaffolds for enhanced mechanoresponse and tenogenesis of mesenchymal stem cells. *Tissue engineering. Part A* **19**, 1360-1372 (2013).

304. le Noble, F., Klein, C., Tintu, A., Pries, A. & Buschmann, I. Neural guidance molecules, tip cells, and mechanical factors in vascular development. *Cardiovascular research* **78**, 232-241 (2008).

305. Responte, D.J., Lee, J.K., Hu, J.C. & Athanasiou, K.A. Biomechanics-driven chondrogenesis: from embryo to adult. *FASEB journal : official publication of the Federation of American Societies for Experimental Biology* **26**, 3614-3624 (2012).

306. Drury, J.L. & Mooney, D.J. Hydrogels for tissue engineering: scaffold design variables and applications. *Biomaterials* **24**, 4337-4351 (2003).

307. Hodde, J. Naturally occurring scaffolds for soft tissue repair and regeneration. *Tissue engineering* **8**, 295-308 (2002).

308. Makris, E.A., Hadidi, P. & Athanasiou, K.A. The knee meniscus: structure-function, pathophysiology, current repair techniques, and prospects for regeneration. *Biomaterials* **32**, 7411-7431 (2011).

309. Agrawal, C.M., Niederauer, G.G. & Athanasiou, K.A. Fabrication and Characterization of PLA-PGA Orthopedic Implants. *Tissue engineering* **1**, 241-252 (1995).

310. Bruns, J., Kahrs, J., Kampen, J., Behrens, P. & Plitz, W. Autologous perichondral tissue for meniscal replacement. *The Journal of bone and joint surgery. British volume* **80**, 918-923 (1998).

311. Puetzer, J.L. & Bonassar, L.J. High density type I collagen gels for tissue engineering of whole menisci. *Acta biomaterialia* **9**, 7787-7795 (2013).

312. Wood, D.J., Minns, R.J. & Strover, A. Replacement of the rabbit medial meniscus with a polyester-carbon fibre bioprosthesis. *Biomaterials* **11**, 13-16 (1990).

313. Klompmaker, J. et al. Meniscal repair by fibrocartilage in the dog: characterization of the repair tissue and the role of vascularity. *Biomaterials* **17**, 1685-1691 (1996).

314. Agrawal, C.M. & Athanasiou, K.A. Technique to control pH in vicinity of biodegrading PLA-PGA implants. *Journal of biomedical materials research* **38**, 105-114 (1997).

315. Macbarb, R.F., Chen, A.L., Hu, J.C. & Athanasiou, K.A. Engineering functional anisotropy in fibrocartilage neotissues. *Biomaterials* **34**, 9980-9989 (2013).

316. Hirai, J., Kanda, K., Oka, T. & Matsuda, T. Highly oriented, tubular hybrid vascular tissue for a low pressure circulatory system. *ASAIO journal* **40**, M383-388 (1994).

317. Hirai, J. & Matsuda, T. Self-organized, tubular hybrid vascular tissue composed of vascular cells and collagen for low-pressure-loaded venous system. *Cell transplantation* **4**, 597-608 (1995).

318. Huang, D., Chang, T.R., Aggarwal, A., Lee, R.C. & Ehrlich, H.P. Mechanisms and dynamics of mechanical strengthening in ligament-equivalent fibroblast-populated collagen matrices. *Annals of biomedical engineering* **21**, 289-305 (1993).

319. L'Heureux, N., Germain, L., Labbe, R. & Auger, F.A. In vitro construction of a human blood vessel from cultured vascular cells: a morphologic study. *Journal of vascular surgery* **17**, 499-509 (1993).

320. L'Heureux, N., Paquet, S., Labbe, R., Germain, L. & Auger, F.A. A completely biological tissue-engineered human blood vessel. *FASEB journal : official publication of the Federation of American Societies for Experimental Biology* **12**, 47-56 (1998).

321. Macbarb, R.F., Chen, A.L., Hu, J.C. & Athanasiou, K.A. Engineering functional anisotropy in fibrocartilage neotissues. *Biomaterials* (2013).

322. Makris, E.A., MacBarb, R.F., Responte, D.J., Hu, J.C. & Athanasiou, K.A. A copper sulfate and hydroxylysine treatment regimen for enhancing collagen cross-linking and biomechanical properties in engineered neocartilage. *FASEB journal : official publication of the Federation of American Societies for Experimental Biology* **27**, 2421-2430 (2013).

323. Bank, R.A. et al. Sensitive fluorimetric quantitation of pyridinium and pentosidine crosslinks in biological samples in a single high-performance liquid chromatographic run. *Journal of chromatography. B, Biomedical sciences and applications* **703**, 37-44 (1997).

324. Fonck, E. et al. Effect of aging on elastin functionality in human cerebral arteries. *Stroke; a journal of cerebral circulation* **40**, 2552-2556 (2009).

325. Vader, D., Kabla, A., Weitz, D. & Mahadevan, L. Strain-induced alignment in collagen gels. *PloS one* **4**, e5902 (2009).

326. Girton, T.S., Barocas, V.H. & Tranquillo, R.T. Confined compression of a tissue-equivalent: collagen fibril and cell alignment in response to anisotropic strain. *Journal of biomechanical engineering* **124**, 568-575 (2002).

327. Grinnell, F. Fibroblast-collagen-matrix contraction: growth-factor signalling and mechanical loading. *Trends in cell biology* **10**, 362-365 (2000).

328. Harris, A.K., Stopak, D. & Wild, P. Fibroblast traction as a mechanism for collagen morphogenesis. *Nature* **290**, 249-251 (1981).

329. Tranquillo, R.T. Self-organization of tissue-equivalents: the nature and role of contact guidance. *Biochemical Society symposium* **65**, 27-42 (1999).

330. Grenier, G. et al. Tissue reorganization in response to mechanical load increases functionality. *Tissue engineering* **11**, 90-100 (2005).

331. Canty, E.G. et al. Actin filaments are required for fibripositor-mediated collagen fibril alignment in tendon. *The Journal of biological chemistry* **281**, 38592-38598 (2006).

332. Chandrasekhar, S. et al. Regulation of type I collagen fibril assembly by link protein and proteoglycans. *Collagen and related research* **4**, 323-337 (1984).

333. Snowden, J.M., Swann, D.A. Effects of glycosaminoglycans and proteoglycan on the in vitro assembly and thermal stability of collagen fibrils. *Biopolymers* **19**, 767-780 (1980).

334. Recuerda, M., Cote, S.P., Villemure, I. & Perie, D. Influence of experimental protocols on the mechanical properties of the intervertebral disc in unconfined compression. *Journal of biomechanical engineering* **133**, 071006 (2011).

335. Khalsa, P.S. & Eisenberg, S.R. Compressive behavior of articular cartilage is not completely explained by proteoglycan osmotic pressure. *J Biomech* **30**, 589-594 (1997).

336. Armstrong, C.G., Bahrani, A.S. & Gardner, D.L. Changes in the deformational behavior of human hip cartilage with age. *Journal of biomechanical engineering* **102**, 214 (1980).

337. Herberhold, C. et al. In situ measurement of articular cartilage deformation in intact femoropatellar joints under static loading. *Journal of biomechanics* **32**, 1287-1295 (1999).

338. Spilker, R.L., Donzelli, P.S. & Mow, V.C. A transversely isotropic biphasic finite element model of the meniscus. *Journal of biomechanics* **25**, 1027-1045 (1992).

339. Spilker, R.L., Nickel, J.C. & Iwasaki, L.R. A biphasic finite element model of in vitro plowing tests of the temporomandibular joint disc. *Annals of biomedical engineering* **37**, 1152-1164 (2009).

340. Ofek, G., Wiltz, D.C. & Athanasiou, K.A. Contribution of the cytoskeleton to the compressive properties and recovery behavior of single cells. *Biophysical journal* **97**, 1873-1882 (2009).

341. Shieh, A.C., Koay, E.J. & Athanasiou, K.A. Strain-dependent recovery behavior of single chondrocytes. *Biomechanics and modeling in mechanobiology* **5**, 172-179 (2006).

342. Guilak, F. & Mow, V.C. The mechanical environment of the chondrocyte: a biphasic finite element model of cell-matrix interactions in articular cartilage. *Journal of biomechanics* **33**, 1663-1673 (2000).

343. Guilak, F., Ratcliffe, A. & Mow, V.C. Chondrocyte deformation and local tissue strain in articular cartilage: a confocal microscopy study. *Journal of orthopaedic research : official publication of the Orthopaedic Research Society* **13**, 410-421 (1995).

344. Hootman, J.M. & Helmick, C.G. Projections of US prevalence of arthritis and associated activity limitations. *Arthritis Rheum* **54**, 226-229 (2006).

345. Lawrence, R.C. et al. Estimates of the prevalence of arthritis and selected musculoskeletal disorders in the United States. *Arthritis Rheum* **41**, 778-799 (1998).

346. V.C. Mow, W.C.H. Structure and function of articular cartilage and meniscus. *Basic Orthopaedic Biomechanics, Raven Press, New York (1997)*, pp. 113–178 (1997).

347. Chen, A.C., Bae, W.C., Schinagl, R.M. & Sah, R.L. Depth- and strain-dependent mechanical and electromechanical properties of full-thickness bovine articular cartilage in confined compression. *J Biomech* **34**, 1-12 (2001).

348. Ficklin, T. et al. Articular cartilage mechanical and biochemical property relations before and after in vitro growth. *Journal of biomechanics* **40**, 3607-3614 (2007).

349. Basser, P.J., Schneiderman, R., Bank, R.A., Wachtel, E. & Maroudas, A. Mechanical properties of the collagen network in human articular cartilage as measured by osmotic stress technique. *Arch Biochem Biophys* **351**, 207-219 (1998).

350. Summey, B.T., Jr., Graff, R.D., Lai, T.S., Greenberg, C.S. & Lee, G.M. Tissue transglutaminase localization and activity regulation in the extracellular matrix of articular cartilage. *J Orthop Res* **20**, 76-82 (2002).

351. Riesle, J., Hollander, A.P., Langer, R., Freed, L.E. & Vunjak-Novakovic, G. Collagen in tissue-engineered cartilage: types, structure, and crosslinks. *Journal of cellular biochemistry* **71**, 313-327 (1998).

352. Beekman, B., Verzijl, N., Bank, R.A., von der Mark, K. & TeKoppele, J.M. Synthesis of collagen by bovine chondrocytes cultured in alginate; posttranslational modifications and cell-matrix interaction. *Experimental cell research* **237**, 135-141 (1997).

353. Bastiaansen-Jenniskens, Y.M. et al. Contribution of collagen network features to functional properties of engineered cartilage. *Osteoarthritis and cartilage / OARS, Osteoarthritis Research Society* **16**, 359-366 (2008).

354. Kagan, H.M. & Sullivan, K.A. Lysyl oxidase: preparation and role in elastin biosynthesis. *Methods Enzymol* **82 Pt A**, 637-650 (1982).

355. Eyre, D.R., Weis, M.A. & Wu, J.J. Advances in collagen cross-link analysis. *Methods* **45**, 65-74 (2008).

356. Steinmann, P.M.R.a.B. Connective Tissue and its Heritable Disorders. (Wiley-Liss, New York, NY; 2002).

357. Siegel, R.C. Lysyl oxidase. *International review of connective tissue research* **8**, 73-118 (1979).

358. Sieibel, M.J., Robins S.P, and Bilezikian, J.P. Dynamics of Bone and Cartilage Metabolism: Principles and Clinical Applications (Academic Press, 2006).

359. Athanasiou, K.A. et al. Biomechanical properties of hip cartilage in experimental animal models. *Clin Orthop Relat Res*, 254-266 (1995).

360. Asanbaeva, A., Masuda, K., Thonar, E.J., Klisch, S.M. & Sah, R.L. Cartilage growth and remodeling: modulation of balance between proteoglycan and collagen network in vitro with beta-aminopropionitrile. *Osteoarthritis Cartilage* **16**, 1-11 (2008).

361. Rivard, C.H., Chaput, C., Rhalmi, S. & Selmani, A. [Bio-absorbable synthetic polyesters and tissue regeneration. A study of three-dimensional proliferation of ovine chondrocytes and osteoblasts]. *Ann Chir* **50**, 651-658 (1996).

362. V.C. Mow, W.C.H.S.a.f.o.a.c.a.m.B.O.B., Raven Press, New York (1997), pp. 113–178.

363. Cox, T.R. & Erler, J.T. Remodeling and homeostasis of the extracellular matrix: implications for fibrotic diseases and cancer. *Disease models & mechanisms* **4**, 165-178 (2011).

364. Tinker, D. & Rucker, R.B. Role of selected nutrients in synthesis, accumulation, and chemical modification of connective tissue proteins. *Physiol Rev* **65**, 607-657 (1985).

365. Opsahl, W. et al. Role of copper in collagen cross-linking and its influence on selected mechanical properties of chick bone and tendon. *The Journal of nutrition* **112**, 708-716 (1982).

366. Heraud, F., Savineau, C. & Harmand, M.F. Copper modulation of extracellular matrix synthesis by human articular chondrocytes. *Scand J Rheumatol* **31**, 279-284 (2002).

367. Pasqualicchio, M., Gasperini, R., Velo, G.P. & Davies, M.E. Effects of copper and zinc on proteoglycan metabolism in articular cartilage. *Mediators of inflammation* **5**, 95-99 (1996).

368. Rowley, D.A. & Halliwell, B. Superoxide-dependent and ascorbate-dependent formation of hydroxyl radicals in the presence of copper salts: a physiologically significant reaction? *Archives of biochemistry and biophysics* **225**, 279-284 (1983).

369. Rowley, D.A. & Halliwell, B. Formation of hydroxyl radicals from hydrogen peroxide and iron salts by superoxide- and ascorbate-dependent mechanisms: relevance to the pathology of rheumatoid disease. *Clin Sci (Lond)* **64**, 649-653 (1983).

370. Dahl, S.L., Rucker, R.B. & Niklason, L.E. Effects of copper and cross-linking on the extracellular matrix of tissue-engineered arteries. *Cell transplantation* **14**, 861-868 (2005).

371. Scarpa, M., Stevanato, R., Viglino, P. & Rigo, A. Superoxide ion as active intermediate in the autoxidation of ascorbate by molecular oxygen. Effect of superoxide dismutase. *J Biol Chem* **258**, 6695-6697 (1983).

372. Eyre, D.R., Wu, J.J. & Woods, P.E. The cartilage collagens: structural and metabolic studies. *J Rheumatol Suppl* **27**, 49-51 (1991).

373. Polan, C.E., Smith, W.G., Hammerstedt, R.H. & Henderson, L.M. Metabolism of hydroxylysine by rats. *The Journal of nutrition* **91**, 143-150 (1967).

374. Sinex, F.M. & Van Slyke, D.D. The source and state of the hydroxylysine of collagen. *J Biol Chem* **216**, 245-250 (1955).

375. Bassleer, C.T., Combal, J.P., Bougaret, S. & Malaise, M. Effects of chondroitin sulfate and interleukin-1 beta on human articular chondrocytes cultivated in clusters. *Osteoarthritis and cartilage / OARS, Osteoarthritis Research Society* **6**, 196-204 (1998).

376. Wandel, S. et al. Effects of glucosamine, chondroitin, or placebo in patients with osteoarthritis of hip or knee: network meta-analysis. *BMJ* **341**, c4675 (2010).

377. Gabay, C., Medinger-Sadowski, C., Gascon, D., Kolo, F. & Finckh, A. Symptomatic effects of chondroitin 4 and chondroitin 6 sulfate on hand osteoarthritis: a randomized, double-blind, placebo-controlled clinical trial at a single center. *Arthritis Rheum* **63**, 3383-3391 (2011).

378. Smith, W.G. & Henderson, L.M. Relationships of Lysine and Hydroxylysine in Streptococcus Faecalis and Leuconostoc Mesenteroides. *J Biol Chem* **239**, 1867-1871 (1964).

379. Tsung, C.M., Smith, W.G., Leach, F.R. & Henderson, L.M. Hydroxylysine metabolism in Streptococcus faecalis. *J Biol Chem* **237**, 1194-1197 (1962).

380. Greenwood D., W.R.J. in Antibiotic and Chemotherapy Anti-infective Agents and Their Use in Therapy., Vol. 8. (ed. G.D. Finch R.G., Norrby S.R., Whitley R.J.) 11-24 (Chuchill Livingstone, London; 2003).

381. Rosenbloom, J. & Prockop, D.J. Incorporation of cis-hydroxyproline into protocollagen and collagen. Collagen containing cis-hydroxyproline in place of proline and trans-hydroxyproline is not extruded at a normal rate. *J Biol Chem* **246**, 1549-1555 (1971).

382. Siegel, R.C. & Fu, J.C. Collagen cross-linking. Purification and substrate specificity of lysyl oxidase. *J Biol Chem* **251**, 5779-5785 (1976).

383. Buckwalter, J.A. & Mankin, H.J. Articular cartilage: tissue design and chondrocyte-matrix interactions. *Instructional course lectures* **47**, 477-486 (1998).

384. Rosenzweig, D.H. et al. Culture of Primary Bovine Chondrocytes on a Continuously Expanding Surface Inhibits Dedifferentiation. *Tissue engineering. Part A* (2012).

385. Mow, V.C., Ratcliffe, A. & Poole, A.R. Cartilage and Diarthrodial Joints as Paradigms for Hierarchical Materials and Structures. *Biomaterials* **13**, 67-97 (1992).

386. Kawamura, S., Lotito, K., Rodeo, S.A. Biomechanics and healing response of the meniscus. *Operative Techniques in Sports Medicine* **11**, 68-76 (2003).

387. Gebremariam, L., Koes, B.W., Peul, W.C. & Huisstede, B.M. Evaluation of treatment effectiveness for the herniated cervical disc: a systematic review. *Spine* **37**, E109-118 (2012).

388. Hunziker, E.B. Biologic repair of articular cartilage. Defect models in experimental animals and matrix requirements. *Clinical orthopaedics and related research*, S135-146 (1999).

389. Khan, I.M., Gilbert, S.J., Singhrao, S.K., Duance, V.C. & Archer, C.W. Cartilage integration: evaluation of the reasons for failure of integration during cartilage repair. A review. *European cells & materials* **16**, 26-39 (2008).

390. Benjamin, M. & Ralphs, J.R. Biology of fibrocartilage cells. *International review of cytology* **233**, 1-45 (2004).

391. Hunziker, E.B. & Quinn, T.M. Surgical removal of articular cartilage leads to loss of chondrocytes from cartilage bordering the wound edge. *The Journal of bone and joint surgery. American volume* **85-A Suppl 2**, 85-92 (2003).

392. Ionescu, L.C. et al. Maturation state-dependent alterations in meniscus integration: implications for scaffold design and tissue engineering. *Tissue engineering. Part A* **17**, 193-204 (2011).

393. Woo, S.L., Vogrin, T.M. & Abramowitch, S.D. Healing and repair of ligament injuries in the knee. *The Journal of the American Academy of Orthopaedic Surgeons* **8**, 364-372 (2000).

394. Bos, P.K., DeGroot, J., Budde, M., Verhaar, J.A. & van Osch, G.J. Specific enzymatic treatment of bovine and human articular cartilage: implications for integrative cartilage repair. *Arthritis and rheumatism* **46**, 976-985 (2002).

395. Jurgensen, K., Aeschlimann, D., Cavin, V., Genge, M. & Hunziker, E.B. A new biological glue for cartilage-cartilage interfaces: tissue transglutaminase. *The Journal of bone and joint surgery. American volume* **79**, 185-193 (1997).

396. Scotti, C. et al. Healing of meniscal tissue by cellular fibrin glue: an in vivo study. *Knee surgery, sports traumatology, arthroscopy : official journal of the ESSKA* **17**, 645-651 (2009).

397. Hunziker, E.B. & Kapfinger, E. Removal of proteoglycans from the surface of defects in articular cartilage transiently enhances coverage by repair cells. *The Journal of bone and joint surgery. British volume* **80**, 144-150 (1998).

398. Takegami, K. et al. Osteogenic protein-1 is most effective in stimulating nucleus pulposus and annulus fibrosus cells to repair their matrix after chondroitinase ABC-induced in vitro chemonucleolysis. *The spine journal : official journal of the North American Spine Society* **5**, 231-238 (2005).

399. Calve, S., Lytle, I.F., Grosh, K., Brown, D.L. & Arruda, E.M. Implantation increases tensile strength and collagen content of self-assembled tendon constructs. *Journal of applied physiology* **108**, 875-881 (2010).

400. Wang, B. et al. Engineering of extensor tendon complex by an ex vivo approach. *Biomaterials* **29**, 2954-2961 (2008).

401. Eleswarapu, S.V., Responte, D.J. & Athanasiou, K.A. Tensile properties, collagen content, and crosslinks in connective tissues of the immature knee joint. *PloS one* **6**, e26178 (2011).

402. Frank, C., McDonald, D., Wilson, J., Eyre, D. & Shrive, N. Rabbit medial collateral ligament scar weakness is associated with decreased collagen pyridinoline crosslink density. *Journal of orthopaedic research : official publication of the Orthopaedic Research Society* **13**, 157-165 (1995).

403. Ahsan, T., Lottman, L.M., Harwood, F., Amiel, D. & Sah, R.L. Integrative cartilage repair: inhibition by beta-aminopropionitrile. *Journal of orthopaedic research : official publication of the Orthopaedic Research Society* **17**, 850-857 (1999).

404. Fujimoto, D. & Moriguchi, T. Pyridinoline, a non-reducible crosslink of collagen. Quantitative determination, distribution, and isolation of a crosslinked peptide. *Journal of biochemistry* **83**, 863-867 (1978).

405. Verdonk, R., Verdonk, P., Huysse, W., Forsyth, R. & Heinrichs, E.L. Tissue ingrowth after implantation of a novel, biodegradable polyurethane scaffold for treatment of partial meniscal lesions. *The American journal of sports medicine* **39**, 774-782 (2011).

406. Rodkey, W.G. et al. Comparison of the collagen meniscus implant with partial meniscectomy. A prospective randomized trial. *The Journal of bone and joint surgery. American volume* **90**, 1413-1426 (2008).

407. Bulgheroni, P. et al. Follow-up of collagen meniscus implant patients: clinical, radiological, and magnetic resonance imaging results at 5 years. *The Knee* **17**, 224-229 (2010).

408. Monllau, J.C. et al. Outcome after partial medial meniscus substitution with the collagen meniscal implant at a minimum of 10 years' follow-up. *Arthroscopy : the journal of arthroscopic & related surgery : official publication of the Arthroscopy Association of North America and the International Arthroscopy Association* **27**, 933-943 (2011).

409. Moriguchi, Y. et al. Repair of meniscal lesions using a scaffold-free tissue-engineered construct derived from allogenic synovial MSCs in a miniature swine model. *Biomaterials* **34**, 2185-2193 (2013).

410. Weinand, C. et al. Healing potential of transplanted allogeneic chondrocytes of three different sources in lesions of the avascular zone of the meniscus: a pilot study. *Archives of orthopaedic and trauma surgery* **126**, 599-605 (2006).

411. Zhang, H., Leng, P. & Zhang, J. Enhanced meniscal repair by overexpression of hIGF-1 in a full-thickness model. *Clinical orthopaedics and related research* **467**, 3165-3174 (2009).

412. Bowles, R.D., Gebhard, H.H., Hartl, R. & Bonassar, L.J. Tissue-engineered intervertebral discs produce new matrix, maintain disc height, and restore biomechanical function to the rodent spine. *Proceedings of the National Academy of Sciences of the United States of America* **108**, 13106-13111 (2011).

413. Ganey, T. et al. Disc chondrocyte transplantation in a canine model: a treatment for degenerated or damaged intervertebral disc. *Spine* **28**, 2609-2620 (2003).

414. Gruber, H.E. et al. Autologous intervertebral disc cell implantation: a model using Psammomys obesus, the sand rat. *Spine* **27**, 1626-1633 (2002).

415. Ionescu, L.C. & Mauck, R.L. Porosity and cell preseeding influence electrospun scaffold maturation and meniscus integration in vitro. *Tissue engineering. Part A* **19**, 538-547 (2013).

416. Ionescu, L.C., Lee, G.C., Huang, K.L. & Mauck, R.L. Growth factor supplementation improves native and engineered meniscus repair in vitro. *Acta biomaterialia* **8**, 3687-3694 (2012).

417. Qu, F., Lin, J.M., Esterhai, J.L., Fisher, M.B. & Mauck, R.L. Biomaterial-mediated delivery of degradative enzymes to improve meniscus integration and repair. *Acta biomaterialia* **9**, 6393-6402 (2013).

418. Randall, J.E. Size of the great white shark (carcharodon). *Science* **181**, 169-170 (1973).

419. Goldman, K.J. Regulation of body temperature in the white shark, Carcharodon carcharias. . *Journal of Comparative Physiology B* **167**, 423-429 (1997).

420. Klimley, A.P., Beavers, S. C., Curtis, T. H., & Jorgensen, S. J. Movements and swimming behavior of three species of sharks in La Jolla Canyon, California. *Enviornmental Biology of FIshes* **63**, 117-135 (2002).

421. Jorgensen, S.J. et al. Philopatry and migration of Pacific white sharks. *Proceedings. Biological sciences / The Royal Society* **277**, 679-688 (2010).

422. Klimley, A.P., Le Boeuf, B.J., Cantara, K.M., Richert, J.E., Davis, S.F., Sommeran, S.V., Kelly, J.T. The hunting strategy of white sharks (Carcharodon carcharias) near a seal colony. *Marine Biology* **138**, 617-636 (2001).

423. Klimley, A.P., Le Boeuf, B.J., Cantara, K.M., Richert, J.E., Davis, S.F., Sommeran, S.V. Radio-acoustic positioning as a tool for studying site-specific behavior of the white shark and other large marine species. *Marine Biology* **138**, 429-446 (2001).

424. Klimley, A.P. in American Scientist, Vol. 82 122-133 (Sigma Xi, The Scientific Research Society, 1994).

425. Nasby-Lucas, N., Dewar, H., Lam, C.H., Goldman, K.J., Domeier, M.L. White shark offshore habitat: a behavioral and environmental characterization of the eastern Pacific shared offshore foraging area. *PloS one* **4**, e8163 (2009).

426. Weng, K.C., O'Sullivan, J. B., Lowe, C. G., Winkler, C. E., Dewar, H., & Block, B. A Movements, behavior and habitat preferences of juvenile white sharks Carcharodon carcharias in the eastern Pacific. *Marine Ecology Progress Series* **338**, 211-224 (2007).

427. Compagno, L.V. in Sharks of the world. (ed. F.a.A.O.o.t.U. Nations) 249 (Rome; 1984).

428. Tricas, T.C., McCosker, J.E. Predatory behaviour of the white shark, Carcharodon carcharias, with notes on its biology. *Proceedings of the California Academy of the Sciences* **43**, 221-238 (1984).

429. Dewar, H., Domeier, M., & Nasby-Lucas, N. Insights into young of the year white shark, Carcharodon carcharias, behavior in the Southern California Bight. . *Enviornmental Biology of FIshes* **70**, 133-143 (2004).

430. Dicken, M.L. First observations of young of the year and juvenile great white sharks (Carcharodon carcharias) scavenging from a whale carcass. *Marine and Freshwater Research* **59**, 596-602 (2008).

431. Fergusson, I.K., Leonard, J.V., Marks, A.M. Predation by White Sharks Carcharodon carcharias (Chondrichthyes: Lamnidae) Upon Chelonians, with New Records from the Mediterranean Sea and a First Record of the Ocean Sunfish Mola mola (Osteichthyes: Molidae) as Stomach Contents. *Enviornmental Biology of FIshes* **58**, 447-453 (2000).

432. Cliff, G., Dudley, S.F.J., Davis, B. Sharks caught in the protective gill nets off Natal, South Africa. 2. The great white shark Carcharodon carcharias (Linnaeus). *South African Journal of Marine Sciences* **8**, 131-144 (1989).

433. Goldman, K.J., & Anderson, S. D. Space utilization and swimming depth of white sharks, Carcharodon carcharias, at the South Farallon Islands, central California. Environmental Biology of Fishes. *Enviornmental Biology of FIshes* **56**, 351-364 (1999).

434. Martin, R.A., Hammerschlag, N., Collier, R. S., & Fallows, C. Predatory behaviour of white sharks (Carcharodon carcharias) at Seal Island, South Africa. *Journal of the marine Biological Association of the United Kingdom* **85**, 1121-1135 (2005).

435. Ferrara, T.L. et al. Mechanics of biting in great white and sandtiger sharks. *Journal of biomechanics* **44**, 430-435 (2011).

436. Wroe, S., McHenry, C. & Thomason, J. Bite club: comparative bite force in big biting mammals and the prediction of predatory behaviour in fossil taxa. *Proceedings. Biological sciences / The Royal Society* **272**, 619-625 (2005).

437. Long, D.J., Jones, R.E. in Great white sharks: the biology of Carcharodon carcharias. (ed. A.P. Klimley, Ainley, D.G.) 293-307 (Academic Press, San Diego, CA; 1996).

438. Summers, A.P., Long, J.H. in Fish Biomechanics Vol. 141. (ed. R.E. Shadwick, Lauder, G.V.) 141-178 (Elsevier Academic Press, London, UK; 2006).

439. Dean, M.N. & Summers, A.P. Mineralized cartilage in the skeleton of chondrichthyan fishes. *Zoology* **109**, 164-168 (2006).

440. Dean, M.N., Chiou, W., Summers, A.P. Morphology and Ultrastructure of Prismatic Calcified Cartilage. *Microscopy and Microanalysis* **11**, 1196-1197 (2005).

441. Elder, B.D., Vigneswaran, K., Athanasiou, K.A. & Kim, D.H. Biomechanical, biochemical, and histological characterization of canine lumbar facet joint cartilage. *Journal of neurosurgery. Spine* **10**, 623-628 (2009).

442. Martin, A.P., Naylor, G.J. & Palumbi, S.R. Rates of mitochondrial DNA evolution in sharks are slow compared with mammals. *Nature* **357**, 153-155 (1992).

443. Cappetta, H. in Handbook Paleoichtyology, Vol. 3B. (ed. H.P. Schultze) 193 (Gustav Fischer Verlag, Stuttgart; 1987).

444. Martin, R.A., Hammerschlag, N., Collier, R.S., Fallows, C. Predatory behaviour of white sharks (Carcharodon carcharias) at Seal Island, South Africa. *Journal of the Marine Biological Association of the United Kingdom* **85**, 1121-1135 (2005).

445. Motta P.J., W.C.D. Advances in the study of feeding behaviors, mechanisms, and mechanics of sharks. . *Enviornmental Biology of FIshes* **60**, 131-156 (2001).

446. Freed, L.E. et al. Chondrogenesis in a cell-polymer-bioreactor system. *Experimental cell research* **240**, 58-65 (1998).

447. Langsjo, T.K. et al. Electron microscopic stereological study of collagen fibrils in bovine articular cartilage: volume and surface densities are best obtained indirectly

(from length densities and diameters) using isotropic uniform random sampling. *Journal of anatomy* **195 (Pt 2)**, 281-293 (1999).

448. Weiss, C., Rosenberg, L. & Helfet, A.J. An ultrastructural study of normal young adult human articular cartilage. *The Journal of bone and joint surgery. American volume* **50**, 663-674 (1968).

449. Akizuki, S. et al. Tensile properties of human knee joint cartilage: I. Influence of ionic conditions, weight bearing, and fibrillation on the tensile modulus. *Journal of orthopaedic research : official publication of the Orthopaedic Research Society* **4**, 379-392 (1986).

450. Dingerkus, G., Seret, B. & Guilbert, E. Multiple prismatic calcium phosphate layers in the jaws of present-day sharks (Chondrichthyes; Selachii). *Experientia* **47**, 38-40 (1991).

451. Orvig, T. Histologic studies of Placoderms and fossil Elasmobranchs. The endoskeleton, with remarks on the hard tissues of lower vertebrates in general. *Ark Zool* **2**, 231-4544 (1951).

452. Janvier, P., Arsenault, M., Desbiens, S. Calcified cartilage in the paired fins of the osteostracan Escuminaspis laticeps (Traquair 1880), from the Late Devonian of Miguasha (Québec, Canada), with a consideration of the early evolution of the pectoral fin endoskeleton in vertebrates. *Journal of Vertebrate Paleontology* **24**, 773-779 (2004).

453. Ten Cate, R.A. in Oral histology: development, structure, and function Edn. 6. (ed. A. Nanci) 376-396 (Mosby, St Louis; 2003).

454. Ramsay, J.B. & Wilga, C.D. Morphology and mechanics of the teeth and jaws of white-spotted bamboo sharks (Chiloscyllium plagiosum). *Journal of morphology* **268**, 664-682 (2007).

455. Langenbach, G.E., Zhang, F., Herring, S.W., van Eijden, T.M. & Hannam, A.G. Dynamic mechanics in the pig mandibular symphysis. *Journal of anatomy* **209**, 69-78 (2006).

456. Derby, M.A. & Pintar, J.E. The histochemical specificity of Streptomyces hyaluronidase and chondroitinase ABC. *Histochem J* **10**, 529-547 (1978).

457. Prabhakar, V. et al. Biochemical characterization of the chondroitinase ABC I active site. *Biochem J* **390**, 395-405 (2005).

458. Malemud, C.J. et al. Phenotypic modulation of newly synthesized proteoglycans in human cartilage and chondrocytes. *Osteoarthritis Cartilage* **3**, 227-238 (1995).

459. Korhonen, R.K. et al. Fibril reinforced poroelastic model predicts specifically mechanical behavior of normal, proteoglycan depleted and collagen degraded articular cartilage. *J Biomech* **36**, 1373-1379 (2003).

460. Rieppo, J. et al. Structure-function relationships in enzymatically modified articular cartilage. *Cells Tissues Organs* **175**, 121-132 (2003).

461. Laasanen, M.S. et al. Novel mechano-acoustic technique and instrument for diagnosis of cartilage degeneration. *Physiol Meas* **23**, 491-503 (2002).

462. Schmidt, M.B., Mow, V.C., Chun, L.E. & Eyre, D.R. Effects of proteoglycan extraction on the tensile behavior of articular cartilage. *J Orthop Res* **8**, 353-363 (1990).

463. Jo, C.H. et al. Degree of degeneration and chondroitinase ABC treatment of human articular cartilage affect adhesion of chondrocytes. *Tissue Eng* **12**, 167-176 (2006).

464. Schwartz, M.H., Leo, P.H. & Lewis, J.L. A microstructural model for the elastic response of articular cartilage. *J Biomech* **27**, 865-873 (1994).